Thermophysics 2011 - Conference Proceedings

16th International Meeting of Thermophysical Society

2nd to 4th November 2011
Valtice, Czech Republic
Brno University of Technology

Book cover design: Vladimír Dvonka, Michal Veselý

Printed by: Brno University of Technology, Faculty of Chemistry, 2011

ISBN: 978-80-214-4345-7

Acknowledgment

Publication of this book was financially supported by the Czech Ministry of Education, Youth and Sports, under project No MSM 6840770031 and by the project "Centre for Materials Research at FCH BUT" No. CZ.1.05/2.1.00/01.0012 from ERDF.

Committees

INTERNATONAL SCIENTIFIC COMMITTEE

Rachel Becker, Civil and Environmental Engineering, Technion, Haifa, ISRAEL
Mark Bomberg, L.C. Smith College of Engineering and Computer Science, Syracuse University, Syracuse, U.S.A.
Robert Cerny, Faculty of Civil Engineering CTU, Prague, CZECH REPUBLIC
Dariusz Gawin, Department of Building Physics & Building Materials, Technical University of Lodz, Lodz, POLAND
John Grunewald, Faculty of Architecture, Dresden University of Technology, Dresden, GERMANY
Ulf Hammerschmidt, Physikalisch-Technische Bundesanstalt,Braunschweig, GERMANY
Shuichi Hokoi, Department of Architecture and Architectural Engineering, Faculty of Engineering, Kyoto University, Kyoto, JAPAN
Ludovit Kubicar, Institute of Physics SAC, Bratislava, SLOVAK REPUBLIC
Xinying Lu, Department of Civil Engineering, Tsinghua University, Beijing, CHINA
Wahid Maref, NRC Institute for Research in Construction, Ottawa, Ontario, CANADA
Peter Matiasovsky, Institute of Construction and Architecture SAC, Bratislava, SLOVAK REPUBLIC
Igor Medveď, Faculty of Natural Sciences, Constantine the Philosopher University, Nitra, SLOVAK REPUBLIC
Zbysek Pavlik, FCE CTU, Prague, CZECH REPUBLIC
Carsten Rode, Department of Civil Engineering, Technical University of Denmark, Lyngby, DENMARK
Staf Roels, Department of Civil Engineering, K. U. LEUVEN, Heverlee Leuven, BELGIUM
Bimal Kumar Sarkar, Department of Physics, School of Advanced Sciences, VIT University VIT University, Vellore, INDIA
Jay Sanjayan, Faculty of Engineering & Industrial Sciences, Swinburne University of Technology, Hawthorn, AUSTRALIA
Henryk Sobczuk, Faculty of Environmental Engineering, Lublin University of Technology, Lublin, POLAND
Oldrich Zmeskal, Faculty of Chemistry BUT, Brno, CZECH REPUBLIC

ORGANIZING COMMITTEE

Oldrich Zmeskal, FCH BUT, Brno, Czech Republic
Tomas Bzatek, FCH BUT, Brno, Czech Republic
Lenka Dohnalová, FCH BUT, Brno, Czech Republic
Zbysek Pavlik, FCE CTU, Prague, Czech Republic
Anton Trnik, FNS CPU, Nitra, Slovak Republic
Milena Pavlíková, FCE CTU, Prague, Czech Republic
Pavla Stefkova, FCH BUT, Brno, Czech Republic
Michal Vesely, FCH BUT, Brno, Czech Republic

HISTORY OF CONFERENCE

The first workshop was organized by ***prof. Stefan Barta*** on January 22, 1996 at the Department of Physics, Faculty of Electrical Engineering and Information Technology at the Slovak University of Technology in Bratislava. The Termophysic's meetings have been established as periodical meetings of scientists working in the field of investigation of thermophysical properties of materials and the problems of heat transfer and measurement of thermophysical and other transport properties of materials.

The Thermophysics as the working group of the Slovak Physical Society was established on the meeting at the Department of Thermophysics of the Slovak Academy of Sciences in Bratislava on June 13, 1997. The aim of the constitution of the working group is to exchange actual information in the field of heat transfer phenomena.

Dr. L'udovít Kubičár acted as the coordinator of the group and organized meetings at the Institute of Physics of the Slovak Academy of Sciences in Bratislava in the years - 1997, 1998 and 1999.

Then ***Dr. Libor Vozár*** from Faculty of Natural Sciences at the Constantine the Philosopher University in Nitra coordinated the activities of the society for the years 2000, 2001 and 2002. The workshops were organized in Nitra, in Račková dolina and Kočovce, respectively.

Next years, the Thermophysics workshop was held in Kočovce again. ***Dr. Peter Matiasovský***, working for the Institute of Construction and Architecture at the Slovak Academy of Sciences in Bratislava, being the chairman of Thermophysical Society for the years 2003, 2004 and 2005 was taking the chair of the workshops.

The last three years the Thermophysics workshop was held in Kočovce again. ***Dr. Jozefa Lukovičova*** from research group at the Department of Physics of Faculty of Civil Engineering at the Slovak University of Technology in Bratislava was taking the chair of the workshops for the years 2006, 2007 and 2008.

Since 2009, the Thermophysics workshop is held in Valtice. ***Prof. Oldrich Zmeskal*** (working at the Institute of Physical and Applied Chemistry and Centre of Material Research at the Faculty of Chemistry of the Brno University of Technology in Brno) and ***Prof. Robert Cerny*** (working at the Department of Materials Engineering and Chemistry at the Faculty of Civil Engineering of the Czech Technical University in Prague) were taking the chairs of the workshops.

Thermophysics 2011 takes place in Valtice - the Moravian town with one of the most impressive Baroque residences of Central Europe and well known wine cellars (Vinné sklepy Valtice)

Content

The Growth and the Decline of Thermoelectric Measurements

Július Krempaský

INPE, Slovak Technical University, Bratislava

Abstract: *An important part of thermophysical measurement is the field ofthermoelectric measurement. This activity involves the measurement of Seebeck's, Peltier's as well as Thompson's coefficients. Some time ago an interest has risen in measurement of so called "figure of merit Z" /Z parameter/, which is defined as a product of squared. Seebeck's coefficient and electrical conductivity divided by thermal conductivity. This quantity determines the effectiveness of the thermoelectric devices. It was proved that the application of some materials in this field should have been dominant, if Z parameter reaches the value about 0.01 1/K or higher. It was expected that the inventing of such materials will be a question of near future only. That was a stimulus for an intensive development of rapid methods of measurement of this parameter and it can be said that such were really found. However, the optimistic prognosis was not fulfilled and the interest for measurement thermoelectric parameters decreased.*

Key words: *thermophysical measurement, thermoelectric devices, Seebeck's, Peltier's and Thompson's coefficients, figure of merit Z*

1. Introduction

It is known that semiconductors generated in the half of the last century an intensive development not only in microelectronics, but stimulated the interest concerning the applicability of these materials also in the field of the production of electricity from heat as well as the generation of head and cold using electrics current. The basis for these interesting applications was the Seebeck's, Peltier's and Thompson's effects. The values of characteristicconstants of semiconductors know in this time signalized that device constructed on the basis of these effects should have been on the level of other classic devices and the optimistic view dictated that after appearance of some better semiconductors these classics devices will be overcome in future by semiconductor ones.

This information started not only an intensive chearching for new progressive constructions for thermoelectric devices, but stimulated also the activity in the development of suitable rapid methods for measuring parameters determinating the effectiveness of these devices. In this situation a new physical quantity appeared - the so called figure of merit Z /Z parameter/, which played a role of a "mean arbiter" at applying semiconductors in the field mentioned above. This quantity contains three fundamental constants: the Seebeck's coefficient, the electrical conductivity and thermal conductivity. It was, therefore, possible to measure this quantity by three separate measurements, but is more topical to prepare a method which should be able to find the value of Z parameter using only one direct measurement. This procedure was successfully realized. We shall analyze these methods in the further text.

2. Basic theory of electric devices

We shall analyze at first a thermoelectric generator which transforms a heat into the electric energy. It is convenient to use for this purpose an electric circuit composed from two semiconductors with opposite type of conductivity (Figure 1) coined together by a metal plate. If competent Seebeck's coefficients are α and competent temperatures T, then the resulting thermoelectric voltage is determined by the formula

$$U = (\alpha_n + \alpha_p)(T_1 - T_2). \tag{1}$$

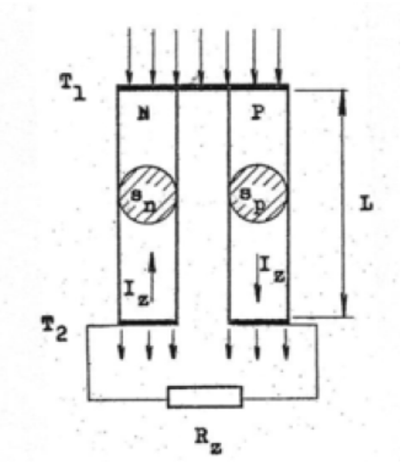

Figure 1: thermoelectric circuit

This phenomenon is accompanied by Peltier's effect, which represents a generation, resp. consumption of heat produced by electric current of the intensity I. Its value is determined by the relation

$$Q = PIt, \tag{2}$$

where P is Peltier's coefficient.

There are of interest for the praxis two quantities: a maximum efficiency and a maximum power. Using a little complicated mathematical procedure it is possible to gain for the first quantity mentioned above the relation (see e.e.)

$$\eta = \frac{T_1 - T_2}{T_1} \frac{\sqrt{1 + Z\overline{T}} - 1}{\sqrt{1 + Z\overline{T}} + T_2 / T_1}, \tag{3}$$

where

$$Z = \frac{(\alpha_n + \alpha_p)^2}{(\sqrt{\lambda_n \rho_n} + \sqrt{\lambda_p \rho_p})^2}. \tag{4}$$

In these formulas $T = (T_1 + T_2)/2$, λ_n and λ_p are thermal conductivities ρ_n and ρ_p are specific electric resistivity. We see that a maximum efficiency of a thermoelectric generator depends on the characteristic quantity, which can beformulated by the relation

$$Z = \frac{\alpha^2 \sigma}{\lambda}, \tag{5}$$

where σ is electrical conductivity. By this way the figure of merit Z entered into the calculation of the efficiency of thermoelectric devices and this is the cause why the measurement of this parameter was highly topical.

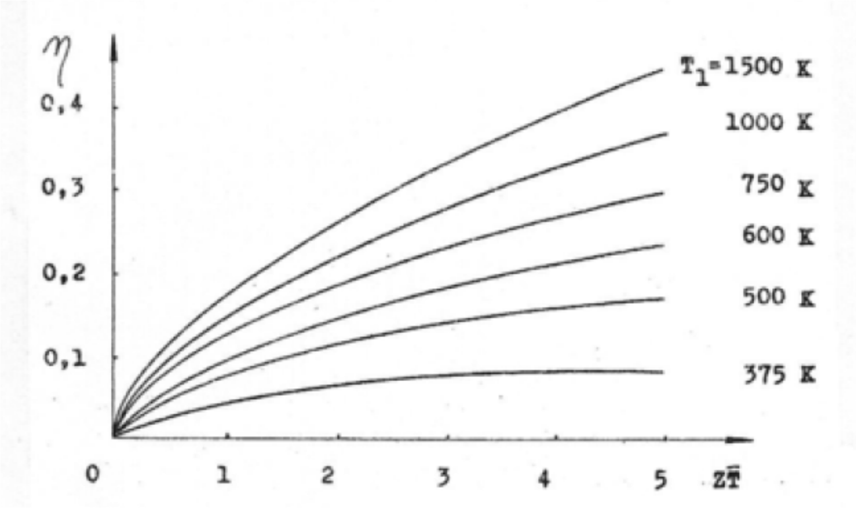

Figure 2: Efficiences of thermoelectric devices

Figure 2 demonstrates how sensitively this parameter influences the efficiency of thermoelectric devices in concrete situations. At (in this time) actual value Z = 0,002 and at temperatures T1 ≈ 600 K and T2 ≈ 300 K the efficiency was about 10%- in contrast wit ideal thermodynamic efficiency, which was 5x larger. It was expected in general that the evolution in technology will bring in near future an increase of the values of figures of merit to the number of order 0.01. In such conditions the efficiency of thermoelectric devices should overcome the efficiencies of classic devices.

Analogical calculations made for generators of heat and cold gave these results

$$\eta_h = \frac{T}{T - T_o}\left(1 - 2\frac{M-1}{ZT}\right), \tag{6}$$

$$\eta_c = \frac{T}{T - T_o}\frac{M - T_o/T}{M+1}, \tag{7}$$

where

$$M = \left\{1 + \frac{1}{2}Z(T + T_o)\right\}^{1/2}.$$

It is clear that also in these cases the Z parameter plays a dominant role.

3. Measurement of the figure of merit Z

According to the definition the figure of merit Z can be measured by separate measurements of characteristic α, σ and λ. This procedure was made more rapid by C,T. Harman [3], who used cylindrically shaped samples. Destructive interference with the samples, which this method requires, was eliminated by Iordanišvili and Trachbrot [4], but the measurements were then less exact. The complicated problem of separating the ohmic potential difference from the thermoelectric in both above methods was solved by Herinckx and Monfils ([5]).

A fundamentally different method of measuring the figure of merit Z is Cutler's method, in which one small-area and one large-area contact are used. Not one of the above measuring methods is suitable for rapid operational checking of the basic material because they require samples of defined geometrical shapes, special preparation, specially prepared contacts etc. From this point of view the more convenient seem methods elaborated in our institute. They use pulse or stationary regime in two-probe or four-probe arrangements with point, linear and circular contacts. Details concerning these methods can be found in papers [7 – 11]. Here we shall present only some interesting results.

a) Pulse two-probe methods

A semi-infinitive sample is used for such measurement. One point contact is a heat source and at a certain suitable distance r there is a recorder of thermal changes. In paper [11] a formula needed for calculation is derived

$$\frac{\alpha^2}{\lambda} = 40{,}98\frac{rU_m^p t_m}{IT_o \Delta t}, \tag{8}$$

where tm is the time in which the thermoelectric voltage has a maximum, U the maximum of this voltage corresponding to their Peltier's heat, I is the intensity of the pulse current, Δ t the duration of the pulse and To is the temperature of the sample before measurement. The value U can easily be found by means of two measurement with the electric current flowing in opposite directions $(U_m^p = (U_m^{p+} - U_m^{p-})/2$ (the influence of the Joule's heat concels, when subtracting).

The applied contacts can be used for measuring the electric conductivity. if in this measurementcurrent I flows through the sample and the ohmic potential difference is U, the electric conductivity is defined by the relation

$$\sigma = \frac{rI_\sigma}{SU_\sigma}, \tag{9}$$

where *S* is cross-section of the sample at the probes. A combination of relations (8) and (9) gives for the figure of merit the formula

$$Z = 40.98\frac{r^2}{ST_o\Delta t}\left(\frac{I_\sigma}{I}\right)\left(\frac{U_m^p}{U_\sigma}\right)t_m. \tag{10}$$

One may choose in the measurement the condition $I_\sigma = I$, so formulas needed for calculation have a simpler form

$$Y = C\frac{U_m^p t_m}{U_\sigma}\ ,\ C = 40.98\frac{r^2}{ST_o\Delta t}\ . \tag{11}$$

The Z parameter could be measured still more easily on the assumption that the contact resistance of the probe and sample is known. In the case of a thin welded wire of radius ro this is (according [12])

$$R = \frac{1}{4r_o\sigma}\ ,\ U_m^p = RI_m^p \tag{12}$$

where I is the current flowing through the circuit. Then it follows from relations written above

$$Z = A\frac{I_m^p t_m}{I}\ ,\ A = 10.24\frac{r}{T_o r_o \Delta t} \tag{13}$$

b) Four probe method

When measuring of semiconductors it is possible to use the four-probe arrangement, which was originally used only for measuring the electric conductivity ([13]). An electric pulse passes through the outer probes (Figure 3) and a thermoelectric voltage is induced between inner probes. If the distances between the probes and their contact resistances are equal, the thermoelectric voltage between inner probes is influenced only by the Peltier's heat. As was shown two measurements must be made for opposite direction of the current pulse. The formula needed for calculation is done in ([11])

$$\frac{\alpha^2}{\lambda} = 20.49\frac{r}{T_0 I\Delta t}\frac{U_m^p}{t_m}\ . \tag{14}$$

If a constant current flows through the outer probes, therelation

$$\sigma = \frac{1}{2\pi r}\frac{I_\sigma}{U_\sigma} \tag{15}$$

is valid and the figure of merit Z can be calculated from the relation

$$Z = \frac{3.26}{T_o\Delta t}\left(\frac{I_\sigma}{I}\right)\left(\frac{U_m^p}{U_\sigma}\right)t_m \tag{16}$$

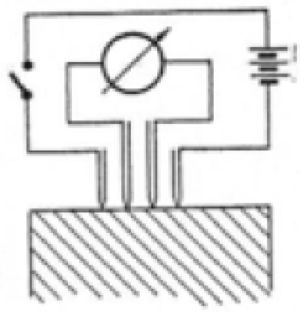

Figure 3: Arrangement with four probes

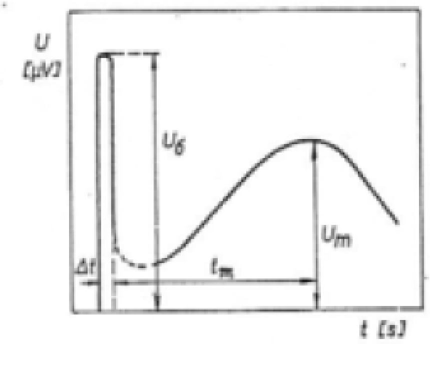

Figure 4: Records at 4-probe method

Of course, it is possible to choose $I_\sigma = I$ and then the figure of merit could be found very rapidly. A graphic record of this measurement is illustrated on the Figure 4.

4. Materials for thermoelectric devices

We have demonstrated that it is necessary for construction of progressive thermoelectric devices to search materials with high value of their figure of merit and these materials must be able to work at high temperatures. The high value of Z parameter needs material with high Seebek's coefficient, high electric conductivity and low thermal conductivity. These conditions were good fulfilled for compound based on bismuth, tellurium, selenium and other, what guaranteed the value 0,002 1/K. It was in general supposed that this value will increase in the future and this optimistic prognosis started - especially in Soviet Union - a very large activity in manufacturing a large spectrum of thermoelectric generators, which is documented e.g. in books ([14]). However, the fate was not favorable for this optimistic prognosis and no materials with higher value of Z parameter like 0,002 were discovered.

A logical result of this evolution was a deep decrease of the interest oriented on thermoelectric application and also the interest concerning thermoelectric measurement practically vanished. The importance of such measurement remained only in the research of fundamental properties of materials.

It is necessary only to hope that an similar fate will realize in thermoelectricity like in superconductivity - nobody expected, but high-temperature superconductors suddenly appeared. But it seems it is only a dream.

References

[1] Krempaský, J. and Lasz, J.: Semiconductors. Scriptum.FEI STU Bratislava, 1978.
[2] Ioffe, A.F.: Fizika spoluprovodníkov. IAN, Moskava-Leningrad, 1967.
[3] Harman, T.c., Cahn, J.H. and Legan, M.J., J. Appl. Phys. 30 (1959), 1351.
[4] Jordanišvili, F.K. and Trachbrot, B., FTT 4 (1962), 122.
[5] Herinckx, C. and Monfils, A., Brit, J., Appl. Phys. 10 (1959), 235.
[6] Cutler, J., J. Appl. Phys. 32 (1961) 1075.
[7] Krempaský, J. Czech, J. J Phys. B 14 (1964), 533.
[8] Krempaský, J. Česk.čas. pro fyziku A 16 (1966), 136.
[9] Krempaský, J.: Meranie termofyzikálnych veličín. SAV Bratislava, 1969.
[10] Kubičar, L. and Krempaský, J., Phys. Stat. Sol. (a) 2 (1970), 739.
[11] Krempaský, J., Čs. čas. fyz. B 12 (1962), 353.
[12] Holm, R.: Electric contacts. Stockholm, 1946.
[13] Valdes, L., Proc. IRE 42 (1954), 420.
[14] Poluprovodniky v nauke i technike I, II.Izd.AN CCCP, Moskva-Leningrad, 1957.

Photoacoustic Spectroscopy: A tool for the investigation of thermal and optical properties of solids

Bimal Kumar Sarkar[1], P. S. Deviprasadh[1], A. S. Verma[2], Sheetal Sharma[2], V. K. Jindal[2]

[1]Department of Physics, VIT University, Vellore 632014, India

Email: bksarkar@vit.ac.in

[2]Department of Physics, Panjab University, Chandigarh 160014, India

Abstract: *Photoacoustic spectroscopic (PAS) technique can be used for investigating the thermal and optical properties of solids. In this technique, one has to detect the photoacoustic signal produced when a sample placed in a cell is irradiated by an intensity modulated beam of light. The amplitude and phase of the photoacoustic (PA) signal depends on the thermal and optical properties of the sample, the most important of which are the specific heat, thermal conductivity, thermal diffusivity, optical absorption coefficient etc. Hence the wealth of information contained in the PA signal can be used to investigate the thermal and optical properties of solids. This enables one to work with essentially transparent media or highly light scattering materials such as powders, amorphous solids, gels and colloids. With this technique it is possible to obtain optical absorption spectra of materials that are completely opaque to transmitted light. In this paper we have emphasized over the theoretical, experimental issues on the application of photacoustic spectroscopy for the investigation of thermal and optical properties of solids.*

Keywords: *Photacoustic spectroscopy, Specific heat, Thermal conductivity, Thermal diffusivity, Optical absorption.*

1. Introduction

The photoacoustic (PA) effect is the generation of an acoustic signal when the sample under investigation, placed inside a closed cell, is irradiated by an intensity modulated beam of light.This phenomenon as detected by alexander Graham Bell in 1880 [1, 2], possesses some unique features. The incident energy in the form of photons is absorbed by the materials. Through the irradiative transition the absorbed energy is converted into thermal energy which in turn reflects the thermal and optical properties of the sample. The photoacoustic (PA) effect is the generation of an acoustic signal when the sample under investigation, is placed inside a closed cell, and is irradiated by an intensity modulated beam of light. In case of gas and liquid samples, the sample fills the entire volume of the cell and the acoustic signals are detected by a microphone and a piezoelectric transducer respectively. In the case of solid samples, the sample fills only a portion of the cell and the remaining volume of the cell is filled with a non-absorbing gas such as air, and a sensitive microphone is suitably placed inside the cell to pick up the acoustic signals. The internal energy levels of the sample are excited by the absorption of incident radiation and upon subsequent de-excitation, all or part of the absorbed photon energy is converted into heat through non-radiative de-excitation processes. In the case of gas and liquid samples, this internal heating causes pressure fluctuations having the same frequency as that of the modulation of the incident beam, which can be detected by the acoustic transducer. In the case of solid samples, the periodic heating of the sample results in a periodic heat flow from the interior of the sample to the surrounding gas which in turn produces pressure fluctuations in the gas which can be detected as an acoustic signal by the microphone. It is also possible to measure the heat generated in a bulk solid sample through the subsequent pressure or stress variation in the sample itself by means of a piezoelectric detector in intimate contact with the sample.

Photoacoustic spectroscopy (PAS) is essentially a combination of optical absorption spectroscopy and calorimetry [3]. From the calorimetric viewpoint, the heat input into the sample is supplied indirectly by the incident beam of light and the rise in temperature is detected by another indirect method using an acoustic transducer instead of a thermal detector. For a typical solid sample, using gas microphone detection system, temperature rise of $\sim 10^{-6}$ ^{0}C can be detected. This acoustic detection has several advantages over conventional thermal detection using temperature sensor such as thermistor or thermopiles in terms of sensitivity, detector rise time and the speed at which measurements can be made. In this paper the theoretical model and application will be presented.

2. Theory

According to Rosencwatg and Gersho (R-G theory) [4,5], in a gas microphone PA cell, the signal depends both on the generation of an acoustic pressure disturbance at the sample-gas interface and on the transport of this pressure disturbance through the gas to microphone. The pressure fluctuations at the sample-gas interface are caused by the periodic heat flow from the sample which is governed by thermal diffusion equations. By solving the thermal diffusion equations for the sample, the backing material on which the sample is mounted and the gas in the cell, the periodic variation in temperature at the sample-gas interface can be obtained. A one-dimensional analysis of the production of a photoacoustic signal in a simple cylindrical cell is shown in figure 1. The cell has a diameter D and length L. It is assumed that the length L is small compared to the wavelength of the acoustic signal and the microphone (not shown in the figure) detects the average pressure in the cell. The solid sample is considered to be in the form of a disc having diameter D and length ℓ. The sample is mounted so that its back surface is against a poor thermal conductor of thickness ℓ''.

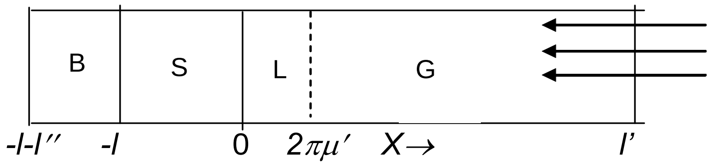

←: Incident light; B: Backing Material; S: Sample; L: Boundary layer of gas; G: Gas column

Figure1. Cross sectional view of a simple cylindrical PA cell.

The thermal diffusion equations are

$$\frac{\partial^2 \theta}{\partial X^2} = \frac{1}{\alpha''}\frac{\partial \theta}{\partial t} \qquad \text{for } -l'' - l \le x \le -l \tag{1}$$

$$\frac{\partial^2\theta}{\partial X^2} = \frac{1}{\alpha}\frac{\partial\theta}{\partial t} - Ae^{\beta x}(1+e^{i\omega t}) \text{ , where } A = \frac{\beta I_0\eta}{2K}\text{; for } -1 \le x \le 0 \tag{2}$$

$$\frac{\partial^2\theta}{\partial X^2} = \frac{1}{\alpha'}\frac{\partial\theta}{\partial t} \quad \text{for, } 0 \le x \le l' \tag{3}$$

Where θ is the temperature and η is the efficiency with which the absorbed light is converted into heat through non-radiative relaxation process.$\alpha = K/\rho C$ is the thermal diffusivity with K, ρ and C being thermal conductivity, density, and specific heat respectively. $a = (\omega/2\alpha)^{1/2}$ is the thermal diffusion coefficient (cm^{-1}) and $\mu = 1/a$ isthe thermal diffusion length (cm). ω denotes the modulation frequency of the incident light beam with absorption coefficient β. To completely specify the solution $\theta(x,t)$, the appropriate boundary conditions are obtained from the requirement of temperature and heat flux continuity at the boundaries $x = 0$ and $x = -l$, and from the constraint that the temperature at the cell walls $x = l'$ and $x = -l-l''$is at ambient.

The general solution for $\theta(x,t)$ in the cell neglecting transients can be written as,

$$\theta(x,t) = \begin{cases} \frac{1}{l''}(x+l+l'')W_0 + We^{\sigma''(x+l)}e^{i\omega t}, -l-l'' \le x \le -l \\ b_1 + b_2x + b_3e^{\beta x} + \left(Ue^{\sigma x} + Ve^{-\sigma x} - Ee^{\beta x}\right)e^{i\omega t}, -l \le x \le 0 \\ \left(1-\frac{x}{l'}\right)F + \theta_0 e^{-\sigma' x}e^{i\omega t}, 0 \le x \le l' \end{cases} \tag{4}$$

where W, U, V, E and θ_0 are complex valued constants, b_1, b_2, b_3, W_0 and F are real valued constants, and $\sigma = (1+i)a$. ◎◎and W represent the complex amplitudes of the periodic temperature at the sample-gas boundary ($x = 0$) and the sample-backing boundary ($x = -l$) respectively. The quantities W_0, F denotes the d.c. components of the temperature at the sample surface $x = 0$ and $x = -l$ respectively.

The explicit solution for θ_0, the complex amplitude of the periodic temperature at the solid – gas boundary ($x = 0$) is given by,

$$\theta_0 = \frac{\beta I_0}{2K\left(\beta^2 - \sigma^2\right)}\left[\frac{(r-1)(b+1)e^{\sigma l} - (r+1)(b-1)e^{-\sigma l} + 2(b-r)e^{-\beta l}}{(g+1)(b+1)e^{\sigma l} - (g-1)(b-1)e^{-\sigma l}}\right] \tag{5}$$

$$\text{where } b = \frac{K''a''}{Ka}, g = \frac{K'a'}{Ka} \text{ and } r = (1-i)\frac{\beta}{2a} \tag{6}$$

The periodic temperature variation at the sample surface as governed by eq.(5) causes thermal waves to diffuse into the gas. The periodic diffusion produces a periodic temperature variation in the gas as given by the component of the solution (4),

$$\theta_{a.c.}(x, t) = \theta_0 e^{-\sigma' x}e^{i\omega t} \tag{7}$$

Because of the periodic heating, this boundary layer of gas expands and contracts periodically and thus can be thought of as acting as an acoustic piston on the rest of the gas column, producing an acoustic signal that travels through the entire gas column. As a result the complex envelope of the sinusoidal pressure variation can be given as

$$Q=\frac{Y\beta}{Ka'\left(\beta^{2}-\sigma^{2}\right)}\left[\frac{(r-1)(b+1)e^{\sigma l}-(r+1)(b-1)e^{-\sigma l}+2(b-r)e^{-\beta l}}{(g+1)(b+1)e^{\sigma l}-(g-1)(b-1)e^{-\sigma l}}\right] \tag{8}$$

where, $Y = \dfrac{I_0 \gamma P_0}{2 T_0 l' \sqrt{2}}$

In case of optically opaque solids,

$$Q = \frac{(1-i)}{2a'}\left(\frac{\mu''}{K''}\right)Y$$ (For thermally thin solids (◎>>l; ◎>>l◎)) (9)

$$Q = \frac{Y}{2a'aK\beta}(\beta-2a-i\beta) \approx \frac{(1-i)}{2a'}\left(\frac{\mu}{K}\right)Y$$ (For thermally thick solids (◎<*l*; ◎>*l*◎) (10)

$$Q = \frac{-i\beta Y}{4a'a^{3}K}(2a-\beta-i\beta) \approx \frac{i\beta\mu}{2a'}\left(\frac{\mu}{K}\right)Y$$ (For thermally thick solids (◎<<*l*; ◎◎*l*◎) (11)

3. PA study of the optical and thermal properties of solids

PA study is carried out for the determination of (i) optical absorption spectra (ii) thermal diffusivity and (iii) specific heat of solids.

3.1. PA determination of the optical absorption spectra

If sample is considered as thermally thick ($\mu >> l$) the Eqn. (5) can be written as

$$\theta_o = \frac{\beta I_o}{2K\left(\beta^{2}-\sigma^{2}\right)} \times \frac{(r-1)}{(g+1)} \tag{12}$$

Now if the PA signal normalized (with black carbon powder) and q be the normalized PA amplitude, then

$$q = \frac{\beta\mu}{\left[(\beta\mu+1)^{2}+1\right]^{1/2}} \tag{13}$$

After simplification the optical absorption can be given as [6,7]

$$\beta = (1/\mu)\frac{\left[q^{2}+q(2-q^{2})^{1/2}\right]}{(1-q^{2})} \tag{14}$$

In Figure 1 the optical absorption spectrum is shown for $Zn_{1-x}Be_xSe$ ternary compound.

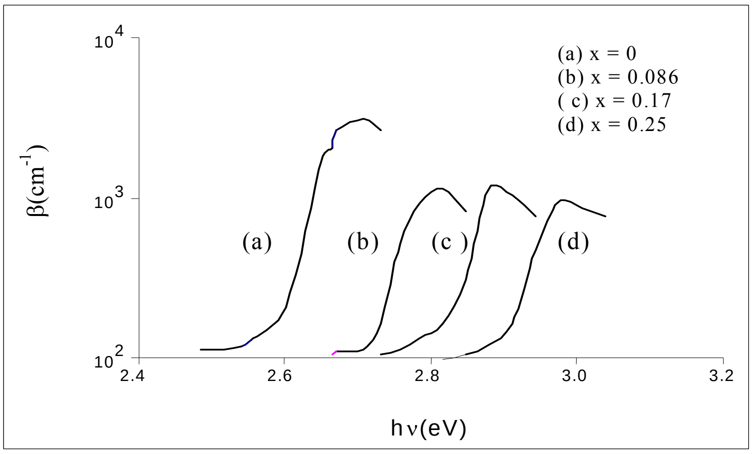

Figure 1: Variation of absorption coefficient (α) of $Zn_{1-x}Be_xSe$ as a function of incident photon energy (hν) with (a) x =0.0, (b) x = 0.086, (c) x = 0.17 and (d) x = 0.26.

3.2. PA determination of thermal diffusivity

Thermal diffusivity of solids can be measured using photoacoustic technique. This is done by measuring the amplitude of the PA signal as a function of the chopping frequency. In the thermally thick regime (μ< l where l is the thickness of the sample) the PA signal is independent of the thermal properties of the backing material on which the sample is mounted, whereas in the thermally thin regime (μ> l) the PA signal get modified by the thermal properties of the backing material as well. For an appropriate thickness of the sample, one can obtain a crossover from the thermally thin regime to the thermally thick regime by increasing the chopping frequency. The amplitude versus chopping frequency plot hence shows a change in slope at the characteristic frequency fc at which the crossover takes place. The characteristic frequency fC is defined by,

$f_C = \alpha / l^2$ (whereα is the thermal diffusivity and l is the sample thickness) (15)

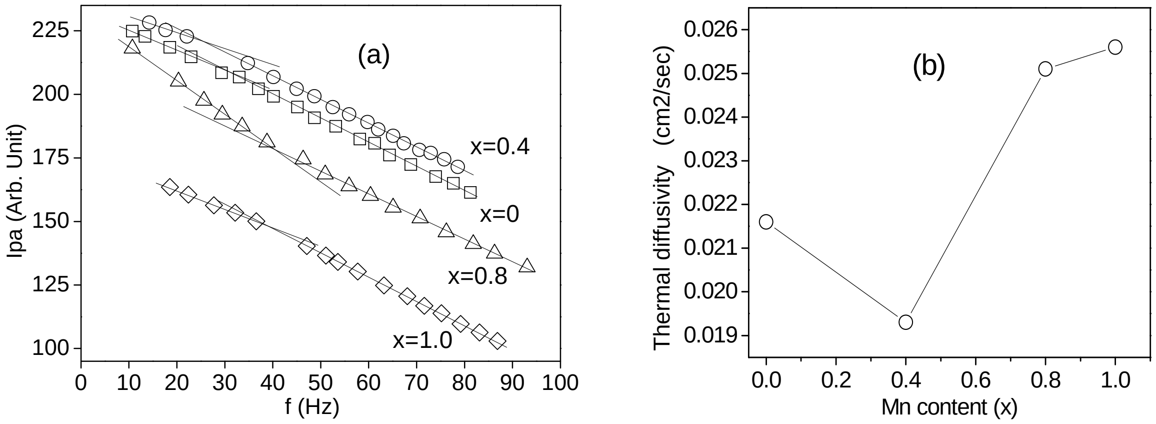

Figure 2: (a) PA signal vs. chopping frequency (f) (b) Thermal diffusivity vs Mn content in $Zn_{1-x}Mn_xTe$ ($0 \leq x \leq 1$) alloys. Estimated characteristic frequency (FC) from figure (a) is used to calculate thermal diffusivity by Eq. (9).

Figure 2 shows the variation of PA signal with chopping frequency and calculated thermal diffusivity data is presented in the same figure.

3.3 PA determination of the specific heat of solids

The R-G theory predicts the amplitude $I_{PA}(T)$ at different temperature (T), of the PA signal to vary as [8],

$$I_{PA}(T) \propto F(T).C(T)^{-1/2}.K(T)^{-1/2} \tag{16}$$

Where C(T) and K(T) are the specific heat and thermal conductivity of the sample respectively. The function F(T) takes into account all the temperature dependent properties of the cell, and the gas that affect the PA signal. F(t) is obtained from the calibration with a standard sample (in our case pure aluminium). Knowing C(T) and K(T) for the standard substance, one can calculate the normalized characteristic function f(T) = F(T)/F(100) using Eq (10). So normalizing the thermal properties of the sample one can get from Eq.(10)

$$\frac{C(T)K(T)}{C(100)K(100)} = \left[\frac{I(100)}{I(T)} f(T)\right]^2 \tag{17}$$

Again from thermal diffusivity data (α = K/ρC), one can calculate the values of α(T)/α(100) or $\frac{K(T)}{K(100)} \times \frac{C(100)}{C(T)}$ at different temperatures. Here we neglect the variation of density (ρ) of the solid in the temperature region of our experiment. Thus with the help of two separate data taken from two separate independent experiments one can find the thermal variation of normalized specific heat of the sample [i.e., C(T)/C(100)]. Thus calculated temperature variation of specific heat of superconductor $Bi_{1.6}Pb_{0.4}Sr_2Ca_2Cu_3O_x$has been shown in figure 3.

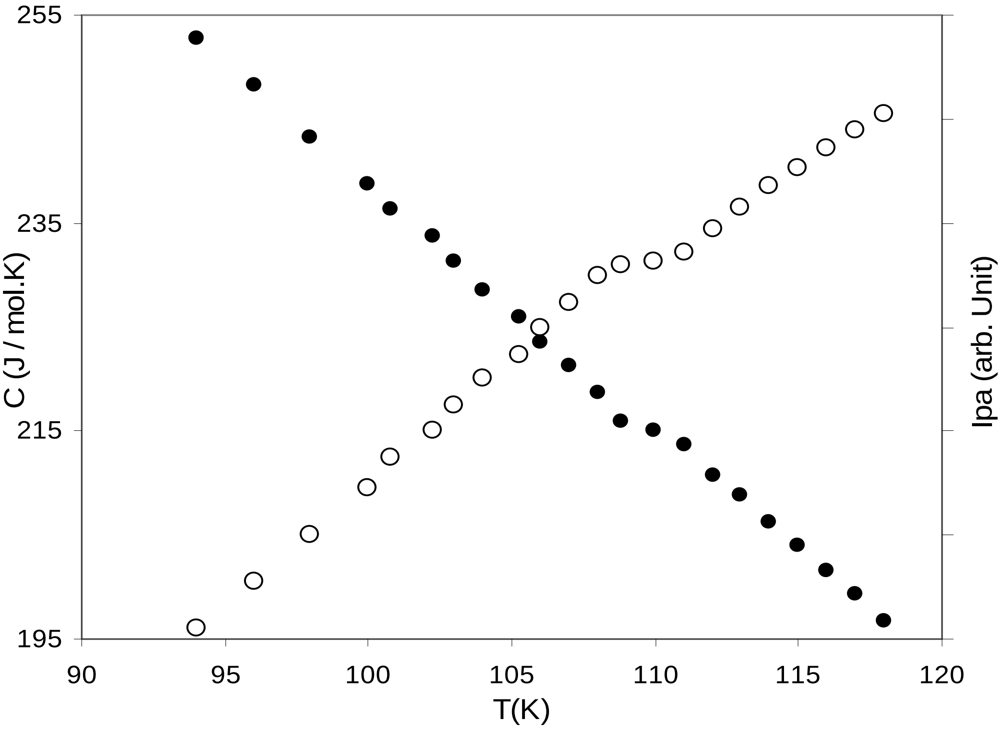

Figure 3: Thermal variation of Ipa(solid circle) and specific. heat(C) of Bi1.6Pb0.4Sr2Ca2Cu3Ox

Conclusion

Photoacoustic spectroscopy is a very sensitive tool for the determination of optical and thermal properties of solids. It has enormous applications in many area of current interest such as study of the thermal diffusivity, heat capacity, optical absorption of solids, estimation of optical band gap, defect states, structural phase transition etc. Photoacoustic spectroscopy can be well utilized for the non-destructive characterization of many solids giving information of their thermal and optical properties.

Acknowledgements

The first author (B. K. S.) is thankful to VIT University, Vellore, for its support and the third author (A. S. V.) acknowledges the assistance given by University Grant Commission, New Delhi, India, under the scheme of Dr. D. S. Kothari Post Doctoral Fellowship.

References

[1] BELL, A. G. On the production and reproduction of sound by light.In *Am. J. Sci.* 1880. 20. 305-324. ISSN: 0002-9599

[2] BELL A. G. Upon the Production of Sound by Radiant Energy.In *Philos. Mag.* 1881. 11. 510-528. ISSN: 1478-6435

[3] SARKAR, B. K., VERMA, A. S., GUPTA, R. C., SINGH, K. Thermal and Optical Properties of $Zn_{1-x}Mn_xTe$ Diluted Magnetic Semiconductor Studied by Photoacoustic Spectroscopic Method. In *Int J Thermophys.* 2010. 31. 620–629. ISSN: 0195-928X

[4] ROSENCWAIG, A. Photoacoustic spectroscopy of solid. In *Opt. Commun.* 1973. 7. 305-308.ISSN:0030-4018

[5] ROSENCWAIG, A., GERSHO, A. Theory of the photoacoustic effect with solids. In *J. Appl. Phys.* 1976. 47, 64-69. ISSN: 0021-8979

[6] SARKAR, B. K., CHAUDHURI, B. K. In *Int. J. Thermophysics.* 2005. 26. 295-303. ISSN: 1572-9567

[7] SARKAR, B. K., VERMA, A. S., DEVIPRASADH,P. S. Temperature inducedbandgapshrinkageinCu$_2$GeSe$_3$: Roleof electron–phononinteraction. In *Physica b.* 2011. 406. 2847–2850. ISSN: 0921-4526

[8] SARKAR, B. K., CHAUDHURI, K., CHAUDHURI, B. K., Photoacoustic spectroscopic method of studying thermal diffusivity and heatcapacity of high Tc superconducting oxide. *Ind. J. Phys.*2000. 74A (3). 211-213. ISSN: 0019-5480

Crystallization processes in disordered materials and Meyer-Neldel rule

Ivan Baník, Jozefa Lukovičová, Gabriela Pavlendová

Department of Physics, Faculty of Civil Engineering, SlovakUniversity of Technology,

Bratislava, SlovakRepublic, e-mail: ivan.banik@stuba.sk

***Abstract**: Many modern electronic solid-state devices such as electrophotographic photoreceptors employed in today's photocopiers, solar cells, organic field-effect transistors (OFETs), and organic light-emitting diodes (OLEDs) are generally based upon noncrystalline materials. Chalcogenide glasses are important group of these materials. They have become attractive materials, which form the basis for phase-change optical recording (CD and DVD) and electronic phasechange memory (PCM) technologies.The aim of research in this area is to increase the reliability of recording information, as well as increased density recording. Differential scanning calorimetry (DSC) is valuable for the quantitative experimental study of crystallization processes in different glassy systems. The crystallization phenomenon can be investigated using isothermal and nonisothermal methods. An understanding of the kinetics of crystallization in glasses is very important for practical application of disordered semiconductors. In this article we present the explanation of the Meyer-Neldel rule in crystallization processes of disordered materials.*

***Keywords**: Crystallization, Meyer-Neldel rule, Diffusion, Activation, Barrier-cluster model*

1. Introduction

The study of amorphous to crystalline phase change is important for the development of new disordered semiconductors (chalcogenide glasses) as better phase change recording materials [1-3]. Various quantitative methods have been suggested to evaluate the level of stability of the glasses. Some of these methods are based on the characteristic temperatures such as the glass transition temperature (T_G), the on-set crystallization temperature (T_0), the peak crystallization temperature (T_C) and the melting temperature (T_M) [4 -7]. More criterionare based on reaction rate constant of crystallization. The determination of rate constant is a subject of great interest from application as well as scientific point of view [4-7]. An understanding of the kinetics of crystallization in glasses is important for the manufacturing of glass-ceramics and in preventing devitrification, too.

1.1 Kinetics of crystallization

Crystallization rates are sometimes measured directly in the microscope [8-11] but this method could not be applied to glasses in which nucleation and crystallizatíon occurred in times below 1h [7]. Differential scanning calorimetry (DSC) is valuable for the quantitative study of crystallization in different glassy systems [11-13]. The crystallization phenomenon in chalcogenide glasses can be experimentally investigated using isothermal and non-isothermal methods. In isothermal method, the sample is brought near to crystallization temperature very quickly and then any physical quantity which changes drastically is measured as a function of time.In non-isothermal method, the sample is heated at a fixed rate and the physical parameter is recorded as a function of temperature. Any physical parameter, which changes drastically, can be taken as a measure of extent of crystallization as a function of time. A disadvantage of the isothermal method is the impossibility to reach a test temperature instantaneously and during the time in which the system needs to stabilize, no measurements are possible. However, non-isothermal methods based on constant heating rate experiment do not have this drawback.

1.2 Isothermal transformation

During the isothermal transformation, the extent of crystallization α of a certain material is represented by the Avrami's equation [14-16]

$$\alpha(t)= 1 - \exp(- (Kt)^n) \tag{1}$$

where K is rate constant and n is the order parameter which depends upon the mechanism of crystal growth. In general, crystallization rate constant K increases exponentially with temperature indicating that the crystallization is a thermally activated process. Mathematically, it can be expressed as

$$K = K_o \exp\left(-\frac{W_c}{kT} \right) \tag{2}$$

Here W_c is the activation energy of crystallization, K_0 the pre-exponential factor and k the universal Boltzmann constant. In Eq. (2) W_c and K_0 are assumed to be practically independent of the temperature (at least in the temperature interval accessible in the calorimetric measurements).

The *a-c* phase transformation in chalcogenide glasses is accompanied by a continuous change of the electrical conductivity σ, which is a sensitive structural parameter. The extent of crystallization α can be calculated using the following relation [17]:

$$\alpha = \left(\frac{\ln\sigma - \ln\sigma_a}{\ln\sigma_c - \ln\sigma_a} \right) \tag{3}$$

The values of σ_a and σ_c were calculated by plotting the time dependence of ln σ during the *a-c* phase transformation for each glassy alloy at different annealing temperatures. Once the values of α as a function of time are known at different isothermal annealing temperatures, the kinetic parameters (K_o and W_c) can be calculated using Eqs. (1-3).

1.3 Non-isothermal crystallization

In non-isothermal crystallization, it is assumed that there is a constant heating rate in the experiment. The relation between the sample temperature T and the heating rateβcan be written in the form:

$$T = T_1 + \beta t \tag{4}$$

where T_1 is the initial temperature. The values of activation energy of crystallization W_c and the pre-exponential factor K_0 in (2) can be (in case of thenon-isothermal crystallization method)evaluated by the equation

$$\ln\left(\frac{\beta}{T_c} \right) = \left(-\frac{W_c}{RT_c} \right) + \ln K_o \tag{5}$$

using the plots of ln(β/T_c) against 1/T_c [3]. In eq. (5),W_c and K_o are assumed to be practically independent of temperature, too. The equation (5) is derived by Augis and Bennett in [18] from the classical Johnson-Mehl-Avrami (JMA) theoretical model [14-16]. This method has an extra advantage that the intercept of ln β/T_C vs. $1/T_c$ gives the value of pre exponential factor K_0 of Arrhenius equation.The experimental results show that W_c values obtained by equation (5) are in good agreement with the W_c values obtained by well known Kissinger's relation [19] and relation of Matusita and Sakka [20]. Eq. (5) has been used by various scientists [4, 21-24].

1.4 Meyer-Neldel rule

The MN empirical rule was discovered by Meyer and Neldel in 1937 at investigation of electrical conductivity of some semiconducting substances [25]. Most semiconductors exhibit an exponential temperature dependence of the conductivity, $\sigma(T)$

$$\sigma = \sigma_0 \exp(-\frac{W}{kT}) \tag{6}$$

where σ_o is a constant and W – activation energy [26-28]. For many classes of materials, especially chalcogenide glasses, amorphous silicon, organic semi-insulators, experimental evidence suggest that a correlation exists between the activation energies and pre-exponential factors of the following form [3, 29]

$$\ln \sigma_0 = bW + \ln \sigma_{00} \tag{7}$$

whereb andσ_{oo} are constant. This relation can be written as

$$\sigma_0 = \sigma_{00} \exp(\frac{W}{kT_0}) \tag{8}$$

hereb = $1/kT_o$. The relation (8) gives the dependence of pre-factor σ_o on the activation energy W and represents Meyer-Neldel empirical rule, or the compensation rule which was discovered by Wilson [30] in 1908. Constant σ_{oo} is often called the Meyer-Nedel pre-exponential factor and kT_o the MN characteristic energy. The MNR is generally observed in disordered materials. In the class of amorphous semiconductors, the MNR has been reported for a-Si:H films in which W is varied by doping by surface absorption, light soaking or by preparing films under different conditions.This rule has also been observed for liquid semiconductors and fullerens. The validity of MNR has been reported in the chalcogenide glasses.However, in case of these glasses this rule is observed by the variation of activation energy W on changing the composition of the glassy alloys in a specific glassy system [3].

Evidence of MN rule [2,3] has been accounted for a number of activated phenomena such as solid state diffusion in crystals and polymers, dielectric relaxation and conduction in polymers, thermally stimulated processes in polymers and electric conduction in amorphous semiconductors, less effort has been done to observe MN rule in kinetic phenomena such as crystallization phenomenon.

1.5 MNR in crystallization processes

The Meyer-Neldel rule in crystallization describes following exponential relation between the activation energy W and the preexponential factor K_o , which appears in the relation (2):

$$K_o = K_{oo} \exp\left(\frac{W_c}{kT_o}\right) \tag{9}$$

Here K_{00} and T_0 are positive constants [3].

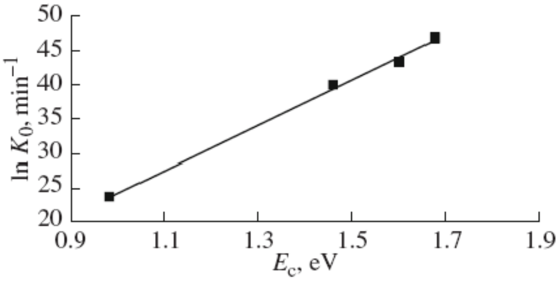

Figure1. Plot of ln Ko versus Ec for $Se_{70}Te_{30}$ *and* $As_{70}Te_{28}$ *M2 (M = Ag, Sb,Zn) glasses [4].*

The applicability of MNR for thermally activated isothermal crystallization in chalcogenide glasses of the Se–Ge–Sb system was firstly reported by Bordas et al. [31,32]. By annealing some Se–Ge–Sb glasses, they observed two crystalline phases: Sb_2Se_3 and $GeSe_2$. According to Bordas et al. such a compensation effect may be attributed to the primary crystallization of Sb_2Se_3 phase.

In the [4] is reported the applicability ofMeyer—Neldel rule for pre-exponential factor of non-isothermal crystallization in $Se_{70}Te_{30}$ and $Se_{70}Te_{28}M_2$ (M = Ag, Sb, Zn) glasses using DSC technique. The authorshave observed strong correlation between pre-exponential factor K_0 and activation energy W_c. As illustration we introduce the obtained results depicted in Figure 1. The resultshows that the activation energy and pre-exponential factor satisfies the Meyer and Neldel rule in form

$$\ln K_o = \ln K_{oo} + \frac{W_c}{kT_o} \qquad (10)$$

2. Explanation of the Meyer-Neldel rule

Many attempts have been made to explain the MNR (compensation effect) for various processes. Up to now there is not the generally accepted theory explaining the MN rule satisfyingly [3].

2.1 MNR at electrical conductivity of semiconductors

Basic ideas concerning the MNR explanation in a case of electric conductivity in non-crystalline semiconductors, namely, in chalcogenide glasses, non-crystalline silicon, Si and Si:H were presented in the works [33-36]. Validity of the Meyer-Neldel rule in non-crystalline semiconductors can be explained assuming that recombination transition of an electron from conduction band to valence band is conditioned by emission of number monoenergetical phonons whose total energy corresponds to the width of forbidden band (and so to the energy extracted in transition). Probability of such complex process is determined by number of emitted phonons. This probability exponentially decreases with increasing number of phonons and consequently with width of the forbidden band. The probability of recombination influences equilibrium concentration of free electrons in conduction band and subsequently electric conductivity. In such a way we have finally obtained the relation which is equivalent to the Meyer-Neldel rule [33-36].

2.2 MNR in crystallization processes

Crystallizationprocessis closely related todiffusionof matter particles. Validity oftheMNR incrystallizationprocesses is - aswe believe– the resultof the validity ofMNR in diffusionof particles. In our article we postulate that the crystallization rate K is directly proportional to the diffusion coefficient D, so $K \sim D$, respectively

$$K = fD \tag{11}$$

where f is a constant. If we prove that the diffusion coefficient D in this case meets MNR rule, we can also confirm the MNR rule for crystallization rate in this case. From the relation

$$D = D_{00} \exp(\frac{W}{kT_0}) \exp(-\frac{W}{kT}) \tag{12}$$

and equation (11) follows

$$K = K_{00} \exp(\frac{W}{kT_0}) \exp(-\frac{W}{kT}) \tag{13}$$

Concerning the correlation between pre-exponentional factor K_o and activation energy W comparing relations (13) and (2) we get

$$K_o = K_{00} \exp(\frac{W}{kT_0}) \tag{14}$$

It is this relationship that describes the experimentally found dependence MNR presented in Figure 1 in logarithmic form. In the following we will focus on an explanation of the MNR in diffusion.

2.3 MNR in diffusion processes

Diffusion is a process proceeding on microscopic level and possessing a broad variety of forms. Diffusion plays important role in solids [4, 26-28]. Numerous micro-structural changes and numerous chemical reactions in solid state take place through solid state diffusion, i.e. the movement and transport of atoms in solid phase [4, 26-28]. Diffusion also takes place along line and surface defects which include grain boundaries, dislocations, inner and outer surface, etc. Observations show that the diffusion often has excitation (activation) character. This is expressed by activation dependence of diffusion coefficient D on temperature T in a form

$$D = D_0 \exp(-\frac{W}{kT}) \tag{15}$$

where W is the activation energy of a diffusion process and D_o je pre-exponential factor. This relation resembles to the relation (8) for electrical conductivity. In a case of diffusion in corresponding formulae instead of electrical conductivity of a semiconductor emerges the diffusion coefficient D. If the MNR is valid then for diffusion pre-exponential factor D_o holds

$$D_0 = D_{00} \exp(\frac{W}{kT_0}) \tag{16}$$

where D_{oo} and T_o are constants. The relation (14) is analogy of the relation (8). For diffusion coefficient of upper mentioned group of substances it holds

$$D = D_{00} \exp(\frac{W}{kT_0}) \exp(-\frac{W}{kT}) \tag{17}$$

2.3.1 Band model for impurity diffusion

Our further aim will be to explain the physical nature of MNR (16) for diffusion processes. We will start our reasoning by so called band model of diffusion. To description of activation processes appears to be suitable the band model like that one, which is successfully used for description of electric properties of semiconductors.One typical feature of that model is existence of forbidden energy gap separating a valence band from a conduction band. The band modelprepared the way for explanation of the MNR by electrical conductivity ofnon-crystalline semiconductors [33-38]. Analogical band approach, likely, is suitable for description of diffusion processes in solids and liquids. The fundamentals of this model will be described later. The band model of particle diffusion – e.g. impurity atoms in a non-crystalline substance, assumes that impurity atoms of a diffusing matter are to be found at low energies in the ground (basic) band therefore in the band of low (nearly zero) mobility. In this simplifying model we shall consider mobility of these particles in the ground (basic) band to be zero. By sufficient energy the particles (atoms) of the ground band can be exited over the forbidden band into the band of non-zero mobility. The atoms need sufficiently enough of energy to this transition. This process is called activation one. The concentration n of impurity atoms in the band of non-zero mobility will be determined by the relation

$$n = n_o \exp(-W/kT) \tag{18}$$

This concentration is closely connected with the coefficient of diffusion $D \approx n$, so that

$$D = D_o \exp(-W/kT) \tag{19}$$

Experiments with diffusion showed that quantities n_o a D_o at the changes of activation energy W very often change in according to empirical Meyer-Neldel rule, namely as

$$n_o = n_{oo} \exp(W/kT_o)$$

resp.

$$D_o = D_{oo} \exp(W/kT_o) \tag{20}$$

wheren_{00}, D_{00} and T_0 are constants. Furher will be shown that MNR dependence (18) can be explained under specific conditions connected with transition of excited atoms from the diffusion band (from a state of non-zero mobility) to the ground – non-active band (of zero mobility).

2.3.2 Dependence of diffusivity D on activation energy W

Our model assumes that there are not energy levels of significant concentration in forbidden band.

Conditions of the MNR validity in a given diffusion process are connected with transition of an atom from the diffusion band into the ground band. A transition of an atom from diffusion band to basic band in disordered materials proceeds predominantly by production of phonons. The total energy of produced phonons will correspond to that one released in atom transition. It appears on the level of energy corresponding to the forbidden band width equal to $2W$. Further, we shall assume that in a substance under consideration dominates phonon production which average energy is ΔE. It means that phonon production of other phonons is negligible. At the transition of an atom from diffusion band to basic band gained energy $2W$ is used for production of N phonons each of them with energy ΔE so that $2W = N\Delta E$ or

$$N = 2W/\Delta E \tag{21}$$

Let w_1 be probability of production of one phonon which energy is equal to ΔE. Probability w_N of production of N phonons of equal energy due to the excited atom – lattice interaction will be

$$w_N = (w_1)^N \tag{22}$$

If we write down probability w_1 as $w_1 = \exp(-\varepsilon_1)$ where ε_1 is a positive value, then probability w_N one can be written with respect to (21, 22) as

$$w_N = \exp(-N\varepsilon_1) = \exp(-\varepsilon_1 2W/\Delta E) = \exp(-bW) \tag{23}$$

where the constant b is given by

$$b = 2\,\varepsilon_1/\Delta E \tag{24}$$

Relation (23) gives at the same time the transition probability of an atom from diffusion to basic band. That one is proportional to the probability of production N phonons and thus proportional to the $\exp(-bW)$. With an increase of activation energy W, the probability of the transition of atom in to basic band according to (23) exponentially decreases.

2.3.3 Equilibrium concentration of excited particles and diffusivity coefficient

An equilibrium concentration n of excited atoms occurring in the diffusion band is a result of two opposite processes: one is a process of generation and the other one is a process of „annihilation of free atoms" in diffusion band. In equilibrium (or steady) state it holds $(\mathrm{d}n/\mathrm{d}t)_{\mathrm{gen}} = (\mathrm{d}n/\mathrm{d}t)_{\mathrm{recom}}$.

We shall assume, that a number n of excited particles generated in a unit time is given as

$$(\mathrm{d}n/\mathrm{d}t)_{\mathrm{gen}} = G = C_1\exp(-W/kT) \tag{25}$$

where C_1 is a constant. For an „annihilation" process we suppose that the relation

$$(\mathrm{d}n/\mathrm{d}t)_{\mathrm{recom}} = R = n.C_2\exp(-bW) \tag{26}$$

is valid. Here C_2 is a constant. The number of annihilation in a unit of time is proportional to the number n. In equilibrium state $R = G$ is valid, so that $C_1\exp(-W/kT) = n\,C_2\exp(-bW)$

From that relation follows for equilibrium concentration n of free atoms

$$n = C_{oo}\exp(bW)\exp(-W/kT) \tag{27}$$

where C_{oo} is determined by the constants C_1 and C_2. It is known that diffusivity coefficient D is proportional to n: $D \approx n$. If mobility of free particles in diffusion band is independent on activation energy W (or that dependence is negligible) one can write with respect to (27)

$$D = D_{oo}\exp(bW)\exp(-W/kT) \tag{28}$$

If we put $b = 1/kT_o$, the relation (28) takes the form identical with (15). At the same time it is valid

$$D_o \approx D_{oo}\exp(W/kT_o) \tag{29}$$

which expresses the Meyer-Neldel rule (14) for diffusion.

3. Discusion.Physical foundation of the diffusion band model

The best arguments in favor of presented hypothesis concerning band model of diffusion can one seek in physics of semiconductors. Just there has been for the first time elaborated and theoretical well-founded band theory of electrical conductivity of semiconductors. It resulted from the solution of the problem of an electron motion in periodic (electric) field of a crystal. If one replaces electron by other particle – say, by diffusing impurity atom – then analogical situation arises. Diffusing atom also is moving in a periodic force field of an atomic lattice. Moving atom is a particle which motion complies with laws of quantum mechanics. The difference is that; the atom has greater mass then electron. It does not change the essence of our analogy. In a case of diffusion it is inappropriate to speak about recombination which is used by semiconductors. That is not significant for creation of a band structure. The band model of diffusion well fits activation character of diffusion and also the MNR for diffusion, as it was shown in preceding section. Moreover, the band model of diffusion enables to understand activation character and validity of the MNR at catalysis and other chemical processes and at phase transitions, too. The Meyer-Neldel rule can not be connected with each kind of diffusion in a solid. Sometime, the Arrhenius relation with constant pre-exponential factor can be valid. The MNR will be valid in case ofsuch diffusion at which the transition from diffuse band into ground band over forbidden band is realized with emission a number of phonons of relative low energies (compare to the width of energy gap). Transfer of particles in a substance proceeds mainly in diffusion band.

Next information about chalcogenide glasses and Meyer-Neldel rule in disordered semiconductors can be found in [39-44].

4. Conclusion

The paper presents an explanation of the validity of the Meyer-Neldel rule in the processes of crystallization in the semiconducting glasses.We consider the validity of this rule for crystallization to be the result of the MNRvalidity in diffusion. Our consideration is based on the assumption that the crystallization process depends primarily on the coefficient of diffusion of particles and the crystallization rate is directly proportional to the diffusion coefficient. Validity of MNR rule for diffusion phenomena is explained on the basis of the band model of diffusion.

References

[1] MEHTA, N.: Chalcogenide Glasses in Electronics and Optoelectronics, A Review on Their Applications, J. Sci. Ind. Res., 2006, vol. 65, p.777–786, (2006).

[2] POPESCU, M.: Physics and Applications of Disordered Materials, INOE Publishing House, (2002).

[3] MEHTA, N.: Current Opinion in SolidState and Material Sci, Vol.14, Issue 5, p.95-106, (2010).

[4] SARASWAT,S., KUSHWAHA,S.S.S.:Glass Phys. Chem.,Vol.35, No.3, p.290, (2009).

[5] HU, L., JIANG, Z.:Journ. Chin. Ceram.Soc. 18, p.315, (1990).

[6] SURINACH, S., BARO, M.D., CLAVAGUERA-MORA, M.T., CLAVAGUERA, N.: Glass Formation and Crystalli-zation in the GeSe2–Sb2Te3 System, J. Mater. Sci., vol. 19, p.3005, (1984).

[7] HRUBÝ, A.: Evaluation of Glass-Forming Tendency by Means of DTA, Czech.J.Phys.B, Vol. 22, No.11,p.1187-1193, (1972).

[8] PRAVEEN, K., SAXENA, N.S.: Journ. of Non-Oxide Glasses, Vol.1, No.2, p.96-102, (2009).

[9] PRAVEEN, K., JAIN, DEEPIKA, K.S., RATHORE, SAXENA, N. S.: Chalcogenide Letters Vol. 5, p.126, (2008).

[10] VAZQUEZ, J., GARCIA, D., BARREDA, G., LOPEZ-ALEMANY, P. L., VILLARES, P., JIMENEZ-GARAY, R..: Journ.of Non-Cryst.Solids 345, p.142, (2004).

[11] SOLIMAN, A. A., EL-DEN, M.B.: Chalcogenide Letters 4, p.35, (2007).

[12] ANIS AHMAD, SAMSHAD,KHAN, A., SINHAL, K., ZULFEQUAR, M.,HUSAIN, M.: Eur. Phys. Journ. Appl. Phys. 38, p.211, (2007).

[13] ABDEL-SATAR, M.A.ABDEL-RAHIM : Int. Journ of Pure and Appl. Phys.3, p.59, (2007).

[14] AVARAMI M.: Journ. Phys. Chem 7, p.1103, (1939).

[15] AVARAMI, M.: Journ. Phys. Chem 8, p.212, (1940).

[16] JOHNSON, W.A., MEHL, R.F.: Trans.Am.Inst.Miner.Eng.l35, p.416, (1939).

[17] MEHTA, N., KUMAR, D., KUMAR, A.: Journ. Phys D: Appl. Phys., Vol.38, p.3953-7,(2005).

[18] AUGIS, J. A., BENNETT, J. E.:Journ. Them.Anal.13, p.283,(1978).

[19] KISSINGER, H. E.: Anal. Chem. 29, p.1702, (1957).

[20] MATUSITA, K., SAKKA, S.: Bull. Inst. Chem. Res. Kyoto Univ. 59, p.159, (1981).

[21] SARASWAT, S., KUSHWAHA, S.S.S., KUMAR, A.: Chalcogenide Letters, Vol.5, No.11,p.281-287, (2008).

[22] LISHCHYNSKYY, I., KABAN, I., HOYER, W., VARVARUK, V.: Physics and Chemistry of Solid States, Vol.11, No.1, p.104-109, (2010).

[23] MEHTA, N., KUMAR, A.: Jour. of Phys. Studies. Vol.10, No.2, p.117-122, (2006).

[24] MEHTA, N., AGRAHARI, S.K., KUMAR, A.: Russian Physics Jounal, Vol. 51, No.3, p. 270, (2008).

[25] MEYER, W., NELDEL, H.: Z. Tech. Phys. (Leipzig), 18, p.588, (1937).

[26] MOTT, N.F., DAVIS, E. A.: Electron processes in non-crystalline materials, Clarendon Press, Oxford 1979, (1979). (Elektronnyje processy v nekrist. veščestvach, Mir, Moskva 1982).

[27] BRODSKY, M.H.: Amorphous semiconductors, Springer Verlag Berlin, Heidelberg - New York 1979, (1979). (Amorfnyje poluprovodniky, Mir, Moskva 1982).

[28] POPESCU,M.A.: Non-crystalline chalcogenides, Solid state science and technology Library, Vol.8, Kluwer academic publishers, Dordrecht/Boston/London, (2000).

[29] SHARMA,R.S., MEHTA,N., KUMAR,A.: Chin.Phys. Lett. Vol. 25, No. 11, p.4079, (2008).

[30] WILSON, H.A.: Philos. Trans. A, 208, p.247, (1908).

[31] BORDAS, S., CLAVAGUERA, N.: Thermochim Acta 1988, 133, p.293-8, (1988).

[32] BORDAS, S., CLAVAGUERA-MORA, MT., CLAVAGUERA, N.: Journ. Non-Cryst Solids, 119, p.232-7, (1990).

[33] BANIK, I.: Journ. of Non-Oxide Glasses, Vol. 1, No. 4, p.267-275, (2009).

[34] BANIK, I.: Chalcogenide Letters, Vol. 6, No. 12, p.629-633, (2009).

[35] BANIK, I.:Journ. of Ovonic Research, Vol.7, No,1, p.15-20, (2011).

[36] BANIK, I.: Optoelectr. and Adv. Mater. Vol.12, No.11, p.2247-2254, (2010).

[37] BANIK, I.: Journ. ofOptoelectr. and Adv. Mater. Vol.11, No.12, p.1915, (2009).

[38] BANIK, I.: Journ. Non-Cryst.Solids, 353, p.1920, (2007).

[39] SINGH, S., SHUKLA,R.K., KUMAR, A.: Journ. Non-Cryst Solids, 351, p.1577-81, (2005).

[40] ZANGENBERG, N.R., NYLANSTED LARSEN, A.: Physica B 340-342, p.780-783, (2003).

[41] SEDDON, A.B.: Journ.of Non-Cryst. Sol. 184,p.44-50, (1995).

[42] PRAKASH, S., KULBIR KAUR, NAVDEEP GOZAL, TRIPATHI, S.K.: PRAMAGA – Journ. of Physsics, Vol 76, No.4., p.629-637, (2011).

[43] SARKAR ,B.K., CHATTERJEE, MUKHERJEE, S., R.K.,CHAUDHURI, B.K. : In J. Mater. Sci. Lett. 1997, 16, p.1499-1502, ISSN: 0251-8028, (1997).

[44] SARKAR, B.K., VERMA,A.S., DEVIPRASAD, P.S.: Physica B 406, p.2847–2850, (2011).

Investigation of thermal diffusivity dependence on temperature of pure and doped YVO4 single crystals
by thermal wave method

Dominika Trefon-Radziejewska, Jerzy Bodzenta

Institute of Physics, Silesian University of Technology, Krzywoustego 2,

44-100 Gliwice, Poland

email: dominika.trefon@polsl.pl

Abstract

Thermal diffusivities of pure and doped YVO_4 *single crystals were measured as a function of the temperature. Two investigated samples were doped with neodymium ions (1 at.% and 2 at.%), one with calcium and thulium ions (0.4 at.% of Ca and 5 at/% of Tm) and one was pure crystal. Measurements were carried out for temperature range 31 - 300˚C. Determination of the thermal diffusivity based on an analysis of thermal wave propagation in the sample.For a detection of temperature disturbance propagating in the sample the mirage effect was used.Obtained results show that the thermal diffusivity decreases with the increase of sample temperature for all investigated crystals. The* YVO_4 *single crystals reveal anisotropy. The thermal diffusivity in [001] direction is considerably higher than in (001) plane. Measurements exhibit that dopants cause lowering of the thermal diffusivity. At the same time the decrease in the thermal diffusivity caused by the temperature growth becomes smaller with growing concentration of impurities.*

Keywords: *YVO_4 crystals; Temperature dependence; Thermal diffusivity; Thermal wave measurement, Doping*

1. Introduction

The yttrium orthovanadate crystal YVO_4 belongs to the tetragonal crystallographic system. The crystallographic structure of it corresponds to the space group D_{4h}[1]. Thanks to doping with trivalent ions of neodymium (Nd^{3+}) it has excellent properties such as high chemical stability and high laser induced damage threshold. The laser cross-section in Nd:YVO_4 is greater than that of Nd:YAG at1064 nm and it exhibits a very high slope efficiency [2]. Neodymium doped vanadate crystals are successfully applied in high power solid state lasers, but they are also very promising for use forhighly efficient laser-diode pumped microlasers [3], as an efficient phosphors [4], polarizer materials [5] and low-threshold laser hosts [6]. In recent years a lot of attention has been paid to YVO_4 doped with thulium ions. A 2 μm Tm^{3+} laser has gained much interest due to its unique and excellent performance in a wide range of application [7]. Doping single crystals allows to modify and to improve their properties. However, introducing dopants into a crystal lattice leads to deterioration of thermal properties. Especially the thermal diffusivity is very sensitive to doping. Additionally, the thermal diffusivity is influenced by the temperature. Because laser systems based on these crystals typically work at elevated temperatures a dependence of it on the temperature must be known.

This paper presents the results of investigations of the thermal diffusivity dependence on the temperature for pure YVO_4 single crystal and crystals doped with different concentrations of trivalent ions: Nd and Tm/Ca. Possible mechanisms of temperatureand doping influence on the thermal diffusivity is discussed. The anisotropy of investigated crystals is taken into account. In the next section samples and the measuring method used for investigation are described. Then results of measurements carried out in the temperature range from 31 to 300°C are shown and discussed. Final conclusions end the paper.

2. Samples

Pure and Nd^{3+} and Tm^{3+}/Ca^{2+}doped YVO_4 crystals were grown by Czochralski method. Details relating to growing process were described elsewhere [8]. Four YVO_4samples were examined: pure, doped with 1 at.% and 2 at.% of Nd^{3+}, and doped with 5 at.% of Tm^{3+} + 0.4 at.% of Ca^{2+}. All samples were cut into rectangular prisms and oriented along main crystallographic directions [100], [010] and [001]. Basic information about samples is collected in Table 1.

Table 1:Basic information about investigated YVO_4 samples

Sample		Dopant	Dimension (10^{-3} m)		
Crystallographic directions			[100]	[010]	[001]
#1	YVO_4	-	10.09	10.19	10.32
#2	YVO_4	1 at.% of Nd	10.09	9.89	10.15
#3	YVO_4	2 at.% of Nd	10.12	9.90	9.10
#4	YVO_4	5 at.% of Tm + 0.4 at.% of Ca	10.21	9.81	10.02

3. Measuring method

Measurement of the thermal diffusivity dependence on temperature of pure and differently doped YVO_4 single crystals were done on an experimental setup utilizing a thermal wave method. The experimental setup consists of a chamber, where the sample is placed between two resistance heaters. They allow sample heating and ensure the same temperature in the whole volume of the sample. To obtain a good thermal insulation of the sample and heaters, the system of the chamber is evacuated to the pressure of a few Pa by scroll vacuum pump (Varian IDP 3). It is possible to modulate the electric current through selected heater with a constant frequency by using a programmable linear power supply (LPS-305). This modulation causes periodic temperature disturbance in the sample, i.e. it generates the thermal wave. In order to follow the temperature of sample surfaces, copper plates with connected thermocouples are placed between the sample and the heaters. To assure low heat resistance thin layers of heat conducting paste are applied at all contacts. The geometry of measurement is shown in Figure 2.At the beginning of each measurement the temperature of the sample is stabilized at a set level. Then the temperature modulation around the set point is applied. In this work experimentswere carried out in the temperature range 31- 300°C. A detection of the temperature disturbance in the sample,is based on the mirage effect. A detecting light beam from He-Ne laser (LASOS 7672) is passing through the sample. The deflection of this beam is registered by a position sensor (Silicon Sensor DL400-7PCBA). The signals from the detector and from both thermocouples are fed to data acquisition unit (Agilent 34970A) and are collectedon a PC. Assuming one dimensional model of heat propagation in thermally thick sample, the phase delay$\Delta\phi$ of the thermal wave at the distance h from a source is given by the formula [9]

$$\Delta\varphi = \sqrt{\frac{\pi f}{\alpha}} h + \varphi_0 \tag{1}$$

where: $f$is the modulation frequency and $\varphi_0$is a constant.

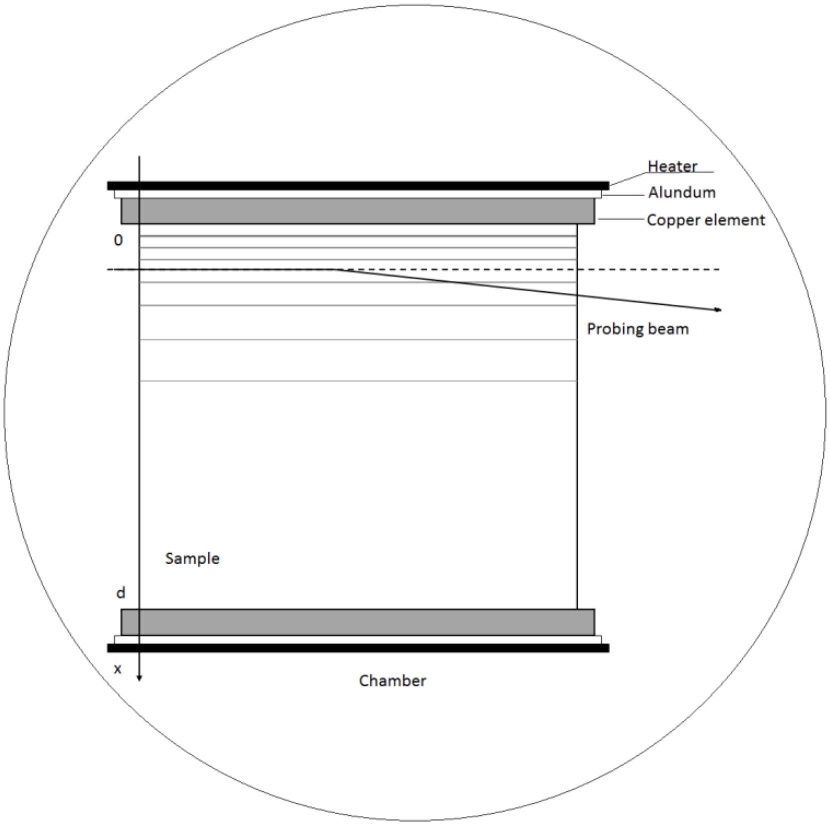

Figure 1: Geometry of measurement

The phase delay can be determined experimentally from measurement of the time delay Δt between the temperature measured by the thermocouple placed between the heater and the sample, and the deflection signal obtained from the position detector for given position of the probing beam. The relation of these values is

$$\Delta\varphi = 2\pi f \cdot \Delta t\ . \tag{2}$$

Measuring the $\Delta\phi$ dependence on h for defined frequency f one can determine the thermal diffusivity α from a simple linear fitting.

4. Experimental results and discussion

Thermal diffusivities of pure and doped YVO_4 crystals were determined for [001] and [010] directions for seven different temperatures in the range from 31 to 300 °C.The symmetry of YVO_4 crystals causes that values measured in (001) plane ([100] and [010] directions) are the same. It was provedin other papers [10,11].The determination of the thermal diffusivity, as it is mentioned in the previous section, was based on linear fitting of the time delay Δt dependence on distance h. Exemplary time dependences of signals from the thermocouple and the position detector registered for pure YVO_4 and the thermal wave propagating in [010] direction are shown in Figure 2.The phase delay was calculated from Equation (2). The phase delay dependence on the probing beam position obtained for pure YVO_4 in [010] direction at 31°C is shown in Figure 3. Thermal diffusivity was obtained by fitting the data with a straight line. In Figure 4 and 5 dependencies of the thermal diffusivity on the temperature determined for all investigated samples are shown.

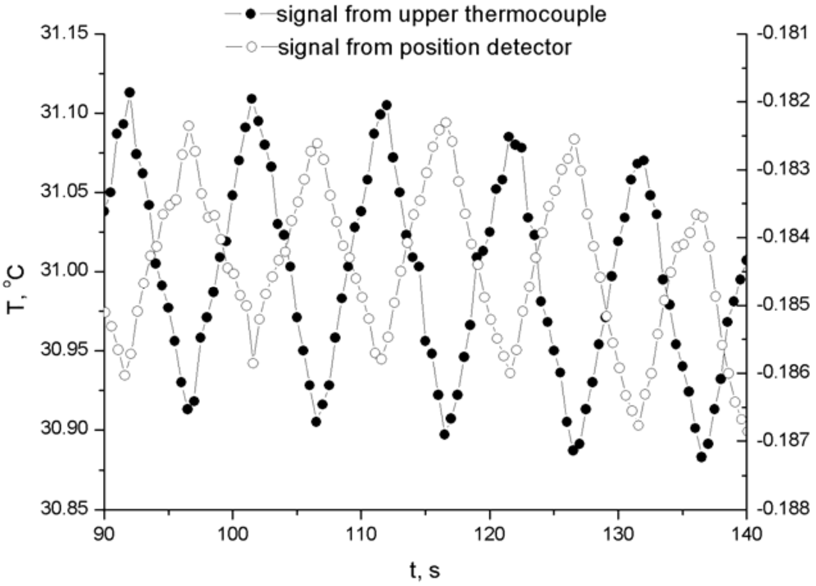

Figure 2: The time delay of temperature disturbance propagating along the pure YVO_4 in [010] direction. The signal from the position detector was measured in a selected distance of probing beam from the modulated upper heater.

For all samples the thermal diffusivity was higher in [001] direction and decreased with increasing temperature. Relative changes in the thermal diffusivity were smaller for doped crystals. It was also observed that the thermal diffusivity of heavily doped samples #3 and #4 approached a constant value at higher temperatures.

Such behaviour can be interpreted in the frame of the phonon theory of the thermal conductivity. The thermal conductivity and, related to it, the thermal diffusivity are determined by the phonon scattering. Two main scattering mechanisms must be taken into account - the phonon-phonon scattering and the phonon scattering on defects. An intensity of the phonon-phonon scatterings grows with growing temperature. This can explain the decrease of the thermal diffusivity observed for all samples when the temperature is growing. Impurity atoms create scattering centres which lead to the deterioration of the thermal diffusivity. The concentration of these centres is proportional to an amount of the dopant. An influence of these additional scattering centres is more pronounced at lower temperatures, when the phonon concentration is lower. At higher temperatures the phonon concentration increases and the phonon-phonon scattering dominates the phonon-impurity scattering. Differences between pure and doped samples become smaller. Probably at very high temperature all samples would exhibit very similar thermal properties. The influence of dopants would be negligible.

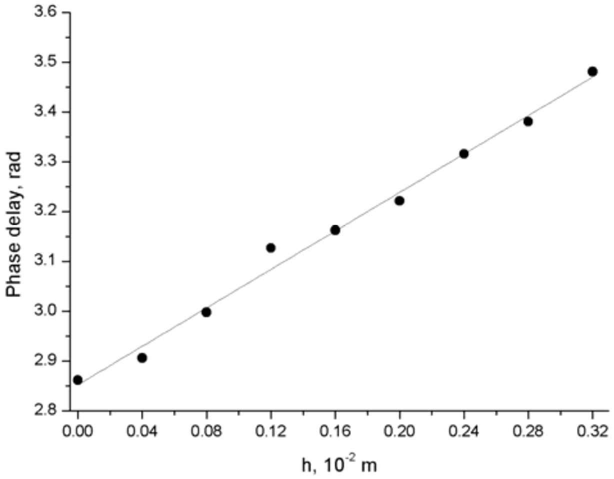

Figure 3: Phase delay of the signal as a function of the distance h from the sample surface measured in pure YVO_4 crystal in [010] direction in 31°C.

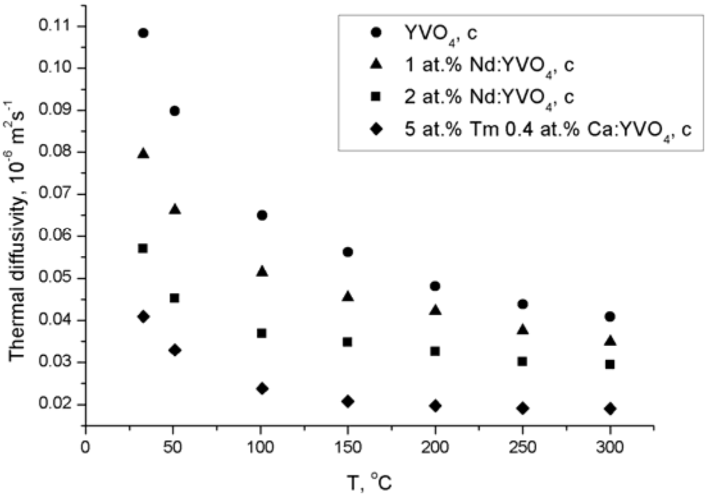

Figure 4: Thermal diffusivity dependence on temperature of pure YVO_4 and doped with 1% and 2% of Nd and with 5% of Tm + 0.4% of Ca measured in [001] direction

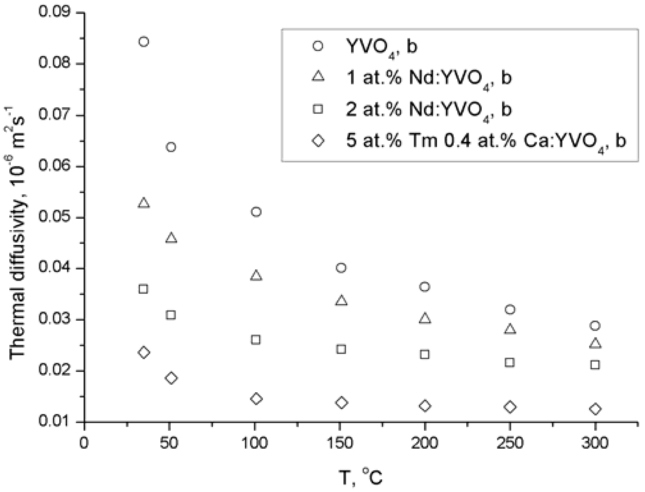

Figure 5: Thermal diffusivity dependence on temperature of pure YVO_4 and doped with 1% and 2% of Nd and with 5% of Tm + 0.4% of Ca measured in [010] direction

5. Conclusion

The carried investigation shows that YVO_4 crystals exhibit higher thermal diffusivity in [001] thanin plane (001). The highest thermal diffusivity was obtained for pure YVO_4 at 31°Cin [001] direction - 0.1084(85) 10^{-6} m^2s^{-1}. For comparison, the thermal diffusivity of the same sample in the same conditions in (001) plane was 0.0843(60) 10^{-6} m^2s^{-1}. The growing concentration of dopants caused decrease in the thermal diffusivity. The relative changes were from about 27% for 1 at.% Nd: YVO_4 to 62% for 5 at.% Tm+0.4 at.% Ca:YVO_4 in [001] direction at 31°C, and from 37% to 72% in [010] direction, respectively (in relation to pure YVO_4). The experimental results confirm the assumption that dopant ions create additional scattering centers of phonons and this mechanism is responsible for the decrease in the thermal diffusivity of doped crystals in comparison with the pure one.

All measured crystals show a decrease in thermal diffusivity with increasing temperature. The largest decrease in thermal diffusivity canbe observed for the pure and low doped samples. The thermal diffusivity drop were from about 60% for pure YVO_4 (in both considered directions)to 50% for 5 at.% Tm+0.4 at.% Ca:YVO_4 in 31-300°C temperature range. At elevated temperatures the influence of doping on the thermal diffusivity becomes less pronounced. The temperature increase causes a rise of phonon-phonon scattering and at higher temperatures this mechanism dominates over the phonon scattering on dopants. General conclusion is that the influence of doping on thermal diffusivity of a material strongly depends on the temperature.

References

[1] http://www.casix.com/product/prod cry yvo4.html

[2] R. A. Fields et al Appl. Phys. Letters 51, 1885 (1987)

[3] K. Shimamura, S. Uda, V.V. Kochurikhin, T. Taniuchi and T. Fukuda, Jpn. J. Appl. Phys. 35, 832 (1996)

[4] M. Prasad, A.K. Pandit, T.H. Ansari, R.A. Singh and B.M. Wanklyn, Phys. Lett. A 138, 61 (1989)

[5] E.A. Maunders and L.G. Deshaser, J. Opt. Soc. 61,684 (1971)

[6] B.H.T. Chai, G. Loutts, X.X. Chang, P. Hong, M. Bass, I.A. Shcherbakov and A.I Zagumennyi, Advanced Solid-State Lasers, Technical Digest vol. 20, Optical Society of America, Washington, DC (1994) p. 41

[7] J. J. Zayhowski, J. Harrison, C. Dill, J. Ochoa, Appl. Opt. 34, 435 (1995)

[8] J. Bodzenta, A. Kaźmierczak-Bałata, T. Łukasiewicz,M. Pyka, Eur. Phys. J. Special Topics 154, 313 (2008)

[9] J. Bodzenta, M. Pyka, J. Phys. IV France 137, 259 (2006)

[10] J. Bodzenta, A. Kaźmierczak-Bałata,K. B. Wokulska, J. Kucytowski, T.Łukasiewicz, B. Hofman, Appl Opt. 48(7), 46 (2009)

[11] J. Kucytowski, K. Wokulska, A. Kaźmierczak-Balata, J. Bodzenta, T. Łukasiewicz, B. Hofman, M. Pyka, Thin Solid Films 516, 8125 (2008)

Effect of temperature on liquid water transport in autoclaved aerated concrete

Kamil Ďurana, Tomáš Korecký, Miroslava Lapková, Jan Toman, Robert Černý

Czech Technical University in Prague, Faculty of Civil Engineering, Department of Materials Engineering and Chemistry, Thákurova 7, 16629 Prague 6, Czech Republic

Abstract: *There are several phenomena affecting water transport in porous materials.Besides the primary one which is the moisture gradient, secondary effects such as temperature, salt concentration, temperature gradient or gravity force are to be taken into account. In this paper, effect of temperature on liquid water transport in autoclaved aerated concrete is studied in the temperature range up to 85 °C.*

Keywords: *moisture diffusivity, moisture, temperature, autoclaved aerated concrete*

1. Introduction

The aim of this study is to determine two effects on moisture transport in porous building materials. These are moisture gradient (so called primary) and temperature (which belongs to so called secondary effects; we disregard gravity and electric or magnetic field as well as concentration of dissolved materials in water). As moisture content significantly affects physical properties [1], it is necessary to evaluate the characteristics describing behavior of material placed in varying moisture and temperature conditions.

We choose *moisture diffusivity* κ *[m²/s]* as a characteristic, according to which one can describe the overall water transport (both liquid and gaseous phase; with respect to temperatures between 25-85°C, we can claim, that contribution of water vapor can be neglected) in porous material, in dependence on moisture content and temperature.Based on molecular physics and thermodynamics, we assume that values of chosen characteristic will grow up with increasing water content or growing temperature.

In experimental part, we used simple method using thin long specimens, placed in specific thermal and hygric conditions and measured moisture content in various distances during specific time period. Measured data were processed by more or less simple mathematics, in order to get moisture diffusivity depending on moisture content for different temperatures.

Among other methods, we should mention chemical (K. Fischer´s method, method of calcium carbide), electromagnetic (spectrometric method, nuclear magnetic resonance, gamma-ray method, radiography or scanning neutron radiography [2]), other electrical (electric resistance method) or traditional physical (pycnometric, tensiometric or hygrometric) methods. Those approaches remain possible to try if our method would show inacceptable errors (error analysis of such procedure is the aim of current study, hence exact results remain still uncovered).

2. Experimental part

2.1 Specimens

In practical part, we chose two types of autoclaved aerated concrete *P1.8 300* and *P4 500* (with different compressive strength and also bulk density). Basic propertiesare shown in Table 1 (those declared by manufacturer Xella [3]; water vapor diffusion resistance factor is stated for both wet and dry state) and Table 2 (those additionally measured by Jerman et al. [4]) below:

Table 1: Material properties declared by manufacturer [3]

Material	**Thermal conductivity [W/m.K]**	**Specific heat capacity [J/kg.K]**	**Water vapor diffusion resistance factor [-]**
P1.8 300	0.08	1000	5/10
P4 500	0.12	1000	5/10

Table 2: Additionally measured properties of used materials [4]

Material	**Matrix density [kg/m³]**	**Total open porosity [% - V$_{ol}$]**	**Bulk density [kg/m³]**
P1.8 300	2 451	87.4	304
P4 500	2 527	80.2	500

Specimens were sawed from an autoclaved aerated concrete block to the dimensions of 40 x 20 x 300 mm. In order to ensure absolute dry state at the very beginning of measurements, all specimens were dried in oven at temperature of 105 °C until the weight remained steady. With respect to demanded one-dimensional water transport, waterproof sheeting was applied over the whole surface apart from both face sides.

2.2 Method of measurement

The setup of experiment consisted of water tank connected with a chamber, where a sponge was placed to ensure continuous wet state, thus almost ideal Dirichlet boundary condition corresponding to the water saturated state was established. The other face side was left openso that in certain time range the boundary condition of zero moisture flux or constant moisture corresponding to the initial state could be assumed. The sample was placed in horizontal position to avoid side-effect of gravity. Thermostatic climatic chamber allowed to keep constant outer conditions, i.e. RH = 50% and temperatures T_i = 25°C, 45°C, 65°C and 85°C.

Moisture content was measured indirectly using a capacitance method. This way, moisture content of each 1 cm of specimen was gained (except for the first and the last one) in specific time periods. In order to relatemoisture meter readings to moisture content values, the specimen was immediatelyafter finishing the experiment cut to 1 cm thick pieces (in direction of moisture flux) and moisture content by mass was measured by gravimetric method (samples were weighted in wet state, dried and weighted again) consequently. That allowed us to interpret former data by using calibration curve known from last measurement (see chapter 3).

This setup naturally brought some inaccuracies to whole method. First, it is factual error of used moisture meter (based on current measurements, we estimate the error of moisture meter reading as approximately 0.8-3.4 [-]; specific value of moisture content depends on calibration curve – see chapter 3), which cannot be neglected. Second, whatever anomaly of specimen´s surface could cause subsequent distortion of measured value (we tried to avoid this by abrading it before the experiment). Finally, we assume that we could not avoid faults caused by weighing, accidental errors and human factor.

2.3 Determination of moisture diffusivity

By measuring moisture contentin the specimen at several time intervals, while there was a horizontal moisture gradient from one side to another, we obtained curves of moisture distribution along the length (with respective transformation according to calibration curve connecting moisture content and capacitance moisture meterreadings). Hence, input parameters for computation of moisture diffusivity were sets of data:

$$u_i = f(x, t) \qquad (1)$$

where$u$ is moisture content by mass [kg/kg], x is distance from wet face side [m], t is time [s] (dried sample was connected with water source in time t = 0s) and f is some function (close to hyperbolic tangent), which does not necessarily be known, because we use measured points only. Index i indicates each measurement.

Desired behaviour of moisture diffusivity in dependence on moisture content was gained by specialized computational programme KADET [5]. It uses method of linear filtration to smooth measured data, calculates moisture diffusivity (with optional fineness) and provides recursive verification of the result (by computing moisture distribution using implemented finite-element-method software TRFEL [6] and displaying it towards measured data) as well.

In this way, we generated each moisture diffusivityvs. moisture content curve for each measured temperature. As our experiments took place in conditions of T = 25°C, 45°C, 65°C and 85°C, we got four dependencies of moisture diffusivity on moisture content for each material. Considering described method, temperature dependence could be expressed neither analytically, nor discrete for more than four values. Yet we claim that for specific temperature interval, studied coefficient can be evaluated by respective curve with tolerable accuracy (we assume that finer scaling of temperature would not bring more accurate results due to total error of stated method).

Moreover, some data had to be excluded from final collection due to their oddness (i.e. position towards other curves, either currently computed or known from former studies [7]; we could not avoid this eventhough we repeated critical measurements), thus we had three lines for each material, differing in temperature from each other. We assign this complication to inhomogeneity of used material (since the experiment was ran on industrial material, we could not assure absolute uniformity of samples; complications with inhomogeneity of such AAC are well known from other experiments).

3. Results

Measured data, calibration curve and recursive verification are shown only for one type of material, just to illustrate the method, only the functions of *moisture diffusivity* κ *[m²/s]* in dependence on moisture content (original moisture content by mass was converted to moisture content by volume, using known bulk density) for various temperatures arepresented for both autoclaved aerated concretes P1.8 300 and P4 500.

Figure 1 shows data measured by capacitance moisture meter. Values at very beginning and the end were not reachable due to size of probe.

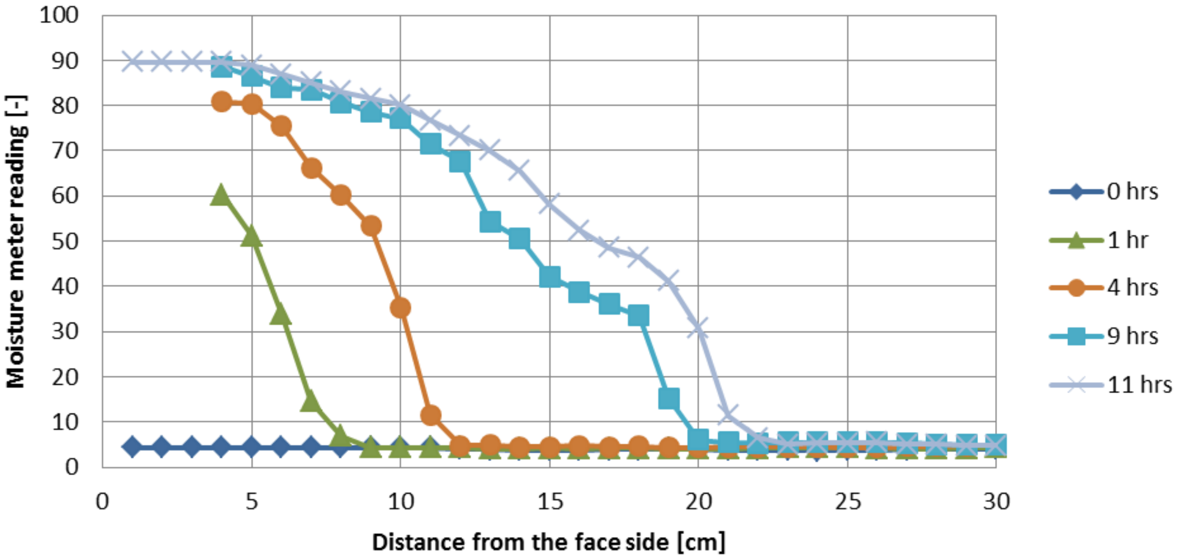

Figure 1: Data measured by capacitance moisture meter, P1.8 300, T = 45°C (each curve represents different time)

By using last measurement (for example curve *11 hours* in Figure 1) in combination with weighing of both wet and dry pieces of sample (gravimetric method), we gained calibration curve for each sample (generally, one can expect bilinear shape of such curve due to percolation threshold, but the observed one was almost unnoticeable, so that we could freely use simple straight line, with respect to reliability of interpolated curve). Considering different samples, we put together single curve for one measurement. Figure 2 shows such example. Reliability and equation are given as well:

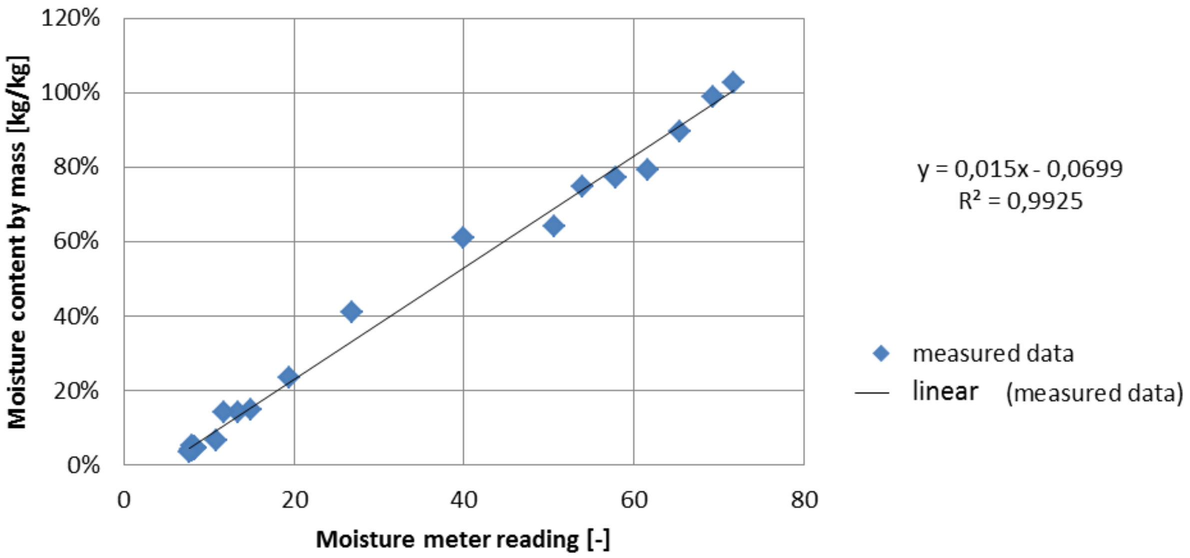

Figure 2: Example of calibration curve, P1.8 300

Combination of measured data and calibration curve allowed us to represent moisture distribution along the specimen in time, which shows Figure 3:

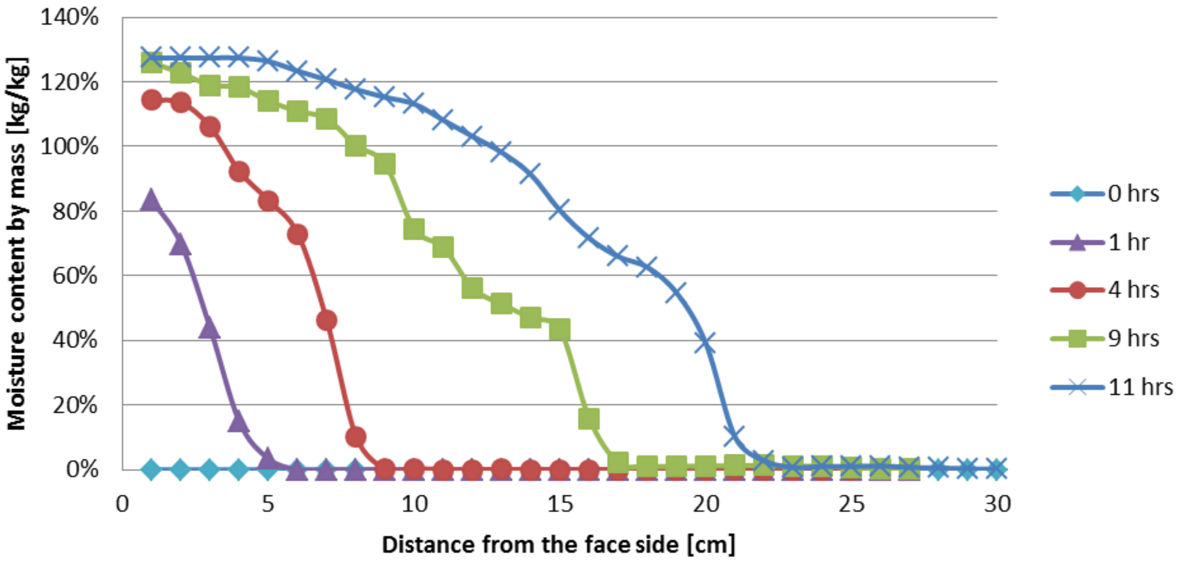

Figure 3: Moisture distribution along the specimen, P1.8 300, T = 45°C (each curve represents different time)

Figure 3 shows, that curves are neither smooth nor regular enough, so that we smoothed them, taking into account the known inaccuracy of used moisture meter.

Subsequently, we computed each moisture diffusivity function. Before putting all results together, thus expressing its dependence on temperature, we verified calculations towards experimental data. As an example of good agreement we present Figure 4, which is also an example of screen in KADET software [5]:

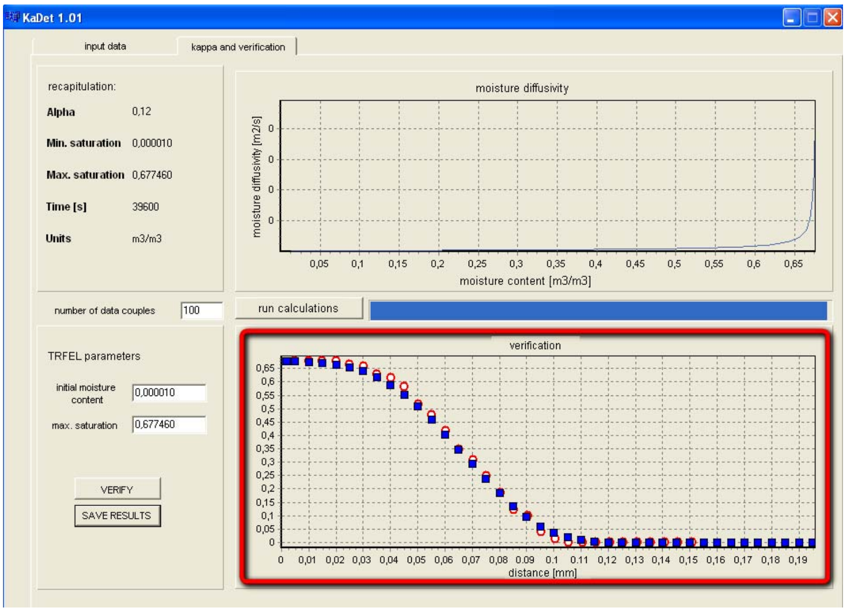

recapitulation:

Alpha 0,12

Min. saturation 0,000010

Max. saturation 0,677460

Time [s] 39600

Units m3/m3

number of data couples 100

TRFEL parameters

initial moisture content 0,000010

max. saturation 0,677460

Figure 4: Screenshot of recursive verification of measured data (white circles with red border) and data computed using determined moisture diffusivity function (blue squares), P4 500, T = 45°C

Finally, Figure 5 and Figure 6 show the results of whole experiment – dependence of *moisture diffusivity κ [m²/s]* on moisture content for various temperatures:

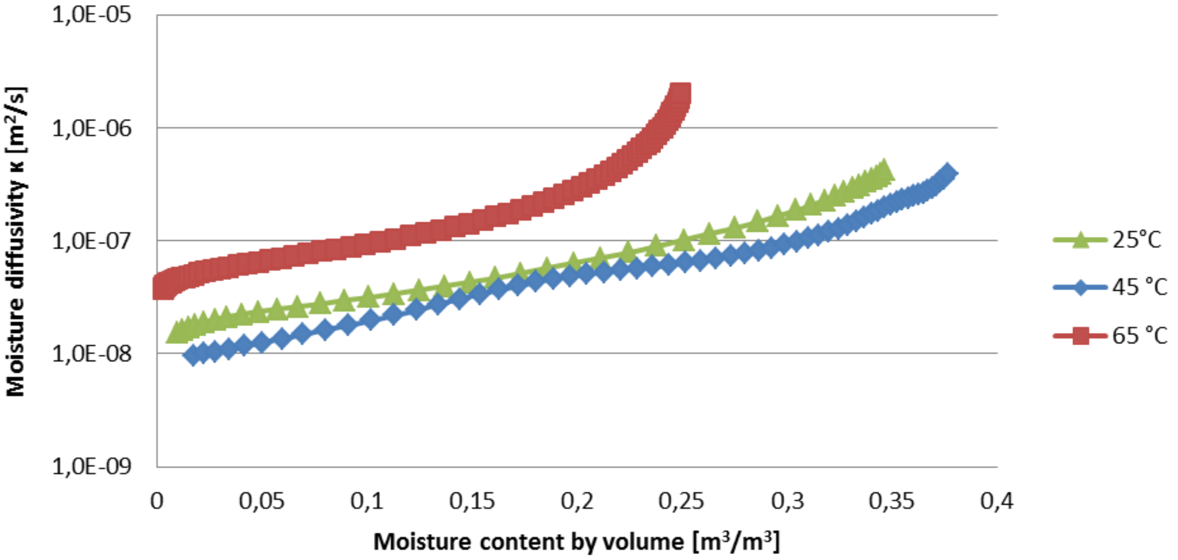

Figure 5: Dependence of moisture diffusivity on moisture content for various temperatures (P1.8 300)

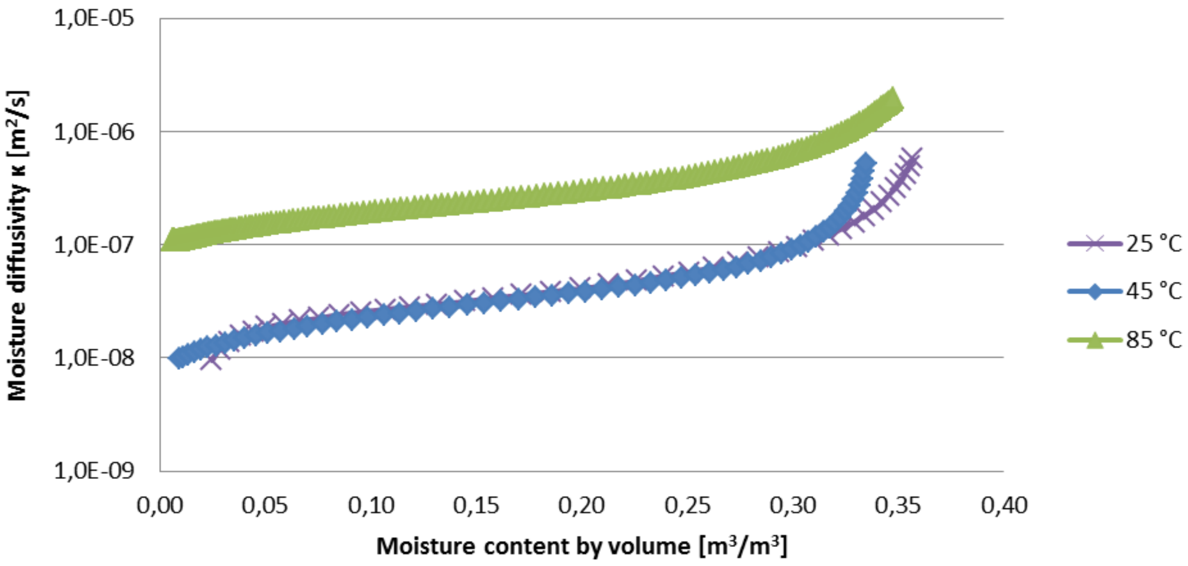

Figure 6: Dependence of moisture diffusivity on moisture content for various temperatures (P4 500)

4. Discussion and conclusions

The dependence of *moisture diffusivity κ[m²/s]*of autoclaved aerated concretes P1.8 300 and P4 500on moisture content was determined for various temperatures up to 85°C. Indirect non-destructive method was used to obtain moisture distribution in several time intervals, thanks to which we were able to calculate desired coefficient using computational inverse analysis.

A significant increase of moisture diffusivity with temperature was observed for temperatures higher than 45°C.On the other hand, there was nearly no noticeable difference between the moisture diffusivity at 25°C and 45°C for both materials, hence we claim that for applications under the temperature of 45°C, one can freely use standard curve measured in laboratory environment.

Steep parts of the moisture diffusivity vs. moisture content curves indicated wet and dry state of material, in other words studied coefficients increased from minimum value around the material´s possible minimum moisture content and reachedtheir maximum value around the moisture content of full saturation. What remains unanswered is the reason of different location of steep growth for each temperature – we expect it to be due to either disparateness of used samples, numerical errors based on insufficient input parameters, or physical changes inside the porous material (for example phase change of water or chemical change of material).

Considering each moisture diffusivity vs. moisture content curve separately, most important (and most reliable) part is the middle one where the trend is nearly exponential (linear on the logarithmic scale) – based on those results, we are able to apply non-constant value of moisture diffusivity coefficient in range of ordinary moisture content (i.e. between nearly dry state and state close to saturation; both beginning and end of curve are less accurate because of numerical method, what is fact that we cannot avoid), which is the most important result of our study.

Acknowledgments

This research was supported by grant of Students Grant Competition, under the number SGS11/100/OHK1/2T/11.

References

[1] TOMAN J. *Influence of temperature and moisture on physical parameters in building materials* - doctoral thesis, Faculty of civil engineering CTU in Prague, Prague, 1992, pp. 2-12, 21-23

[2] PEL L. – KETELAARS A. A. J. – ADAN O. C. G. – VAN WELL A. A. Determination of moisture diffusivity in porous media using scanning neutron radiography. In *International Journal of Heat and Mass Transfer*, Volume 36, Issue 5, 1993, Pages 1261-1267

[3] Xella – technical parameters of products. URL: http://www.xella.cz/downloads/czk/product/ytong-lambda.pdf [vis. 2011-06-23]

[4] JERMAN M. – KOČÍ V. – VÝBORNÝ J. – ČERNÝ R. Thermal and hygric properties of autoclaved aerated concrete. In *Thermophysics 2010*, Brno: University of Technology, 2010, p. 102-108. ISBN 978-80-214-4166-8.

[5] KADET – Authorized software, Department of Material engineering and chemistry, Faculty of Civil engineering, CTU in Prague. Available on http://tpm.fsv.cvut.cz/vz/software17.php [vis. 2011-06-23]

[6] KRUIS J. – KOUDELKA T. – KREJČÍ T. Efficient computer implemnentation of coupled hydrothermo-mechanical analysis. In *Mathematics and Computer Simulation*, 2008

[7] JERMAN M. - KEPPERT M. - VÝBORNÝ J. - ČERNÝ R. Moisture and heat transport and storage characteristics of two commercial autoclaved aerated concretes In: *Cement Wapno Beton*. 2011, vol. 16/78, no. 1, p. 18-29. ISSN 1425-8129.

Comparison of water transport in the sandstones with different porosity

Danica Fidríková , Ľudovít Kubičár

Institute of Physics, Slovak Academy of Sciences, Slovak republic

Abstract: *Influence of moisture on materials leads to changes of physical and chemical properties. Materials with different porosities saturate by various mechanisms. This paper is focused on water transport and moisture determination in various porous structures. The Hot-ball method is used for determination of the moisture in the material. Sandstones with different porosities, 21%, 17,8% and 1,5% water porosities were investigated. Process of water transport or moisture transport is closely related to porous structure. Porosity affects transport properties of the material and it is necessary to know the way and mechanism distributing the water in materials with different porosities. Measurements were carried out by thermal conductivity sensors (Hot-ball sensor) located in different positions along path of water movement. Principle of Hot-ball sensor (thermal conductivity sensor) is based on Hot-ball method for measuring thermal conductivity. The specimens were put in vertical position into a vessel in which a constant water level about 3mm above the bottom was kept. In this manner prepared specimens were placed in a chamber with constant surrounding humidity and temperature. Local moisture content in porous stone is inspected using Hot-ball method, where the measured values of thermal conductivity are correlated to the water content. Experimental set up for investigation of water diffusion in stones is described. Results of water transport in different sandstones are presented.*

Keywords: *water transport, humidity, porosity, thermal conductivity, sandstones*

Introduction

The knowledge of transport of moisture in porous building materials is basic for the estimation of long term performance of buildings and is strongly dependent on the climatic conditions [1]. The mechanism of fluid flow inside the pores is complicated due to the presence of various phases and their interactions with the solid rock matrix. In order to fully understand the transport mechanisms at this scale, one needs to have a better picture of the actual porous structure of rock [2]. Experimental and theoretical research in such materials concentrates to processes of heat and moisture transport in porous structure. If a building material is in contact with water it absorbs moisture by capillary suction then it is capillary active, if it does not, it is regarded as hydrophobic. Climatic parameter for moisture accumulation is relative humidity.

The transport in pores is not possible to describe by simple analytical equations. Currently mathematical models include boundary and initial conditions that describes the experiment. Then the mathematical formulation of mass transfer at the macroscopic level in porous media is usually based on diffusion equations. These were first established by Philip and de Vries (1957). Later, a more fundamental basis for these equations was given by Whitaker (1977) and Bear and

Bachmat (1990). If gravity is neglected, the moisture transport for the one-dimensional isothermal problems that will be considered here can be described by a non-linear diffusion equation:

$$\frac{\partial\theta}{\partial t} = \frac{\partial}{\partial x}(D_\theta \frac{\partial\theta}{\partial x}) \tag{1}$$

In this equation θ [m^3m^{-3}] is the volumetric moisture content and D_θ [m^2s^{-1}] the moisture diffusivity. In this diffusion model all mechanisms for moisture transport, i.e., liquid flow and vapor diffusion, are combined into single moisture diffusivity, which is dependent on the actual moisture content. The moisture diffusivity D_θ has to be determined experimentally for the porous medium of interest. By measuring the transient moisture profiles during the various transport processes, i.e., drying and absorption, the diffusion coefficient can be determined directly [3].

Experimental studies are focused on determining the moisture content in the certain area of material around sensors to determine the laws by which spread of moisture. The transport in porous structures cannot be described by simple analytical equations. To determine the characteristics of moisture transfer it is necessary to know humidity of the ambient air.

Measurement of thermophysical properties consists of the evaluation of thermal conductivity, thermal diffusivity and specific heat and it provides insight into the optimal selection of a material. Determination of thermophysical parameters of materials has two parts. In the first, heat equation is solved for given boundary and initial conditions and due to solution we get a temperature function, which describes the temperature distribution in the sample. Temperature function includes parameters as time and parameters characterizing the thermophysical properties of the material. Specification of the boundary and initial conditions, and the temperature function receive additional parameters, such as contact thermal resistance, coefficient of heat transfer, etc. Therefore, it must take into account the possibility of technical realization of the experiment. In the second part, the experiment is realised that allows determination of the temperature field of a specimen. Then we can calculate the thermophysical parameters from the temperature function and experimental data [4]. Moisture of material is closely related to its pore structure, usually modeled as an interconnected system of capillaries with different radius. For the quantitative determination of the capillary suction forces it is customary to use a cyliner capillary model, as shown in figure 1.

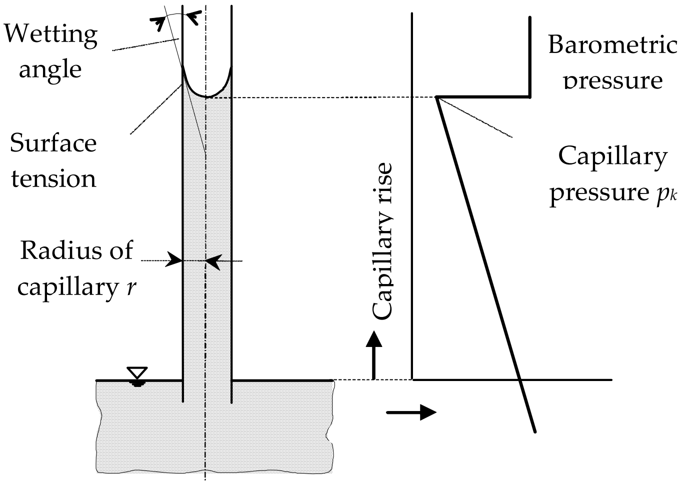

Figure 1 *Schematic view of the water column (left) in a cylinder capillary model*

Principle of experimental method

There are many experimental methods for measuring thermophysical parameters. Transient methods are based on the generation of the dynamic temperature field inside the sample. The measuring process can be described as follows: first, the temperature of the sample is stabilized and uniform; then a small disturbance is applied to the sample by use of a heat pulse, or by use of a heat flux in the form of a step-wise function. From the parameters of the temperature response to this small disturbance the thermophysical parameters can be calculated, according to the model used. In practice, the temperature response is up to 10 K (Figure 2). We use the transient method based on the hot-ball method.

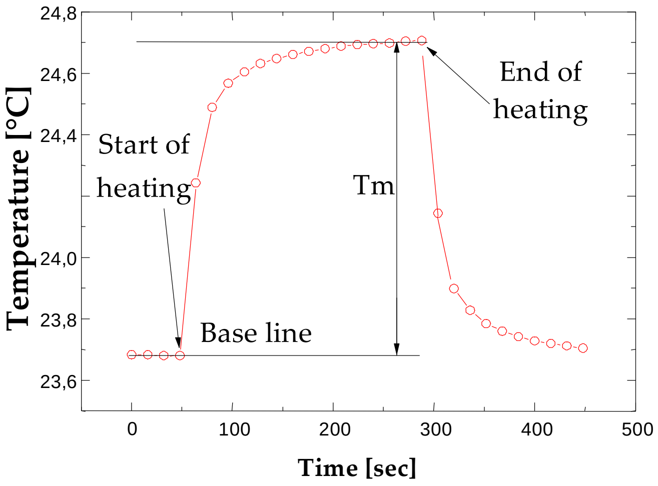

Figure 2 *The temperature response for constant production of heat*

The sensor is made of two components of a thermometer (thermistor) and a resistance (patented). These components are mutually glued together by epoxy. After curing the epoxy the sensor is ready to calibrate. The diameter of the finished sensor is in the range of 2 to 2,3 mm.

The working equation of the Hot-ball sensor is based on an ideal model which assumes a constant heat flux F per surface unit from the empty sphere of radius r_b into the infinitive medium for times $t > 0$. Then the temperature distribution within the medium is characterized by the function [4]

$$T(t, r_b) = T_0 \left\{ 1 - \exp(u^2) \Theta^*(u) \right\} \tag{2}$$

where $T_0 = \dfrac{q}{4\pi r_b \lambda}$, $u = \dfrac{\sqrt{at}}{r_b}$ λ is thermal conductivity and a is thermal diffusivity. $\Theta^*(u)$ is the complementary error function. Function (1) can be derived from the partial differential equation governing heat conduction, considering the initial condition $T(0, r) = 0$ and the boundary condition $-\lambda \dfrac{\partial T}{\partial r}_{r=r_0} = ql(t)$. For time tending to infinity, $t \to \infty$ equation (1) reduces to its steady-state form

$$T_m = \frac{q}{4\pi r_0 \lambda} \tag{3}$$

Rearranging the latter equation one obtains the working equation of the hot-ball sensor [4]

$$\lambda = \frac{q}{4\pi r_0 T_m} \tag{4}$$

Experiment and results

For the experiments sandstones with 21%, 17,8% and 1,5% water porosities were used. The specimens were dried under vacuum and moisturized to water saturated state to calculate its porosities. The same initial conditions for all specimens were established. The specimen was fixed in specimen holder in vertical position shown in figure 3 and inserted into the device. The temperature of 25 °C and ambient humidity 30% was kept during experiment. One-dimensional transport process under isothermal climatic conditions was realized. A special mechanism (Figure 3) was used to keep a constant water level in about 2 mm from the bottom. In order to determine the quantitative amount of vapor and liquid water transport amount within the specimens three Hot-ball sensors are fixed in certain positions. Three RTM devices (Transient MS) were used to collect data on local values of the moisture by measuring the thermal conductivity due to Hot-ball probes. The total increase of moisture of each specimen is measured by weighting (integral moisture). Integral moisture shows the change in weight depending on the increase of water content in the specimen over a period of saturation. Saturation was performed on specimen of sandstones, where first capillary saturation in the specimens was observed. The macrostructure and conditions of the experiment must deliberate in measuring thermophysical parameters in heterogeneous materials. The heat spreads throughout the system, and it is very difficult to isolate the sample from its surroundings. Therefore, we are keeping the specimens at constant temperature and also at constant humidity.

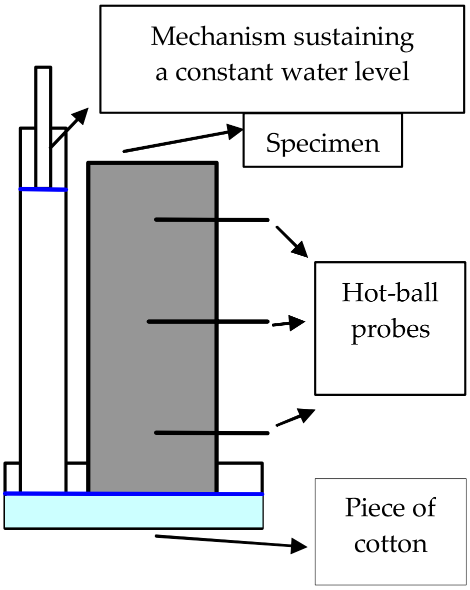

Figure 3 *Placing specimens during the experiment*

Transport properties such as thermophysical properties are affected by macrostructure of specimens. These properties in the material are also affected by the humidity. Sorption curve for the entire range of moisture retention curve are used to express the relationship between humidity and moisture. Depending on structure of materials we have different trend of the sorption curves (Figure 4). Capillary flow and flow on the surface can participate on water transport depending on total pressure gradient.

Experimental data obtained by measuring devices RTM are shown in Figure 5. Gradual saturation of the specimen depending on the position of Hot-ball sensors can be found. Saturation strongly depends on of porosity in materials. A complete picture about the processes of saturation water in the material with certain porosity can be obtained after saturation. Then the values q/Tm (ratio of the constant output power to change of the temperature during a measuring cycle) are converted to percentage increase of the moisture in the specimen. This conversion is done by linearization of values q/Tm to moisture content. Figure 5 shows plots of the local values q/Tm for different sensor positions as a function of the time. Simultaneously integral moisture is plotted as a function of time. Both parameters, namely local parameter q/Tm and integral moisture change due to water transport into the specimen. The experiment shows that we are able to describe not only the increase of moisture by weight, but by using the Hot-ball method also the local value of q/Tm. The latter can be recalculated to local value of moisture. In fact it is able to determine the thermal conductivity of the specimen in a certain position. The graphs in figure 5 describe the gradual transport of water in sandstones with different porosity in areas where thermal conductivity probes (Hot-ball probes) are located. These probes were in all three specimens at the same positions. Thus the graphs represent the transport of water in the first step of saturation, i.e. in the sorption saturation region. Parameter q/Tm reaches values above the saturation for the specimen of 21 % porosity very fast in the bottom and in the middle sensor position. This is typical for materials which contain larger pores as well as micropores.

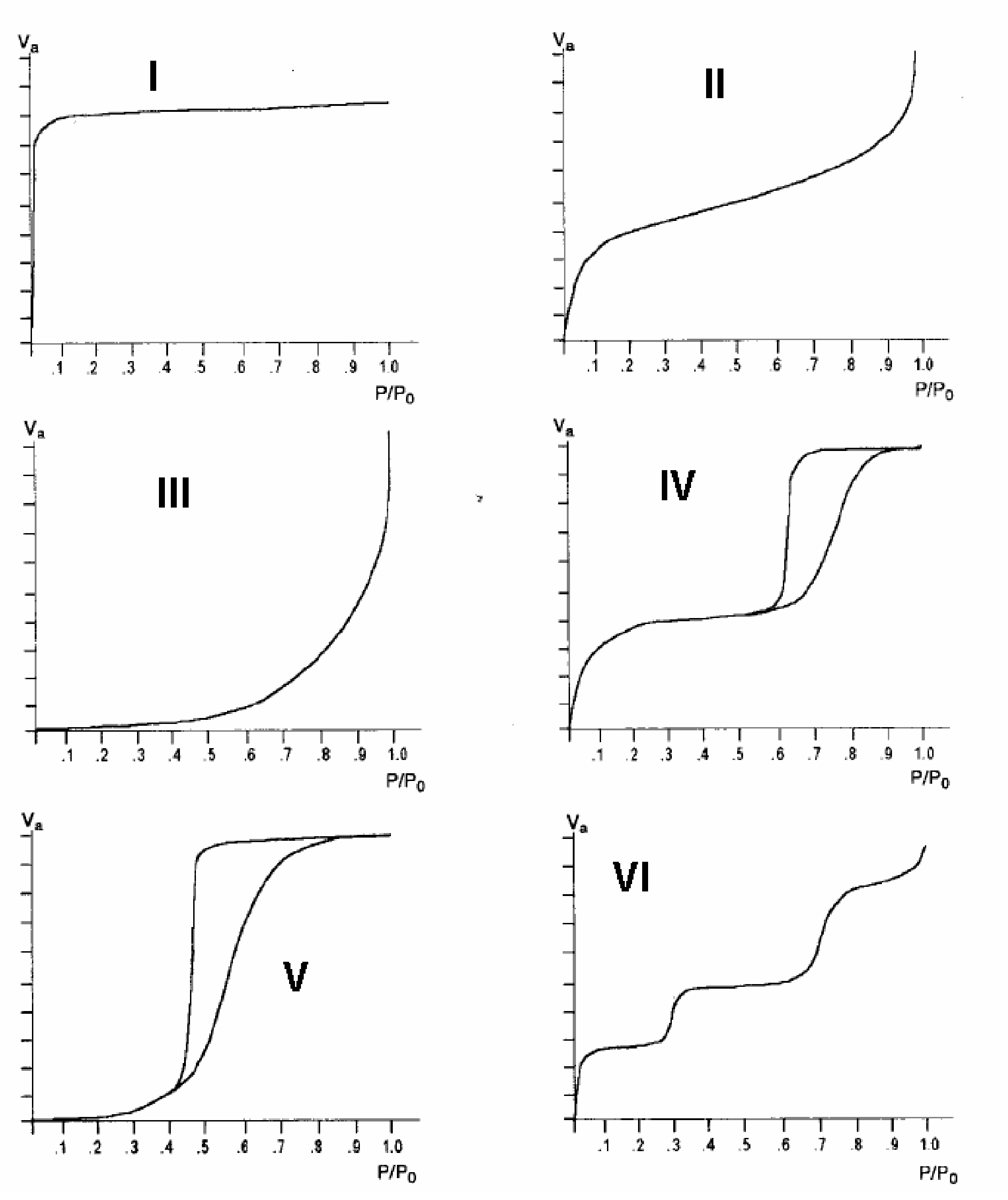

__Figure 4__ Types of sorption isotherm by BET classification

While the top probe in this specimen of sandstone shows the effect saturation of water vapour from the ambient atmosphere instead of regular transport of water from store. In the specimen with 17.8 % water porosity (Figure 5 middle column) in all three positions the transport of water is dependent on distance from the water source. It characterizes the gradual increase of the water content at local positions. From these three graphs we can see transport of water from bottom to top in time sequence. In the specimen with lowest porosity (1,5%) (Figure 5 third column), graphs from bottom sensor and top sensor have typical course for the low-porous materials. This specimen shows a strong capillary saturation. Capillaries in such materials are narrow and a high capillary pressure should exist for such materials. In agreement with figure 1 one can see that the radius of capillary r is smaller, the water increase is higher. But in middle part of the specimen, the curve grows very slowly. This corresponds to very low-porous materials where boundary conditions play any role in the transport of water in the sample**.**

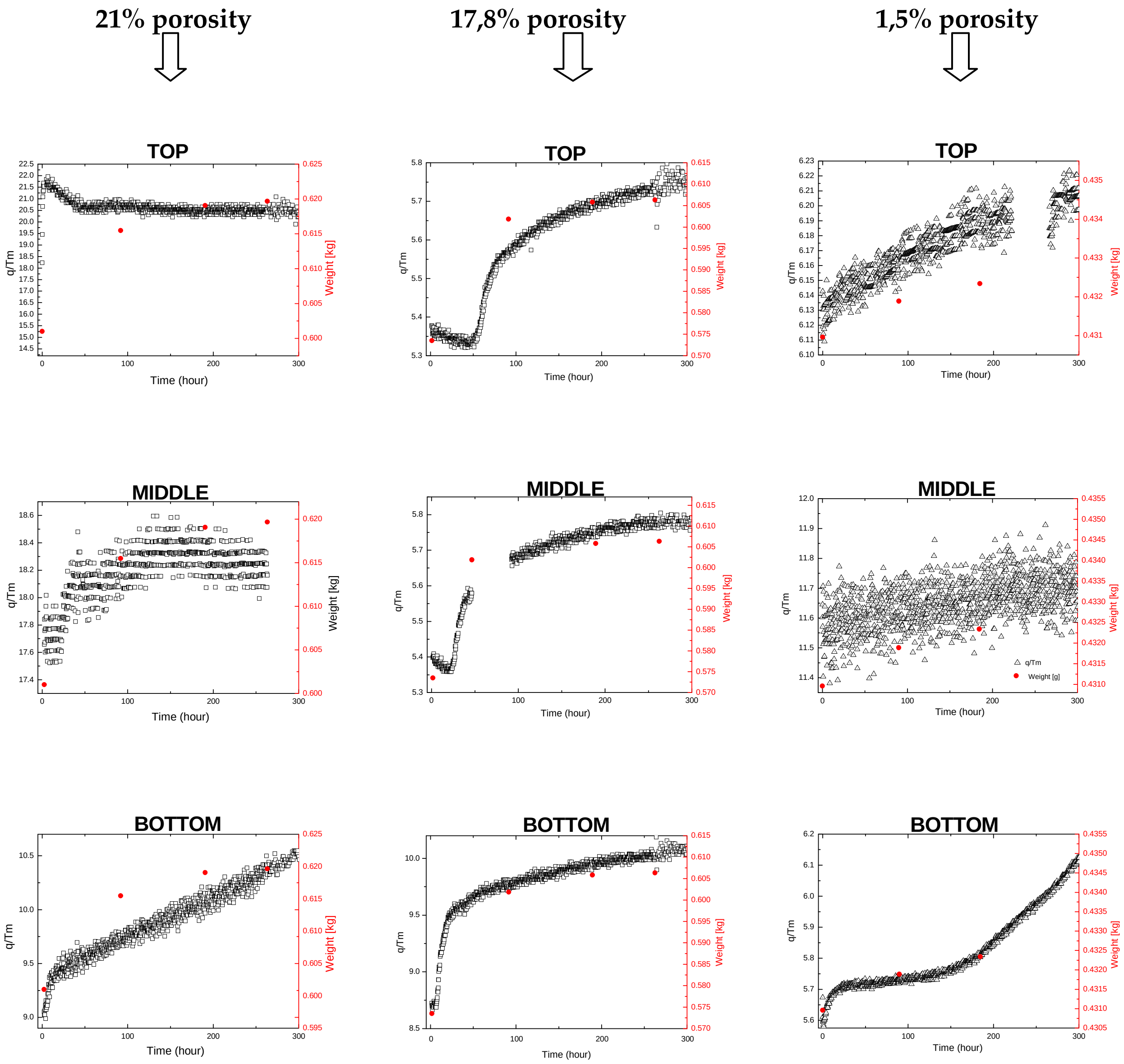

Figure 5 *Graphs of saturation in sandstone with different porosity*

Acknowledgements

The paper was supported by the project APVV LPP–0442–09

References

[1] Terheiden, K.: Simultaneous measurement of vapor and liquid moisture transport in porous building materials, Building and Environment 43, 2008, str. 2188-2192

[2] Bera, B., Mitra, S. K., Vick, D.: Understanding the micro structure of Berea Sandstone by the simultaneous use of micro-computed tomography (micro-CT) and focused ion beam-scanning electron microscopy (FIB-SEM), Micron 42, 2011, 412–418

[3] Pel, L., Kopinga, K., Brocken, H.: Moisture transport in porous building materials, HERON, Vol. 41, No. 2, 1996, ISSN 0046-7316

[4] Kubičár, Ľ.: Rýchla metóda merania základných termofyzikálnych parametrov, Veda Bratislava, 1988, str. 17 – 100

[5] Vretenár, V., Fidríková, D., Dieška, P., Štofaník, V., Kubičár, Ľ.: Accuracy Analysis of the Transient Hot-Ball Method for Measurement of Thermophysical Parameters, Veda Bratislava, 2011, ISBN 978 - 80 - 969672 - 4 - 7

Estimation of thermophysical parameters of polytetrafluoroethylene (PTFE) by a hybrid method

Marcin Gapski[1], Piotr Koniorczyk[1], Janusz Zmywaczyk[1]

[1] Faculty of Mechatronics, Military University of Technology (MUT), Kaliskiego 2,

00-908 Warsaw, Poland

***Abstract**: In this paper a hybrid method is presented for simultaneous estimation of the thermal conductivity λ and the specific heat c_p of polytetrafluoroethylene (PTFE) insulation material during single measurement. The experimental setup consisted of a thin-layer Kapton heater put symmetrically into the sample which was divided into two parts. Temperature histories were recorded at the back face of the samples using the K-type thermocouples and the FLIR SC5000 infrared camera. Thermophysical parameter estimation process was based on simulated and real measurement signals which were brought up to the temperature excess θ_m (t) at the back face of the sample placed next to the heater. The ownestimation results were compared with reference values from literature.*

***Keywords**: inverse problem, thermophysical parameters, hybrid method, PTFE, differential evolution*

1. Introduction

A hybrid method of estimation the temperature-dependent thermophysical parameters is presented. The method of differential evolution (DE) developed by Storn and Price [3] is used at the beginning of calculations.DE is a stochastic parallel direct search evolution strategy optimization method that is fairly fast and reasonably robust. DE is used for multidimensional nonlinear functions but does not use the gradient of the problem being optimized, which means that DE is capable of handling nondifferentiable objective functions as opposed to classic optimization methods. DE can therefore also be used on optimization problems that are not even continuous, are noisy and change over time. Differentialevolution is a method from a commonly known group of metaheuristics methodswhich makes few or no assumptions about the problem being optimized and can search very large spaces of candidate solutions. However, metaheuristics such as DE do not guarantee an optimal solution to be ever found.Presented in this paper hybrid method which is the conjunction of differential evolution and coefficient inverse techniquehas all the advantages of both methods and guarantees the best solution to be found. Confirmation of this may be the results of simultaneous estimation of temperature-dependent thermal conductivity $\lambda_r(T)$, $\lambda_z(T)$ and specific heat $c_p(T)$given in [7] where the author used DE to find initially a set of the coefficients which represent the unknown temperature depending thermophysical parameters in a priori given base of functions.Havingsuch a starting point the Levenberg-Marquardt procedure was next applied to findthe minimum of a mean-square functional .In contrast to the work[7] the input data to inverse problemi.e. the temperature histories at some locations of sample and the heat flux was knownfrom experiment. The aim of this work was to identify the thermal conductivity λ and the specific heat c_p ofPTFE insulation material based on a contact (K-type thermocouple) and contact-less (IR camera) temperature measurementduring single experimentusing hybrid inverse method.

The PTFE insulation material with density $\rho = 2197$ kg/m^3 [2, 4] is widely used in the semiconductor, medical, chemical, automotive, electrical, aerospace, filtration, wire & cable and petrochemical industries. Moreover PTFE is mostly known as a non-stick coating found on cookware. The polytetrafluoroethylene has a coefficient of friction that is one of the lowest of any material. PTFE is also extremely abrasion and corrosion resistant and can be applied in a wide range of temperatures, from 260°C down to -270°C. PTFE also has excellent flame resistance due to its extremely high melting point, along with a very low rate of smoke generation and heat release. Additionally, The original properties of PTFE products remain the same for a very long service life even after extended time periods in water and at extreme temperatures. Furthermore, PTFE is resistant to atmospheric aging and is not affected by ultraviolet light.http://www.amicon.com/ptfeproperties.htm - BacktoTop

2. Problem formulation and solution (method description)

A hybrid method used in estimation process proposed in the paper consists of two methods: differential evolution and inverse coefficient technique. The method of differential evolution (DE) is used at the beginning of calculations. Like evolution strategies, DE first uses mutation and crossover operators to create child vectors.In [3] two mutation operators were presented:

$$\mathbf{v}_i^{(h)} = \mathbf{u}_a^{(h)} + F \cdot \left(\mathbf{u}_b^{(h)} - \mathbf{u}_c^{(h)}\right), \quad i = 1, \ldots, \mathrm{NP} \tag{1}$$

$$\mathbf{v}_i^{(h)} = \mathbf{u}_a^{(h)} + K \cdot \left(\mathbf{u}_{opt}^{(h)} - \mathbf{u}_i^{(h)}\right) + F \cdot \left(\mathbf{u}_b^{(h)} - \mathbf{u}_c^{(h)}\right), \quad i = 1, \ldots, \mathrm{NP} \tag{2}$$

where$\mathbf{v}_i$is a trial vector, which is used next in the crossover operation to create a child vector.The population members $\mathbf{u}_a^{(h)}, \mathbf{u}_b^{(h)}, \mathbf{u}_c^{(h)}$ are chosen at random. $F \in [0,1]$ is a real number that is constant throughout the optimization process. $K \in [0,1]$ is also a real number, $\mathbf{u}_i^{(h)}$is the ith best fit member of the population in generation h and $\mathbf{u}_{opt}^{(h)}$ is the best fit population member in generation h. Each vector has D-elements andNP stands for the size of population for each generation h. In subsequent years, other mutation operators have been developed. Which scheme works best is problem specific.

After the mutation operation is used to create $\mathbf{v}_i$ trial vector, a crossover operation is used to create child $\mathbf{y}_i$:

$$y_{j,i}^{(h+1)} = \begin{cases} v_{j,i}^{(h+1)} & \text{if } (r_j \le CR) \text{ or } j = r_i \\ u_{j,i}^{(h)}, & \text{otherwise} \end{cases} \tag{3}$$

Where r_i, $r_j$arerandom numbers and $CR$is a crossover probability. Each of them is a real number from the range [0, 1]. CR remains constant during the entire optimization process.In this way, the$i$th child vector $\mathbf{y}_i$ will have characteristics of the ith trial vector created by mutation and of the$i$th parent. Figure 1 presents creation of a child vector for a problem with 5 unknowns:

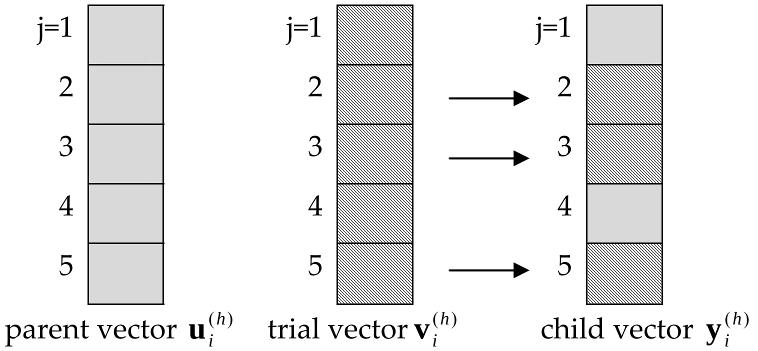

Figure 1: The creation process of a child vector from the parent and trial vectors

The selection process in DE is a direct competition between the *i*th parent and the *i*th child:

$$\boldsymbol{u}_i^{(h+1)} = \begin{cases} \boldsymbol{y}_i^{(h)}, & \chi^2\left(\boldsymbol{y}_i^{(h)}\right) \leq \chi^2\left(\boldsymbol{u}_i^{(h)}\right) \\ \boldsymbol{u}_i^{(h)}, & \text{otherwise} \end{cases} \tag{4}$$

This guarantees that every member of the population in generation (h+1)is as good or better than the corresponding member in generation(h). In earlier generations, when the differences between population members used by the mutation operator will be relatively large, mutations will also be relatively large, leading to better exploration of the entire search space.In later generations, when population members become similar as the minimum is approached, mutations will become smaller, which allows for better fine-tuning of the unknown parameters.

The main purpose of the differential evolution in the hybrid method is to preliminary determine the values of unknown thermal conductivityλ and the specific heat c_p of PTFE. Next step is to use the inverse coefficient technique with the previously calculated thermophysical parameters as a starting point in optimization procedure. It is important to mention that in the identification procedure only the thermal conductivity $\lambda_z$and the specific heat c_p were taken into account and the thermal conductivity λ_r and the heat transfer coefficient h_r,$h_z$played the role of additional degree of freedom.These parameters{λ_r , h_r, h_z } allow for a better fit the model thermal respond to the experimental one resulting from difficult to estimate heat losses and contact resistances. The boundary-value problem of heat conduction is shown in figure 2. Analytical or numerical solution of the direct problem as well as deterministic method of solving coefficient inverse problem were presented in [5, 6]so there is no need to repeat them here.In the present hybrid method DE procedure was adopted from [8] and the calculation procedure was as follows:

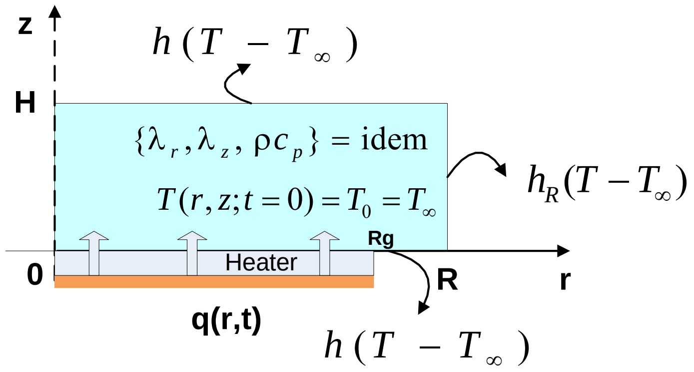

Figure 2: Physical model

A. Differential evolution -vector of population $\mathbf{v} = [c_p,\ \lambda_r,\ \lambda_z,\ h_r,\ h_z]^{\mathrm{T}}$

- (DEparameters): D=5, NP = 20, CR = 0.6, K=F=0.8, *iter_max*=20, refresh=5

- searching range of parameters:

$$\mathbf{v}_{\min} = [500,\ 0.01,\ 0.1,\ 0.01,\ 0.01]^{\mathrm{T}},\quad \mathbf{v}_{\max} = [2000,\ 50,\ 0.5,\ 50,\ 50]^{\mathrm{T}}$$

Remark: searching range for c_p and λ_z can be determined using transient pulse method as x_{min}= 0.5x*,x_{max} = 1.5x*, where x=c_p or x = λ_z and x* is calculated based onthe position of the maximumtemperature excesson the rearsurface of the sampleof thickness*H*

B. Deterministic inverse procedure

- starting point = $\mathbf{v}_{opt}$, where $\mathbf{v}_{opt}$ stands for optimal solution from DE method
- Levenberg-Marquardt optimization procedure to find the minimum of mean-square functional

3. Experiment and the results

The sketch of experimental setup is shown in figure 4 and the view from infrared camera of a set (back face of the sample – insulation ring – clamps) is visible in Figure 3. The rectangular thermal pulse of duration t_g (much shorter than the final time of measurement t_f) was generated by the electric thin-layer Kapton heater (0.2mm thickness, $6.645\cdot10^{-4}$ m^2 effective heating area) using a stabilized DC power supply PPS 2017 automatically controlled by an own computer program environment. Temperature Th3 was measured by using K-type thermocouple of diameter 80μm made by OMEGA applying 9-Ch scanner card Keithley 2001 TCSCAN. In addition to this the FLIR SC5000 infrared camera with spectral range 2.5÷5.1 μm, 640×512 pixels perframe and 5-100 Hz sampling frequency was used to record the temperature histories at the back side of the sample. The time of pulse duration was chosen to be equal to t_g = 2s, the voltage amplitude was U= 40V and the current was I = 0.516A. The unknown emissivity of PTFE was determined to be equal to ε=0.9.

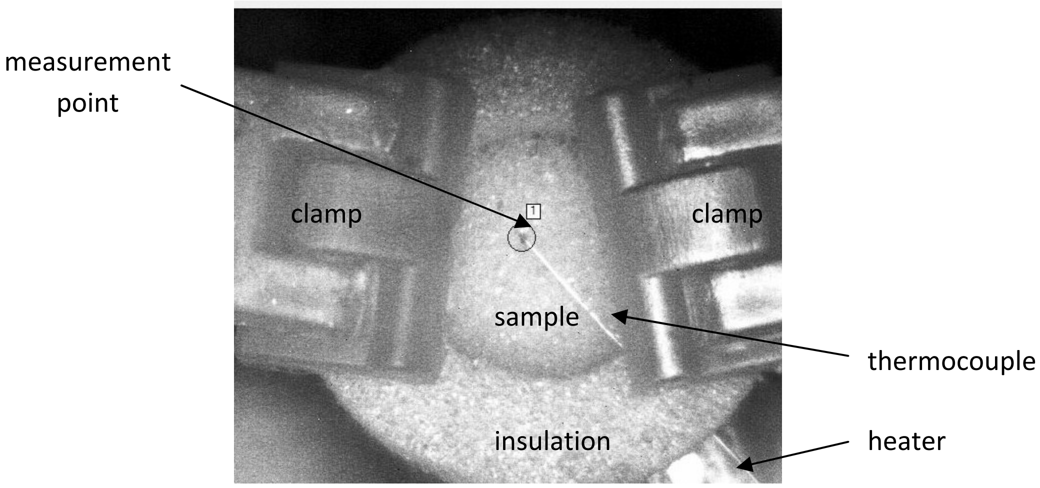

Figure 3: Back face of the sample with pointed measurement point (view from the infrared camera)

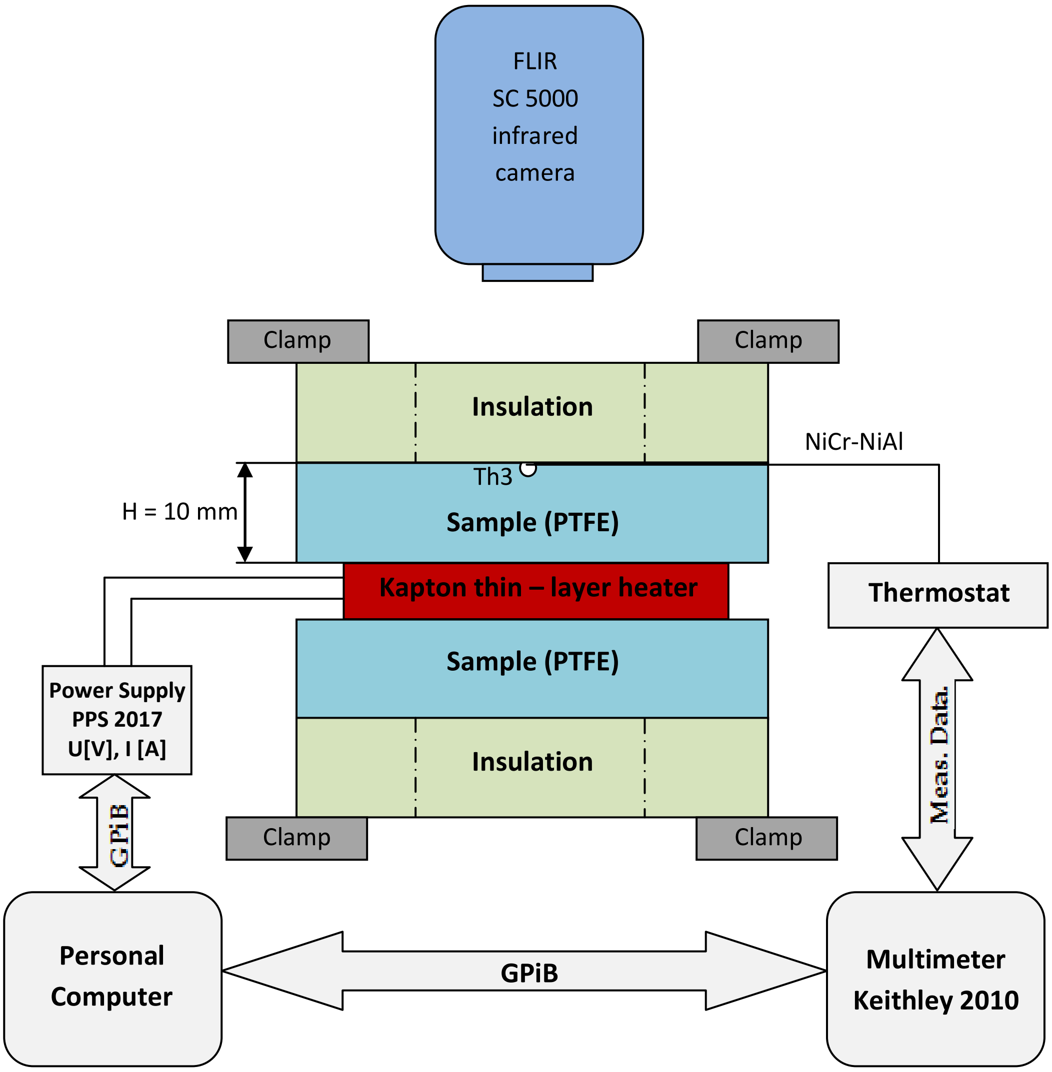

Figure 4: Sketch of measurement setup (scale not preserved)

In figure5 Done can observe a peak in the registered by IR camera signal (*f*= 10Hz)at the back face of the sample corresponding to the moment of switching on the heater and of duration equals t_g. This situation occurs only during measurement of PTFE and can be observed only by using infrared camera. One can observe also in this figure that just after switching off the heater the temperature increase registered by camera at the back face of the PTFE sample amounted to 0.1K. Signals registered by K-type thermocouple do not show such behaviour (Figure 5C).The observed effect for PTFE is connected with its high transmissivity within the IR camera spectral measurement range from 2.5μm to 5.1μm and reduces the temperature excess at the back face of the sample during its measurement with IR camera. Following this effect the results of parameter estimation obtained by inverse technique may differ from each other depending on which way the sample's temperature was measured.

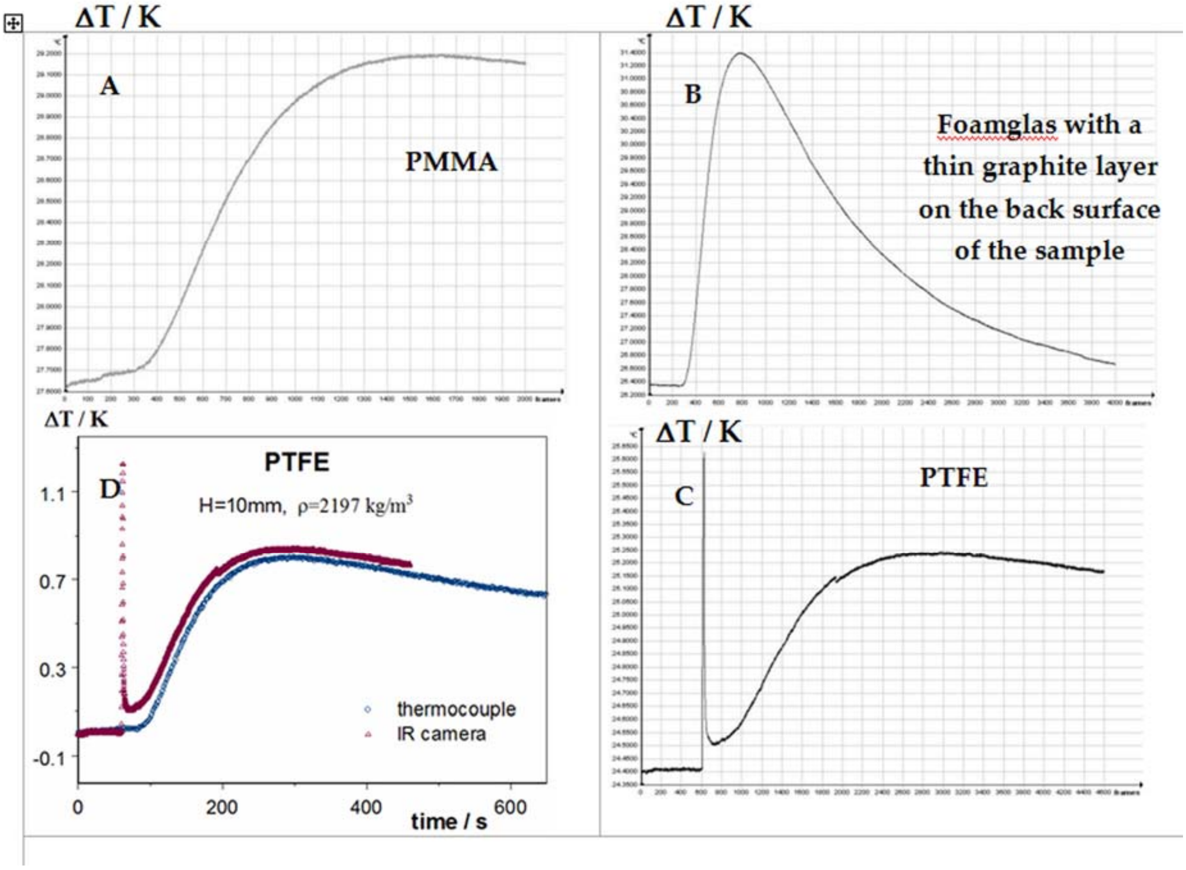

Figure 5: Registered temperature histories Th3 obtained from infrared camera for different materials

In figure 6 comparison ofthe calculated and the measured temperature is presented. It is clearly visible that the results obtained just after DE calculations with respect to the both signals are not consistent in the whole time interval (Figure 6A). A visible improvement of this situation is reached when the hybrid method was used (Figure 6B).

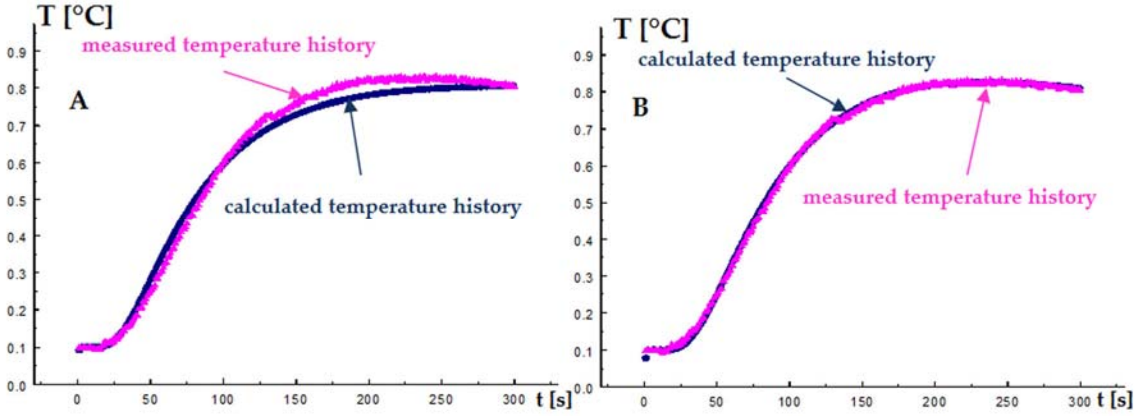

Figure 6: Measured by IR cameraand calculated temperature histories at Th3. A) after DE calculations only, B) after entire hybrid method calculations

The results of parameter estimation obtained after DE calculations,entire hybrid method and pulse transient method are shown in Table 1.In the last column reference values of thermophysical parameters for PTFE are presented.

Table 1.Results of parameter estimation for PTFE at T_0*=24.4*^{0}*C (values in brackets - thermocouple)*

Parameter	DE method	Hybrid method	Pulse transient method	Reference values
λ_z[W/m/K]	0.2187 (0.3287)	0.2811 (0.2936)	0.4318 (0.4018)	~**0.27** [1]
c_p [J/kg/K]	773.75 (1012.16)	805.85 (1020.9)	939.44 (877.96)	~**1090**[1, 2]
a [m^2/s]×10^{-7}	1.286 (1.478)	1.588 (1.309)	2.092 (2.082)	~**1.25** [1], ~**1.8**[4]

Analysing the results of parameter estimation for PTFE given in Table 1 one can observe that the values of thermal conductivity λ_z and thermal diffusivity $a$obtained from pulse transient method are overestimated with respect to the ones from DEandhybrid methods. Maximum percentage deviation $(\Delta\lambda_z/\lambda_z)_{max}$ in case of IR camera temperature measurements amounts to19.0%,4.1%, 59.3% for DE, hybrid and pulse transient method, respectively.Similarly, for specific heat the percentage deviation$(\Delta c_p/c_p)_{max}$ in that case amounts to 29.0%, 26.1%, 13.8%, respectively. In case of temperature measurements using K-type thermocouple the percentage deviation $(\Delta\lambda_z/\lambda_z)_{max}$ = { 21.7%,8.7%, 48.8%} and for $(\Delta c_p/c_p)_{max}$={7.1%, 6.3%, 19.5%} with respect to DE, hybrid and pulse transient methods.

Discrepancy of results obtained using pulse transient method with respect to DE or hybrid method can be explained by very simplified physical model of heat transfer in case of pulse transient in which the boundary conditions correspond to a semi-infinite body.

It is worth mentioning that PTFE temperature characteristics of $c_p$have some peak involvingtwo separate maxima at 23.5°C and 31.6°C with c_p values equal to about 1900 J/kg/K and 1300 J/kg/K. respectively . According to Blumm et al [1]itmeans that two overlapped transitions occur in this temperature range [1]. This effect was also observedby Panas et al [2]. One can also observe that values of λ_z and c_p obtained from differential evolution are lower than results from the hybrid method. Differential evolution is able to give values closer to reference ones nevertheless process of estimation would be much longer. This is one of the reasons to use deterministic technique in the second part of calculations in the hybrid method.

Conclusion

The hybrid method presented in the paper seems to be very efficient technique. It has all the advantages of both evolution and deterministic methods. Thanks to differential evolution it guarantees finding the global minimum and preliminary determining the range of estimated parameters. Thereafter the second technique is used to find quickly the best final solution of the inverse problem. The possibility of implementing any inverse method, apart from the coefficient inverse technique used here, makes the hybrid method very universal computational tool.

Unfortunately the complicated nature of polytetrafluoroethylene insulating material at the room temperaturemakes it difficult to evaluate propriety of obtained values of the specific heat. The experiment has to be performed at different temperatures and for other materials to unambiguously prove its usability.

Another interesting finding of the carried out experimentsis the heater effect observed on registered by the FLIR SC5000 infrared camera temperature history of PTFE at the back face of the sample.PTFE turned out to be the only material from examined so far by us that shows the temperature peak strictly correlated with the heater placed on the opposite surface of the sample. This effect requires spectrophotometric analysis of PTFE and will be carried out in the nearest future.

Acknowledgments

This research was supported by the Dean grant of Mechatronics Faculty of MUT, number: 955/2011.

References

[1] BLUMM J.; LINDEMANNA.; MEYERM.*Characterization of PTFE Using Advanced Thermal Analysis Techniques,* International Journal of Thermophysics, **35** (2010), p. 1919 – 1927

[2] PANAS A. J.; CUDZIŁO S.; TERPIŁOWSKI J.*Investigation of thermophysical properties of metal-polytetrafluoroethylene pyrotechnic compositions,* High Temperature – High Pressure, **34** (2003), p. 691-698

[3] STORN R., PRICE K. *Differential Evolution - a Simple and Efficient Heuristic for Global Optimization over Continuous Spaces*, Journal of Global Optimization, Kluwer Academic Publishers,**11** (1997), p. 341 - 359.

[4] TERPIŁOWSKIJ., *A modified flash method for determination of thermal diffusivity in semitransparent solids exposed to laser radiation*, archives of thermodynamics, **25** (2005), No.2, p. 39-68

[5] ZMYWACZYK J.; WIELGOSZ M.; KONIORCZYK P.; GAPSKI M.*Identification of some thermophysical and boundry parameters of black foamglas by an inverse method*, Proc. Thermophysics 2009, 29-30 Oct. 2009 Valtice, Chech Republic, p. 235-251

[6] ZMYWACZYKJ.; GAPSKIM.*Estimation of thermophysical parameters of stainless steel 1H18N9T by an inverse method,* Proc. Thermophysics 2010, 3-5 Nov. 2010 Valtice, Chech Republic, p. 253-261

[7] ZMYWACZYK J : *Numerical estimation of the temperature-dependent thermophysica lparameters using hybrid method of differential evolution and theLevenberg-Marquardt algorithm*, archives of thermodynamics, 28 (2007), No.1, p. 89-106

[8] http://www.icsi.berkeley.edu/~storn/code.html#f90c

Simplified and full mathematical models of concrete degradation during slow heating to high temperature- a comparative study

Dariusz Gawin[1], **Francesco Pesavento**[2]

[1]Department of Building Physics and Building Materials, Technical University of Lodz, Al. Politechniki 6, 90-924 Łódź, Poland, email: Dariusz.Gawin@p.lodz.pl

[2]Department of Structural and Transportation Engineering, University of Padova,via Marzolo 9, 35131 Padova, Italy, email: pesa@caronte.dic.unipd.it

Abstract: *The paper deals with modelling hygro-thermal performance and thermo-chemical degradation of concrete exposed to slow heating. Physical phenomena taking place in the material pores in such conditions are very complex and mutually coupled, thus rather complicated nonlinear mathematical models are needed to describe them. One of the most reliable numerical models of concrete at high temperature, widely validated experimentally, was developed by Authors in the last 10 years. FE simulations performed with this model are computationally costly, hence it cannot be applied for analyses of the whole large concrete structures. The aim of the paper is to simplify the model, by neglecting some chosen physical phenomena or flux components, and to evaluate differences between the simulation results obtained with the simplified models and with the full one. An extensive numerical study is performed with five simplified models, neglecting convective heat transport, latent heat of water vaporization, latent heat of concrete dehydration, water mass sources due to dehydration or the effect of concrete damaging on the material permeability. These simplifications in modelling of slowly heated concrete are considered and their effect on the results of FE simulations is analyzed. The simulations performed clearly show that only convective heat transfer and latent heat of dehydration can be neglected without a negative impact on the accuracy of simulations. All other simplifications considered can produce very different results with respect to the full model.*

Keywords: *Concrete degradation, High temperature, Hygro-thermal phenomena, Numerical modelling.*

1. Introduction

Reliableprediction of concrete structures durability duringslow heating to high temperature is of importance when designing concrete structures of nuclear power stations or nuclear waste disposals. To obtain the evolutions of temperature, moisture content, gas pressure and degradation processesin such conditions, rather complex mathematical models are required, [1 - 6]. One of the most reliable numerical models of concrete at high temperature, widely validated experimentally, was developed by Authors in the last 10 years [3 - 6]. It considers the porous and multiphase nature of concrete, phase and chemical transformations, different behaviour of moisture below and above the critical temperature of water, mutual interactions and couplings between the thermal, hygral and degradation processes, as well as several material nonlinearities. For these reasons, the modelis computationally costly and cannot be used for analyses of large concrete structures. Hence, for the latter purpose a simplified modelshouldbe developed. Though, there is still an open question which physical and chemical phenomena can be neglected in modelling of heated concrete structures without a significant loss of accuracy and reliability of numerical simulations. The aim of this paper is to simplify the model, by neglecting some chosen physical phenomena or flux components, and to evaluate differences between the simulation results obtained with the simplified models and with the full one for a concrete structure exposed to a slow heating.

2. Mathematical model

The state of concrete at high temperature is described by 4 primary state variables, i.e. gas pressure, p^g, capillary pressure, p^c, temperature, T, and displacement vector, $\mathbf{u}$, as well as 3 internal variables describing advancement of the dehydration and deterioration processes, i.e. degree of dehydration, Γ_{dehydr}, chemical damage parameter, V, and mechanical damage parameter, d. The model consists of 7 equations: 2 mass balances (continuity equations of water and dry air), enthalpy (energy) balance, linear momentum balance (mechanical equilibrium equation) and 3 evolution equations. For convenience of the Reader, the final form of the model equations, expressed in terms of the primary state variables, are listed below. The full development of the model equations is presented in [4].

Mass balance equation of dry air takes into account both the diffusive and advective air flow, the variations of the saturation degree with water and air density, as well as the variations of porosity caused by: dehydration process, temperature variation, skeleton density changes due to dehydration and by skeleton deformations. The mass balance has the following form:

$$\begin{aligned}&-n\frac{D^sS_w}{Dt}-\beta_s\left(1-n\right)\left(1-S_w\right)\frac{D^sT}{Dt}+\left(1-S_w\right)\alpha\, div\,\mathbf{v}^s+\frac{\left(1-S_w\right)n}{\rho^{ga}}\frac{D^s\rho^{ga}}{Dt}+\frac{1}{\rho^{ga}}div\,\mathbf{J}_g^{ga}\\&+\frac{1}{\rho^{ga}}div\left(n\left(1-S_w\right)\rho^{ga}\mathbf{v}^{gs}\right)-\frac{\dot{m}_{dehydr}}{\rho^s}\left(1-S_w\right)-\frac{\left(1-n\right)\left(1-S_w\right)}{\rho^s}\frac{\partial\rho^s}{\partial\Gamma_{dehydr}}\frac{D^s\Gamma_{dehydr}}{Dt}=0,\end{aligned}\qquad(1)$$

where S_w means the water saturation degree, n the porosity, β_s the thermal expansion of solid skeleton, α the Biot's coefficient, ρ^{ga} the density of dry air, $\mathbf{J}_g^{ga}$ the diffusive mass flux of air in the gas phase, $\mathbf{v}^{gs}$ the skeleton velocity, $\mathbf{v}^{gs}$ the velocity of gas with respect to the skeleton.

Mass balance equation of gaseous and liquid water considers the diffusive and advective flows of water vapour and water, the mass sources related to phase changes of vapour and dehydration, and the changes of porosity caused by variation of: temperature, dehydration process, variation of skeleton density due to dehydration and deformations of the skeleton, as well as the variations of: water saturation degree and the densities of vapour, ρ^{gw}, and liquid water, ρ^w. This gives the following equation:

$$\begin{aligned}&n\left(\rho^w-\rho^{gw}\right)\frac{D^sS_w}{Dt}+\left(\rho^wS_w+\rho^{gw}S_g\right)\alpha\, div\,\mathbf{v}^s-\beta^*_{swg}\frac{D^sT}{Dt}+S_gn\frac{D^s\rho^{gw}}{Dt}+S_wn\frac{D^s\rho^w}{Dt}\\&+div\left(nS_g\rho^{gw}\mathbf{v}^{gs}\right)+div\left(nS_w\rho^w\mathbf{v}^{ws}+\mathbf{J}_g^{gw}\right)-\left(\rho^wS_w+\rho^{gw}S_g\right)\frac{\left(1-n\right)}{\rho^s}\frac{\partial\rho^s}{\partial\Gamma_{dehydr}}\frac{D^s\Gamma_{dehydr}}{Dt}\\&-\frac{\dot{m}_{dehydr}}{\rho^s}\left(\rho^wS_w+\rho^{gw}S_g\right)=-\dot{m}_{dehydr}\end{aligned}\qquad(2)$$

where β^{*}_{swg} is thermal expansion coefficient of the multiphase medium, $\dot{m}_{dehydr}$ the mass source of water due to dehydration and $\mathbf{J}^{gw}_{g}$ the diffusive mass flux of vapour in the gas phase.

Enthalpy balance equation of the multi-phase medium, accounting for the conductive and convective heat flows, the heat effects of phase changes and dehydration process, and heat accumulation by a material, can be written as follows:

$$\left(\rho C_p\right)_{eff}\frac{\partial T}{\partial t}+\left(\rho_w C^w_p\mathbf{v}^w+\rho_g C^g_p\mathbf{v}^g\right)\cdot grad\,T-div\left(\chi_{eff}\,grad\,T\right)=-\dot{m}_{vap}\Delta H_{vap}+\dot{m}_{dehydr}\Delta H_{dehydr}, \tag{3}$$

where χ_{eff} and $\left(\rho C_p\right)_{eff}$ meanthe effective thermal conductivity and capacity of moist concrete, obtained from experiments, ΔH_{vap} and ΔH_{dehydr} the enthalpies of evaporation and dehydration, while the vapour mass source is given by:

$$\begin{aligned}\dot{m}_{vap}&=-\rho^w n\frac{\partial S_w}{\partial t}-\rho^w S_w\,\alpha\,div\mathbf{v}^s+\beta^{*}_{sw}\frac{\partial T}{\partial t}-div\left(n\,S_w\rho^w\mathbf{v}^{ws}\right)+\dot{m}_{dehydr}\left(1-\frac{\rho^w S_w}{\rho^s}\right)\\&-\left(1-n\right)\frac{\rho^w S_w}{\rho^s}\frac{\partial\rho^s}{\partial\Gamma_{dehydr}}\frac{\partial\Gamma_{dehydr}}{\partial t}.\end{aligned}\tag{4}$$

Equation (4) is obtained from the water mass conservation equation, considering the advective flow of water, the mass sources related to dehydration and the changes of porosity caused by: variation of temperature, dehydration process, variation of skeleton density due to dehydration and deformations of the skeleton, as well as the variations of water saturation degree.

Linear momentum conservation equation of the multi-phase medium, has the following form:

$$div\left[\left(1-d\right)\left(1-V\right)\mathbf{\Lambda_0}:\left(\boldsymbol{\varepsilon}_{tot}-\boldsymbol{\varepsilon}_{th}-\boldsymbol{\varepsilon}_{tchem}-\boldsymbol{\varepsilon}_{tr}\right)\right]+\rho\mathbf{g}=0, \tag{5}$$

where $\mathbf{\Lambda_0}$ means the elasticity tensor of undamaged material, **g** the acceleration of gravity, *d* the isotropic damage parameter, ρ the density of moist material, and $\boldsymbol{\varepsilon}_{tot}$, $\boldsymbol{\varepsilon}_{th}$, $\boldsymbol{\varepsilon}_{tchem}$ and $\boldsymbol{\varepsilon}_{tr}$ are total, thermal, thermochemical and transient strain tensors, respectively.

More details about the mathematical model, and in particular constitutive relationships used (material functions), as well as numerical solution of the model equations can be found in [4, 6].

3. Numerical analyses

The presented in [1, 2, 7] literature review, concerning hygro-thermal performance and deterioration of concrete at high temperature, shows that the most commonly used simplifications during modelling of heated concrete are: neglecting convective heat flux, neglecting mass and/or heat sources due to phase changes or dehydration process, and neglecting effect of thermal deterioration and/or cracking of concrete on its permeability. To analyse effect of the aforementioned simplifications of the mathematical model, presented in section 2, on the results of numerical simulations concerning performance of concrete during slow heating to high temperature, the following cases are considered:

1) omitting convective heat transport, referred on the graphs as "no CONV";

2) omitting latent heat of vaporization ("Qvap=0");

3) omitting latent heat of dehydration ("Qdeh=0");

4) omitting mass source due to dehydration and the heat source caused by it ("DMhyd=0");

5) omitting coupling between intrinsic permeability and concrete material damage ("no K(D));

The simulations were performed for the initial value -boundary problem, concerning a 60-cm concrete wall, heated fromtwo sidesby ambient air whichtemperature is increasing with the rate of 2 K/min. The following initial conditions were assumed: temperatureT_0= 293.15K (20^{o}C), relative humidityϕ_0=50%, gas pressure p^g=101325 Pa and complete lack of thermal and mechanical deterioration, i.e. $◎_{dehydr,0}$=0, d_0=0 andV_0=0. Simulations were performed for the period of 8 hours with the time step $◎t$= 1s. Due to symmetry, computations were performed for one half of the wall thickness, modelled with the mesh of 100 (100×1) 8-noded isoparametric finite elements of equal size (3mm×10mm), containing 503 nodes and 2515 degree of freedom.The following main material properties for concrete were used: porosity n= 5.1%, thermal conductivity χ_{eff} =1.4 W/m^{2}K, intrinsic permeability k_0= 2·10^{-19} m^2 andcompressive strength f_c= 80 MPa.The full set of material data used in the simulations is given in [7].

The evolution of temperature, gas pressure and mechanical damage at four different distances from the heated surface, obtained for the simulations performed with the full model, are presented in Figures 1 - 3. After 8 hours of heating temperature of a surface layer reached about 930^{o}C (~1200 K), at the distance of 2.4 cm ~735^{o}C, at 6 cm ~475^{o}C, while in a core zone (i.e. deeper than 10 cm) it remained below 300^{o}C, Figure 1. Due to temperature increase water evaporated, what was accompanied by a gas pressure increase up to about 7.5 bars, Figure2, and in the temperature range from ~200^{o}C to ~300^{o}C the gas phase was composed mainly of vapour.Due to heating concrete was exposed to a gradual thermo-chemical degradation (up to ~90% in a surface layer) and to mechanical damage (cracking) due to high gas pressure and constrained thermal dilatation of a surface layer, Figure 3.

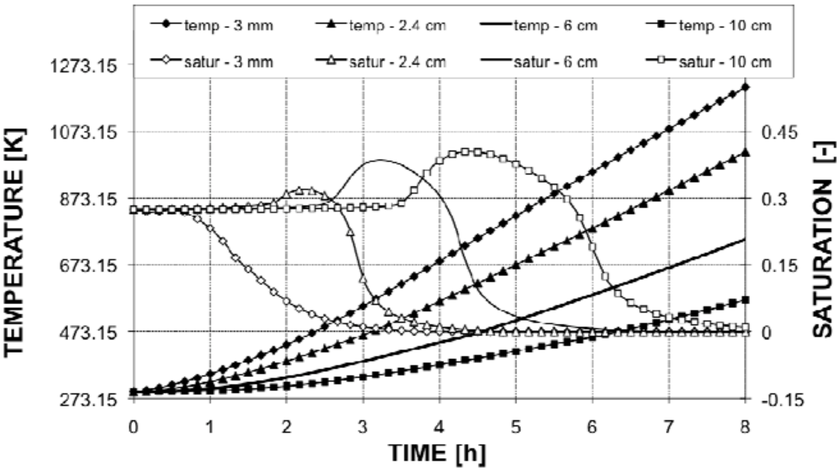

Figure 1. A concrete wall heated with the rate of 2 K/min – the evolutions of temperature and saturation degree at four different distances from the heated surface, obtained fromsimulation with the full model.

The resultsobtained with the simplified models considered in this paper, are presented in Figures 4 - 6 as the differences between an actual model and the reference (full) one. The evolution of the variables,which are most important during assesment of durability of concrete structures at high temperature, i.e. temperature *T*(*t*), gas pressure $p^g(t)$ and mechanical damage *d*(*t*), is analyzed.In particular, the distance of2.4 cm from the wall surface was chosen, because it is endangered by thermal spalling phenomenon. To evaluate a 'temporary' and an‘averaged’ in space and timeagreement between solutions for a variable *f*(*x*,*t*) (*f*= *T*, p^g and *d*),obtained with the considered models and with the reference one, the following relationships were used:

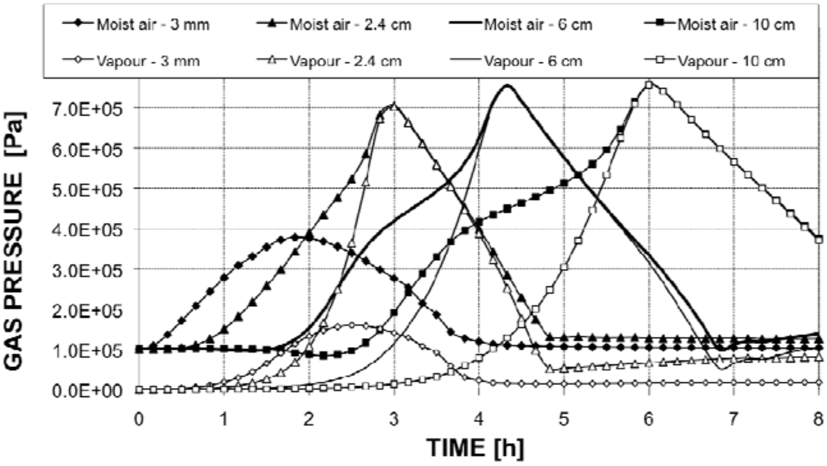

Figure 2. A concrete wall heated with the rate of 2 K/min – the evolutions of gas- and vapour pressure at four different distances from the heated surface, obtained fromsimulation with the full model.

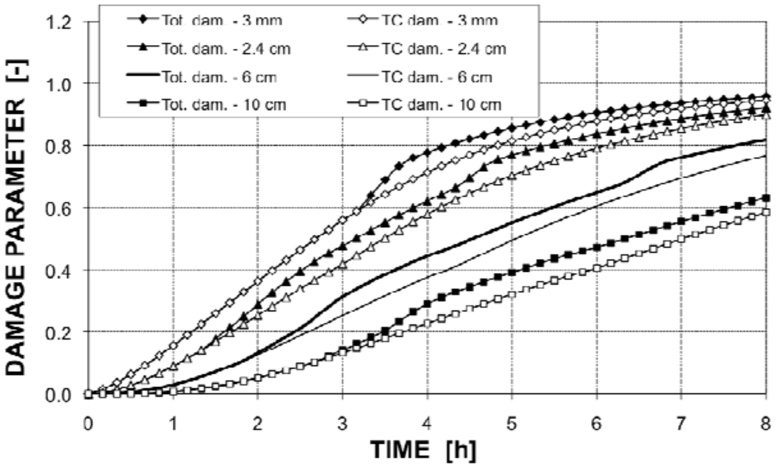

Figure 3. A concrete wall heated with the rate of 2 K/min – the evolutions of total and thermo-chemical damage at four different distances from the heated surface, obtained fromsimulation with the full model.

$$\bar{\delta}_{ref}\left[f(x,t)\right]=\frac{\max\left[\left|f(x_k,t_n)-f_{ref}(x_k,t_n)\right|\right]}{\max\left[\Delta f_{ref}\left(0\le x\le x_{\max},0\le t\le t_{\max}\right)\right]}, \tag{6}$$

$$\bar{\delta}_{ref}\left[f(x,t)\right]=\sum_{x_k}\sum_{t_n}\left[\frac{f(x_k,t_n)-f_{ref}(x_k,t_n)}{\max\left[\Delta f_{ref}\left(0\le x\le x_{\max},0\le t\le t_{\max}\right)\right]}\right]^2, \tag{7}$$

where t_n are values of time when the simulation results were saved (i.e. every 10 min during the whole analyzed process), and x_k are the considered positions, x_k = 0.3cm, 2.4cm, 3.3cm, 6.0cm and 10.0cm from the heated surface. In the above formula the normalized differences of variables $f\left(x_k, t_n\right)$ (i.e. divided by the maximal changes of those variables within the whole analyzed process) are used in order to enable comparing the results for different variables. The values of $\bar{\delta}_{ref}$ and the maximal relative differences $\bar{\delta}_{\max}$, obtained for the considered cases of simplified model are given in Table 1. The diverging solution was obtained for case 5, hence the data concerning it are marked with a star.

The results of analysis presented in Table 1 clearly show that the smallest difference in comparison to the full model, both from the 'time averaged' and 'temporary' point of view, were observed for cases 1 and 3, i.e. for the simplified models omitting convective heat transport and latent heat of dehydration. The results for case 2 confirmed that the vapour mass source due to dehydration is of importance when analysing performance of heated structures. Neglecting the coupling between intrinsic permeability and concrete material damage resulted in a very high gas pressures and rapid increase of mechanical damage parameter what caused diverging solution (marked with a star in Table 1).

Table 1: Relative errors of the analyzed state variables for the considered cases of simplified models.

Case	$\bar{\delta}_{ref}\left[T(x,t)\right]$	$\bar{\delta}_{ref}\left[p^g(x,t)\right]$	$\bar{\delta}_{ref}\left[d(x,t)\right]$	$\sum_m \bar{\delta}_{ref}(f_m)$	$\bar{\delta}_{\max}(T)$	$\bar{\delta}_{\max}(p^g)$	$\bar{\delta}_{\max}(d)$	$\sum_m \bar{\delta}_{\max}(f_m)$
	[-]	**[-]**	**[-]**	**[-]**	**[-]**	**[-]**	**[-]**	**[-]**
1	0.0132	0.000763	0.00674	0.020703	0.002	0.016	1.435	1.453
2	2.122	0.0873	1.376	3.5853	0.013	0.074	1.435	1.522
3	0.299	0.0138	0.192	0.5048	0.011	0.046	1.435	1.492
4	2.485	0.0583	4.252	6.7953	0.018	0.248	1.435	1.701
5*	14.262*	0.109*	528.371*	542.742*	0.007*	5.958*	3.453*	9.418*

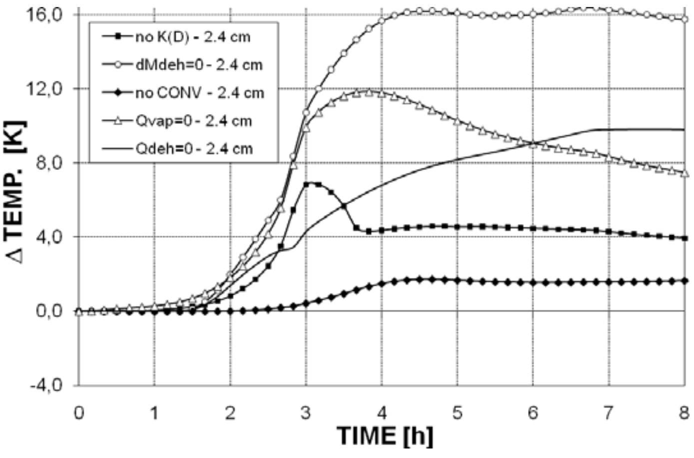

Figure 4. A wall heated with the rate of 2 K/min – the differences of the temperature evolutions with respect to the full model, obtained for the distance of 2.4 cm from the surface for different cases of the simplifiedmathematical models.

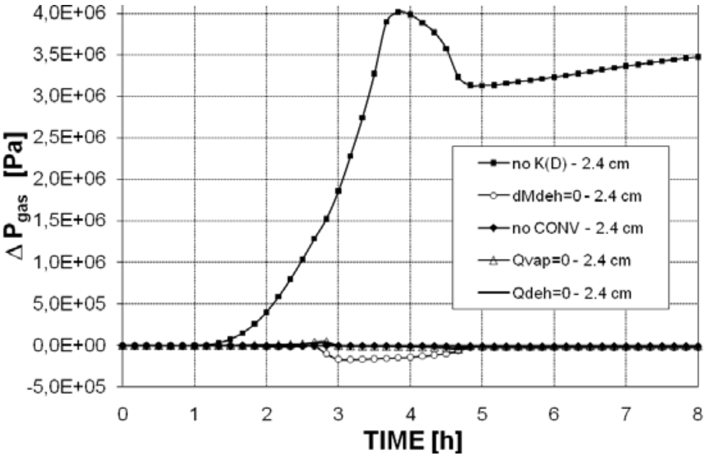

Figure 5. A wall heated with the rate of 2 K/min – the differences of the gas pressure evolutions with respect to the full model, obtained for the distance of 2.4 cm from the surface for different cases of the simplifiedmathematical models.

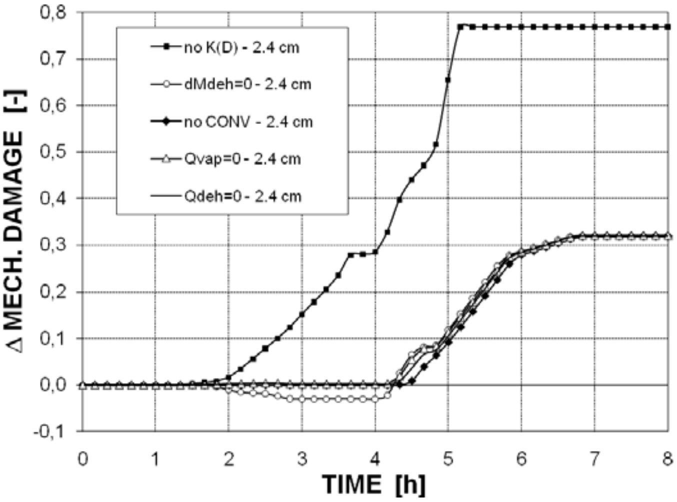

Figure 6. A wall heated with the rate of 2 K/min – the differences of the mechanical damage evolutions with respect to the full model, obtained for the distance of 2.4 cm from the surface for different cases of the simplifiedmathematical models.

4. Conclusions

The simulations performed here for a slowly heated 1-D concrete structure and those presented in [7], concerning 1-D and 2-D structures heated at both small and high rate (fire conditions), have clearly showed that only convective heat transfer can be neglected without a negative impact on the accuracy of simulation results. All other model simplifications, especially those related to the characteristic features of heated concrete, like the phase changes of water and concrete dehydration process during heating and related to them heat- and mass sources or sinks, the effect of concrete degradation (cracking) on the increase of material permeability, or the thermal creep strains of concrete during first heating, can produce very different results with respect to the model considering all the aforementioned physical phenomena. Hence, in general, such 'oversimplified' models of heated concrete may not be used for reliable prediction of concrete structures performance, and in particular for assessment of the thermal spalling risk at high temperature. For slowly heated concrete, latent heat of dehydration may be omitted as well, but mass source of vapour related to the latter process should be considered during simulations.

Acknowledgments

The first author's research was partially funded by the project POIG.01.01.02-10-106/09-00 “Innovative means and effective methods to improve the safety and durability of building structures and transportation infrastructures in the strategy of sustainable development” at the Technical University of Lodz, Poland, within the “Innovative Economy Strategic Programme” funded by EU. The research was also partially funded by the strategic project STPD08JA32 "Algorithms and Architectures for Computational Science and Engineering" funded by the University of Padova, Italy.

References

[1] BAZANT, Z.P. - KAPLAN, M.F. Concrete at High Temperatures: Material Properties and Mathematical Models. Longman, Harlow. 1996. ISBN 0-582-08626-4.

[2] PHAN, L.T. - CARINO, N.J. - DUTHINH, D. - GARBOCZI, E. (eds.)., Proceedings of International Workshop on Fire Performance of High-Strength Concrete, NIST Special Publication 919, Gaitherburg (MD), USA. 1997.

[3] GAWIN, D. - MAJORANA, C.E. - SCHREFLER, B.A. Numerical analysis of hygro-thermic behaviour and damage of concrete at high temperature. In Mechanics of Cohesive-Frictional Materials.1999. 4. p. 37 - 74. ISSN 1096-9853.

[4] GAWIN, D. - PESAVENTO, F. - SCHREFLER, B.A. Modelling of thermo-chemical and mechanical damage of concrete at high temperature. In Computer Methods in Applied Mechanics and Engineering.2003. 192. p. 1731 - 1771. ISSN 0045-7825.

[5] GAWIN, D. - PESAVENTO, F. - SCHREFLER, B.A. Modelling of deformations of high strength concrete at elevated temperatures, In Concrete Science and Engineering/ Materials and Structures. 2004. 37(268). p. 218 - 236. ISSN 1871-6873.

[6] GAWIN, D. - PESAVENTO, F. - SCHREFLER, B.A. Towards prediction of the thermal spalling risk through a multi-phase porous media model of concrete. In Computer Methods in Applied Mechanics and Engineering.2006. 195(41-43). p. 5707 - 5729. ISSN 0045-7825.

[7] GAWIN, D. - PESAVENTO, F. - SCHREFLER, B.A. What physical phenomena can be neglected when modelling concrete at high temperature? A comparative study. Part 2: Comparison between models. In Solids andStructures, 2011.48(13). p. 1945 - 1961. ISSN 0020-7683.

Drying shrinkage of autoclaved aerated concrete

Miloš Jerman, Jaroslav Výborný, Robert Černý

Department of Materials Engineering and Chemistry, Faculty of Civil Engineering,
Czech Technical University in Prague, Thákurova 7, 166 29 Prague 6, Czech Republic

Abstract: *Autoclaved aerated concrete (AAC) is a commonly used building material which is favoredby many designers due to its good thermal properties, low bulk density, and easy and fast building. However, failures in the AAC constructionsin a form of cracking of interior or exterior surfaces were observed in the past which could possibly lead to serious consequences for practical applications of AAC. In this paper, moisture-induced length change of AAC is investigated as a very important parameter for designers. According to the producers' data sheets, the shrinkage of AAC is 0.5 mm/m betweenthe volumetric moisture contents of 40% and 5%. It agrees well with the results obtained in this paper. However, the highestlength changes are found between 5% andthe dry material. This property of AAC which is not considered by designers because of unavailability of necessary data may be responsible forsurface cracking in some cases.*

Keywords: *autoclaved aerated concrete, drying shrinkage, contact dilatometer*

1. Introduction

The volumetric changes in autoclaved aerated concrete (AAC) occur due to drying, temperature change or carbonation. Drying shrinkage depends on material composition.For example, drying shrinkage of aerated concrete with only cement as the binder is reported to be significantly higher than that produced with lime or lime and cement [1].Additivessuch as fly ash have also influence on volumetric changes ofAAC. In normal concrete, fly ash has no effect on volumetric changes [1], and in self compacted concrete the addition of fly ash into mixture can decrease drying shrinkagesignificantly [2].Drying shrinkage of AAC is widely different from normal concrete probably of coarse aggregates in the latter. The shrinkage of AAC with fly ash is two times higher than for AAC with sand[1,3].

Other volumetric changes could be due to carbonation. Principle of carbonation is tobermorite reaction with atmospheric carbon dioxide in the presence of moisture,

$$5CaO \cdot 6SiO_2 \cdot 5H2O + 5CO_2 \longrightarrow 5CaCO_3 + 6SiO_2 + 5\,H_2O \qquad (1)$$

Carbonation shrinkage reached approximately 0.25% after 40 days at a CO_2 concentration of 3% vol. Higher CO_2 concentration leads to quicker shrinkage [4].

In this paper, the drying shrinkage of AAC is investigated. Drying shrinkage is induced by water loss ofthe material.

2. Tested materials

Three types of AAC (P 1.8-300, P 2-350λ, and P 4-500)were produced by Xella CZ.AAC P 2-400 was delivered by company H+H.For all AAC the silica sand as filler was used.The basic properties of studied AAC (bulk density, porosity and matrix density) are summarized in Table 1 [5,6].

Table 1: Basic physical properties of AAC

Material	Matrix density [kg m^{-3}]	Porosity [% vol.]	Bulk density [kg m^{-3}]
P1,8-300	2451	87.4	304
P2-350 λ	2048	81.9	363
P2-400	2140	80.7	407
P4-500	2527	80.2	500

3. Experimental method

Various methods can be used for the measurement of length changes, such as the methods employing the changes in the electric resistance, capacitance, inductance, the interference optical methods, the methods based on using the mirror and the scale. In this paper, the linear shrinkage was measured by contact dilatometer. The experiment was carried out under isothermal conditions.

The drying shrinkage test was done on 40x40x160 mm samples in accordance with Czech standard ČSN EN 13009 [7]. Square gauge plugs were glued on both the face sides of the specimen to facilitate length change measurements.

In the first step, the tested samples were immersed into water for 48 hours. Then they were placed into polyethylene bags for 48 hours. After that, their initial length was measured by contact dilatometer. This value was compared with the etalon. Tested sample in contact dilatometer is shown in Figure 1a, the contact dilatometer with etalon is in Figure1b.In the next step, the samples were kept in a climatic chamber with controlled relative humidity and temperature. The temperature was 25 ±2 °C, the relative humidity 80%.Then the samples were periodically weighted until constant mass values wereachieved. After that the next length by contact dilatometer was measured.

The hygric expansion/shrinkage coefficient [mm/m] was calculated according to the formula

$$\varepsilon_{\mathrm{CS,i}} = \frac{\left(L_{C0} - L_{Ci}\right) - \left(L_{inv,0} - L_{inv,i}\right)}{L_C} * 1000 \tag{2}$$

whereL_c is initial length of test sample, L_{C0} reading on the electronic dial of the length changes at tested sample at timet_0, L_{Ci}length of tested sample at timet_i, $L_{inv,0}$reading on the electronic dial of the length of constant etalon at time t_0, $L_{inv,i}$reading on the electronic dial of the length of constant etalon at timet_i.

Moisture content by mass u[kg/kg] for each time of the measurement$t_i$was determined according to the formula

$$u = \frac{m_i - m_d}{m_d - m_{plug}} \tag{3}$$

where m_i is mass of the wet sample at timet_i „ $m_d$mass of the dried sample, m_{plug}mass of the gauge plugs, and then recalculated to moisture content by volume w as

$$w = u\frac{\rho_d}{\rho_w} \tag{4}$$

whereρ_d is bulk density and ρ_w density of water.

Figure 1a, b Device for measurement of linear hygric expansion/shrinkage at normal temperatures, on the left with tested sample, on the right with etalon

4. Experimental results and discussion

Experimental results are summarized in Figures 2, 3 and Table 2. According to the producers' data sheets, the shrinkage of AAC is 0.5 mm/m between the volumetric moisture contents of 40% and 5%. It agrees reasonably well with our data. From water saturated condition to 0.05 m^3/m^3 was drying shrinkage approximately 0.35 mm/m for AAC P 4-500, P 2-400, P 2-350. The highest shrinkage in this range was observed for AAC P 1.8-300 (0.40 mm/m). However, the highestlength changes were achieved for all materials between the volumetric moisture content of 0.05 m^3/m^3 and dry state.As it is shown inTable 2, the total drying shrinkage was similar for all types of AAC (approximately 1 mm/m),with the lowest value for P 4-500 andthe highest value for AAC P 1.8-300.

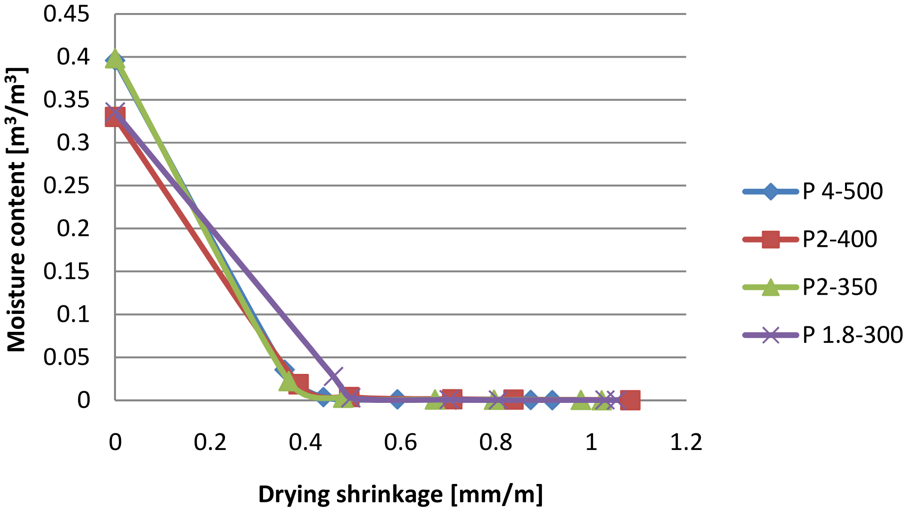

Figure2. Drying shrinkage of 4 types of AAC

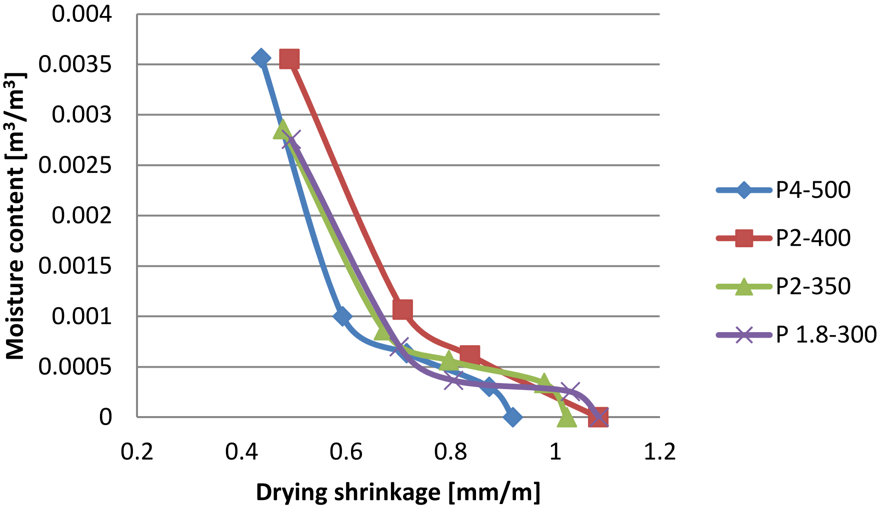

Figure 3. Drying shrinkage of 4 types of AAC for low moisture content

Table 2. Total drying shrinkage of 4 types of AAC

AAC	Total drying shrinkage [mm/m]
P 4-500	0.92
P 2-400	1.08
P 2-350	1.02
P 1.8-300	1.09

5. Conclusion

The experimental data presented in this paper showed that drying shrinkage of all four studied types of AAC increased with decreasing moisture content and the increase was fastest in the range of very low moistures. This was apparently due to the loosening of van der Waals forces bonding water molecules to the pore walls as a consequence of removal of the surface phase of water at drying.This feature of the AAC drying process which is commonly not considered by designers because of unavailability of necessary data may be responsible for surface cracking in some cases.

Acknowledgments

This research was supported by the Czech Science Foundation, under project No. 103/09/0016.

References

[1] Ramamurthy K., Narayanan, N. Influence of composition and curing on drying shrinkage of aerated concrete, Materials and Structures/Matériaux et Constructions, Vol. 33, 2000, p. 243-250

[2] Ma K., Xie Y., Long G., Luo Y., Drying Shrinkage of Medium Strength SCC, Second International Symposium on Design, Performance and Use of Self-Consolidating Concrete SCC 2009, RILEM Publications, Bagneux 2009, p. 657-663.

[3] Narayanan, N., Ramamurthy, K. Structure and properties of aerated concrete: a review, Cement & Concrete Composites, Vol. 22, 2000, p. 321-329

[4] Matsushita F., Aono Y., Shibata S., Calcium silicate structure and carbonation shrinkage of a tobermorite-based material,Cement and Concrete Research, Vol. 34, 2004,p. 1251 – 1257.

[5] Výborný, J., Jerman, M., Černý, R., Tepelné a vlhkostní transportní charakteristiky nových pórobetonových výrobků, Stavební obzor, Vol. 20, 2011, p. 7-11.

[6] Jerman, M., Keppert, M., Výborný, J., Černý, R., Moisture and heat transport and storage characteristics of two commercial autoclaved aerated concretes, Cement, Wapno Beton, Vol. 16/78, 2011, p. 18-29.

[7] ČSN EN 13009 Tepelně vlhkostní chování stavebních material a výrobků – Stanovení součinitele vlhkostní roztažnosti, Český normalizační institut, 2001.

Experimental determination of material characteristics of cellular concrete necessary for service life assessment studies

Miloš Jerman, Jaroslav Výborný, Robert Černý

Department of Materials Engineering and Chemistry, Faculty of Civil Engineering, Czech Technical Universityin Prague, Thákurova 7, 166 29 Prague 6, Czech Republic,

e-mail: milos.jerman@fsv.cvut.cz

***Abstract**: Water and heat transport parameters of two different autoclaved aerated concretes commercially produced in Czech Republic are investigated. Moisture diffusivity and specific heat capacity are determined as functions of moisture content, thermal conductivity as a function of both moisture content and temperature. Experimental results show that in particular the dependence of water and heat transport parameters on moisture content is very significant. However, the data given by the material producers are mostly given as single values only, mostly in dry state. In the light of the experimental findings obtained in this paper this is quite insufficient for any service life assessment studies utilizing hygrothermal performance analyses.*

***Keywords:** Aerated autoclaved concrete, water transport properties, thermal properties*

1. Introduction

In the current durability assessments of building envelope systems based on autoclaved aerated concrete (AAC) a complex view is often missing. Precise and serious analyses of hygrothermal performance of the new AAC technologies based on sound scientific knowledge are not performed very frequently. However, AAC-based building envelopes should be designed as a system consisting of AAC, internal and external finishes and possibly also thermal insulation layer, and in this design process, the details have to be solved using suitable methods.The quality of any computational simulation study aimed at the service life assessment depends primarily on the quality of input parameters. In this paper, water and heat transport parameters of two commercial AAC products are measured and compared with the data available in common databases. The measured data will be used in hygrothermal computer simulation studies, and the obtained moisture and temperature fields will be utilized in service life analyses.

2. Materials

Two different commercial AAC were studied in this paper. The first of them (P 4 500) was produced by Xella CZ and second one (P 2 400)by H+H Czech Republic. In Table 1 data of material properties, which are published by the producers in their data sheets [1, 2] are presented. Water vapor diffusion resistance factor is shown for both states, wet and dry, according to Czech and European standards. Thermal conductivity and specific heat capacity are measured only in dry state.

Table 1: Parameters of AAC according to the producer's data sheet

Material	Thermal conductivity [W $m^{-1}K^{-1}$]	Specific heat capacity [J kg^{-1} K^{-1}]	Water vapor diffusion resistance factor [-]
P 2400	0.10 (dry state)	1000	5/10
P 4 500	0.12 (dry state)	1000	5/10

3. Experimental methods

3.1 Basic physical parameters

As basic physical material characteristics, bulk density [kg m^{-3}], open porosity [Vol.-%] and matrix density [kg m^{-3}] were determined. The matrix density ϱ was measured by helium pycnometry, bulk density ϱ_b by measuring the mass and dimensions of specimens. The total porosity P was calculated as

$$P = 1 - \frac{\rho_b}{\rho} \tag{1}$$

3.2 Water vapour transport properties

The cup method was used for determination of water vapour transmission properties [3]. The measurement is carried out in steady state under isothermal conditions. It is based on one-dimensional water vapour diffusion, measuring the diffusion water vapour flux through the specimen and on measuring partial water vapour pressure in the air under and above specific specimen surface. The measurements were done at 25°C in a period of two weeks. The steady state values of mass loss determined by linear regression for the last five readings were used for the determination of water vapour diffusion coefficient. In the dry cup method the sealed cup containing dried $CaCl_2$ (the equilibrium relative humidity above the desiccant was 5%) was placed in an air-conditioned box with 50% relative humidity. Otherwise the measurement was done in the same way as in the wet cup method.

The water vapour diffusion coefficient D [m^2 s^{-1}] was calculated from the measured data according to the equation:

$$D = \frac{\Delta m \cdot d \cdot R \cdot T}{S \cdot \tau \cdot M \cdot \Delta p_p} \tag{2}$$

where Δm [kg] is the amount of water vapour diffused through the sample, d [m] the sample thickness, S [m^2] the specimen surface, τ [s] the period of time corresponding to the transport of mass of water vapour Δm, Δp_p the difference in water vapour pressurein the air under and above specific specimen surface, R the universal gas constant, M the molar mass of water, T[K] the absolute temperature. On the basis of the diffusion coefficient D, the water vapour diffusion resistance factor μ was determined:

$$\mu = \frac{D_a}{D} \tag{3}$$

where D_a is the diffusion coefficient of water vapour in the air.

The samples for determination of water vapour transport properties had a shape of cylinder with diameter of 100 mm and height of 20 mm.

3.3 Liquid water transport properties

3.3.1 Water absorption coefficient

The water absorption coefficient was measured using a standard experimental setup [4]. The specimen was water and vapour-proof insulated on four lateral sides and the face side was immersed 1-2 mm in the water. The automatic balance allowed recording the increase of mass. The water absorption coefficient A [kgm^{-2}s$^{-1/2}$] was then calculated using the formula:

$$i = A \cdot \sqrt{t} \tag{4}$$

where i is the cumulative water absorption [kg m^{-2}], t the time from the beginning of the suction experiment. The water absorption coefficient was then employed for the calculation of the apparent moisture diffusivity in the form:

$$\kappa_{app} \approx \left(\frac{A}{w_c - w_0} \right)^2 \tag{5}$$

where w_c is the saturated moisture content [kgm^{-3}] and w_0 the initial moisture content [kgm^{-3}].

The samples for determination of water absorption coefficient had a size of 50 x 50 x 20 mm.

3.3.2 Moisture diffusivity in dependence on moisture content

For determination of moisture diffusivity depending on moisture content the inverse analysis of moisture profiles using Boltzmann transformation was used. The moisture profiles were measured by the capacitance method which was calibrated gravimetrically.The dimensions of tested specimen were 20 x 40 x 300 mm. Their lateral sides were water- and vapour-proof insulated and a face side was in contact with water. The moisture diffusivity was calculated as

$$\kappa(u_x) = \frac{1}{2t_0 \left(\frac{du}{dx} \right)_{x_0}} \int_{x_0}^{\infty} x \frac{du}{dx} dx. \tag{6}$$

where u is the moisture content by mass, u_x is the value of moisture content at the position $x=x_0$.

3.4 Thermal properties

The thermal conductivity and specific heat capacity were measured by the commercial device ISOMET 2104 (Applied Precision, Ltd.). ISOMET 2104 is a multi-functional instrument for measuring thermal conductivity, thermal diffusivity, and volumetric heat capacity. It is equipped with various types of optional probes, needle probes are for porous, fibrous or soft materials, and surface probes are suitable for hard materials. The measurement is based on the analysis of the temperature response of the analyzed material to heat flow impulses. The heat flow is induced by electrical heating using a resistor heater having a direct thermal contact with the surface of the sample. The measurements in this paper were done using the surface probe. Thermal properties were measured in laboratory conditions at the average temperature of 25°C. The measurement of thermal conductivity and specific heat capacity in dependence on moisture content was done from the dry state to fully water saturated state.

The samples for determination of heat transport and storage properties had a size of 70 x 70 x 70 mm.

4. Experimental results and discussion

4.1 Basic physical parameters

The results of basic properties measurement are summarized in Table 2. The bulk density both AAC agreed with producers data sheet. The porosity of both AAC was similar, but matrix density was much higher for AAC P4 500 which indicated different production technology.

Table 2:Basic physical properties of AAC

Material	Matrix density [kgm^{-3}]	Total porosity [Vol.-%]	Bulk density [kgm^{-3}]
P 2 400	2140	80.7	407
P 4-500	2527	80.2	500

4.2 Water vapour transport properties

Water vapour transport properties are shown in Table 3. P4 500 exhibited lower water vapour diffusion resistance factor than P2 400, which did not correspond with its higher bulk density. However, as indicated by the higher matrix density, the topology of the pore space of P4 500 might differ from P2 400. The μ values were for the wet cup method about 50% lower than the data given in the producers' data sheets, for dry cup and P4 500 they agreed with the producer's data, but P2 400 had μ 40% higher. However, it should be noted that the producers probably used only some estimated data because their μ values were the same for products with large differences (300-500 kg m^{-3}) in bulk density.

Table 3:Water vapour diffusion properties of AAC

Material	D [10^{-6} m^{2}s^{-1}]		μ [-]	
	5/50 RH %	97/50 RH %	5/50 RH%	97/50 RH%
P 4 500	2.6	7.5	9.7	3.0
P 2 400	6.2	7.3	14	3.7

4.3 Liquid water transport properties

4.3.1 Water absorption coefficient

Water transport properties are shown in Table 4. P 4 500 achieved about 50% higher water absorption coefficient than P 2 400. This did not correspond with its higher bulk density, similarly as in the case of water vapour transport parameters. So, the different pore topology of both materials played probably a significant role here as well.

Table 4:Liquid water transportproperties of AAC

	A [kg m^{-2} s$^{-1/2}$]	κ[m^2 s^{-1}]
P4 - 500	0.044	7.6*10^{-9}
P2 - 400	0.027	7.1*10^{-10}

4.3.2 Moisture diffusivity in dependence on moisture content

Example of measured moisture profiles is shown in Figure 1.

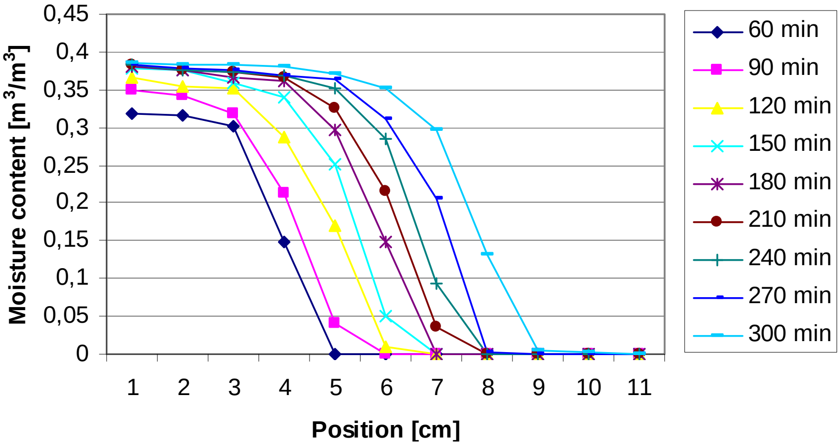

Figure 1: Moisture profiles of P 4 500

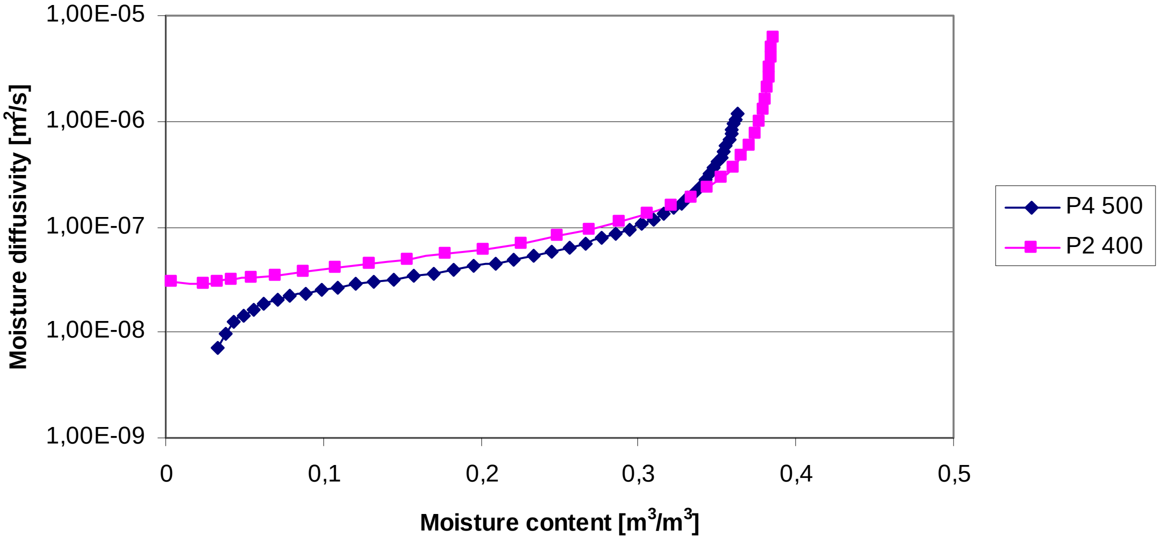

Figure2: Moisture diffusivity in dependence on moisture content

The calculated moisture diffusivity κ of both materials is presented in Figure 2. P2 400 exhibited higher κ in almost the whole range of moisture content which did not agree well with the apparent moisture diffusivity values in Table 4. Also, the κ values in Figure 2 were much higher than those in Table 4. This might be due to the uncertainties in calculating the apparent moisture diffusivity using Eq. (5). The saturated moisture content in the denominator was assumed to be the value obtained in the water vacuum saturation experiment. However, the differences could not be explained even with using the capillary saturation values. Another possible explanation of the obtained differences could be the different experimental setups in both cases. The apparent moisture diffusivity was determined using an experiment taking place in vertical position, and the moisture profiles used for calculation of moisture dependent moisture diffusivity were measured in horizontal position. So, the effect of gravity could be important.

4.4 Thermal properties

Thermal conductivity in dependence on moisture content of measured samples is shown in Figure 3. The data for P4 500 were higher in the whole range of moisture content but the differences were up to 10% only. This was in accordance with the higher bulk density of P4 500.

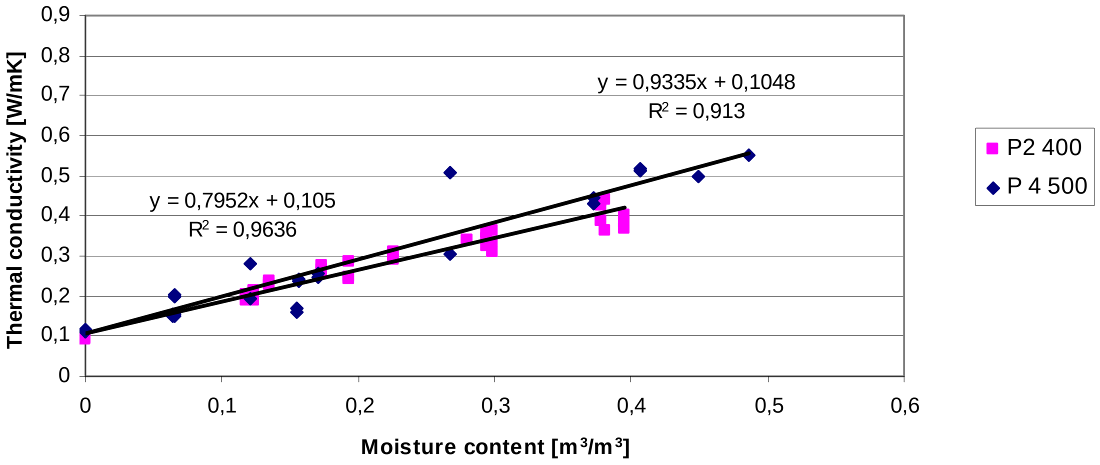

Figure 3: Thermal conductivity in dependence on moisture content

Thermal conductivity in dependence on temperature is summarized in Table 5. Thermal conductivity of both materials increased with increasing temperature, for P4 500 it was systematically higher than for P2 400.

Table 5: Thermal conductivity of AAC in dependence on temperature

Material/temperature	2 °C	10 °C	15 °C	25 °C	30 °C	40 °C
P 2-400	0.0839	0.0857	0.0921	0.0927	0.0985	0.0991
P 4-500	0.9410	0.1060	0.1088	0.1218	0.1288	0.1438

The difference between the values measured at 2°C and 40°C was much lower than that obtained by comparing the data for dry and water saturated samples. So, the dependence of thermal conductivity on temperature was much weaker than on moisture.

The data for thermal conductivity in dry state at 25°C agreed well with the data given by the producers (Table 1). For P2 400 the measured thermal conductivity was even lower than in the producer's data sheet.

The specific heat capacity as a function of moisture content is presented in Figure 4.The values in dry state were for both materials up to 10% higher than in Table 1 but the declared data (1000 J/kgK) seemed to be just estimated values rather than exactly measured.

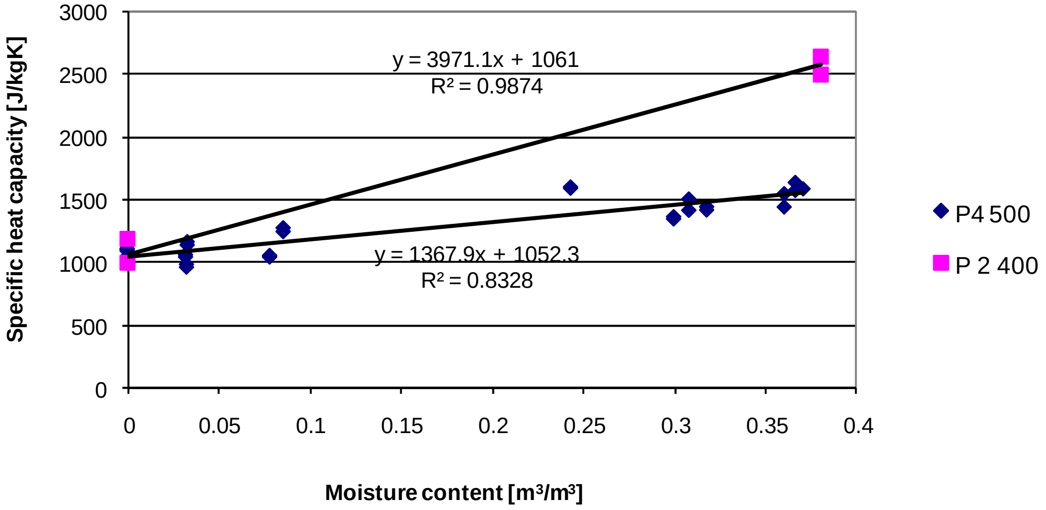

Figure 4:Specific heat capacity in dependence on moisture content

5. Conclusions

The experimental results presented in this paper showed that the data given by the AAC producers were mostly given with reasonable accuracy. However, their extent was far from satisfactory.The catalogue lists of AAC producers were found to be confined to water vapor transport parameters and heat transport and storage parameters, both given in the form of a single value. Therefore, even for a very active and responsible designer it would be quite difficult to gather enough data for a serious hygrothermal analysis of AAC-based building envelope systems. The absence of some important hygric properties such as liquid water transport parameters in the producers' declarations greatly limits the quality of any hygric analysis which can be done in the common design process in building practice. This paper partially helped in dealing with the lack of necessary parameters for commercial AAC used in the practice but it is necessary to continue in this effort and provide similar data also for other typical AAC products.

Acknowledgements

This research has been supported by the Czech Science Foundation, under grant No. 103/09/0016.

References

[1] Xella, 2010. Technical parameters of products.URL: <http://www.xella.cz/downloads/czk/product/ytong-lambda.pdf> [cit. 2010-01-26]

[2] H+H, 2010. Technical parameters of products. URL: <http://www.hplush.cz/c/document_library/get_file?folderId=528926&name=DLFE-11218.pdfl> [cit. 2010-01-26]

[3] Roels, S., Carmeliet, J., Hens, H., Adan, O., Brocken, H., Černý, R., Pavlík, Z., Hall, C., Kumaran, K., Pel, L. & Plagge, R. 2004. Interlaboratory Comparison of Hygric Properties of Porous Building Materials. Journal of Thermal Envelope and Building Science 27: 307-325.

[4] Kumaran, M.K. 1999. Moisture diffusivity of building materials from water absorption measurements.*Journal of Thermal Envelope and Building Science*, 22, 349-355.

Mortars containing municipal solid waste incineration ashes – mechanical and thermal properties

Martin Keppert, Eva Vejmelková, Zbyšek Pavlík

Department of Materials Engineering and Chemistry, Faculty of Civil Engineering, Czech Technical University in Prague, Thákurova 7, 166 29 Prague 6, CzechRepublic

Abstract: *Municipal solid wastes incineration (MSWI) is in fact process converting the solid wastes to energy and ashes – bottom ash and fly ash. The ashes are nowadays mostly chemically treated in order to reduce the environmental risks due to high content of heavy metals and organic pollutants and landfilled. Obviously the possibility to use the MSWI ashes for production of a marketable product would be favorable. Such product has to prevent the leach out of dangerous components from the ashes to environment (i.e. immobilizate heavy metals). A promising approach is immobilization of heavy metals in cementitious matrix because the chemical composition of these ashes – except the high heavy metals content – is rather similar to coal fly ash. Such cementitious immobilizate can be used as building material instead of common cement based concrete or mortar. The physical properties of the resulting immobilizate are obviously influenced by the presence of the MSWI ash. The present paper deals with influence of four kinds of MSWI ashes on strength and morphology of the cement mortars which consequently influences also their thermal properties. It was found that the influence of MSWI ashes on mortars strength is highly dependent on the chemical composition of the particular used ash; the thermal properties are influenced by all ashes in the approximately identical way.*

Keywords: *MSWI ashes, thermal conductivity, strength*

1. Introduction

Materials generated in Municipal Solid Waste Incineration (MSWI) can be divided into two fundamental groups: bottom ash (BA) and fly ash (FA). Especially fly ashes are toxic due to high content of heavy metals and (in some technologies) organic compounds (POPs - Persistent Organic Pollutants). There is lot of technologies for FA treatment and stabilization, both commercial and under development [1]. An alternative way, which is also under development yet, is utilization of MSWI ashes (BA and FA) for production of building materials which is inspired by common using of coal fly ash.

The high variability in composition and properties id for MSWI ashes typical; it is caused by different composition of incinerated waste (both locally and in dependence on season) and by differences in incineration facility technology. Hence the utilization of MSWI ashes has to be evaluated individually. There is several approaches to application of MSWI ashes in civil engineering. It is possible to use ashes as concrete admixture in raw state as a partial replacement of cement or aggregates. It is usually accompanied with certain loss of compressive strength due to unfavourable chemical composition of MSWI ashes [2]. Very often makes problems the presence of aluminium in metallic form in BA; aluminium is corroded in alkaline environment prevailing in concrete while hydrogen is evolved [3]. Other problematic components are sulfates and chlorides. It is possible to wash the salts by plain water or various solutions [4] but the pozzolanity of ash can be lost [5]. Another approach is ashes vitrification – melting and grinding of cooled slag to fine powder. It is possible to vitrify MSWI bottom ash itself [6] or with additive glass [7]. There is also a possibility to adjust SiO_2/CaO ratio in the slag by quartz sand during melting in order to obtain high pozzolanity [8].Vitrification of MSWI ashes consumes obviously higher capital and operational costs than washing. MSWI fly ash has been successfully tested also as component of raw materials mixture for production of Portland clinker [9]. Yang et al. [10] prepared from MSWI ashes and additives low-melting glass-ceramics. Another approach presents using of MSWI as raw material for agglomerated lightweight aggregates [11].

Motivation of this research is to evaluate the effect of several kinds of untreated MSWI ashes on mechanical and thermal properties of cementitious composites.

2. Materials and experimental methods

The studied ashes (fly ashes from boiler - FA1 and FA2 - and from Electrostatic precipitator - ESP; bottom ash BA) were collected in a modern Czech MSWI facility. The plant is equipped with acid extraction of heavy metals from fly ashes; such treated ashes are mixed with bottom ash and sold as material for banks, road construction etc. In this work the ashes were studied in raw state – before treatment.

Chemical composition of untreated ashes (only major elements) is summarized in Table 1. For civil engineering application in cementitious materials is important especially high content of sulfates in all ashes and chlorides in ESP (above limits given by technical standards for concrete admixtures [12, 13]). Another unfavorable factor is high content of zinc in ESP fly ash; zinc is retarding the cement hydration. It is possible to observe increase of ashes "salty" character from BA to ESP.

Table 1: Chemical composition of MSWI ashes (major components).

	FA1	FA2	ESP	BA
SiO_2	15.9	19.6	9.9	33.5
Al_2O_3	8.0	9.7	4.2	15.8
Fe_2O_3	2.9	3.4	1.9	8.4
CaO	25.7	25.6	13.0	19.4
MgO	2.1	2.4	1.2	2.0
SO_3	28.8	14.9	15.7	9.3
ZnO	2.8	2.5	8.0	0.8
Na_2O	5.4	5.9	17.9	3.6
K_2O	4.4	4.4	8.4	1.9
TiO_2	1.6	1.6	0.8	1.5
Cl	0.7	7.3	15.1	1.1
$\sum$	98.1	97.5	96.0	97.1

The MSWI ashes were used as partial replacement of siliceous sand (0/4 mm) in cementitious mortars (Table 2). The amount of water in ashes containing mortars was higher than in reference MREf in order to maintain good workability of fresh mixtures. Cement CEM I 42.5 R was used as principal binder. The mixtures were mixed in laboratory mixer and specimens were casted and then stored in environment of 100 % RH.

Bulk density ϱ, matrix density ϱmat and porosity ψ were determined by means of hydrostatic weighing. The pore size distribution was measured by mercury intrusion porosimetry (Pascal 140 + 440, Thermo). The thermal conductivity and specific heat capacity were measured using the commercial device ISOMET 2104 (Applied Precision, Ltd). The measurement is based on analysis of the temperature response of the analyzed material to heat flow impulses. The compressive and bending strength of mortars was measured by standard method using 160x40x40 mm prisms.

Table 2: Composition of mortars containing MSWI ashes.

Component	MRef	MFA1	MFA2	MESP	MBA
	kg/m^3				
CEM I 42.5 R	580	580	580	580	580
Sand 0/4 mm	1750	1575	1575	1575	1575
Water	300	390	390	390	390
FA1	-	175	-	-	-
FA2	-	-	175	-	-
ESP	-	-	-	175	-
BA	-	-	-	-	175

3. Results and discussion

The fundamental physical properties of mortars are summarized in Table 3. The main effect of MSWI ashes presence in mortars is increase of porosity (and obviously related decrease of bulk density). The highest increase of porosity causes the boiler fly ash FA1. This fly ash reduces also compressive strength in the most negative way (Table 3).

Table 3: Selected fundamental, mechanical and thermal properties of mortars containing MWSI ashes.

	◎	◎$_{mat}$	◎	R_c	R_b	◎$_{dry}$	c_{dry}
	[kg/m^3]	[kg/m^3]	[%]	[MPa]	[MPa]	[W/(mK)]	[J/(kgK)]
MRef	2058	2450	16.0	53.5	5.0	1.67	826
MFA1	1820	2403	24.2	29.0	5.5	1.16	780
MFA2	1961	2517	22.1	40.0	6.0	1.16	729
MESP	1990	2546	21.8	52.5	7.0	1.27	854
MBA	1950	2516	22.5	32.0	4.5	1.23	644

The closer view on mortars' pore system provides mercury intrusion porosimetry (Figure 1). Bottom ash BA causes increase of capillary pores volume while the fly ashes act in both capillary and gel pores. It is probably due to more siliceous character of BA while more salty fly ashes are more influencing also the hydration and thus the morphology of gel pore system. Especially the most salty ESP causes significant increase in gel pores´ volume while its effect on capillary pores is not observed. Sort of strange is certain positive effect of ashes on bending strength while the compressive strength is decreasing after addition of all kinds of ashes. The decrease of compressive strength is caused by high content of sulfates in ashes which is causing sulfate corrosion of cementitious materials.

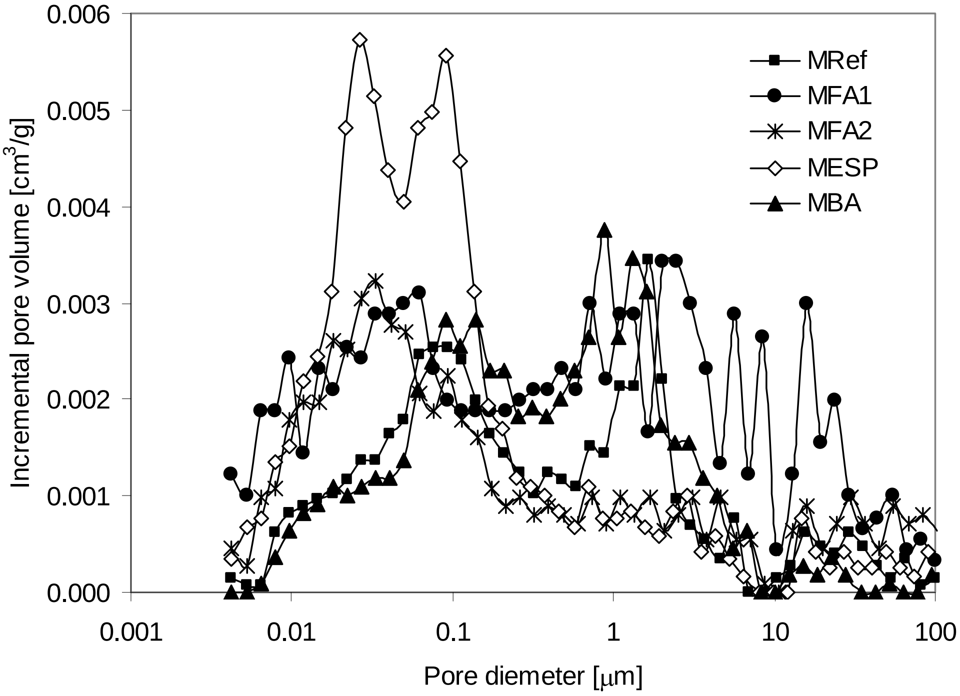

Figure 1: Dependence of thermal conductivity upon moisture and porosity of mortars.

The thermal conductivity in dried state λ_{dry} is presented in Table 3. Thermal conductivity of mortars containing ashes is significantly lower the in case of reference mortar MRef. It is in agreement with the observed higher total porosity of MSWI mortars. There are any big differences between particular ashes; their effect on thermal conductivity is roughly the same. The presented values of specific heat capacity do not able to postulate any conclusion since the used experimental method is just approximate.

In Figure 2 are plotted values of thermal conductivity as function of specific moisture content and also porosity of particular samples. The thermal conductivity of all mortars is increasing with moisture content as can be expected. This increase is faster (i.e. has higher slope) in the less porous reference mortar; the maximum moisture content was 0.08 kg/kg. The slopes of thermal conductivity increase in (more porous) MSWI mortars are lower; the maximum water content in MSWI mortars was about 0.12 kg/kg. Finally it can be observed that all MSWI mortars behave in a similar way, all points fall in a cloud.

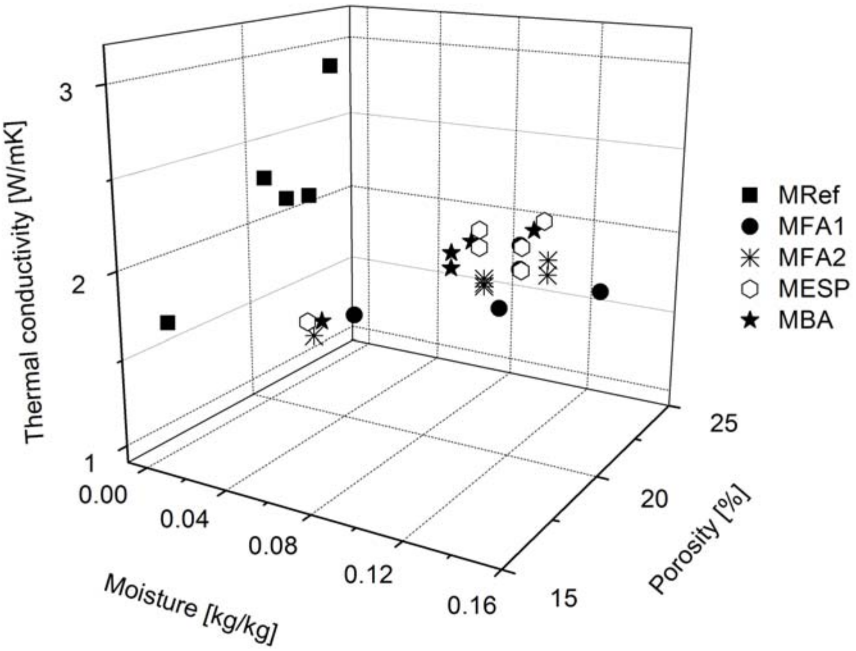

Figure 2: Dependence of thermal conductivity upon moisture and porosity of mortars.

4. Conclusions

The untreated MSWI ashes applied as partial replacement of fine aggregates in cementitious mortars influence significantly properties of mortars. All ashes reduced the compressive strength due to high content of sulfates. The effect of ashes on pore system is dependent on the ash character; while the bottom ash (it has siliceous nature) is increasing only the capillaries volume, the more salty fly ashes are influencing also the hydration processes and cause increase of both capillary and gel pores. Nevertheless the total porosity is comparable in all MSWI mortars. The thermal conductivity of MSWI mortars is lower when compared to reference mortar due to higher porosity. The effect of moisture content on thermal conductivity is positive as expected, but the increase less steep than in reference mortar.

Acknowledgments

This research has been supported by the Czech Science Foundation under projectNo. P104/11/0438.

References

[1] *Management of APC residues from W-t-E plants; An overview of management options and treatment methods*,2nd Ed., International Solid Waste Association, Copenhagen, 2008, pp 116.

[2] PERA, J. – COUTAZ, L. – AMBROISE, J. – CHABABBET, M. Use of Incinerator Bottom Ashin Concrete. In *Cement and Concrete Research*.1997. 27. p. 1–5

[3] MÜLLER, U. – RÜBNER, K. The Microstructure of Concrete Made with Municipal Waste Incinerator Bottom Ash as an Aggregate Component. In Cement and Concrete Research.2006. 36.p. 1434–1443

[4] GAO, X. – WANG, W. – YE, T. – WANG, F. – LAN, Y. Utilization of Washed MSWI Fly Ash as Partial Cement Substitute with the Addition of Dithiocarbamic Chelate. In *Journal of Environmental Management*.2008. 88.p. 293–299

[5] AUBERT, J.E. – HUSSON, B. – VAQUIER, A. Use of Municipal solid waste incineration fly ash in concrete. In *Cement and Concrete Research*. 2004. 34. p. 957 – 963

[6] FERRARIS, M. – SALVO, M. – VENTERELLA, A. – BUZZI, L. – VEGLIA, M. Use of Vitrified MSWI Bottom Ashes for Concrete Production. *Waste Management*. 29.p. 1041–1047

[7] LEE, T.C. – RAO, M.K. Recycling municipal incinerator fly- and scrubber-ash into fused slag for the substantial replacement of cement in cement-mortars.*Waste management*. 2009. 29. p. 1952-1959

[8] LEE, T.C. –LI, Z.S. Conditioned MSWI ash-slag-mix as a replacement for cement in cement mortar.In*Construction and Building materials*. 2010. 24. p. 970-979

[9] WANG, L. – JIN, Y. – NIE, Y. – LI, R. Recycling of municipal solid waste incineration fly ash for ordinary Portland cement production: A real-scale test. *Resources, Conservation and Recycling*. 2010. 54. p. 1428-1435

[10] YANG, J. – XIAO, B. - BOCCACCINI, A. R. Preparation of low melting temperature glass-ceramics from municipal waste incineration fly ash. Fuel. 2009. 88. p. 1275-1280

[11] CIOFFI, R. – COLANGELO, F. – MONTAGNARO, F. – SANTORO, L. Manufacture of artificial aggregate using MSWI bottom ash. 2011. *Waste Management*. 31. p. 281-288

[12] ČSN EN 450. Fly ash for concrete.Definition, specifications and conformity criteria.European Committee for Standardization.

[13] ČSN EN 12620. Aggregates for concrete.European Committee for Standardization.

A Transient Analysis of Water Vapor Transport in Porous Materials in Dependence on Relative Humidity

Jan Kočí, Jiří Maděra, Zbyšek Pavlík, Eva Vejmelková, Robert Černý

Czech Technical University in Prague, Faculty of Civil Engineering, Department of Materials
Engineering and Chemistry, Thákurova 7, CZ-166 29 Prague, Czech Republic

Abstract: *The knowledge of dependence of water vapor diffusion coefficient on relative humidity is crucial for application of building materials in real conditions. Material parameter obtained in this way can provide very valuable information not only for building designers, but it can be very effectively used in sophisticated simulation tools of buildings' performance. In this paper, a transient analysis of water vapor transport is presented which brings significant shortening of time necessary for experimental work. Usually, the steady state cup method requires time within a range of weeks, whereas the transient method requires less than half of that time.*

Keywords: *water vapor diffusion coefficient, cellular concrete, transient method*

1. Introduction

Water vapour transport in porous building materials has serious impact on materials' durability and service life. The presence of higher relative humidity in building materials related to high sorption properties leads to negative events like decrement of thermal insulation function, hydration of absorbed inorganic salts followed by rising of hydration pressures, and overall dampness of materials.Also the algae and fungi growth can be observed in case of high relative humidity in materials. On that account, the building engineers and researchers must deal with the problem of water vapour transport within the porous structure of building materials, and investigate the material parameters characterising the water vapour transport.

For determination of material parameters describing the water vapour diffusion in porous building materials, the steady state cup method in different experimental arrangement is the most often used technique. This method is the most popular for its simplicity and is generally considered as reliable and relatively accurate. However, back in 2004, in the framework of EU-initiated HAMSTAD project, the involved researches have referred to the necessity of improvement of the vapour diffusion experiment based on cup method. Within the HAMSTAD project, five independent laboratories studied the water vapour transmission in accordance to prEN ISO 12572 [1]. They have measured three different materials (nominally ceramic brick, calcium silicate, and cellular concrete). All three materials were measured at three different values of relative humidity and 5 samples per relative humidity were used. For all three materials the results of the different laboratories were in the same order of magnitude. However, although the experiments were carried out according to an existing ISO standard, the water vapour resistance data showed surprisingly high differences. The range between the highest and lowest values was two to four times higher than the low value. The obtained results of water vapour diffusion experiments are summarized in [2], where the authors put several possible causes for the obtained differences of measured diffusion parameters. It was found out that the calcium chloride flocks used to obtain 0% relative humidity in the cup were often not dry enough resulting in a higher relative humidity in the cup and a lower gradient across the specimen. They also remarked that the manual handling of the cups and the small distance between solution level and specimen may bring the specimens in contact with the salt solution, disturbing the results. In addition, the standard prEN ISO 12572 gives examples of different suitable cups, allowing variation in shape and cups. Whether these variations influence the measuring accuracy is not known. On this account, the authors [1] concluded that all the above given causes for the observed differences of obtained results require a further study, what should result in an improvement of the existing standards.

Although the researches involved in HAMSTAD project addressed the necessity to improve existing standards to scientific and professional community already in 2004, no further development of the steady state cup method can be observed until now. Herein, also other substantial problems of steady state cup method of water vapour diffusion parameters measurements must be stated. As the intensive research on water transmission proved, the water vapour diffusion properties depend on relative humidity in material. Therefore, the existing standards based on cup method require measurement in several pairs of relatively humidity [3]. However, from these measurements, only step-wise relationship between diffusion parameters and relative humidity is accessed within highly time-consuming experiments.

On this account one must look for a new, advanced method for determination of relative humidity dependent water vapour transport properties. This method must not be time-consuming, simple enough in experimental arrangement and sufficiently reliable.Such requirements can meet the combined experimental/computational technique presented in this paper based on measurement of relative humidity profiles and their inverse analysis using computational modelling involving genetic algorithms.

2. Combined experimental/computational technique for determination of water vapour diffusion permeability as a function of relative humidity

2.1 Experimental

For the application of computational inverse analysis, knowledge on relative humidity distribution along the sample length which is oriented in parallel to water vapour transport must be known. Therefore, an experimental apparatus for relative humidity profiles measurement within 1-D water vapour transport was devised. It consists of two airtight chambers that are separated by measured sample that has usually rod shape. The sample is provided by water vapour proof insulation on all the lateral sides what ensures 1-D water vapour flux through the studied material. In the first chamber, a state close of high relative humidity is kept while in the second one, there is a state close to 0% relative humidity. In this way, simulation of gradient of partial water vapour pressure is performed. For monitoring of relative humidity fields, the capacity hygrometric sensors are used. There are placed into the before bored holes in specific distances along the sample length in such manner that no disturbance of water vapour flux through the sample occurs. The basic schema of the apparatus is given in Figure 1. Within the measurement, the rod shaped sample having dimension 70/100/350 mm was studied. Before the measurement, 16 holes for the mini-hygrometry sensors were bored. Then, the sample was insulated on all the lateral sides by epoxy resin, dried at 60°C, and placed into the measuring apparatus. After the sensors positioning, the apparatus was hermetically closed, and the water vapour transport through the sample simulated. In the first chamber, saturated water solution of K_2SO_4 was used for simulation of high relative humidity typically close to 97 % [4]. In the second chamber, silica gel maintained low relative humidity that typically reached value close to 1.5 %. The water vapour transport was then continuously monitored and relative humidity profiles measured.

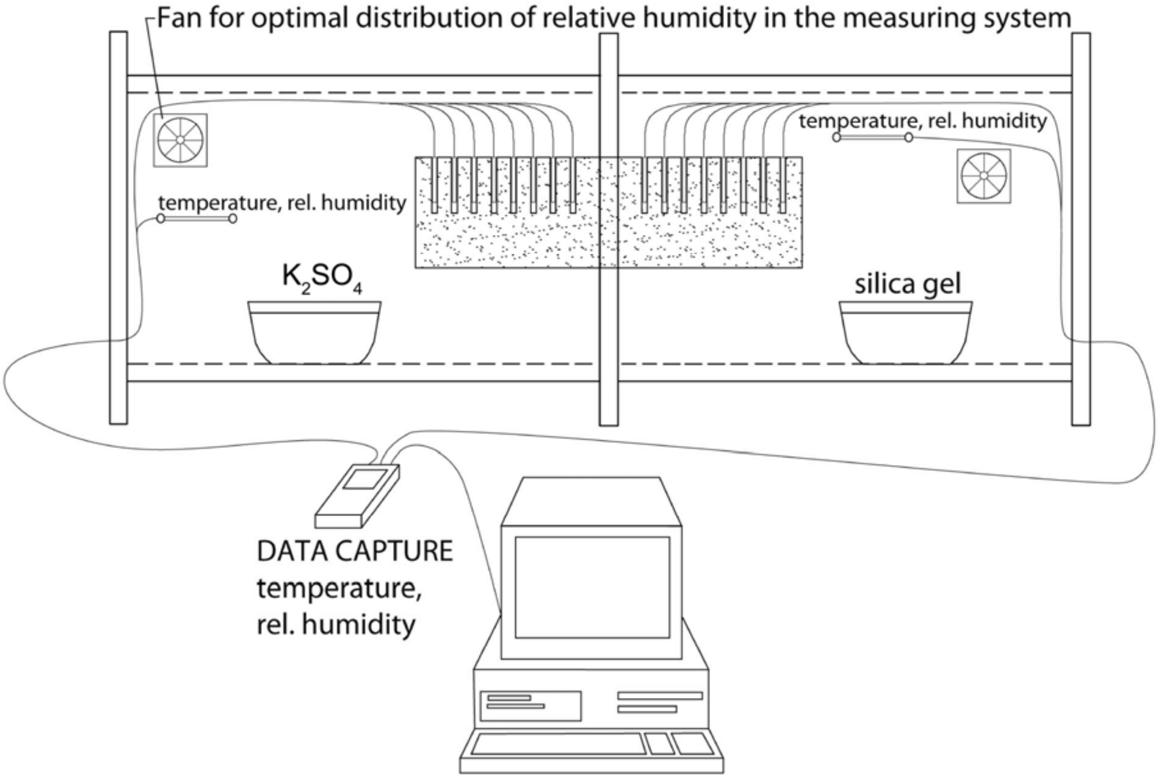

Figure 1:Experimental set-up of relative humidity profiles measurement

2.2 Computational

The measured relative humidity profiles were analysed within the coupled inverse and forward analysis that was performed using computer code HEMOT [3] and GRADE genetic algorithm [5]. Within this process, the optimised water vapour permeability vs. Relative humidity function was found by the use of GRADE code and verified by agreement between data calculated by HEMOT code and measured within the transient experiment. Within the performed calculations, also the effect of water vapour transfer coefficient on the simulated relative humidity profiles was studied.

2.3 Computer code HEMOT (Heat and Moisture Transport)

The numerical simulation tool HEMOT has been developed at the Department of Materials Engineering and Chemistry, Faculty of Civil Engineering, Czech Technical University in Prague in order to support coupled heat and water transport in porous building materials. It allows simulation of transport phenomena in constructive building details for 1D and 2D problems, whereas the basic variables characterizing the hygro-thermal state of building constructions (temperature, moisture content, relative humidity) can be obtained as functions of space and time. The mathematical formulation of coupled heat and moisture transport equations is done according to [5] and the code works on the basis of finite element method. A particular advantage of HEMOT code is the possibility of investigation of variants concerning different constructions, different materials and different climatic loads. Constructive details of buildings and building materials can be optimized using the numerical simulation, and the reliability of constructions for different given indoor and outdoor climates can be judged.HEMOT is using the material database as a data source, which simplifies computations and allows obtaining more complex results.

2.4 GRADE algorithm

Genetic algorithms belong to a group of evolution algorithms, which includes also evolution strategies and genetic programming. At present, genetic algorithms belong to the most modern optimization methods available. They follow an analogy of processes that occur in living nature within the evolution of live organisms during period of many millions of years. The principles of genetic algorithms were first proposed in [7] and the details on this technique can be found in the books by [8] and [9].

In genetic algorithm, a population of individuals (chromosomes), which encode candidate solutions to an optimization problem, evolves toward better solutions. The evolution usually starts from randomly generated population and happens in generations. In each generation, the fitness function of every individual in the population is evaluated, multiple individuals stochastically selected from the current population (based on their fitness) and modified using genetic operators (cross-over, mutation) to form a new population. The new population is then used in the next iteration of the algorithm. Commonly, the algorithm terminates when either a maximum number of generations has been produced (a satisfactory solution probably have not been reached), or a satisfactory fitness level has been reached for the population.

The GRADE algorithm [5] used for optimization of water vapour transport parameters was developed at Department of Mechanics, Faculty of Civil Engineering, Czech Technical University in Prague from its previous version called SADE [10]. Comparing to the SADE algorithm, GRADE operates with a few new features and modifications. These modifications reduce the number of external parameters of the algorithm and thus increase the convergence rate of the algorithm for smooth objective functions with just one optimum. This algorithm uses the simplified differential operator, but contrary to the differential evolution, the GRADE method uses the algorithmic scheme very similar to the standard genetic algorithm.

As the first step, the initial population is generated randomly and the objective function value is assigned to all chromosomes in the population. The size of the population is defined as the number of variables of objective function multiplied by parameter *pop_rate*.

Several new chromosomes are created using the mutation operator. Total number of mutations depends on the value of parameter called *radioactivity*.

Other new chromosomes are created using the simplified differential operator crossing-over. The total amount of chromosomes is now two times higher than in the beginning.

Each newly created chromosome is evaluated by objective function.
The amount of chromosomes in the population is reduced by operator called selection. Hence, the amount of individuals is decreased to its original value.

Steps 2-5 are repeated until stopping criterion is reached.

The scheme of optimization is shown in Figure 2.

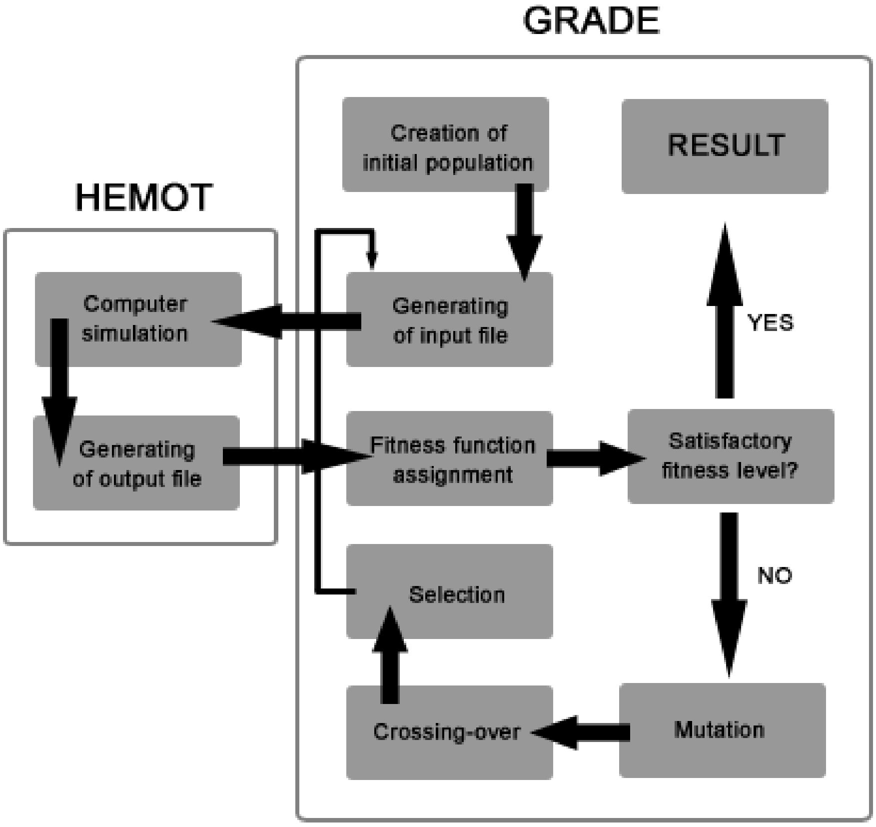

Figure 2:Scheme of optimization using GRADE algorithm and HEMOT simulation tool

3. Results and discussion

The combined experimental/computational technique described above was used for the assessment of water vapour permeability of cellular concrete as afunction of relative humidity. We used cellular concrete material P2-350 Lambda produced by Ytong.

The measured relative humidity profiles were analysed within the inverse and forward analysis process and the water vapour permeability as afunction of relative humidity optimised by GRADE algorithm was calculated. The water vapour permeability was accessed as a function given by five points only, because of the calculations severity.

In Figure 3, there are presented typical relative humidity fields measured within the transient experiment together with the relative humidity calculated by HEMOT code using the optimised water vapour permeability function. Within the computational optimisation, also the value of water vapour transfer coefficient was fitted, whereas the data presented in Figure 3 were calculated for water vapour transfer coefficient equal to 6.76E-09 s/m (with regard to partial vapour pressure). We can see relatively good agreement between measured and calculated data, where the optimised water vapour permeability function was used as input material parameter implemented into the water vapour balance equation.

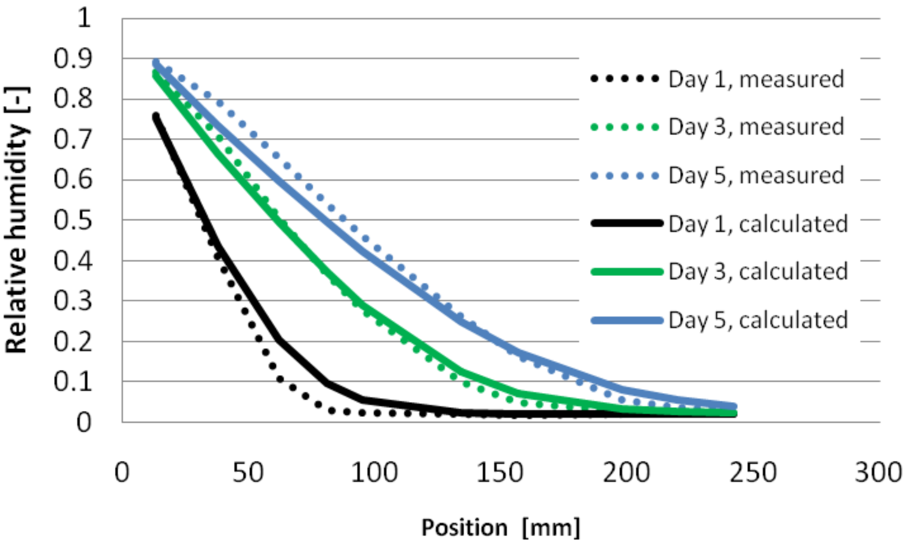

Fig 3.Relative humidity profiles measured within the transient experiment and calculated using HEMOT code

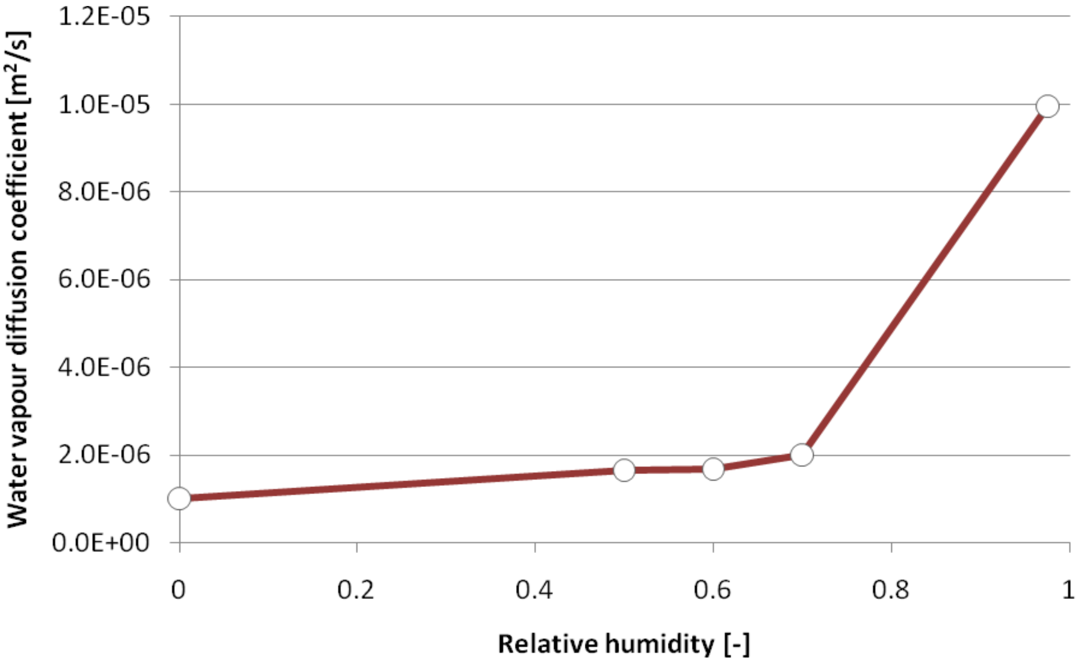

Fig 4.Water vapour diffusion coefficient of studied cellular concrete

The water vapour diffusion coefficient optimised by GRADE algorithm is presented in Fig 4. We can see its high dependence on relative humidity what is crucial for application of studied cellular concrete in building practice. In case of high relative humidity, the studied material will allow fast water vapour transport what will consequently lead to its high moistening related to volume changes, decrement of thermal insulation function etc. Especially the changes of relative humidity could lead to serious material inner mechanical loading accompanied by cracking and spalling. On the other hand, the studied material will enable management of the interior conditions of buildings from the point of view of water vapour evaporation through the building envelopes based on cellular concrete. In this way, the optimal life conditions of buildings'residentswill be ensured.

4. Conclusions

In this paper, we presented a combined experimental/computational technique for determination of water vapour diffusion coefficient dependent on relative humidity. The knowledge of dependence of water vapour diffusion coefficient on relative humidity is crucial for application of building material in real conditions. Material parameter obtained in this way provide very valuable information not only for building designers, but it can be very effectively used in sophisticated simulation tools of buildings' performance. Last but not least, the presented technique brings significant shortening of time necessary for experimental work. Usually, the steady state cup method requires time within range of weeks, whereas the transient method requires less than half of that time. Such savings of time put really high potential into the transient method and make good prerequisites for its wider application in material research.

Acknowledgements

This work has been financially supported by the Ministry of Education, Youth and Sports of Czech Republic, under project SGS10/127/OHK1/2T/11 and by the Czech Science Foundation, under grant No. 103/09/0016.

References

[1] EN ISO 12572. 2000. Hygrothermal performance of building materials and products, determination of water vapour transmission properties. The European Committee for Standardization, Brussels.

[2] ROELS S., CARMELIET, J., HENS, H., ADAN, O., BROCKEN, H., ČERNÝ R., PAVLÍK Z., HALL CH., KUMARAN K., Pel L. & Plagge R. 2004. Interlaboratory Comparison of Hygric Properties of Porous Building Materials. Journal of Thermal Envelope & Building Science, Vol. 27, No. 4, pp. 307-325.

[3] ČERNÝ R. 2010 (ed.). Complex System of Methods for Directed Design and Assessment of Functional Properties of Building Materials: Assessment and Synthesis of Analytical Data and Construction of the System. Czech Technical University in Prague, CTU Press, Prague.215 p.

[4] JIŘIČKOVÁ M. 2004. Application of TDR Microprobes, Minitensiometry and Minihygrometry to the Determination of Moisture Transport and Moisture Storage Parameters of Building Materials.CTU Prague.102 p.

[5] KUČEROVÁ A. 2007. Identification of nonlinear mechanical model parameters based on softcomputing methods. PhD thesis, Ecole Normale Supérieure de Cachan.

[6] KÜNZEL H. M. 1995. Simultaneous Heat and Moisture Transport in Building Components.PhD Thesis, Fraunhofer IRB Verlag, Stuttgart.

[7] HOLLAND, J. H. 1975. Adaptation in natural and artificial systems: an introductory analysis with applications to biology, control and artificial intelligence. Internal report. Ann Arbor: University of Michigan Press.

[8] GOLDBERG, E. D. 1989. Genetic algorithms in search, optimization and machine learning.Reading, Addison-Wesley.

[9] MICHALEWICZ, Z. 1996. Genetic algorithms + data structures = evolution programs, 3rd ed. Berlin, Springer.

[10] HRSTKA, O. (WWW). Homepage of SADE
http://klobouk.fsv.cvut.cz/~ondra/sade/sade.html

Computational analysis of energy efficiency of selected building envelopes provided with thermal insulation systems

Václav Kočí, Jan Kočí, Jiří Maděra, Robert Černý, Xinying Lu

Department of Materials Engineering and Chemistry, Faculty of Civil Engineering,Czech Technical University in Prague, Thákurova 7/2077, 166 29 Prague, Czech Republic, vaclav.koci.1@fsv.cvut.cz

Department of Civil Engineering, Tsinghua University, Beijing 100084, China

Abstract: *Energy efficiency of selected building envelopes provided with thermal insulation systems is studied in the paper. A diffusion-type model is used for the description of coupled heat and moisture transport aimed at the determination of the total energy loss/gain. The computational implementation of the model leads to a system of two non-linear partial differential equations with the moisture accumulation function as additional condition. The construction of the computer code is based on the application of the general finite element computer simulation tool SIFEL (SImple Finite ELements) developed in the Department of Mechanics, Faculty of Civil Engineering, Czech Technical University in Prague. The code can provide basic state variables (moisture content, relative humidity, temperature) as functions of space and time for a given part of building structure. Heat flux on both interior and exterior surfaces is calculated on hourly basis and integrated to obtain the total energy loss/gain. As boundary conditions, climatic data corresponding to typical years in Ostrava, Beijing and Hong Kong are applied. A set of computational simulations of hygrothermal conditions in the studied envelopes is done for different material compositions and different climates. The data analysis provides information on the most advantageous material composition with respect to the energy efficiency of thermal insulation systems.*

Keywords: *energy efficiency, building envelopes, thermal insulation systems*

1. Introduction

Thermal insulating systems are nowadays integral part of buildings. Their composition very depends on climatic conditions of building's region. Quality of thermal insulating system has positive influence on energy performance of buildings, because its major part composes from heating energy. It is impossible to use unified thermal insulating system widely; it should be designed according to the individual requirements using suitable design method to meet the conditions given by appropriate standards. Of course, the design method is also implemented in standard [1], however it does not assume the presence of moisture which is changing all the year and negatively affects thermal insulating capabilities of building envelope. In this paper, energy efficiency of several types of building envelopes under different climatic conditions is accomplished using computational analysis of coupled heat and moisture transport. That means, the moisture content is not neglected so the results are more accurate.

2. Computational analysis

2.1 Mathematical model

Künzel's mathematical model of heat and moisture transport [2] was used in the simulations which can be formulated as

$$\frac{d\rho_v}{d\varphi}\frac{\partial\varphi}{\partial t} = div\left[D_\varphi grad\varphi + \delta_p grad(\varphi p_s)\right] \tag{1}$$

$$\frac{dH}{dT}\frac{\partial T}{\partial t} = div(\lambda gradT) + L_v div\left[\delta_p grad(\varphi p_s)\right] \tag{2}$$

where ϱv is the partial density of moisture, ϕ relative humidity, δp permeability of water vapour, ps partial pressure of saturated water vapour, H enthalpy density, Lv heat of evaporation, λ thermal conductivity and T temperature,

$$D_\varphi = D_w \frac{d\rho_v}{d\varphi} \tag{3}$$

is liquid moisture diffusivity coefficient, Dw capillary transport coefficient.

The computational analysis was accomplished by computer code HEMOT, which was developed at the Department of Material Engineering and Chemistry, Faculty of Civil Engineering, CzechTechnicalUniversity in Prague on the basis of the general finite element package SIFEL [3].

2.2 Properties of materials involved in building envelope

In this paper we assumed load bearing wall made from AAC in thickness of 300 mm provided with different types of thermal insulation in thickness of 100 mm (expanded polystyrene, hydrophobic and hydrophilic mineral wool). There is 10 mm thick adhesive layer between AAC and thermal insulation. The wall is provided from interior and exterior side with 10 mm thick plaster developed especially for AAC constructions.

The values of material parameters were taken from [4 - 6] and are summarized in Table 1. We used following symbols: ϱ – bulk density [kg/m^3], ψ – porosity [%], c – specific heat capacity [J/kgK], μ – water vapor diffusion resistance factor [-], λdry – thermal conductivity in dry conditions [W/mK], λ_{sat} – thermal conductivity in water saturated conditions [W/mK], κ - moisture diffusivity [m^2/s], w_{hyg} – hygroscopic moisture content by volume [m3/m3].

Table 1: Material characteristics of involved materials

	AAC P2-400	Adhesive layer Mamut M2	Baumit MVR Uni	Expanded polystyrene	Hydrophobic mineral wool	Hydrophilic mineral wool
ϱ [kg/m^3]	412	1430	1402	50	270	71
ψ [%]	80.3	42.6	44.4	97.0	88.0	96.0
c [J/kgK]	1250-1385	1020	1020-1780	1300	630	810
μ [-]	3.7-14.4	12.4	4.5-12.4	50	2.1-3.7	4.3

λ_{dry} [W/mK]	0.094	0.481	0.443	0.040	0.045	0.043
λ_{sat} [W/mK]	0.434	2.022	1.380	0.560	0.246	0.246
κ [m^2/s]	1.12e-9	1.07e-9	1.59e-9	2.10e-11	2.51e-10	8.4e-6
w_{hyg} [m^3/m^3]	0.019	0.201	0.042	0.001	0.007	0.000046

2.3 Initial and boundary conditions

Initial and boundary conditions should be as realistic as possible. This was the reason why we used climatic data in the exterior in the form of Test Reference Year for Ostrava, Beijing and Hong Kong which contained long-term average data. They were obtained using Meteonorm software, version 6.1 [7], which is meteorological database and computer program for climatological calculations for every location on the globe.

On the interior side we used constant values of relative humidity 55% and temperature 21°C.

2.4 Energy efficiency calculations

When the energy efficiency is evaluated, the results obtained in third year of simulation are taken into account. At first, the heat fluxes in boundary elements of building envelope cross-section are calculated according to the relation

$$q = \lambda \frac{dT}{dx}, \tag{4}$$

whereq denotes the heat flux [W/m2envelope], ◎◎is thermal conductivity depending on moisture content [W/mK], dT is difference between temperatures of two nodes defining the element [K] and dx is size of the element [m].

The value of thermal conductivity is determined from calculated moisture content according to the linear function characterized by values of ◎dry and ◎sat in Table 1 of Baumit MVR Uni plaster.

The energy efficiency per annum can be then calculated as integral of time function of heat flux according to the relation

$$Q = \int_{1.Jan}^{31.Dec} q(t)dt, \tag{5}$$

whereQ denotes the energy efficiency per annum [kWh/m2envelopea] and q(t) is time function of heat flux [W/m2envelope].

3. Computational results

Figs. 1 – 3 show hourly values of heat flux on interior (red) and exterior side (blue) of building envelope. The heat flux on exterior side is much more variable because of climatic conditions, sun radiation in particular. The figures are very similar, so only the representatives are chosen. Figure 1 shows the hourly values of heat flux on interior and exterior side of building envelope provided with EPS under Beijing's climatic conditions, Figure 2 shows values of heat flux of building envelope provided with hydrophilic mineral wool under Hong Kong's climatic condition and Figure 3 shows values of heat flux of building envelope provided with hydrophobic mineral wool under Ostrava's climatic condition.

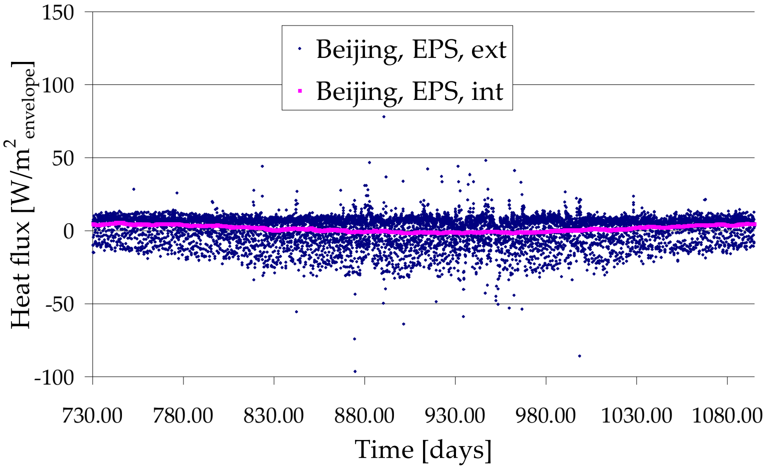

Figure 1: Heat fluxes on interior and exterior side, Beijing, EPS

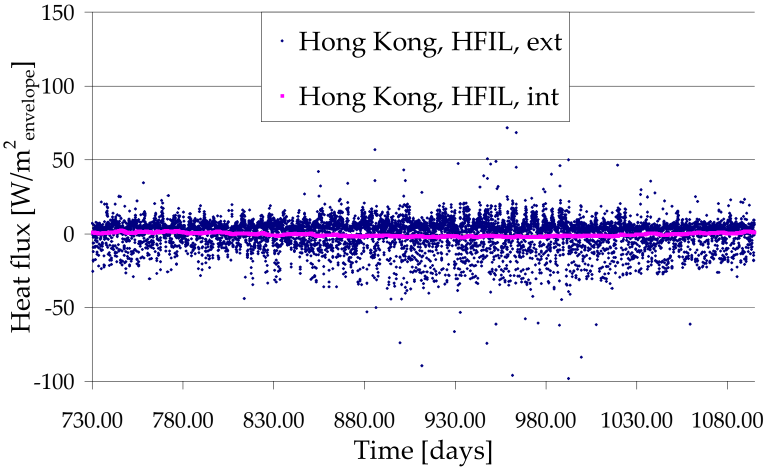

Figure 2: Heat fluxes on interior and exterior side, Hong Kong, hydrophilic mineral wool

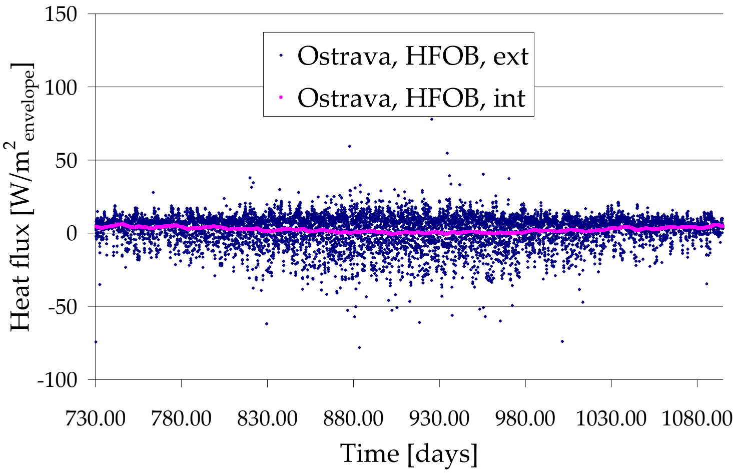

Figure 3: Heat fluxes on interior and exterior side, Ostrava, hydrophobic mineral wool

When the heat fluxes were calculated, the values of thermal conductivity depending on moisture content were used. These values on exterior side differ significantly according to the climatic region and its humidity as shows Figure 4. The values on interior side are also different but not as much as in previous case (Figure 5).

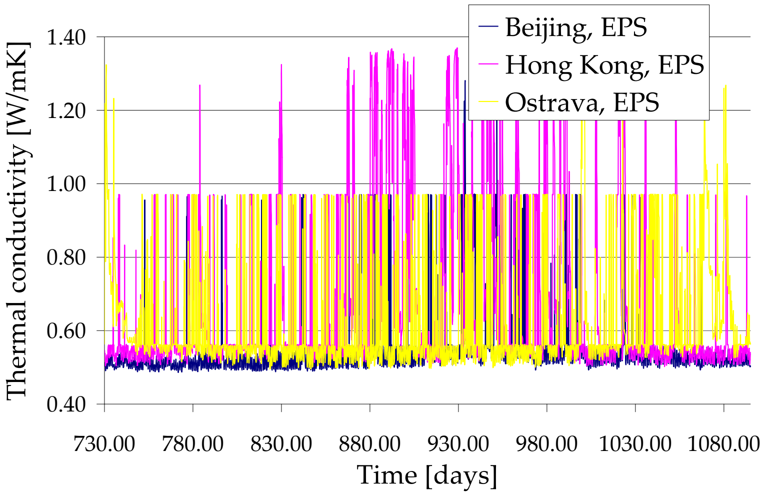

Figure 4: Values of thermal conductivity on exterior side, EPS

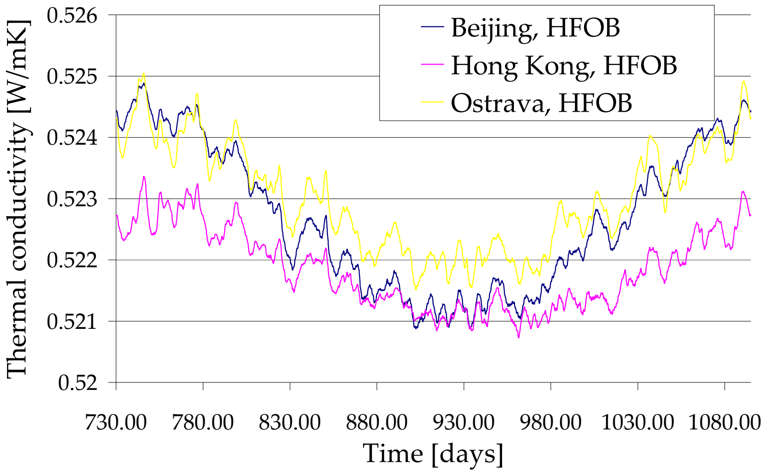

Figure 5: Values of thermal conductivity on interior side, hydrophobic mineral wool

The energy efficiency per annum given by integral of time function of heat flux is summarized in Table 2. We obtained two values, on interior and exterior side. Because the calculations were accomplished in non-steady state, these values are different. This is caused by heat accumulation inside the building envelope. As the decisive values we assumed the results on interior side which is not as affected by hourly climatic changes as the exterior side.

The plus sign of energy efficiency means the energy loss, it can be understood as the amount of heating energy necessary to keep constant values of temperature 21 °C in interior. On the other hand, the minus sign can be understood as the amount of energy consumption on cooling to keep the temperature at 21 °C.

Table 2: Energy efficiency results

	Beijing	**Hong Kong**	**Ostrava**
EPS	**14,1 kWh/m^{2}envelopea**	**-3,7 kWh/m^{2}envelopea**	**19,4 kWh/m^{2}envelopea**
Hydrophobic mineral wool	**14,9 kWh/m^{2}envelopea**	**-3,6 kWh/m^{2}envelopea**	**20,5 kWh/m^{2}envelopea**
Hydrophilic mineral wool	**15,0 kWh/m^{2}envelopea**	**-5,0 kWh/m^{2}envelopea**	**21,5 kWh/m^{2}envelopea**

4. Discussion

According to the results presented in this paper the efficiency of thermal insulations is highly dependent on climatic conditions of given region. Whereas Ostrava experiences an oceanic climate with warm summers and relatively cold winters, Beijing has monsoon-influenced humid continental climate, characterized by hot, humid summers and generally cold, windy, dry winters. As Ostrava and Beijing are cities with similar temperature development during a year, we included one more Chinese city – Hong Kong. Hong Kong has a humid subtropical climate. Summer is hot and humid with occasional showers when typhoons are most likely, sometimes resulting in flooding or landslides. Winters are mild and usually start sunny, becoming cloudier towards February; the occasional cold front brings strong, cooling winds. The most temperate seasons are spring, which can be changeable, and autumn, which is generally sunny and dry.

Whereas the thermal insulation in Ostrava and Beijing protects the buildings against cold, its function in Hong Kong is quite contrary – protects the building against warm. Thus in Ostrava and Beijing major part of energy consumption is allotted to heating, in Hong Kong to cooling (see Table 2).

The efficiency of thermal insulation is influenced by its moisture, so it can be said it depends on humidity of climate. Thus the highest efficiency is reached when insulation with lowest water saturation and moisture diffusivity and highest water vapor diffusion resistance factor is used. If these parameters of used insulation materials are compared, the most preconditions for highest efficiency has polystyrene, which was also confirmed by the computational results for Ostrava and Beijing. From that point of view, the worst option is to choose hydrophilic mineral wool, which can increase the heating costs from 6.4 to 10.1 % in relatively dry climate of Ostrava and Beijing and up to 35% under climatic conditions of Hong Kong.

On the other hand, under moist climatic conditions of Hong Kong, the thermal conductivity of saturated EPS is higher than for hydrophobic mineral wool, so better efficiency is achieved when hydrophobic mineral wool is assumed.

5. Conclusions

In this paper, the energy efficiency of several types of building envelopes under different climatic conditions has been analyzed. The envelope consisted of AAC provided with three different types of thermal insulation, namely EPS and hydrophobic and hydrophilic mineral wool. Climatic conditions of Ostrava, Beijing and Hong Kong were assumed.

The results of this paper showed, best choice from point of view of energy efficiency is to choose expanded polystyrene under Ostrava's and Beijing's climatic conditions and hydrophobic mineral wool under Hong Kong's climatic conditions. Generally can be affirmed, application of EPS is advantageous under dry climatic conditions and application of hydrophobic mineral wool is suitable only in humid climates.

All the results were achieved using computational analysis of coupled heat and moisture transport which is more advantageous than assessment according to the standards, because the liquid moisture transport is not neglected and the results are then more accurate.

Acknowledgements

This research has been supported by the Ministry of Education, Youth and Sports of the CzechRepublic, under project No ME10112.

References

[1] ČSN 73 0540. Thermal protection of buildings.Prague: Czech Office for Standards, Metrology and Testing, 2007.

[2] Künzel, H. M. Simultaneous Heat and Moisture Transport in Building Components, Ph. D. Thesis. IRB Verlag, Stuttgart. 1995.

[3] Černý, R. (ed.). Complex System of Methods for Directed Design and Assessment of Functional Properties of Building Materials: Assessment and Synthesis of Analytical Data and Construction of the System, Prague: CTU. pp. 192-201. 2010.

[4] Jerman, M., Kočí, V., Maděra, J., Výborný, J., Černý,R. Water and Heat Transport Parameters of Materials Involved in AAC-based building envelopes. In: Proceedings of the 1st Central European Symposium on Building Physics 2010. Lodz: TechnicalUniversity of Lodz, pp. 39-46. 2010.

[5] Grunewald, J. DELPHIN 4.1 – Documentation, Theoretical Fundamentals, TU Dresden, Dresden. 2000.

[6] Jiřičková, M. and Černý, R., Effect of Hydrophilic Admixtures on Moisture and Heat Transport and Storage Parameters of Mineral Wool, Construction and Building Materials, 20, 425-434, 2006.

[7] Meteonorm Version 6, software version 6.1.0.20 of April 2010, METEOTEST, Switzerland, 2010.

Computational modeling of coupled heat, moisture and salt transport in a typical building envelope

Václav Kočí[1], Jiří Maděra[2],Robert Černý[3]

Department of Materials Engineering and Chemistry, Faculty of Civil Engineering, Czech Technical University in Prague, Czech Republic, Thákurova 7/2077, 166 29 **Prague 6**

1vaclav.koci.1@fsv.cvut.cz, 2madera@fsv.cvut.cz, 3cernyr@fsv.cvut.cz

Abstract: Coupled heat, moisture and salt transport in a massive concrete structure provided with thermal insulation system is modeled using a finite-element computer simulation tool. In a set of simulation runs, the application of four different types of concrete is analyzed. It is found that from the point of view of frost resistance all the studied concretes are equivalent. From the point of view of salt accumulation, the most suitable option is to use concrete containing metakaolin as partial replacement of Portland cement.

Keywords: coupled heat, moisture and salt transport, service life, building envelope, computational modeling

1. Introduction

Degradation of building materials is caused by many factors. The most principal are chemical and mechanical corrosion. As a mechanical corrosion we can assume the influence of weather conditions, particularly the destruction effect of freezing water which is contained in building materials. Phase conversion of water goes along with volume increase and this is the main mechanism leading to material destruction.

Building materials can be frost-resistant in varying degrees which depends on their material characteristics. The frost resistance could be defined by experimental methods. However, more complicated is to determine the amount of freezing cycles which arise during the year in real building structure. Freezing cycle can appear only when two conditions are met. The first condition is the presence of overhygroscopic (liquid) moisture, the second a temperature below water freezing point. So we have to observe the hygrothermal performance of studied material and compare the thermal and hygric state in parallel. Computational analysis is the best instrument for this operation. The amount of freezing cycles depends in the first instance on climatic conditions and material composition used in building envelope.

Under real conditions, there are salts transported together with water as well. To obtain results as realistic as possible, it is necessary to implement transport of salts into used computational model. In this paper we are dealing with service life of different types of concretes. Simultaneously with water and heat transport, salt transport is considered as well. Salt presence affects service life of concretes in two ways: salt crystallization can cause mechanical destruction of concrete or can negatively affect its hygric performance. These two mechanisms are taken into account when service life is estimated.

2. Experimental

Determination of frost resistance of concretes and exterior render was accomplished at Brno University of Technology [1] under laboratory conditions. As the original reference is in Czech language and may not be accessible for the majority of readers, we will present some details of the measuring procedure here.

For lime-cement plaster (LCP), the specimens in size of 40 × 40 × 160 mm were made, for concretes 100 x 100 x 400 mm. Temperature in the laboratory was 21±1°C, relative humidity was 45±5%. Frost resistance tests of both LCP and concretes - concrete modified by fly ash (CF), metakaolin (CM), slag (CS) and reference concrete without any modification (CR) - were carried out according to ČSN 73 1322/Z1:1968 [2]. The samples were tested after 28 days of concrete maturing and standard curing. The total test required 100 freezing and thawing cycles. One cycle consisted of 4 hours freezing at -20°C and 2 hours thawing in 20°C warm water. The results of frost resistance tests are presented in Table 1.

Table 1: Number of freezing cycle causing damage of material

	LCP	**CF**	**CM**	**CS**	**CR**
Number of freezing cycles	**> 103**	**> 100**	**> 100**	**> 100**	**> 100**

3. Computational

3.1 Description of the building envelope

In this paper we assumed concrete wall made of different types of concrete (CF, CM, CS or CR) provided with thermal insulation system (mineral wool). The wall was provided with lime-cement plaster on interior and exterior side. By the same token we assumed the cases when the thermal insulation system was not present. The material combination is shown in Figure 1.

Hygrothermal performance was investigated in concrete in a point close to the interface with render.

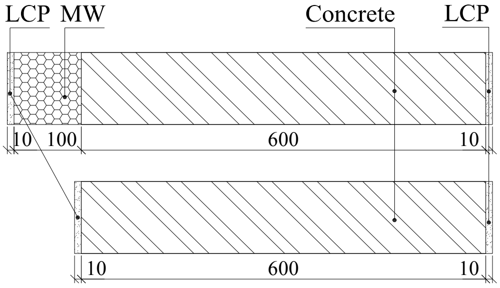

Figure 1: Scheme of concrete wall

3.2 Input parameters

As the input parameters we need to know characteristics of used materials, boundary and initial conditions.

Basic material characteristics of analyzed materials are shown in Table 2 and Figure 2. We used following symbols: ϱ – bulk density [kg/m^3], ψ– porosity [%], c – specific heat capacity [J/kgK],

μ – water vapor diffusion resistance factor [-], λdry – thermal conductivity in dry conditions [W/mK], λsat – thermal conductivity in water saturated conditions [W/mK], κ - moisture diffusivity [m^2/s], whyg – hygroscopic moisture content by volume [m^3/m^3], D - salt diffusion coefficient [m^2/s]. All these parameters were measured in laboratory of transport processes at the Department of Materials Engineering and Chemistry, Faculty of Civil Engineering, Czech Technical University in Prague [3, 4].

Table 2: Basic material characteristics of concretes

	CF	CM	CS	CR	LCP	MW
ϱ [kg/m^3]	2356	2366	2334	2380	1550	170
ψ [%]	12.5	13.0	9.7	12.3	40	89
c [J/kgK]	692	728	720	672	1200	840
μdry cup [-]	44.63	32.44	17.70	15.80	7	3
μw.10t cup [-]	17.18	20.99	8.99	6.60	0.7	0.055
λdry [W/mK]	1.550	1.565	1.632	1.660	2.4	1.2
λsat [W/mK]	1.940	2.085	2.077	2.085	$7.3.10^{-7}..10^{3}.2w$	$5.1.10^{-10}..10^{3}.12w$
κ [m^2/s]	$6.49.10^{-9}$	$4.09.10^{-9}$	$3.77.10^{-9}$	$7.15.10^{-9}$	0.03	0.0073
whyg [m^3/m^3]	0.074685	0.106943	0.089000	0.083300	$8.97.10^{-7}$	4.10^{-11}
D [m^2/s]	$6.88.10^{-8}$	$7.98.10^{-8}$	$9.85.10^{-8}$	$1.9.10^{-7}$		

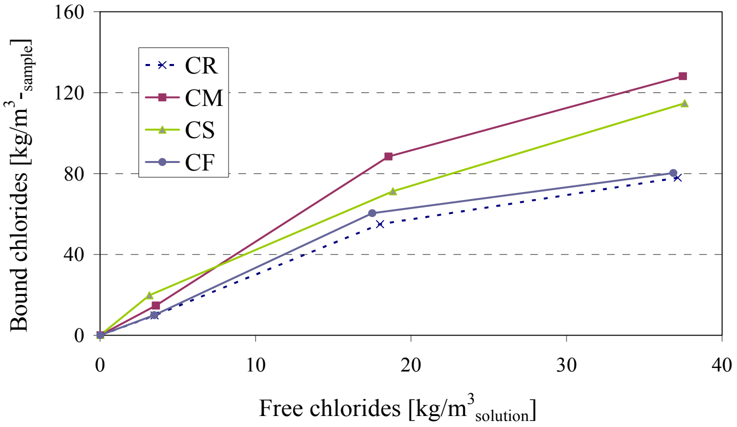

Figure 2: Chloride binding isotherms of used types of concrete

3.3 Computational model

A diffusion-advection model is used for basic description of coupled heat, moisture and salt transport in porous building materials, taking into account both water movement due to the moisture gradient and dispersion effects within the liquid phase due to the concentration gradient. Salt crystallization in the porous body is modeled using an equilibrium model. The effect of salt bonding on the pore walls is taken into account as well. The original moisture and salt transport modeling treatment chosen by Pel et al. [5] was modified and extended. The basic idea that the mechanism of salt solution transport can be described by Bear and Bachmat diffusion-advection model [6] taking into account not only the influence of moisture flow on salt transport but also the effect of salt bonding on pore walls is preserved. In addition to the effects taken into account in the original model from Pel et al. [5], salt crystallization and water vapor transport are introduced into the model. Also, contrary to the model of Pel et al. [5] the dispersion effects in the liquid phase are considered as significant. The heat transport is included as well. The modified mathematical model can be formulated as follows:

$$\begin{aligned}&\frac{\partial (wC_f)}{\partial t} H(C_{f,sat} - C_f) = \\ &= \frac{\partial}{\partial x}\left(wD \frac{\partial C_f}{\partial x}\right) + \frac{\partial}{\partial x}\left(C_f \kappa \frac{\partial w}{\partial x}\right) - \frac{\partial C_b}{\partial t} - \frac{\partial C_c}{\partial t}\end{aligned} \tag{1}$$

$$\frac{\partial w}{\partial t} = \frac{\partial}{\partial x}\left(\kappa \frac{\partial w}{\partial x}\right) + \frac{\partial}{\partial x}\left(\frac{\delta}{\rho_w} \frac{\partial p_v}{\partial x}\right) \tag{2}$$

$$\frac{\partial C_c}{\partial t} = \frac{\partial \left[w\left(C_f - C_{f,sat}\right)\right]}{\partial t} H\left(C_f - C_{f,sat}\right) \tag{3}$$

$$\rho c \frac{dT}{dt} = \frac{\partial}{\partial x}\left(\lambda \frac{\partial T}{\partial x}\right) + \frac{\partial}{\partial x}\left(L_v \delta \frac{\partial p_v}{\partial x}\right) \tag{4}$$

where Cf is the concentration of free salts in water [kg/m3 of the solution], Cb the concentration of bonded salts in the whole porous body [kg/m3 of the sample], D the salt diffusion coefficient [m2/s], w the volumetric moisture content [m3/m3], κ the moisture diffusivity [m2/s], Cc the amount of crystallized salt [kg/m3 of the sample], Cf,sat the saturated free salt concentration [kg/m3 of the solution], H the Heaviside step unit function, H(x≥0)=1, H(x<0)=0, δ the water vapor diffusion permeability [s], pvthe partial pressure of water vapor [Pa], ϱw the density of water [kg/m3], Lvthe latent heat of evaporation of water [J/kg],λ the thermal conductivity [W/mK], ϱ the bulk density [kg/m3], c the specific heat capacity [J/kgK] and T the temperature [K].

3.4 Boundary and initial conditions

Initial and boundary conditions should be as realistic as possible. This is the reason why we used wide climatic data set for the exterior. The most reliable results were achieved with Test Referent Year (TRY) for Prague, which contained average climatic data for 30 years. On interior side we used constant value of relative humidity 55 % and temperature 21°C.

Initial relative humidity of used materials was set on 50%, initial temperature on 21 °C and initial concentration of free chlorides was 10 kg/m3 of the solution. When salt source was not assumed, simulation was done for 5 years. When salt source was assumed, the simulation was done for 150 years.

3.5 Source function of salt transport

Before modeling of salt transport can be started, it is important to describe source function at first. It is further necessary to know, which way the salt is getting into the construction. There are several possibilities: chemical reactions of building material and environment, usage of building, activities of living organisms, etc. The most significant influence has salt dissolved in water penetrating into building. Amount of salt dissolved in water depends on local conditions, but it can be much higher due to human activities, especially due to application of de-icing salt, which is source of chlorides first of all.

As the source function has not been ever published and its shape is depending on local conditions, we had to estimate it based on set of input parameters. We went from public notice, which determines amount of de-icing salt (NaCl) to 20 g/m2 in one road spreading (day limit is 60 g/m2). Based on evaluation of temperature (Figure 3) and rainfall (Figure 4) from long-term climatic data, we determined average amount of snowfall during reference year relative to particular hours. In these hours we took using de-icing salt as granted. This led to increase of salt concentration in water which has impact on salinity of building masonry.

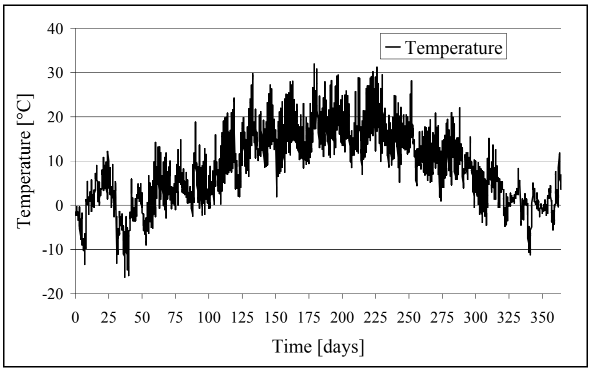

Figure 3: Long-term climatic data – temperature

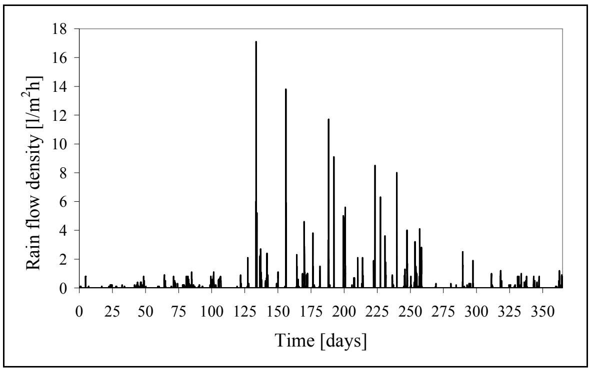

Figure 4: Long-term climatic data – rainfall

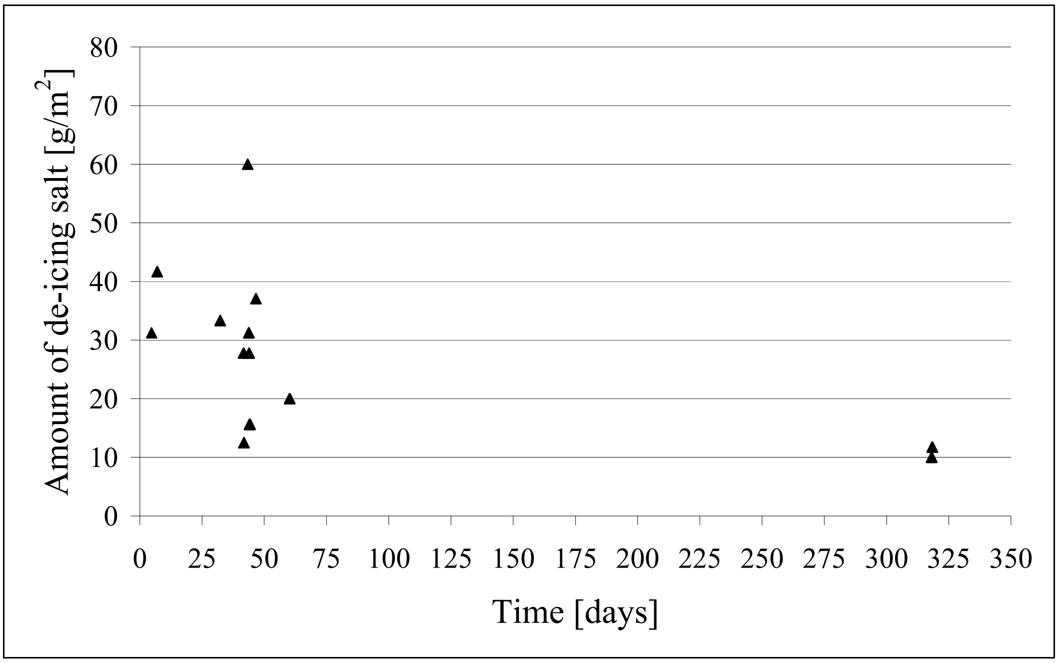

Figure 5: Amount of applied de-icing salt

Figure 5 shows average amount of applied de-icing salt during one year. Threshold of crystallization of chlorides is 189 kg/m3solution which correspond to maximal solubility of chlorides.

4. Computational results

4.1 Concrete wall provided with exterior render

The most predisposed type of concrete to creation of freezing cycles is the reference concrete. However, due to low moisture content during the studied period there is not any freezing cycle. Overhygroscopic moisture content is reached only in summer months when the temperature is above zero.

In concrete modified by fly ash, the overhygroscopic moisture content is reached once per a reference year, but as in the previous case this happens in summer month so there are not any possibilities of creation of freezing cycles. In other types of concrete the overhygroscopic moisture content is not reached at all. All the results are similar to result on Figure 6.

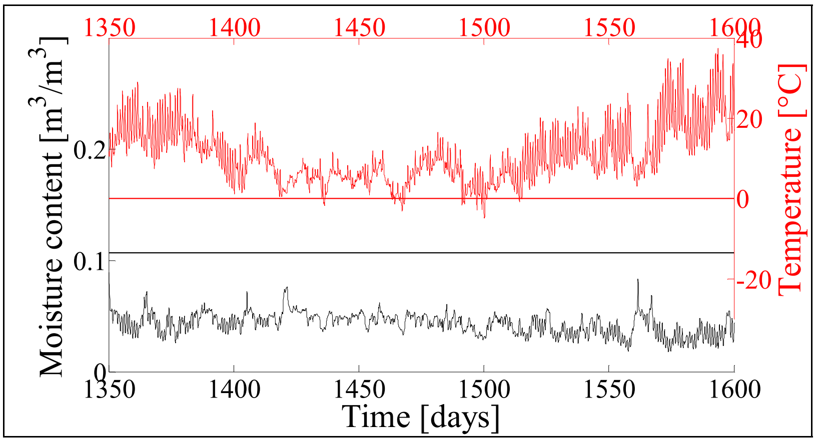

Figure6: Time dependence of temperature and moisture content in CM, no salt source considered

In Figure 7, the steady-state of salt concentration (when no salt source was under consideration) in CM is presented. When salt source is considered, distribution of salt amount during 150 years of simulation is shown in Figure 8. Increase of salt concentration more in detail is presented in Figure 9.

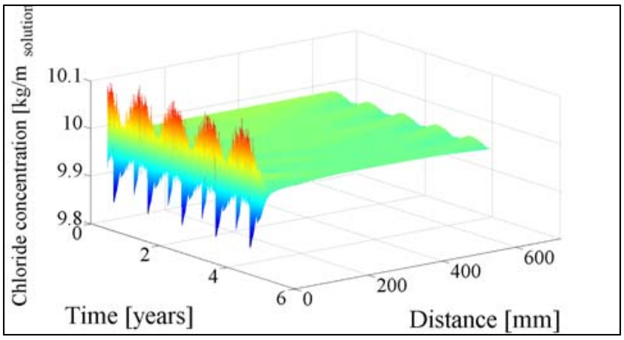

Figure 7: Steady-state of salt distribution in CM, no salt source

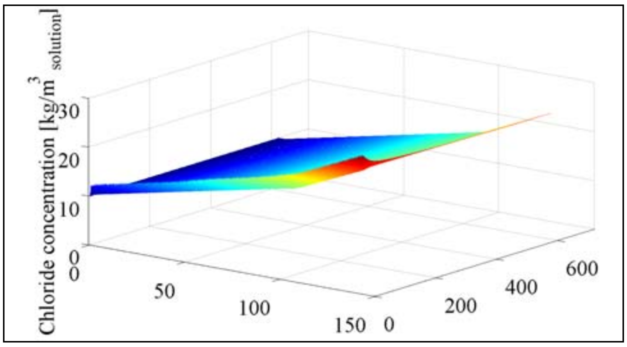

Figure 8: Increase of salt concentration in CM considered during 150 years, salt source

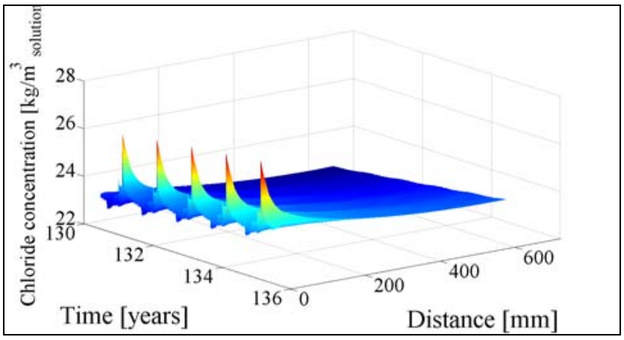

Figure 9: Increase of salt concentration in CM between 130th and 135th year, salt source considered

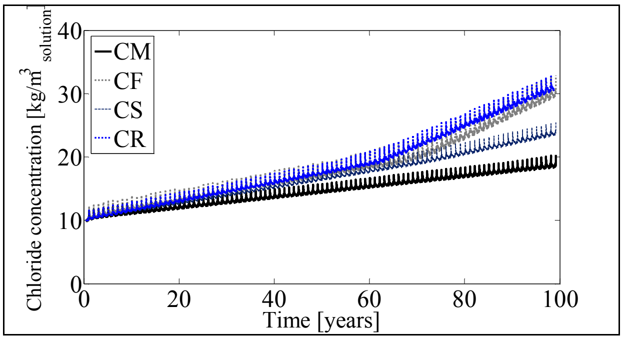

Figure 10: Rate of salt concentration increase in different types of concrete provided with exterior render

In case of other types of concretes when salt source is under consideration, the shape of curve of salt concentration increase is almost identical, only differences are in rate of increase, which is shown in Figure 10.

As it is shown in Figure 10, best results from the point of view of salt accumulation are achieved, when concrete modified by metakaolin is used. On the other hand, the worst results are observed when reference concrete is considered.

4.2 Concrete wall provided with mineral wool and exterior render

In this material combination, mineral wool prevents temperature in concrete to drop below zero. Contained water is then not allowed to get frozen practically in all types of concrete. Typical hygrothermal behavior of all types of concretes is presented in Figure 11.

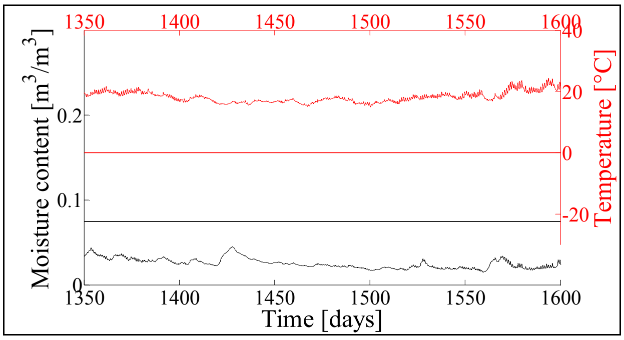

Figure 11: Time dependence of temperature and moisture content in CF provided withmineral wool, no salt source considered
no salt source considered

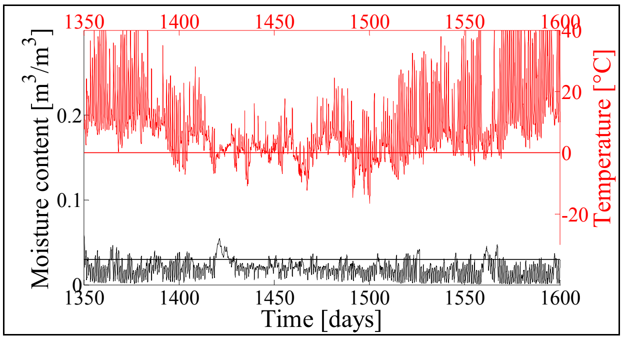

Figure 12: Time dependence of temperatureand moisture content in exterior render applied on CF provided with mineral wool,

While concrete is reliably protected against effects of freezing water, exterior render is exposed to abnormal strain thanks to low moisture diffusivity of mineral wool. This causes that number of freezing cycles in exterior render during one year is about 25 in all types of concrete, no matter if salt source is considered. Typical hygrothermal behavior of exterior render is presented in Figure 12.

Influence of mineral wool on salt accumulation in concrete is not too significant. When salt source is considered, distribution of salt amount during 150 years of simulation is shown in Figure 13. Increase of salt concentration more in detail is presented in Figure 14.

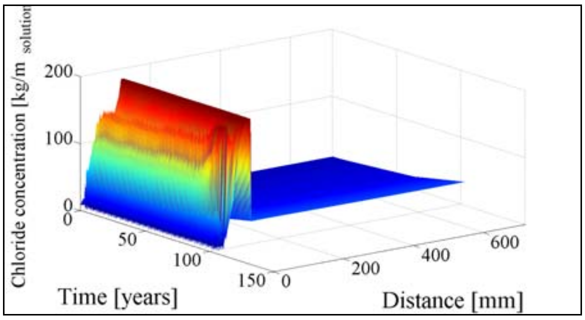

Figure 13: Increase of salt concentration in CF during 150 years, salt source considered

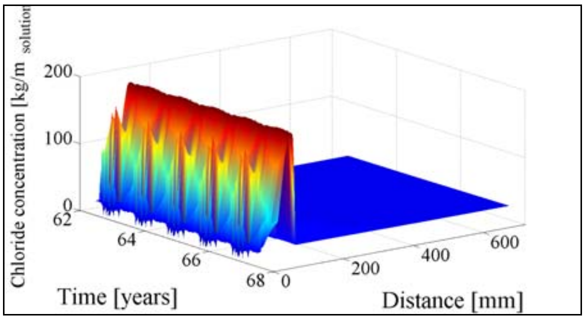

Figure 14: Increase of salt concentration in CF between 62nd and 67th year, salt source considered

In case of other types of concretes when salt source is under consideration, the shape of curve of salt concentration increase is almost identical, only differences are in rate of increase, which is shown in Figure 15.

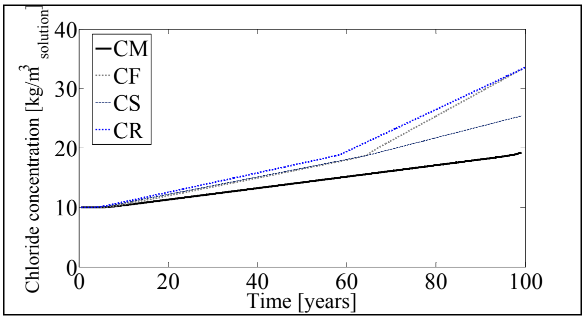

Figure 15: Rate of salt concentration increase in different types of concrete provided with mineral wool and exterior render

Best results are achieved again when concrete modified with metakaolin is considered. Worst results from the point of view salt accumulation gives reference concrete and concrete modified by fly ash.

5. Discussion

In this computer simulation only the liquid moisture appearance caused by rain was considered. However, there can be locations on building, which are exposed to water originating from other sources. This can be the case of a socle part of building and places with wrong construction details solution. In these cases, the number of freezing cycles during one year could be much higher.

Although concrete wall built from all the types of investigated concrete provided with exterior render does not show indications of freezing of the contained moisture, the wall made from reference concrete is very close to it. As we considered only reference year which is based on long-term average of relative humidity and temperature, the freezing cycles cannot be completely excluded in every particular year; in real weather conditions deviations from the average values may appear which could lead to creation of some freezing cycles. Basically, this is caused by the low value of moisture diffusivity of concrete which does not allow for a relatively fast release of contained moisture.

If we investigate concrete wall provided with thermal insulation system, namely mineral wool, due to propitious thermal insulating properties the temperature in the concrete will never drop below zero which makes freezing of water impossible. However, mineral wool has very low value of moisture diffusivity. Therefore, the moisture can not be transported to concrete in sufficient amount and its amount in exterior plaster remains relatively high for long time. The exposure to low temperatures causes then freezing of this water.

Results of simulation show that amount of salt contained in building construction does not have significant influence on hygric behavior of used materials. However under real conditions, the influence of salts on hygric behavior could be expected. This phenomenon was not revealed because of missing dependence of sorption isotherms on salt concentration of building materials.

As the results show, modification of concrete has significant impact on salt accumulation. Best behavior was achieved with modification by metakaolin, worst results with modification by fly ash or without any modification. This is corresponding to shape of chloride binding isotherms shown in Figure 2. However, threshold of chlorides crystallization is reached in more than 400 years in all cases, so in overall durability considerations is salt crystallization not the limiting factor.

6. Conclusions

An assessment of the service life of new types of concrete using combined computational-experimental approach was presented in the paper. In the experimental part, durability of selected concretes was determined in terms of their frost resistance. A diffusion-type model was used for the description of coupled heat, moisture and salt transport aimed at the identification of the number of frost cycles in a real structure. In a practical application of the model, a concrete wall provided with exterior thermal insulation system and both exterior and interior renders was analyzed. Influence of salt presence on hygrothermal performance of used building materials was evaluated.

Acknowledgements

This research has been supported by the Ministry of Education, Youth and Sports of the CzechRepublic, under project No MSM: 6840770031 and SGS10/128/OHK1/2T/11.

References

[1] ONDRÁČEK, M. – SEDLMAJER, M. - ROVNANÍKOVÁ, P. Mrazuvzdornost a odolnost proti CHRL vysokohodnotných betonů s alternativními silikátovými pojivy. Sborník mezinárodní konference 14.Betonářské dny 2007, Hradec Králové, 2007. ČBS ČSSI, pp. 427-431.

[2] ČSN 73 1322/Z1:1968, Concrete testing – Hardened concrete – Frost resistance. Czech Standardization Institute, Prague. 2003.

[3] JIŘIČKOVÁ, M. - ČERNÝ, R. Effect of Hydrophilic Admixtures on Moisture and Heat Transport and Storage Parameters of Mineral Wool. Construction and Building Materials, Vol. 20, pp. 425-434. 2006.

[4] VEJMELKOVÁ, E. - KEPPERT, M. - PAVLÍKOVÁ, M. - ČERNÝ, R., ONDRÁČEK, M. - SEDLMAJER,, M. Effect of alternative silicate binders on properties of cement-based composites. Energy Efficiency and New Approaches. Proceedings of the Fourth International Building Physics Conference, Istanbul: Beysan Matbaacilik ve Reklamcilik, pp. 25-32. 2009.

[5] PEL, L. - KOPINGA, K - Kasschieter E. F. Saline absorption in calcium-silicate brick observed by NMR scanning, J. Phys. D: Appl. Phys., Vol. 33, pp. 1380–1385. 2000.

[6] BEAR, J. - Bachmat, Y. Introduction to Modeling of Transport Phenomena in Porous Media, Vol. 4, Kluwer, Dordrecht. 1990.

Computational and experimental analysis of heat and moisture transport in a critical detail of a contact thermal insulation system

Jan Kočí, Zbyšek Pavlík, Robert Černý

Department of Materials Engineering and Chemistry, Faculty of Civil Engineering, Czech Technical University in Prague, Thákurova 7, 166 29 Prague, Czech Republic

e-mail: jan.koci@fsv.cvut.cz

Abstract: *Computational modeling represents useful tool for the assessment of thermal function of newly designed building materials and structures. However, the accuracy of computer simulations is strictly dependent on the reliability of input data. Among them, especially experimental determination of material parameters represents the most serious problem from the point of view of their availability and sufficient accuracy. On that account, the computer codes used for simulations of thermal performance of investigated structures and materials must be firstly calibrated for specific studied conditions. In this paper, a semi-scale experiment simulating a critical detail of a contact thermal insulation system is used in the calibration of a computer simulation tool for modeling coupled heat and moisture transport in building materials.*

1. Introduction

Mathematical models of heat and moisture transport are very effective tools in the prediction of hygrothermal performance of building envelopes, and they are logically frequently used in scientific envelope design at present. On that account, several computer codes enabling simulation and assessment of hygric and thermal building's function were developed until now. During the past twenty years, researches have made significant advances in the development of Heat, Air, and Moisture Transport (HAM) models [1] and several computer models and codes are now commercially or publicly available to the users. As examples of this type of codes Delphin [2, 3], LATENITE, MOIST, TCCC2D [4, 5], hygIRC [6], WUFI [7], TRANSMAT [8] can be mentioned.

Although these computer codes are considered to be universal and reliable, certain limitations of their application have to be given. It must be taken into account that any computational code can provide reliable information only in the case that the quality of input data is very good. This is not always true, because the standard lists of thermal and hygric material parameters are often not complete, and also do not include the dependencies on basic state variables of heat and moisture transport. In addition, the models always work with some parameters, which are not known explicitly (for instance hygric and thermal interface and surface resistances), and often neglect some effects (for instance Soret and Dufour effects), which can possibly be important under specific conditions. Therefore, the models have to be tested very thoroughly before they can be applied to the serious analysis and modeling of long-term hygric and thermal performance of building materials and their multi-layered systems.

The laboratory measurement of thermal and hygric transport and storage properties in the necessary range of external conditions is the first unavoidable condition for a proper application of any mathematical model. Experimental determination of temperature and moisture fields in building envelopes for the sake of calibration of a particular mathematical model is the second critical task. For this purpose, the field measurement of temperature and moisture fields on a building site can be used. In this way, the hygrothermal performance of a particular structure can be assessed, as well as effectiveness of newly developed materials and technological solutions. Also the validation and calibration of mathematical models of coupled heat and moisture transport in porous building materials and components can be done.

Monitoring temperature and moisture fields on building sites will certainly always remain the final and decisive stage of testing the performance of building structures. However, it should really be considered as the final step, when all principal problems are already resolved and the risk of failure is minimal. The costs of building a special test house are quite high and using private buildings for testing purposes might result in difficult problems if the designed solutions do not work as expected.

A semi-scale experiment for testing the hygrothermal performance of a building structure presents a logical bridge filling the gap between the laboratory measurements of hygrothermal properties and full-scale test house measurements of field variables of heat and moisture transport. A semi-scale measuring system for determination of temperature and moisture fields [9] should be designed in such a way that it simulates conditions, which are as close as possible to the real conditions on a building site, but it should still maintain its laboratory character, so that the expenses can be kept considerably lower compared to a real test house. If these requirements are well met, the application of flexible semi-scale testing systems can be considered as a reasonable solution for the improvement of the model validation and calibration procedure.

In this paper, semi-scale testing of a critical detail is employed for obtaining the basic information on hygrothermal performance of a building envelope system with newly designed interior thermal insulation. This information is utilized in improvement of the input data of the computer code TRANSMAT 6.2 for simulation of combined heat and moisture transport. Long-term hygrothermal performance of the analyzed envelope is then simulated using the code TRANSMAT 6.2 with improved input data so that the accuracy of the performed calculation is done on higher level.

2. Semi-scale experiment

2.1 Semi-Scale Testing System

For investigation of hygrothermal performance of the building structure studied in this paper, the semi-scale measuriement system NONSTAT was utilized. The NONSTAT system consists of two main parts, namely the climatic chambers’ system and the monitoring and data storage part. The climatic chambers’ system is composed of two Feutron climatic chambers for simulation of semi-real climatic conditions very close to reality (temperature and relative humidity changes are simulated) and by connecting tunnel for placing the tested structure. If the tested specimen is sealed in the tunnel, the moisture and heat transport can be simulated in the tested structure. For simulation of rainfall, the optional sprinkler device can be used. For measurement of heavy specimens, the testing tunnel is supported by hydraulic trolley. The schematic view of the applied semi-scale system is given in Figure 1.

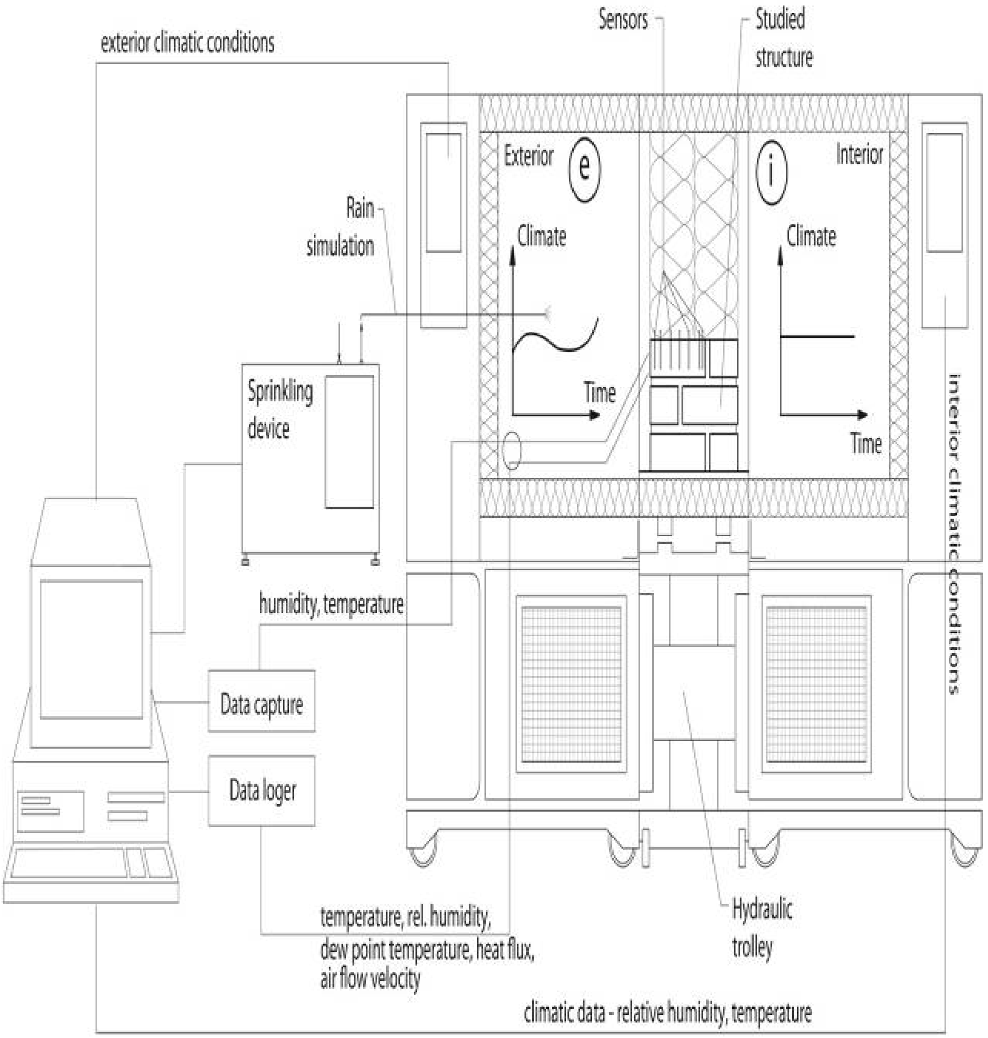

Figure 1: Schematic description of applied semi-scale system

In the presented experiment, monitoring of relative humidity and temperature changes in the specific places of the studied construction detail was done. For this purpose, sophisticated system of probes produced by Ahlborn was used. The accuracy of particular sensors was as follows: capacitive relative humidity sensors applicable in the range of humidities 5-98 % ±2 %, temperature resistance sensors ± 0.4°C in the temperature range from –20 °C to 0°C, and± 0.1 °C in the range from 0°C to 70°C. The whole measuring system was operated by a computer, including the climatic data entry into the exterior climatic chamber. The details on the system including the measuring technology can be found in [9, 10].

2.2 The Studied Construction Detail of Building Envelope

A new type of interior thermal insulation system on the basis of the hydrophilic mineral wool was analyzed in the semi-scale experiment. The insulation system was applied on the fragment of the brick wall with part of the window frame and glazing. The composition of the investigated building envelope was formed from the exterior to the interior by load bearing structure - brick wall 600 mm thick, water vapor retarder KAM (Sakret) on cement glue principle in the thickness of 10-15 mm, dual density hydrophilic mineral wool based insulation material DU (Rockwool) of 100 mm thickness, and water vapor permeable plaster FFP (Sakret) with the thickness of 15 mm. Figure 2 shows the simplified 1-D the scheme of the tested structure.

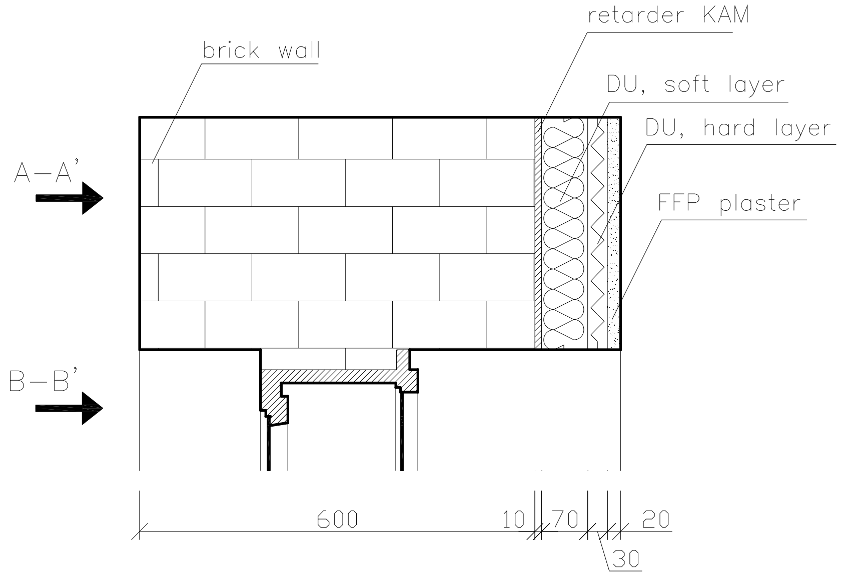

Figure 2: Scheme of the studied structure including investigated cross sections

2.3 Sample Arrangement and Measuring Technology

The process of sample preparation can be divided in three phases: walling the studied structure, installation of the probes to the sample, and positioning of the sample into the tunnel between climatic chambers. The walling of the studied structure was done in the standard way using dry retarder and plaster mixtures and wet technological process. The sensors for monitoring temperature and relative humidity were placed to the investigated construction to beforehand bored holes. The upper part of the bore opening was closed by silicon sealing. The placing of the sensors was done regarding to the complete knowledge on relative humidity and temperature distribution in the studied detail and with respect to possible condensation zones. The placing of the sensors is closely described in the next part of this paper, where computer generated mesh was adjusted to sensors positioning.

After positioning all sensors, the prepared sample was placed into the connecting tunnel, which was then connected by sleeve connectors with the climatic chambers. The sample, placed into the connecting tunnel, was thermally insulated from the tunnel wall using extruded polystyrene boards in combination with mineral wool and provided with a water- and water vapor-proof coating. In this way, 1-D moisture and heat transport was ensured (Figure 3a, b).

When the climatic chambers were connected, the climatic conditions in both of them were set up. In the chamber, which should simulate interior climatic conditions, the constant conditions typical for common residential houses were chosen. In the chamber, simulating exterior climatic conditions, the real climatic data of temperature and relative humidity of the reference year for Prague, Czech Republic, were used. The data corresponded to time interval of October 10 to February 14. In this way, the most unfavorable winter climatic conditions were simulated.

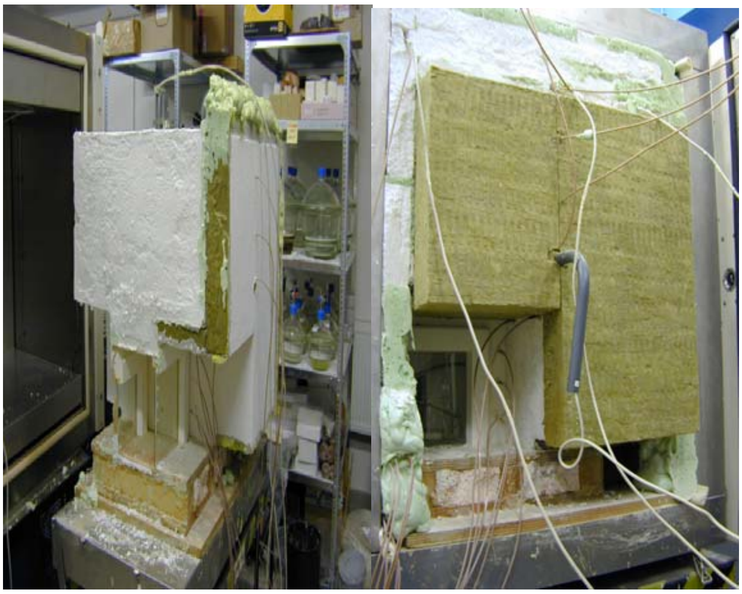

Figure 3a, b Sample arrangement

3. Computational analysis and code validation

Within the computational analysis of experimental situation, validation of computer code TRANSMAT 6.2 was done. This simulation tool was originally developed in Department of Materials Engineering and Chemistry, Faculty of Civil Engineering, Czech Technical University in Prague in order to support the investigation of the coupled heat, moisture and salt transport in porous building materials [11, 12]. It enables simulation of thermal and hygric behaviour of constructive building details in 1-D or 2-D arrangement. The construction of the code is based on the application of the general finite element computer simulation tool SIFEL (SImple Finite ELements) developed in the Department of Mechanics, Faculty of Civil Engineering, Czech Technical University in Prague [13]. Using this code, the basic variables characterizing the hygrothermal state of building structures (temperature, moisture content, relative humidity, salt concentration) can be obtained as functions of space and time.

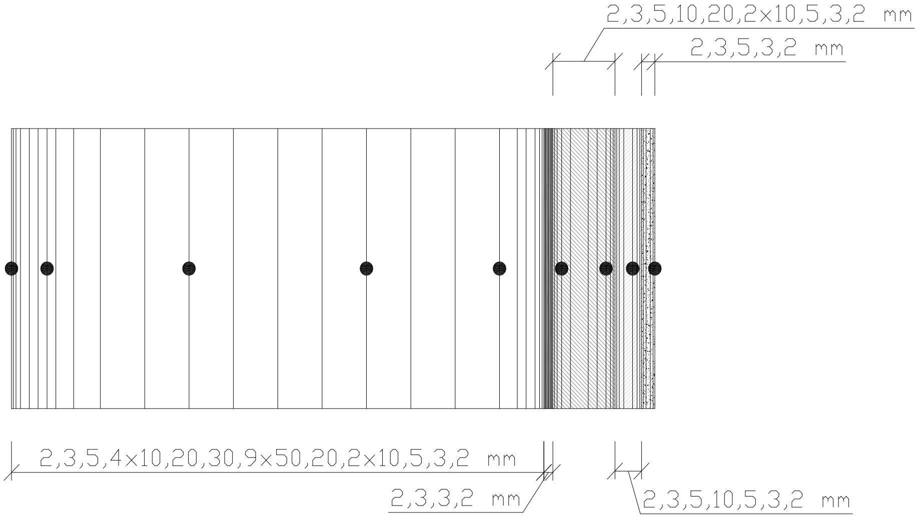

Figure 4 Sensors placing and computer generated mesh, section A-A′

In the computer implementation of the analyzed hygrothermal performance problem, the computer generated mesh was adjusted in sections A-A′, B-B′, to the positions of the sensors in the measured envelope (Figs. 4, 5) so that the same data could be obtained both in the experiment and in the calculations.

As input data, material parameters determined in our laboratory during previous experiments were employed [14, 15] except for the material parameters of wooden window frame and air that were taken from the database of the computer code TRANSMAT 6.2. The following parameters were used: density, specific heat capacity, open porosity, water vapor diffusion coefficient, and thermal conductivity in dependence on moisture content, apparent moisture diffusivity, sorption isotherms and water vapor diffusion resistance factor. The initial conditions for calculations were chosen as data measured in the semi-scale experiment for time $t = 0$.

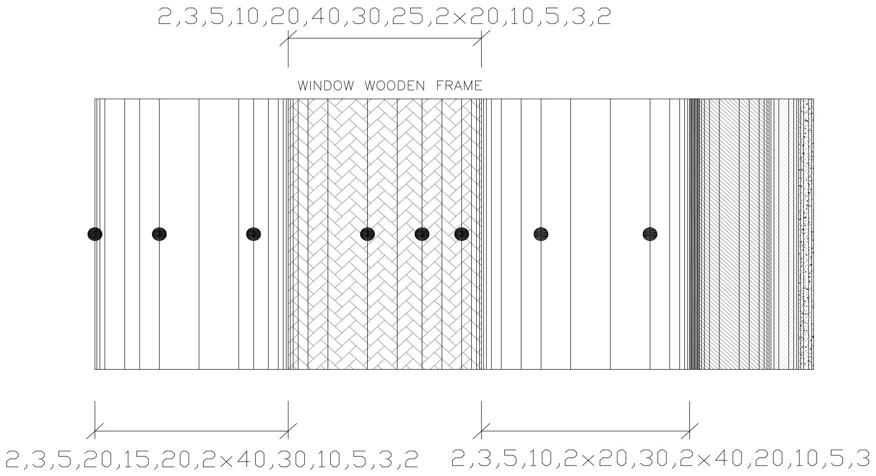

Figure 5 Sensors placing and computer generated mesh, section B-B′

4. Results and discussion

The measured and calculated temperature and relative humidity profiles determined in the validation tests of TRANSMAT 6.2 code are presented in Figs. 6–9.

The results obtained during the semi-scale experiment have shown that some high values of hygroscopic moisture were found in the brick wall during the whole time of the experiment, and a part of it remained there until the end of the winter period (see Figs. 7, 9 for the situation in the end of winter period). However, it should be noted that the conditions of the experiment were more severe than in the reality. In the beginning of the experiment, the brick wall was freshly built in the laboratory, i.e., it contained relatively high amount of moisture and was at room temperature. The climatic conditions of the end of October then have led to a fast increase of relative humidity and even water condensation in a part of the wall. This water could not be fully removed from the wall during the winter period because of the limited possibility of the water transport to the exterior and of the continuous transport of water vapor from the interior to the load bearing structure increasing the total amount of water in the brick. On the other hand, the hydrophilic mineral wool material DU remained dry during the whole critical part of the year, which is clearly a consequence of the high values of its moisture transport parameters. Therefore, the hygrothermal performance of the wall could be considered as relatively good in general.

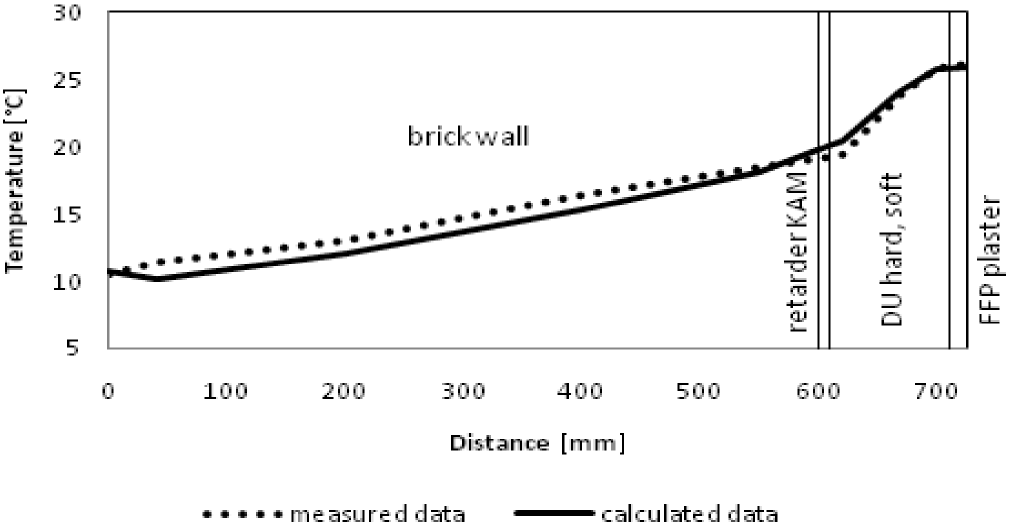

Figure 6 Temperature profiles, section A-A′, February 1

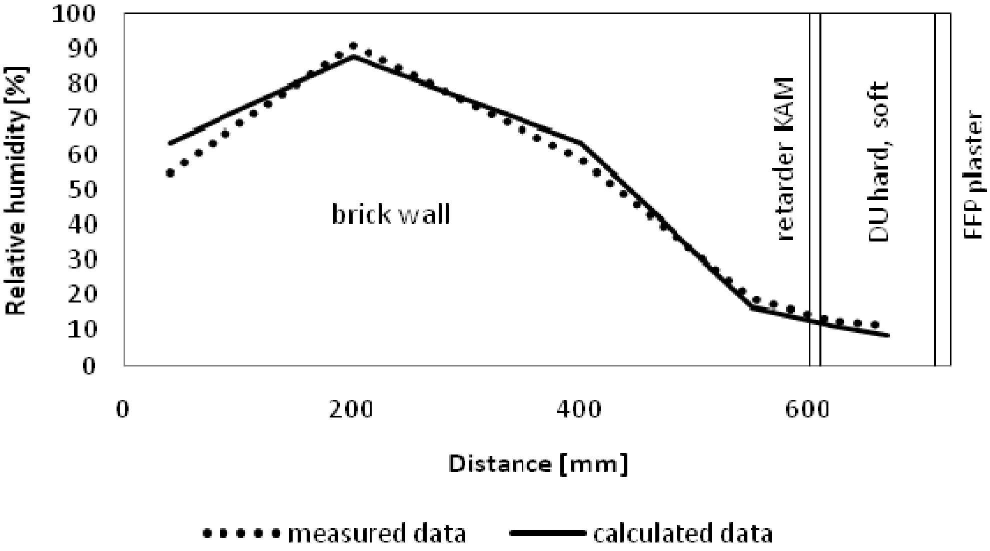

Figure 7 Rel. humidity profiles, section A-A′, February 1

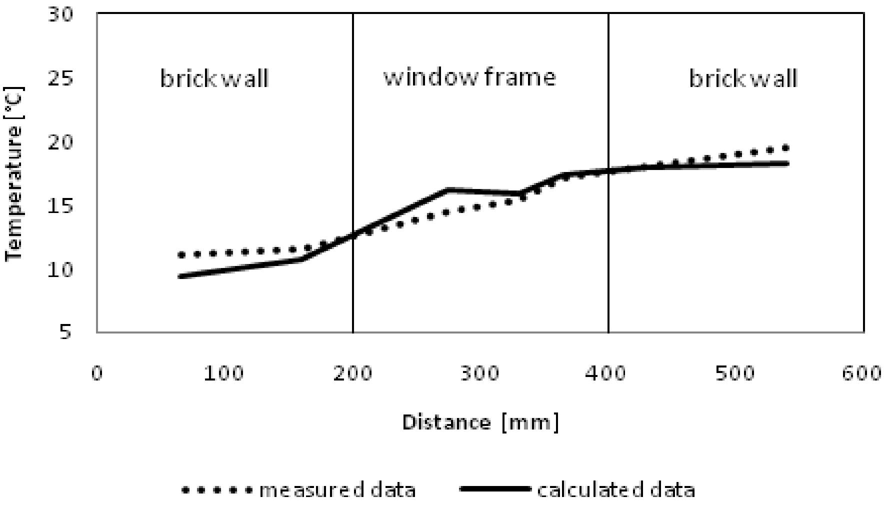

Figure 8: Temperature profiles, section B-B′, February 1

The computational simulation performed with input material parameters mentioned above [14, 15] has shown in the first step only slight agreement with the experimental data. Therefore, we have started the inverse modeling process to achieve a better agreement and to calibrate the TRANSMAT 6.2 code for the studied problem.

The main problems were in relative humidity profiles. Therefore, we tried to modify hygric parameters, which were not determined in the dependence on moisture content, especially water vapor diffusion resistance factor of ceramic brick and water vapor retarder KAM. We have also formed the moisture dependent moisture diffusivity functions to achieve more reliable results. In summary, we have tested 35 combinations of the mentioned hygric parameters. The best results were achieved with the modified hygric parameters given in Tabs. 1 - 4. Within the validation and calibration of TRANSMAT 6.2 code, the modification of standard heat and moisture transfer coefficients was necessary. The final results are presented in Table 5.

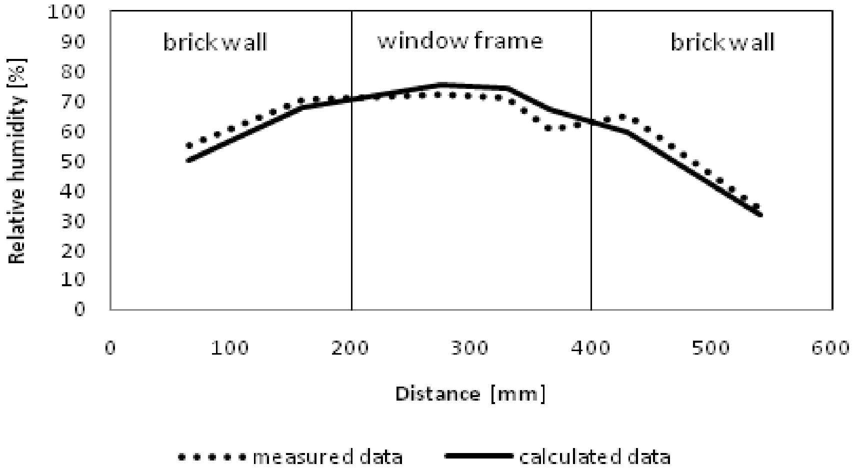

Figure 9 Rel. humidity profiles, section B-B', February 1

The data presented in Tabs. 1 – 4 clearly document the necessity of determination of liquid as well as of gaseous moisture transport parameters in dependence on moisture content. Without using moisture dependent moisture diffusivity function, it would not be possible to achieve sufficient agreement between measured and calculated data. For the practical application of HAM models represents this finding crucial information, since many researchers and practitioners do not include this dependence in their calculations. The same material and structural behavior can be assumed also in the case of gaseous moisture transport, where the water vapor diffusion resistance factor will be changed with moisture content.

Looking at the comparison of measured and calculated results presented in Figs. 6 – 9, one can see that the differences are typically very low, for temperature as well as for relative humidity profiles. On that account we can conclude, the overall agreement is acceptable for the studied problem and the validated code TRANSMAT 6.2 can be considered reliable for long-term hygrothermal analysis of investigated building envelope.

Since the applied computer code TRANSMAT 6.2 was validated and calibrated for the studied structure, long-term simulation of tested building envelope was performed in the final part of the paper. Within these simulations, 5 years cycle of climatic conditions of the Prague reference year was applied on the exterior side of the brick wall provided with newly designed interior thermal insulation system. These results are presented in Figs. 10 – 13.

Table 1 Modified hygric parameters of ceramic brick

Parameter	Original	Modified
Moisture diffusivity (m^2/s)	1.52e-09	Moisture dependence (m^3/m^3) 0.00 - 1.52e-09 0.90 - 5.52e-09 0.315 - 1.52e-08
Water vapor diffusion resistance factor (-)	8.1	25.0

Table 2 Modified hygric parameters of retarder KAM

Parameter	Original	Modified
Moisture diffusivity (m^2/s)	5.43e-08	Moisture dependence (m^3/m^3) 0.0000 - 5.43e-09 0.0016 - 5.43e-08 0.468 - 5.43e-07
Water vapor diffusionresistance factor (-)	10.6	7.0

Table 3 Modified hygric parameters of DU soft layer

Parameter	Original	Modified
Moisture diffusivity (m^2/s)	6.12e-07	Moisture dependence (m^3/m^3) 0.0000 - 6.12e-07 0.0016 - 9.12e-06 0.96 - 6.12e-05

Table 4 Modified hygric parameters of DU hard layer

Parameter	Original	Modified
Moisture diffusivity (m^2/s)	1.22e-06	Moisture dependence (m^3/m^3) 0.000 - 1.22e-06 0.002 - 4.22e-06 0.93 - 1.22e-05

Table 5 Modified transfer coefficients

Parameter	Original	Modified
Heat transfer – interior ($W/m^2 K$)	25	35
Heat transfer – exterior ($W/m^2 K$)	8	5
Moisture transfer – exterior (s/m)	5.88e-08	5.88e-07

The calculated results clearly demonstrate the satisfactory hygrothermal function of studied brick wall with interior thermal insulation system based on hydrophilic mineral wool. Within the five years simulation, no overhygroscopic moisture was observed in the wall as well as in thermal insulation layer. Looking at temperature function of investigated envelope fragment, the benefit of thermal insulation application was quite obvious. This finding proved the applicability of developed insulation system for ceramic brick based envelopes.

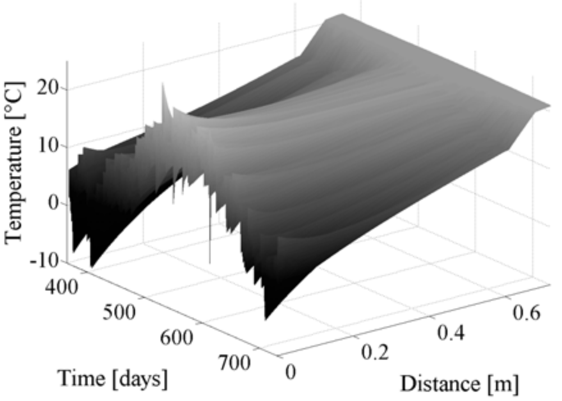

Figure 10 Temperature distributions in the studied structure during 5th year of simulation, section A-A′

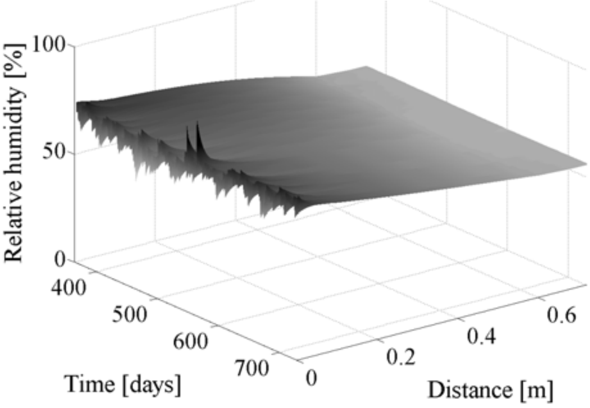

Figure 11 Relative humidity distributions in the studied structure during 5th year of simulation, section A-A′

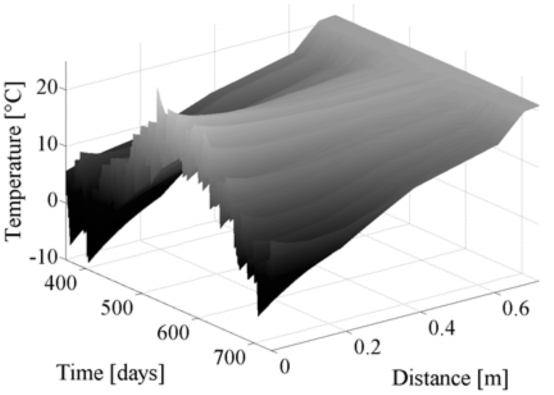

Figure 12 Temperature distributions in the studied structure during 5th year of simulation, section B-B′

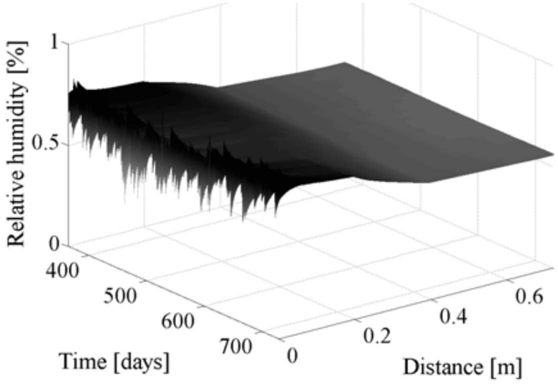

Figure 13 Relative humidity distributions in the studied structure during 5th year of simulation, section B-B′

5. Conclusions

The semi-scale experimental analysis of hygrothermal performance of the building envelope with the interior thermal insulation system in difference climate conditions presented in the paper has demonstrated the possibility of application of semi-scale systems in the process of design and testing of new building structures and new technological solutions. The performed experiment has shown the applicability of semi-scale tests in the moisture and temperature management of building structures. In a combination with computational analysis it can also be applied for calibration and validity tests of current or newly developed computational models solving the problem of combined moisture and heat transport.

The semi-scale experimental testing of a brick wall provided by an interior thermal insulation system with hydrophilic mineral wool insulation and water vapor retarder on the surface of the load bearing structure has shown a reasonable hygrothermal performance of the wall, particularly taking into account that the initial conditions were much worse than in the reality.

In the future work it will be necessary to return to the laboratory measurements and to completely determine material parameters as functions of temperature and moisture content. Then it will be possible to start the inverse modeling process with better initial conditions and to determine the interface resistance factors between the layers of the studied multi-layered building structure.

Acknowledgements

This research has been supported by the Ministry of Education, Youth and Sports of the Czech Republic, under project No MSM: 6840770031.

References

[1] Hens, H., 1996, *Heat, Air and Moisture Transport*, Final Report, Vol. 1, Task 1: Modeling, International Energy Agency Annex 24, Laboratorium Bouwfysica, K. U. Leuven, Belgium.

[2] Häupl, P., Fechner, H., Grunewald, J., Xu, Y. and Stopp, H., 1997, Numerical simulation of moisture behaviour within different flat roof structures, *Proc. of CIB W40 meeting*, Kyoto.

[3] Grunewald, J., 2000, DELPHIN 4.1 - Documentation, Theoretical Fundamentals, TU Dresden, Dresden.

[4] ASTM, 1994, *Moisture control in buildings*, edited by H. R. Trechsel, Philadelphia, ASTM.

[5] IEA, 1996, Modelling, Final Report, IEA ECBCS Annex 24.

[6] Kumaran, M.K.and Wang, J., 2002, *How well should one knot the hygrothermal properties of building materials?*A Thermal and Moisture Transport Property Database for Common Building and Insulating Materials, Appendix I, Final Report from ASHRAE Research Project 1018-RP.

[7] Künzel, H.M., 1995, *Simultaneous Heat and Moisture Transport in Building Components*, IRB-Verlag, Sttutgart.

[8] Bíca, L., Maděra, J. and Černý, R., 2006, A Computer Simulation Tool for Modeling Heat and Moisture Transport in Building Materials, *Computational and Experimental Analysis of Structure and Properties of New Building Materials from Nano- to Macrolevel III*, Prague CTU, 75-84.

[9] Pavlík, Z., Pavlík, J., Jiřičková, M., Černý, R., 2002, "System for Testing the Hygrothermal Performance of Multi-Layered Building Envelopes," *Journal of Thermal Envelope and Building Science*, Vol. 25, pp. 239-249.

[10] Pavlík, Z., 2004, *Development of a Semi-scale Technique for the Assessment of Hygro-thermal Performance of Multi-layered Systems of Building Materials*, CTU Report, Vol. 8, No. 1, CTU Prague.

[11] Kočí, V., Maděra, J., Černý, R. and Rovnaníková, P., 2009, Application of a combined computational-experimental approach for service life estimate of exterior plasters of historical buildings. *Structural Studies, Repairs and Maintenance of Heritage Architecture XI*, C. Brebbia, (ed.), WIT Press, Southampton, pp. 303-314.

[12] Kruis, J. and Maděra, J., 2009, Numerical Analysis of Coupled Problems with Discontinuities, *Proceedings of the 12th International Conference on Civil, Structural and Environmental Engineering Computing*, Stirling, Civil-Comp Press Ltd, p. 273.

[13] Kruis, J., Koudelka, T. and Krejčí, T., 2010, "Efficient computer implementation of coupled hydro-thermo-mechanical analysis", *Mathematics and Computers in Simulation*, vol. 80, pp. 1578-1588.

[14] Jiřičková, M. and Černý, R. 2002, Thermal and Hygric Properties of Mortars and Water Vapor Retarders for Interior Thermal Insulation Systems, *Proceedings of 11th Symposium for Building Physics*, TU Dresden, Vol. 1, pp. 319-328, Dresden.

[15] Jiřičková M., 2004, Application of TDR Microprobes, Minitensiometry and Minihygrometry to the Determination of Moisture Transport and Moisture Storage Parameters of Building Materials, *CTU Report*, Vol. 8, No. 2, CTU Prague.

Hygrothermal assessment of typical and critical details of selected thermal insulation systems

Jan Kočí, Václav Kočí, Jiří Maděra, Robert Černý, Xinying Lu

[1]Department of Materials Engineering and Chemistry, Faculty of Civil Engineering, Czech Technical University in Prague, Thákruova 7, CZ-166 29 Prague 6, Czech Republic, e-mail: jan.koci@fsv.cvut.cz

Department of Civil Engineering, Tsinghua University, Beijing 100084, China

Abstract: *The hygrothermal performance of several contemporary building envelopes is studied using computational simulations of coupled heat and moisture transport. So far, these constructions were designed using traditional methods according to technical standards which do not seem to be convenient for such design. In this paper some representative typical and critical details were chosen and assessed by computer simulation tool Hemot, which was developed at the Faculty of Civil Engineering, Czech Technical University in Prague. The simulation of transport phenomena is done for several 2-D problems. The basic variables characterizing the hygrothermal state of the studied building envelopes (temperature, moisture content, relative humidity) are obtained as functions of space and time. Constructive details of thermal insulation systems can be optimized in this way, using the results of numerical simulation, and their reliability for different given indoor and outdoor climates can be assessed.*

Keywords: *typical and critical details, computer simulation, heat and moisture transport*

1. Introduction

The basic function of the envelope or enclosure of a building or structure is to protect the covered or otherwise conditioned interior spaces from the surrounding environment. This fundamental need for shelter is a concept that is as old as the recorded history of mankind. However, as our needs have evolved and technologies have advanced, the demand placed on designers to both understand and integrate, a wide range of increasingly complex materials, components, and systems into the building enclosure has grown in equal proportion.

Most research in thermal performance of buildings is aimed at experimental or computational analysis of building envelopes [1] – [8]. On the other hand it is important to say, that moisture influence on thermal performance of the building is not often mentioned in technical literature. An example is given in [9] and [10]. For determination of coupled heat and moisture transport according to contemporary standards, a simplified methods based on Glaser's model are used. Although Glaser's method proved its functionality in many practical applications, it must be remembered, that in more complicated details, where transport of liquid water has to be taken into account, this method fails due to diverging from physical reality. This can for example results in prediction moisture accumulation in such location in the structure, where this accumulation absolutely does not arise. Interior thermal insulation system without vapor barrier is a typical example where Glaser's method is unusable.

We can state, that design of thermal insulation systems is mostly done on empirical base only or with using simplified hygrothermal analyses, which are strictly defined in national standards. These standards also contain requirements for the materials and constructions that can be used in thermal insulation systems. Such technique is convenient, but not optimal, for standard residential buildings, where designing process of thermal insulation system is a routine. On the other hand, in case of designing modern buildings (especially high-rise) or application of newly developed insulation materials and systems, we cannot rely on empirical knowledge or experience from previous constructions. In addition to this, the technical standards are not flexible and cannot react on rapid progress in materials science. Therefore we should use more sophisticated ways to assess more complicated details and construction from the hygrothermal point of view.

2. Selected typical and critical details

Exterior wall types commonly associated with above-grade building enclosure design and construction can generally be classified as follows: as a barrier wall, a cavity wall or a mass wall. The mass walls are the oldest types of wall systems, which have been studied many times in the past. These wall types come under effect of Glaser’s model, therefore we are not interested in mass wall any further and the following summary of the characteristics of each wall type is restricted to cavity and barrier walls only. The above mentioned wall types may contain many critical details which must be assessed by comprehensive building envelope quality assurance program. Such programs are developed at Department of Materials Engineering and Chemistry, Faculty of Civil Engineering, Czech Technical University in Prague. In this section we bring some of these critical details, which are to be assessed (Figs. 1 and 2).

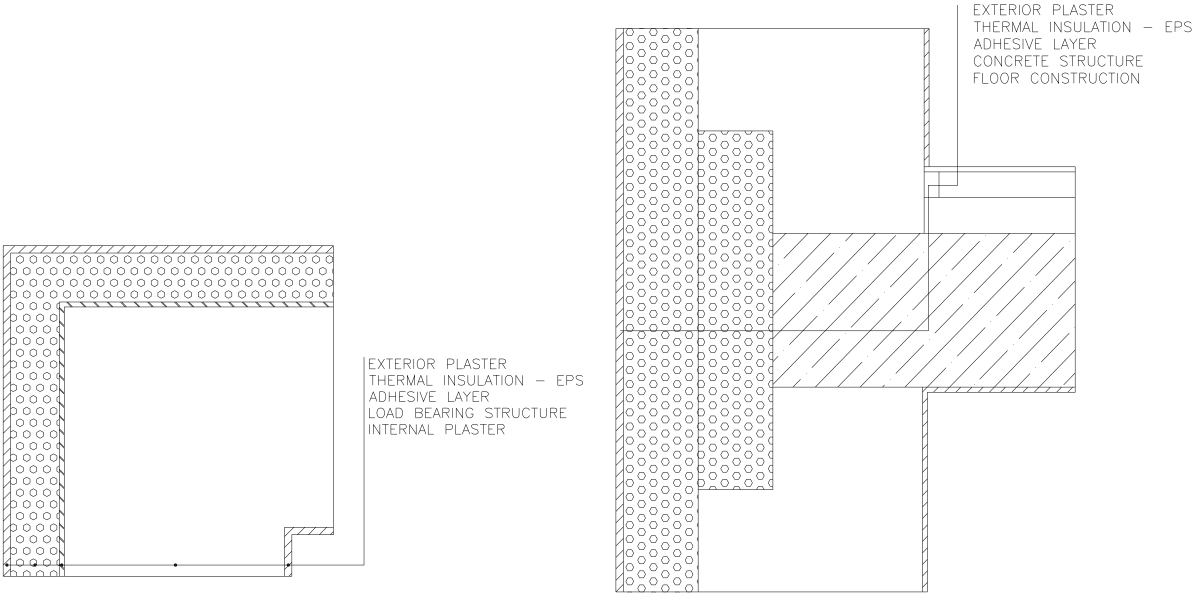

Figure 1a,b: Outer corner with exterior thermal insulation (horizontal section) and load-bearing structure with ceiling provided with external thermal insulation (vertical section)

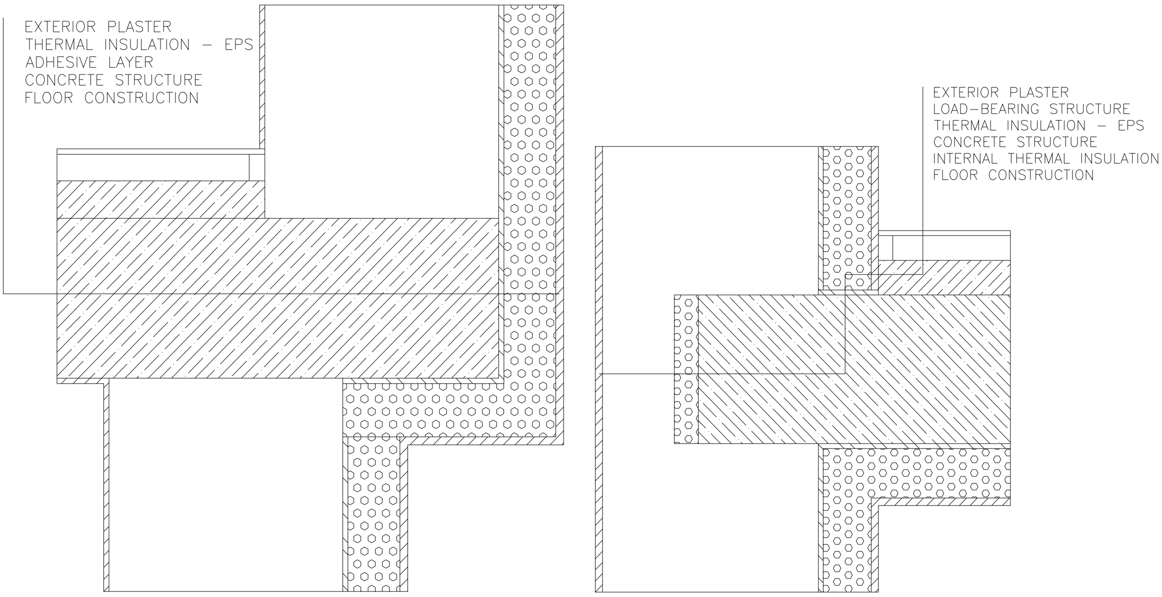

Figure 2a,b: Wall offset with external thermal insulation (vertical section) and load-bearing structure with ceiling provided with internal thermal insulation (vertical section)

3. Computer simulation

The numerical simulation tool HEMOT has been developed at the Department of Materials Engineering and Chemistry, Faculty of Civil Engineering, Czech Technical University in Prague in order to support coupled heat and water transport in porous building materials [11]. It allows simulation of transport phenomena in constructive building details for 1D and 2D problems, whereas the basic variables characterizing the hygro-thermal state of building constructions (temperature, moisture content, relative humidity) can be obtained as functions of space and time. The mathematical formulation of coupled heat and moisture transport equations is done according to Künzel [12] and the code works on the basis of finite element method. A particular advantage of HEMOT code is the possibility of investigation of variants concerning different constructions, different materials and different climatic loads. Constructive details of buildings and building materials can be optimized using the numerical simulation, and the reliability of constructions for different given indoor and outdoor climates can be judged. HEMOT is using the material database as a data source, which simplifies computations and allows obtaining more complex results.

Boundary conditions were assumed for different climatic locations – Czech Republic (Ostrava) and China (Beijing). Whereas Ostrava experiences an oceanic climate with warm summers and relatively cold winters, Beijing has monsoon-influenced humid continental climate, characterized by hot, humid summers and generally cold, windy, dry winters.Both Ostrava and Beijing are cities with similar temperature development during a year, but different relative humidity development. Boundary conditions for Ostrava and Beijing were obtained using Meteonorm software, version 6.1 [13], which is meteorological database and computer program for climatological calculations for every location on the globe.

4. Materials characteristics

Basic material parameters of used materials are shown in Table 1. We used the following symbols: ◎ – bulk density [kg/m^3], ◎ – porosity [%], ◎ – water vapor diffusion resistance factor [-], w_{hyg} – hygroscopic moisture content by volume [m^3/m^3], ◎ – moisture diffusivity [m^2/s], c – specific heat capacity [J/kgK], ◎dry - thermal conductivity in dry conditions [W/mK], ◎sat - thermal conductivity in water saturated conditions [W/mK]. All these parameters were measured in Laboratory of Transport Processes of the Department of Materials Engineering and Chemistry, Faculty of Civil Engineering, Czech Technical University in Prague [14-16].

Table 1: Properties of applied materials

	Interior plaster	Exterior plaster	Expanded polystyrene	Adhesive layer	Ceramic brick	Concrete
ρ [kg/m^3]	1384	1550	50	1430	1670	2380
ψ [%]	47.3	40.0	97.0	42.6	37.5	12.3
c_{dry} [J/kgK]	1028	600	1300	1020	1202	672
c_{sat}[J/kgK]	1719	1200	1300	1020	1202	872
$\mu_{dry\ cup}$ [-]	12.6	7	50	12.4	19.5	15.8
$\mu_{wet\ cup}$ [-]	7.1	7	50	12.4	19.5	6.6
λ_{dry} [W/mK]	0.366	0.700	0.040	0.481	0.50	1.66
λ_{sat} [W/mK]	1.186	2.400	0.560	2.022	0.65	2.085
κ_{app} [m^2/s]	1.360e-7	7.290e-7	2.100e-11	1.070e-9	2.650e-7	7.150e-9
w_{hyg} [m^3/m^3]	0.031	0.030	0.001	0.201	0.048	0.0833

5. Simulation results & discussion

All simulations were performed for 6 years under two different boundary conditions – for Ostrava and Beijing. Comparing these simulation results we discovered that relative humidity in the construction details reached higher values under climate of Ostrava, whereas Beijing's climate brought more extreme temperatures to the construction. Trying to find critical points in the construction details, we are focused on moisture presence in the structure and therefore we present only relative humidity outputs. The temperature distribution is very similar for both climatic boundary conditions.

The simulation results are presented for two days chosen as representative for winter and summer period. The date 30th July, year 6 was chosen as typical day for summer period and 31st January, year 6 was chosen as typical day for winter period.

The simulation results of an outer corner provided with thermal insulation are shown in Figure 3. Critical point of this detail is located in the corner of thermal insulation where relative humidity reached about 80 % in summer and 84 % in winter period. For Beijing climate the relative humidity is ranging between 71 % (summer) and 76 % (winter).

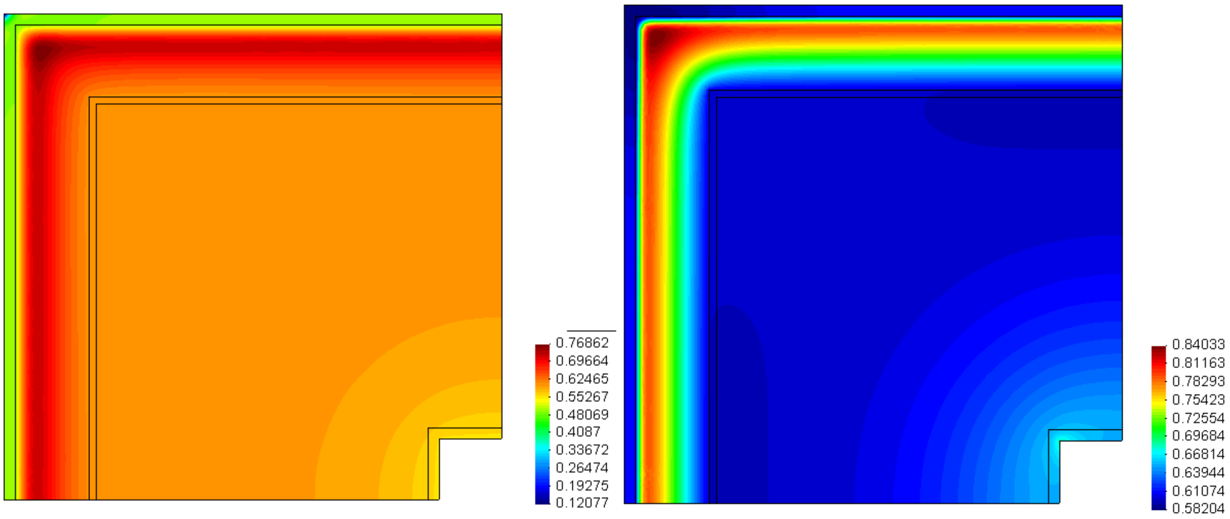

Figure 3: Relative humidity distribution for summer (left) and winter (right) period – outer corner, Ostrava

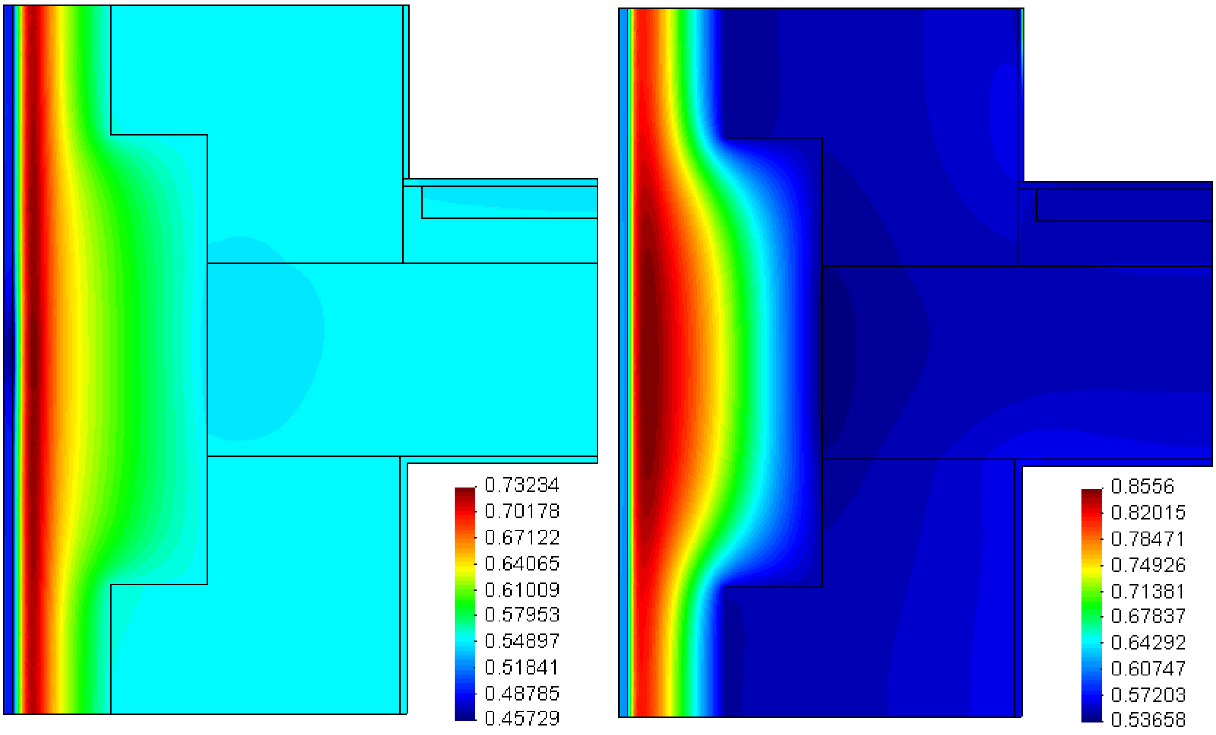

Figure 4: Relative humidity distribution for summer (left) and winter (right) period – load-bearing structure with ceiling provided with external thermal insulation, Ostrava

The simulation results of load-bearing structure provided with external thermal insulation are shown in Figure 4. Critical point of this detail is located again in the thermal insulation, few millimeters under the plaster. Relative humidity reached about 75 % in summer and almost 90 % in winter period. For Beijing climate the critical value of relative humidity is about 68 % for both summer and winter period.

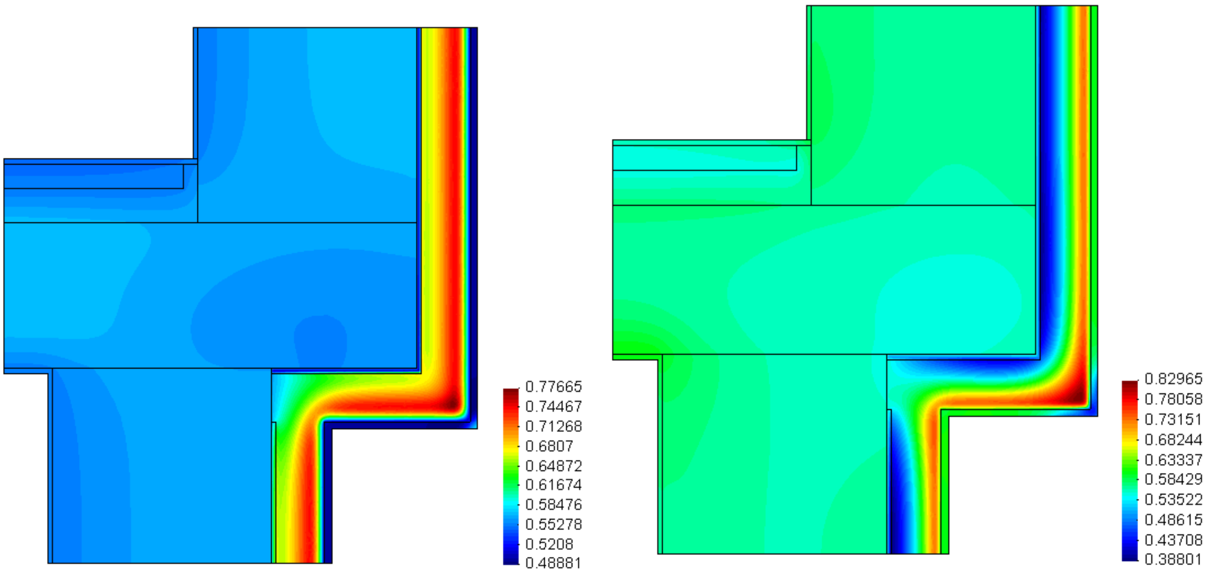

Figure 5: Relative humidity distribution for summer (left) and winter (right) period – wall offset, Ostrava

The simulation results of wall offset provided with external thermal insulation are shown in Figure 5. Critical point of this detail is located in the outer corner of thermal insulation, few millimeters under the plaster. Relative humidity reached about 80 % in summer and almost 85 % in winter period. For Beijing climate the critical point was found on the interface between thermal insulation and load-bearing structure, where the values of relative humidity were about 95 %.

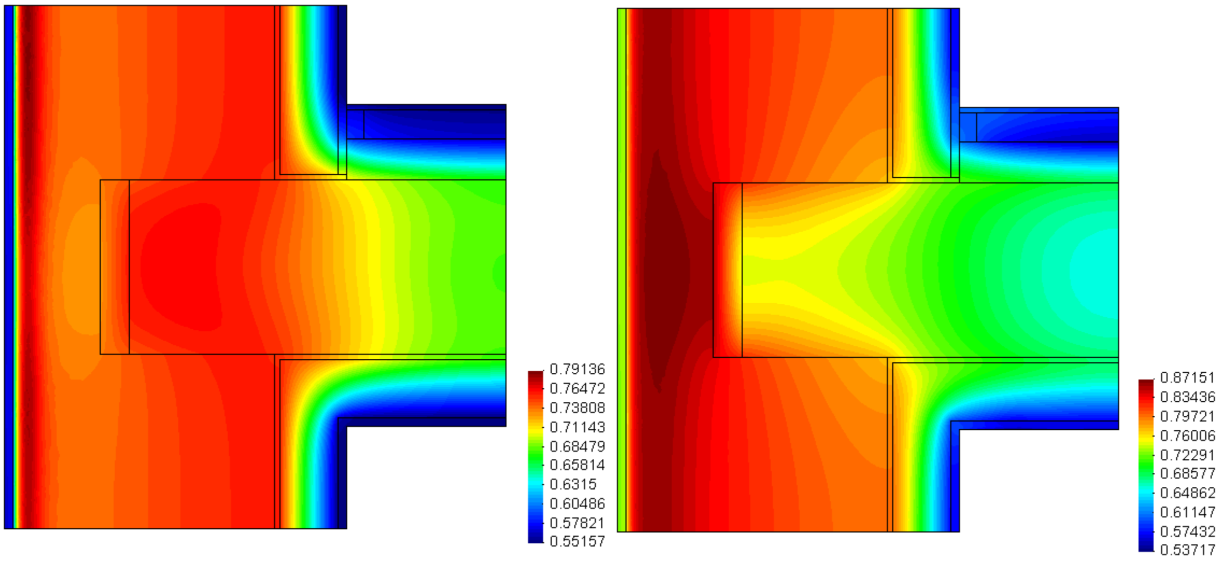

Figure 6: Relative humidity distribution for summer (left) and winter (right) period – load-bearing structure with ceiling provided with internal thermal insulation, Ostrava

The simulation results of last detail – load-bearing structure with ceilings provided with internal thermal insulation is shown in Figure 6. Here we can clearly see that increased values of relative humidity are within whole load-bearing structure.

In the previous paragraphs we showed simulation results and found some critical points in the selected details that must be assessed very carefully during designing phase. In the simulations we used reference years only, so in some cases the results might be much worse. The relative humidity in critical points of the details is to large degree affected by local rains, which may be especially in China long-time and very heavy. Therefore, special attention should be given to proper selection of external plaster when designing such details. In Figure 7 we can see an example of relative humidity as a function of time in the critical point in wall offset provided with external thermal insulation (previously showed in Figure 2a and Figure 5).

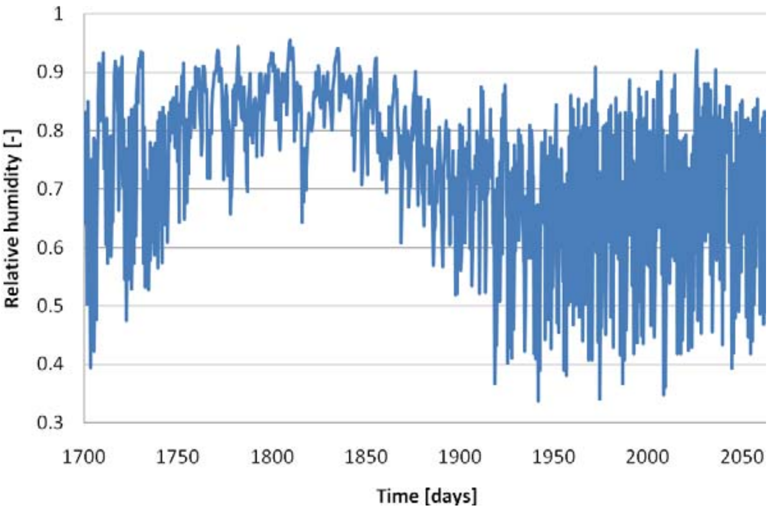

Figure 7: Relative humidity distribution in critical point of wall offset provided with thermal insulation, Ostrava

Conclusion

In this paper, hygrothermal performance of several typical and critical construction details of contemporary buildings was analyzed. It was demonstrated that such details should not be assessed by routine methods defined by national standards. Even well known Glaser's method should not be used for their assessment. The Glaser's method and other simple methods given by national standard should be used only in case of really simple building envelopes. In the other cases we recommend to use numerical simulation tools to discover potential weak points and to prevent water condensation in construction details.

Acknowledgements

This research has been supported by the Ministry of Education, Youth and Sports of the Czech Republic, under project No ME10112.

References

[1] G. F. Jones, and R. W. Jones. Steady-state heat transfer in an insulated, reinforced concrete wall: theory, numerical simulations, and experiments. *Energy and Buildings*, Vol. 29, Issue 3, 1999, pp. 293–305.

[2] T. Nussbaumer, R. Bundi, Ch. Tanner, and H. Muehlebach.Thermal analysis of a wooden door system with integrated vacuum insulation panels.*Energy and Buildings*, Vol. 37, Issue 11, 2005, pp. 1107–1113.

[3] P. T. Tsilingiris. Parametric space distribution effects of wall heat capacity and thermal resistance on the dynamic thermal behavior of walls and structures. *Energy and Buildings*, Vol. 38, Issue 10, 2006, pp. 1200–1211.

[4] Z. Yılmaz. Evaluation of energy efficient design strategies for different climatic zones: Comparison of thermal performance of buildings in temperate-humid and hot-dry climate. *Energy and Buildings*, Vol. 39, Issue 3, 2007, pp. 306–316.

[5] B. Yesilata, and P. Turgut. A simple dynamic measurement technique for comparing thermal insulation performances of anisotropic building materials.*Energy and Buildings*, Vol. 39, Issue 9, 2007, pp. 1027-1034.

[6] M. M. Eftekhari. Comparative thermal performance of new and old houses.*Energy and Buildings*, Vol. 25, Issue 1, 1997, pp. 69-73.

[7] R. Levinson, W. Delp, D. Dickerhoff, and M. Modera. Effects of airflow infiltration on the thermal performance ofinternally insulated ducts. *Energy and Buildings*, Vol. 32, Issue 3, 2000, pp. 345–354.

[8] T .M. I. Mahlia, B. N. Taufiq, Ismail, and H.H. Masjuki. Correlation between thermal conductivity and the thickness of selected insulation materials for building wall.*Energy and Buildings*, Vol. 39, Issue 2, 2007, pp. 182–187.

[9] C. J. Simonson, Y. X. Tao, and R. W. Besant. Thermal performance and hysteresis in fibrous insulation exposed to moisture and step changes in the cold temperature boundary condition. *Energy and Buildings*, Vol. 21, Issue 3, 1994, pp. 251-257.

[10] M. Matilainen, J. Kurnitski, and O. Seppanen.Moisture conditions and energy consumption in heated crawl spaces in cold climates.*Energy and Buildings*, Vol. 35, Issue 2, 2003, pp. 203–216.

[11] Černý R., Complex System of Methods for Directed Design and Assessment of Functional Properties of Building Materials: Assessment and Synthesis of Analytical Data and Construction of the System. CTN CTU in Prague, 192 – 201. 2010.

[12] Künzel H. M.,.Simultaneous Heat and Moisture Transport in Building Components.PhD Thesis, Fraunhofer IRB Verlag, Stuttgart, 1995.

[13] Meteonorm Version 6, software version 6.1.0.20 of April 2010, METEOTEST, Switzerland, 2010.

[14] Pernicová, R., Pavlíková, M., Pavlík, Z., Černý, R. Vliv metakaolinu na mechanické, tepelné a vlhkostní vlastnosti vápenných omítek. Metakaolin 2007. Brno: VUT FAST, 70-77. 2007.

[15] Vejmelková, E., Černý, R. Application of Alternative Silicate Binders in the Production of High Performance Materials Beneficial to the Environment. In: Proceedings of the 2008 World Sustainable Building Conference [CD-ROM]. Balnaring, Victoria: ASN Events Pty Ltd, 520-525, 2008.

[16] Pavlíková, M., Pavlík, Z., Černý, R. Hygric and Thermal Properties of Materials Used in Historical Masonry. In: Proceedings of the 8th Symposium on Building Physics in the Nordic Countries. Lyngby: Technical University of Denmark, BYG.DTU, 903-910, 2008.

Properties study of reflexive thermal-insulation multilayer for external constructions

Daniel Kopkáně[1], Karel Trojan[2],Jaroslav Nováček[3]

Institute of Technology of Building Materials and Components, Faculty of Civil Engineering, Brno University of Technology, Czech Republic, Veveří 95,662 37 Brno

[1]kopkane.d@fce.vutbr.cz, [2]karel1.trojan@gmail.com, [3]novacek.j@fce.vutbr.cz

Abstract: *The article is devoted to the issue of reflective thermo-insulation systems. These systems use sandwich compositions consisting of air layers and layers of material with low emissivity coating to suppress the transmission of radiant heat. There are experimentally determined thermal resistances of air layer with respect to its internal divisions and emissivity of internal surfaces and wetake into account theeffect ofmediumtemperature on thethermalresistance. The article is devoted to further verification thermal-technical properties of a particular reflective thermal insulation.*

Keywords: *heat radiation, thermal resistance, reflexive thermo-insulating system, emissivity, air layers*

1. Introduction

Everybody knows there is three basic ways of spreading of heat energy: conduction, convection and radiation. The radiation seams to be neglected or was in the past. Nowadays we can see increasing interest about radiation properties of building materials. It is no wonder since the radiation is about the same magnitude as convection if comparing heat flows in common conditions.

On the market of thermal insulations can be seen boom of insulations based on multiple layers of aluminum foils with some distant layers (air bubble wrapping foils, polyurethane foils etc.) between them. The paper presents some of related results obtained in Physical laboratory of Department of Building materials on Faculty of Civil engineering, Brno University of Technology.

2. Theoretical background

2.1 Radiation

Every object in Universe with non-zero temperature do emits electromagnetic waves. The amount of radiated energy depends on its surface: its temperature, area and quality. The quality is being expressed by so called emissivity – marked as ε. This material property expresses ability of material to radiate energy as ratio of maximal theoretical amount so for real materials it lies between 0 to 1. Emissivity is often strongly depending wavelength. The fundamental equations to describe radiation are Planck's law (1), Stefan-Boltzman's (2) and Kirchhoff's law (3).

$$E(\lambda,T)=\frac{2.h.c^2}{\lambda^5}\cdot\frac{1}{e^{h.c/\lambda.k.T}-1}, \tag{1}$$

where is: E - energy emitted by blackbody radiator [W.m^{-2}.μm^{-1}] , $h = 6{,}625\ .\ 10^{-27}$ erg.s (Planck constant), $k = 1{,}38\ .\ 10^{-16}$erg.K^{-1} ´(Boltzman constant) and $c = 3\ .\ 10^{10}$ cm.s^{-1} (speed of light).

$$q_{rad} = \varepsilon\ .\ c_b\ .\ T^4, \tag{2}$$

where is: q_{rad} - radiated heat flux [W.m^{-2}], ε - emissivity of surface [-], c_b - Stefan-Boltzman constant [$c_b \approx 5{,}67032.10^{-8}$ W.m^{-2}.K^{-4}] and T - absolute temperature of surface [K].

$$R + A + T = 1, \tag{3}$$

where is: R - reflection, A - absorption and T - transition of electromagnetic radiation by surface.

The outcomes of those physical laws are:

- The radiation strongly depends on emissivity and temperature (see Figure 1),
- All around is huge amount of electromagnetic energy, however since the objects radiates on themselves, we recognize just the subdivision of those radiation heat flows,
- As the temperature goes down the radiation drops quickly and the radiations is being realized on still longer wavelengths and the mail band for common temperatures (0 to 30°C) lies between 8 to 15 microns of wavelength (so called long infra red or LIR for short),
- Materials with high reflection have low radiation and vice versa.

Those finding are very important for further understanding to this topic. The common materials tend to have fairly high emissivity in LIR (above 0,9) so the thermal radiation is thereforealso high. The possibility for reduction of radiation flow is effective reduction in emissivity of surfaces by utilization of metals. Metals have naturally low emissivity mainly if polished. The most utilised is aluminum (low cost, easy to handle). For applications on windows several, more sophisticated coatings have been developed (so called heat mirror etc.) however for purpose of this study only aluminum was measured.

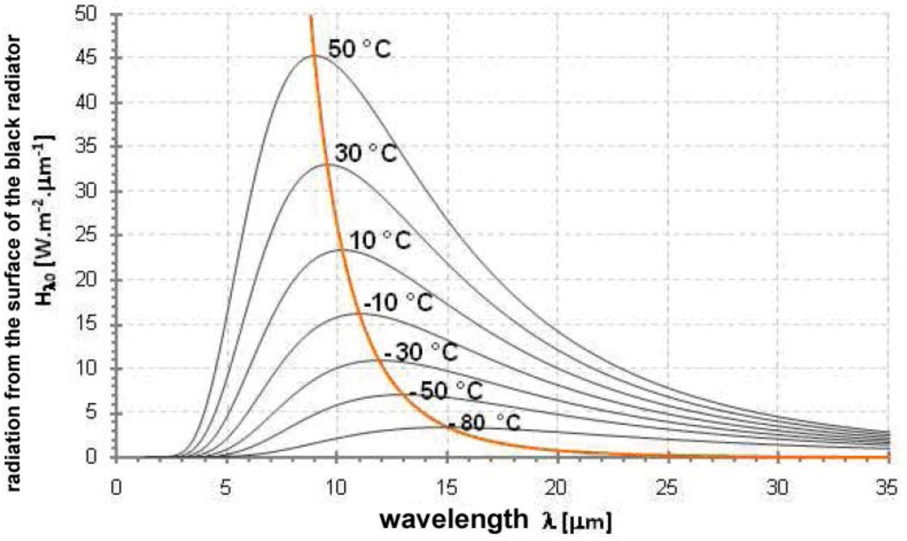

Figure 1: Graphical representation of emitted energy of black body radiator as function of surface temperature and wavelength of electromagnetic radiation [3]

2.2 Convection

Energy transfer between opposite sides of air layer is very complicated phenomenon, which can by simplify described by heat transfer coefficient. This coefficient contains influence of viscosity ofthe flowingmedium, flow velocity, flow direction, surface roughness and other parameters.

Value of energy transmitted by convection between flowing medium and solid surface is given by Newton's equation:

$$q = -h.(T_{\text{medium}} - T_{\text{solid}}) \tag{4}$$

where is: q - heat flux [W.m^{-2}], T_{medium} - thermodynamic temperature of flowing medium [K], T_{solid} - thermodynamic temperature of solid surface [K], h - heat transfer coefficient [W.m^{-2}.K^{-1}].

2.3 Thermal properties of air layer

Heat transfer in closed air layer is complicated mix of conduction, convection and radiation.Major influence on thermal resistance has emissivity value of internal surfaces whichaffects radiation intensity and thickness of air gap whichaffects possibility of air flowing. Heat transfer by conduction is negligible in most cases.

Following graph in figure 2 shows development of thermal resistance of closed air gap for winter conditions as function of gap thickness and in respect to direction of heat flow. We cansee that thethermal resistance of closed air gap issteeplyincreasesto a thickness of20 mm,beyond this value furtherincrease of the gapthicknesshas nota major impact.

This factis the reason,why we are working with a uniform thickness of air layers of 20 mm in all followingexperiments.

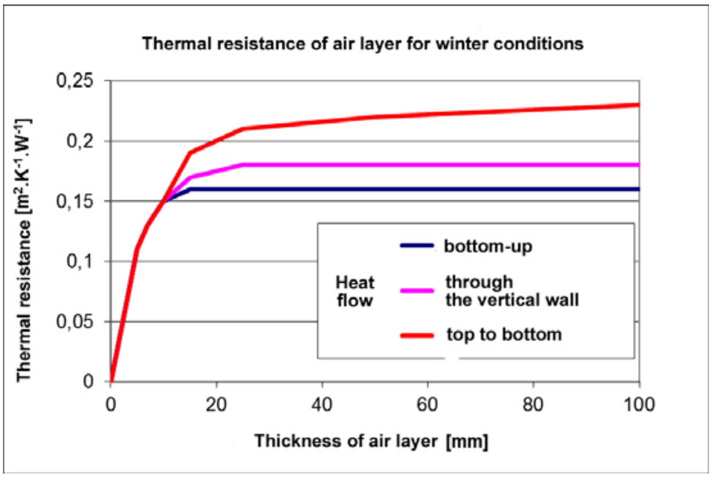

Figure 2: Thermal resistance of closed air gap according to ČSN 730540; valid for winter conditions and internal surfaces with emissivity ε≥0,8. [4]

3. Measurement device for determination of thermal resistance

Thermal resistance R appears as an ideal variable for comparison ofreflectiveand contactthermalinsulators. This parameter issuccess fully avoids problems of comparing the thermal conductivity and properties of layers suppress the spread of heat by radiation and convection. To determine the thermal resistance of the reflective insulating material was there fore used the following equipment and methodology.

The used device Holometrix is designed to measure the thermal conductivity of building materials in the according to ČSN EN 12664 „Thermal performance of building materials and products - Determination of thermal resistance by means of guarded hot plate and heat flow meter methods - Dry and moist products of medium and low thermal resistance".Specifically, the method of measurement with one plate (single-specimen apparatus)[5].

The device function is to set different temperatures on oppositesides of the plate specimen (top heating and bottom cooling plate) and subsequent measurement of heat flowing through the sample.

The measurements have one specific aspect related to construction on the measuring device: the heat flow in being realized from top to bottom. In conventional insulation, where is the main mechanism for energy transfer conduction which is isotropic, this aspect has no influence on results. However in case of present of air, the results are strongly depending on orientation of the sample since the heat flow is depending on its direction.

4. Thermal properties of divided air layer

Firs set of measurements has aim to compare effect of different materials on overall heat flow.

Basic idea is to measure air layer with defined thickness of 40mm. The distance of hot and cold plate was granted by two frames made of polystyrene of 20mm thickness (see Figure 3).In next steps the air layer was divided by different materials: polypropylene foil, paper sheet and aluminum foil respectively. The purpose is to affect convection and radiation as main mechanisms of heat transfer. The conduction is being assumed as minor effect here because of construction of measuring device (see Figure 3).

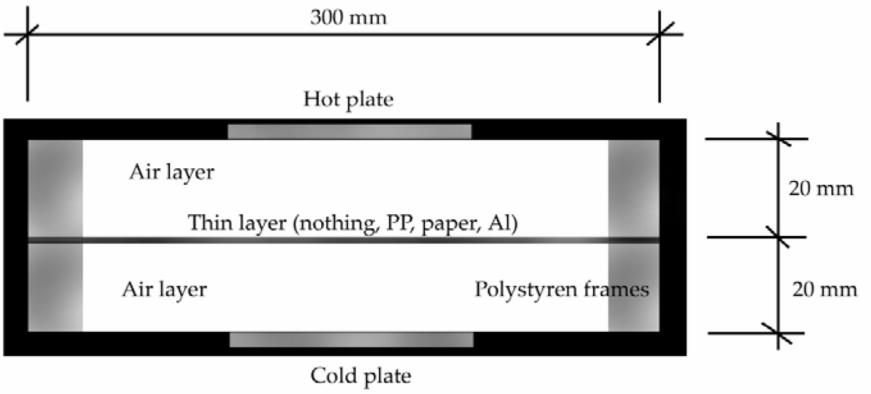

Figure 3: Scheme of measuring composition

The expectations are:

Just air layer 40mm – the air flow is limited just by distance and by difference in density of air with different temperature; there is no barrier for radiation, however the heat is being emitted from the heated spot only.

Polypropylene foil with two air gaps of 20mm – the foil makes barrier for air flow; the radiation is being effected by less then 10% (assumption), since the polypropylene foil is transparent for infra thermal radiation (however there will be some infrared emission form the foil itself).

Paper sheet – effective barrier for air flow; the radiation is in interaction with the material because it is not transparent however it is able to absorb and to emit thermal radiation very well – the emissivity of paper is about 0,93 between 8-14microns [1].

Aluminium foil – like in other cases there is barrier spreading the air layer in two separated gaps, moreover the aluminum has emissivity less the 0,1 so the heat transfer by radiation was highly retarded.

Table 1: Results of thermal resistance measurement according ČSN EN 12664

Composition of layers / thickness	Thermal resistance R [m^2.K.W^{-1}] (mean temperature: 10°C ; temperature gradient of hot and cold plate: 20°C)	Equivalent thermal conductivity λ_{eq}[W.m^{-1}.K^{-1}]
air layer 40mm	**0,23**	**0,176**
air layer 20mm polypropylene foil 0,02mm air layer 20mm	**0,25**	**0,162**
air layer 20mm paper sheet 0,1mmair layer 20mm	**0,38**	**0,104**
air layer 20mm aluminum foil 0,02mm air layer 20mm	**1,06**	**0,038**

As can be seen in table 1 the difference between performance of 40mm of air and two layers of air separated by polypropylene foil is just negligible. The reason lies in fact that thermal radiation can easily pass through the foil. In the other hand the air flow is in this configuration relatively ineffective because of direction from top to bottom. The result obtained with paper sheet is significantly better obviously due to kind of barrier to thermal radiation (since the transparency to thermal radiation is only significant difference here). In the end can be seen how significant the radiation is as the aluminium foil performance is the best by far. In this case is the radiation retarded on both sides: due to low emissivity the foil is not directly heated and the heat past by air convection is not radiated toward cold plate (of course to certain point according to its emissivity).

5. Thermal properties of simple air layer with different emissivity of internal surfaces

The next experiment aimed to measure heat transfer realized over air layer in case of surface with common emissivity ($\varepsilon \geq 0,9$) versus case where low emissivity surface (LES) is on one or both sides ($\varepsilon \leq 0,15$). The experiment setup can be seen on figures 4, 5 and 6. The LES is in this case aluminium foil glued to plywood board (PWB).

The real effect of LES can be compared with conventional insulation if equivalent thickness will be calculated. The idea is to subtract thermal conductivity of the PWB from the total thermal resistance as measured. The equivalent thickness is then expressed as amount of conventional insulation with lambda 0,04 W.m^{-1}K^{-1} required for same thermal resistance. The results are presented in table 2.

As mentioned above, the results are related to head flow form top to bottom. In other configurations the results will be different.

In subsequent figures of schemes of measuring compositions is consideredthe followingmarking:

1- hot plate, 2 – cold plate, 3 – polystyrene frame, 4 – plywood board (PWB), 5 – low emissivity surface (LES), 6 – air gap, 7 – measuring chamber.

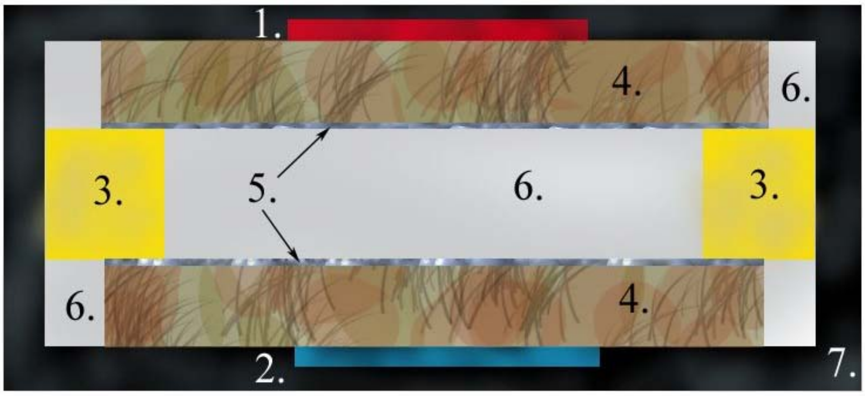

Figure 4: Scheme of measuring composition LES to LES

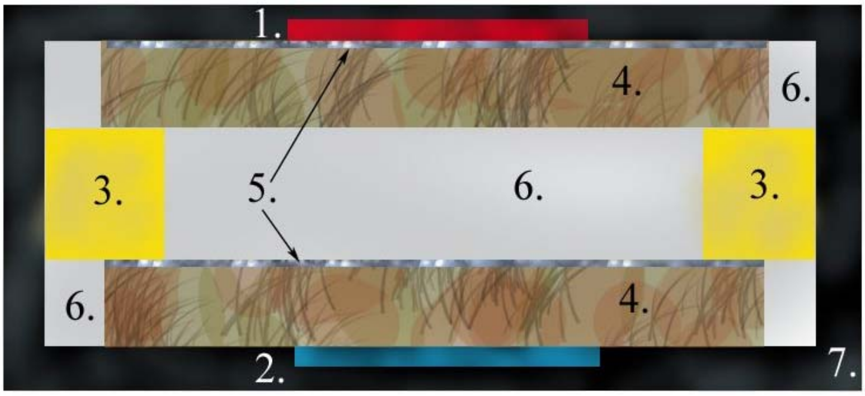

Figure 5: Scheme of measuring composition PWB to LES

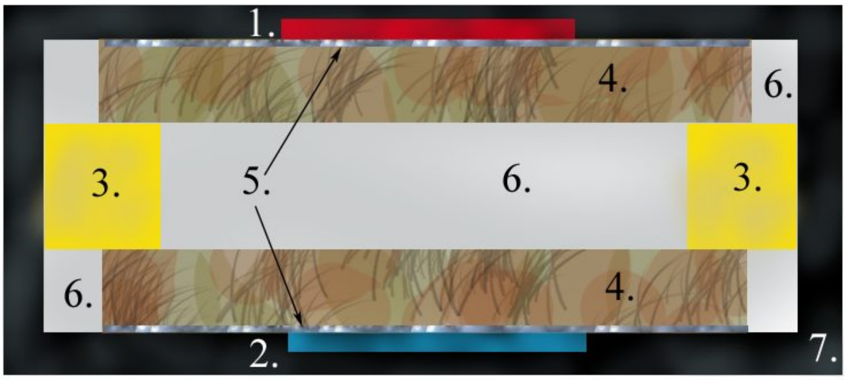

Figure 6: Scheme of measuring composition PWB to PWB

Table 2: Experimental values of thermal resistance Rof construction compositions

Composition	Thermal resistance ofmultilayer$R$ [$m^2.K.W^{-1}$]
LES to LES	1,051
PWB to LES	1,010
PWB to PWB	0,537
plywood board (separate contact measurement)	0,195

For the assessment of effect ofcoating onthermal resistance of layerscan be calculatedequivalentthickness ofconventional contactinsulation, which should be adequate to thermalresistance.The calculation isperformedas:

$$d = R \,.\, \lambda, \qquad (5)$$

where is: d - equivalent thickness of conventional thermal insulation [m], R - thermal resistance of 20mm thick air layer [$m^2.K.W^{-1}$], λ - thermal conductivity of conventional insulation (λ = 0,04 $W.m^{-1}.K^{-1}$).

Substituting into the formulathe following values were calculated.

Table 3 : Calculated values of equivalent thickness of conventional contact insulation

Composition	Thermal resistance of 20mm thick air layer [$m^2.K.W^{-1}$]	Equivalent thicknessof conventional thermal insulation [mm] (λ = 0,04 $W.m^{-1}.K^{-1}$)
LES to LES	0,661	26,5
PWB to LES	0,621	24,8
PWB to PWB	0,148	5,9

As can be seen the performance of plywood boars with low emissivity surface are very good. In fact, it this particularly case the thin layer of aluminium can substitute thermo-insulative role of polystyrene. However, this is valid for direction of heat flow from top to bottom and in case of dry surfaces. Presence of condensate will ruin low emissivity and therefore thermal resistance. Another important (and obvious) results is about influence of second LES. Since the emissivity of PWB is about 0,94 and LES less than 0,1 application of LES on one side leads to dramatic reduction in heat flow. Addition of the other LES has just minor effect.

6. Thermal properties of the basic type of reflexive thermo-insulating multilayer

The next set of experiments was carried on commercially available thermal insulation based on the composition of foils with low emissivity surfaces with transparency distance inter layers (foil with air bubbles). The measurements were realized according to same concept like above described experiments with polystyrene frames for predefined air layer (see figure 1). Direct contact measurements were carried on the same compositions as well.

In subsequent table is consideredthe followingmarking: A – thin polypropylene foil with both side aluminium coating, B – transparent polypropylene foil with air bubbles in thickness of 4 mm, a.l. – air layer.

Table 4 : Experimental values of thermal resistance Rof construction compositions

		Thermal resistance R [$m^2.K.W^{-1}$] (mean temperature / temperature gradient of hot and cold plate [°C])				Equivalent thicknessof conventional thermal insulation [mm] ($\lambda = 0{,}04$ $W.m^{-1}.K^{-1}$)
Composition of layers	Thickness [mm]	10/10	10/20	35/30		10/20
a.l. 20mm-ABA-a.l. 20mm	44,6	0,66	0,65	0,54		26,2
a.l. 20mm-ABABA-a.l. 20mm	47,4	0,78	0,79	0,68		31,6
a.l. 20mm-ABABABA-a.l. 20mm	50,7	0,91	0,90	0,79		36,2
a.l. 20mm-ABABABABA-a.l. 20mm	55,1	1,14	1,17	0,97		46,7

Composition of layers (contact measurement)	Thickness [mm]	10/10	10/20	35/30		10/20
ABA	4,3	-	0,13	-		5,0
ABABA	8,7	-	0,23	-		9,3
ABABABA	13,2	-	-	-		-
ABABABABA	17,5	-	0,45	-		17,9

For better illustration are the results compared with calculated equivalent thickness of conventional insulation (similar to foam polystyrene). As can be seen the reflective multilayer insulation have in contact measuring thermal properties slightly better, therefore the λ is less then 0,04 $W.m^{-1}.K^{-1}$. In case of presence of air layers, the insulation performance seams to be somehow lower. This is probably related to fact, that multilayer insulation tends to created pillow-like shape as it is compressed between polystyrene frames. The outcome is significantly reduced thickness of the air layer; therefore such results can be problematically compared with results obtained on with plywood boards.

7. Conclusions

The paper presented some results measured on different types of compositions related to low emissivity surface applications. It has been proved, that thermal radiation is significant part of overall thermal flow even in common conditions. In some cases it can be comparable to conventional insulations and/or it can be good addition to the thermo isolative systems. The possibilities of such applications are definitely not fully exploited jet.

Received results will be invalid in the case of internal surface condensation. Surface condensation is fundamentally changing the surface emissivity and cancels the effect of suppressing the radiant flux, because the emissivity of liquid water is given as $\varepsilon = 0.98$. In addition, the presence of liquid water also reduces the thermal resistance due to higher component heat conduction. Condition of thecondensate formation andpreventits formation in reflexive thermo-insulation systems aresubject to our furtherresearch.

Acknowledgements

This paper was created with financial support of internal project FAST-S-11-47 VUT Brno and project CEZ MŠMT č. 0021630511.

References

[1] http://www.infrared-thermography.com/material-1.htm (August 2011).

[2] KOPKÁNĚ, D.; NOVÁČEK, J.; ŠŤASTNÍK, S. Metodika měření reflektance stavebních materiálů. In *sborník konference Maltoviny 2010.*Brno, VUT Brno. 2010. p. 1 - 12. ISBN 978-80-214-4204-7.

[3] STEUER, R. Studium fyzikálních vlastností materiálů vnějšího zateplení budovz hlediska snížení vlhkostní zátěže. Brno, 2008. 134 s. Ph.D. Thesis. Vysoké učení technické v Brně.

[4] ČSN 730540. *Thermal protection of buildings*. Praha: Český normalizační institut. 2005.

[5] ČSN EN 12664. *Thermal performance of building materials and products - Determination of thermal resistance by means of guarded hot plate and heat flow meter methods - Dry and moist products of medium and low thermal resistance.* Praha: Český normalizační institut. 2001. 72 p.

Hysteretic effects ofmoisture storage of calcium silicate insulation boards

Olga Koronthalyova[1], **Peter Matiasovsky**[1], **Juraj Veselsky**[2], **Daniel Szabo**[2]

[1]Institute of Construction and Architecture SAS, Slovak Academy of Sciences, Dubravska c. 9, SK-84503 Bratislava, Slovakia, email:usarkoro@savba.sk

[2]Slovak Technical University, Faculty of Civil Engineering, Radlinskeho 11, SK-813 68 Bratislava, Slovakia

Abstract: *Significance of hysteretic effects on hygroscopic moisture storage of calcium silicate insulation boards (CS)is investigated. The water vapour adsorption, desorption and scanning curves of CS were measured in relative humidity (RH) range from 0 to 98% by the standard desiccator method, consisting in conditioning the samples in desiccators under constant RH and temperature (23°C). The hygric performance of CS specimen under dynamic conditions - cyclic changing RH and constant temperature - was tested in a climatic chamber with precise control of temperature and relative humidity. The test was performed with 24/48 hours step changes between 53 and 81% of RH. The moisture uptake and release during the dynamic test was determined by a continuous weighing of the specimen. The results of the dynamic test are compared with numerical simulation, using the steady - state hygric properties. The both static as well as dynamic measurements have shown a presence of hysteretic behaviour. Based on the analysis of the experimental results a significance of hysteretic effects on hygro-thermalperformance of CS in the hygroscopic range is discussed.*

Keywords: *Hysteretic effect, water vapour sorption, cyclic changing relative humidity, calcium silicate insulation board.*

1. Introduction

In the simulations of the hygro-thermal behaviour of building structures the moisture capacity of building materials is the most frequently expressed using the main adsorption curve or the mean of the adsorption and desorption curve. However in actual circumstances the materials in building structures are exposed to changing boundary conditions. Therefore – in case of presence of the hysteretic effects - their actual moisture capacity and consequently moisture content correspond to the moisture capacity/content of the scanning curves between the adsorption and desorption curve. The measurements of the scanning curves of the building materials are not very frequent.Some building materials scanning curves can be found in [1-3]. The measured scanning curves of wood have been presented for example in [4-5].

The aim of the study was to determine the actual primary drying scanning curves of the CS material and to assess the significance of the hysteretic effects on itshygro-thermal performance.

Calcium silicate is an inorganic high porous fibre-reinforced thermal insulation material composed of the hydrous calcium silicate and the cellulose reinforcing fibres. Some types of calcium silicate have been developed as thermal insulation materials applicable from the indoor side of envelope parts of buildings. For these types of CS, the pore size distribution with high portion of pores (80-90%) in the relative narrow pore radius interval (10^2-10^3 nm) is typical [6].

In the hygroscopic region, the thermal conductivity of CS is relatively strongly dependent on the moisture content [6]. Therefore if hysteretic effects significantly affect its actual moisture content, they should be involved also in an evaluation of its thermo-insulation ability.

2. Experimental part

The tested material is characterised by the following basic parameters: bulk density, open porosity and capillary moisture content. The bulk density was calculated from volume and mass of the dried out specimens (oven drying at 105°C). The capillary moisture content was determined from a time-controlled capillary water uptake experiment, the open porosity from the water saturation test.

The water vapour resistance factorwas measured by the standard dry-cup (0 – 53% RH – silica-gel and climatic chamber) and wet-cup (100 – 53% RH - water and climatic chamber) methods [7].

The water vapour main adsorption and desorption isotherms as well as scanning curves were determined by the standard gravimetric desiccator method, which consists in conditioning the samples in desiccators under constant relative humidity and temperature (23°C) until the static equilibrium is achieved [8]. The measurements are done for eight values of RH: 12%, 33%, 53%, 75%, 79.5%, 85%, 94% and 98%. The dimensions of the samples were ca 40 x 40 x 30 mm. The samples were oven dried beforehand at 105 °C. The mass of the samples was weighed by means of electronic scales with the accuracy 0.001g.

The dynamic test was performed in climatic chamber at the Faculty of Civil Engineering Slovak Technical University. The test was performed with 24/48 hours step changes between 53 and 81% RH. The temperature was kept at constant value 23 ± 0.3°C (Figure 1). RH changes in the chamber were controlled by dry and wet air streams. The relative humidity near the sample was monitored by the capacity RH sensor and the temperature was measured by the resistance sensor Pt 100. The dimensions of the measured specimen were: 293 x 190 x 39.1 mm.

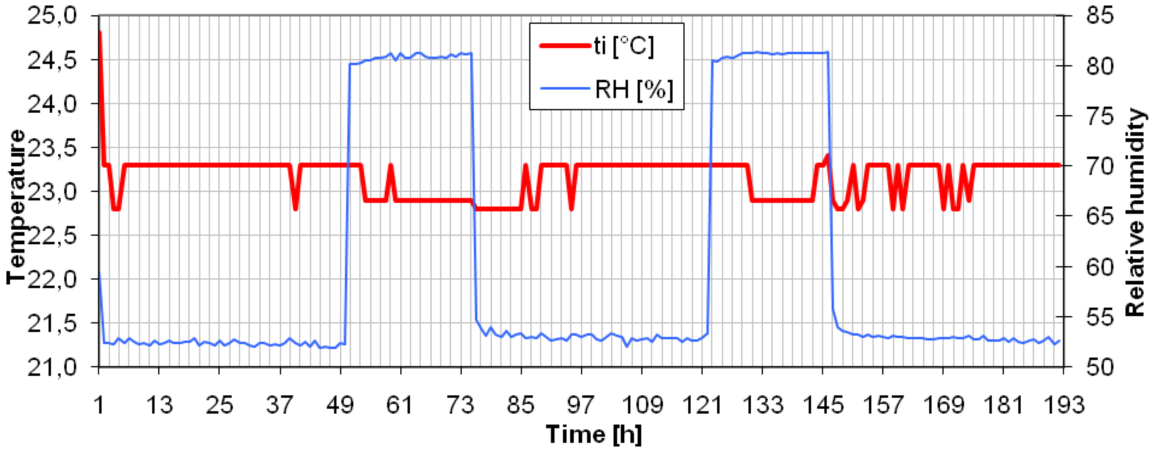

Figure 1: Measured temperature and relative humidity courses during the dynamic test in climatic chamber

The specimen was sealed on all but two surfaces by epoxy in order to guarantee 1D water vapour flow, the area of active surfaces was 0.11134 m^2. The weight of the sample was measured by the balance Sartorius with the accuracy 0.1g. The weight of sample, temperature and RH in the chamber were registered every hour.

3. Numerical simulation

The 1D simulation tool WUFI (version 2.2) is used for the moisture content calculations of CS sample during the dynamic test. Based on the simulation results, the sample mass courses are calculated. The time step of 1 hour and the mesh size of 0.65 mm were applied in calculations.

The air flow velocity near the sample was estimated to 1.3 m/s. On the base of the similarity relations and the Lewis relation the value of the surface film coefficient for diffusion $\beta_v = 7.35 \cdot 10^{-8}$ s /m was determined, which has been used in simulations.

4. Results and discussion

The determined basic material properties of the CS as well as its water vapour resistance factors (μ) are in Table 1.

Table 1: Measured basic material properties and μ-values of CS

Bulk density [kg/m^3]	**Open porosity [-]**	**Capillary moisture content [m^3/m^3]**	**μ (dry cup) [-]**	**μ (wet cup) [-]**
280	0.90	0.87	4.5	2

The measured main adsorption and primary desorption scanning isotherms from RH of 98, 94, 85 and 79.5 % are presented in Figure 2. As it can be seen from Figure 2, the hysteretic effects are noticeable in case of desorption from RH higher than 80%. On the other hand the hysteretic loop between the main adsorption and desorption from 98% RH is narrow and the obtained volumetric equilibrium moisture content values in the range of lower RH (RH ≤75%) are below 1% even in case of desorption from 98%. The adsorption curve as well as desorption ones are characterised by a steep increase/decrease in the interval of high humidity (above ca 85 %), but

Table 2: Mean values of moisture capacity (kg/m^3) for main adsorption curve and primary scanning desorption curves

RH interval	**Main adsorption**	**Desorption from 98% RH**	**Desorption from 94% RH**	**Desorption from 85% RH**	**Desorption from 79.5% RH**
11.3-53%	5.3	5.8	5.0	4.9	4.8
53-75%	10.7	8.4	7.3	7.1	8.5
75-85%	46.5	26.3	19.0	21.6	26.8
85-94%	100.8	111.1	80.0	-	-
94-98%	718.2	634.2	-	-	-

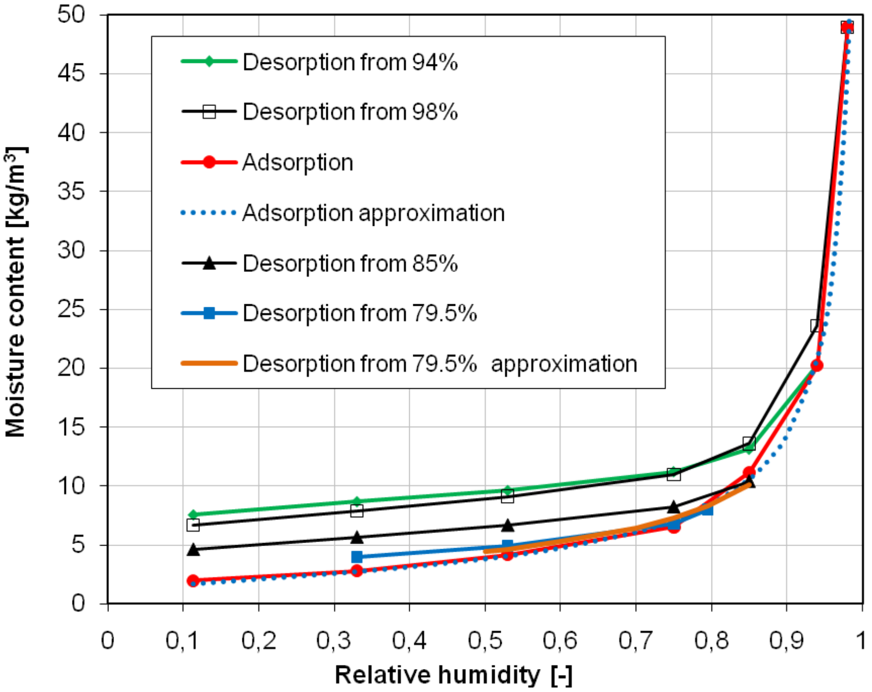

Figure 2: Measured main adsorption isotherm and desorption isotherms from relative humidity of 98, 94, 85 and 79.5 % RH. Approximation functions (Eq. 1), used for main adsorption and desorption from 79.5 % RH.

the differences between the adsorption and desorption moisture capacity are not very significant. In region of lower RH (below 80%) the slopes of the main adsorption and desorption curves are practically the same (Table 2).

After desorption from 85% and 79.5% RH also the 1st scanning adsorption curves from 11.3% and 33 % RH have been measured. In both cases the course of the 1st scanning adsorption curve is practically identical with the preceding desorption one.

The measured mass changes of the CS specimen during the dynamic test are presented in Figure 3. During the of moisture release phase some weak hysteretic effects can be observed, however the mass change during the second moisture release is practically identical with the first one, that indicates that quasi steady state is achieved.

The results of the dynamic test are compared with numerical simulation. Two calculations have been done: in the first calculation the measured main adsorption isotherm was used as the moisture storage function while in the second one desorption curve from 80% was used. In the simulations, the main adsorption and the desorption curve from 79.5% RH are fitted by the relation of van Genuchten type (1):

$$w(\varphi) = w_{max} \cdot (1-(A \cdot \ln\varphi)^{n1})^{n2} \tag{1}$$

where ϕ is the relative humidity, w_{max}, A, n1, are parameters (Table 3); n2=(1-n1)/n1.

The comparison between the measured and by relation (1) approximated adsorption and desorption curves is shown in Figure 2.

Table 3: Equation (1) parameters for main adsorption and desorption from 79.5% RH

Main adsorption			**Desorption from 79.5% RH**		
w_{max}[kg/m³]	**A**	**n1**	**w_{max}[kg/m³]**	**A**	**n1**
588	1900	1.7	588	8000	1.567

The water vapour resistance factor moisture dependence was approximated in the simulations by the following relation:

$$\mu(\varphi) = \frac{1}{a + b \cdot \exp(c \cdot \varphi)}, \tag{2}$$

where a, b, c, are the parameters: a = 0.22, b = 0.00047 and c = 8.5

The comparison of the measured and simulated CS sample mass changes is presented in Figure 3. The simulation using the main adsorption is in very good agreement with the measured 1st moisture uptake. Starting from the 1st moisture release, the measured results coincide with the simulation using desorption from 80%. Taking into account that the desorption curve from 80% and the main adsorption are relatively close (Figure 2), it is possible to note that the calculated specimen mass is very sensitive to the moisture storage function used. The results of dynamic test simulation also confirm that starting from the 1st moisture release, the processes of adsorption and desorption can be described by the same moisture storage function. It is in an agreement with the static measurements results, when in case of desorption from 85 and 79.5% RH, the 1st scanning adsorption curve is practically identical with the preceding desorption one.

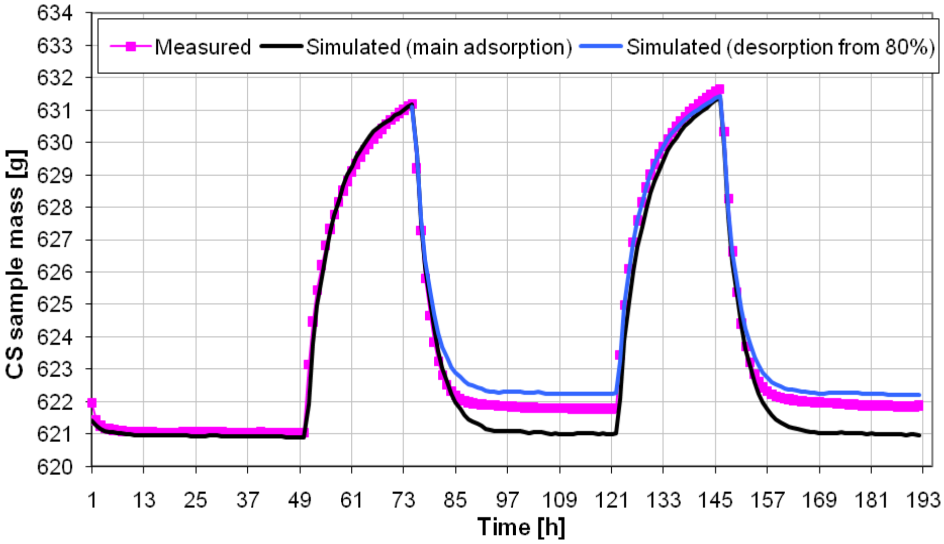

Figure 3: Measured and simulated mass changes of CS specimen during dynamic test

In order to evaluate the possible effect of the noticed CS hysteresis on its actual thermal conductivity under cyclic changing of RH, the obtained differences of moisture content between the main adsorption curve and the desorption from 98% are analysed. The highest differences between the values are noticed in the RH range from 33% to 55 %, where the volumetric moisture contents differ by 0.5% (Figure 2). Taking into account the CS thermal conductivity moisture dependence [6], the higher moisture content of the desorption curve can cause the thermal conductivity increase no more than of 20%.

5. Conclusions

The moisture storage properties of CS material under static conditions and under cyclic changes of RH are determined in the hygroscopic region.

The static as well as dynamic test show the presence of the hysteresis effects in CS hygroscopic moisture storage. The hysteretic effects are practically negligible in case of desorption from relative humidity lower than 80%. In case of desorption from the higher relative humidity, the presence of hysteresis is noticeable, but due to narrow hysteretic loop the effect of hysteresis on the hygrothermal performance, namely for evaluation of thermo-insulation ability of CS material is not significant.

In case of CS material under cyclic changes of relative humidity, the primary desorption curves can be used as the moisture storage functions with the sufficient accuracy.

Acknowledgments

This research was supported by the Slovak Grant Agency VEGA (Grant No. 2/0159/10).

References

[1] Hansen, K. K. *Sorption isotherms, A catalogue*. Department of Civil Engineering, Technical University of Denmark, 1986

[2] Koronthalyova, O. Water vapour sorption hysteresis of autoclaved aerated concrete and burnt clay brick. In *Proceedings of the 1st Central European Symposium on Building Physics,* Technical University of Lodz. 2010. p. 47-53. ISBN 978-83-7283-367-9

[3] Koronthalyova,O. Water vapour sorption of building materials – modelling of scanning curves. In*Proceedings of the 9th Nordic Symposium on Building Physics, NSB 2011,* Editors: J. Vinha, J. Piironen, K. Salminen, Department of Civil Engineering, Tampere University of Technology, Tampere, Finland. 2011. p. 655-662. ISBN 978-952-15-2573-5

[4] Peralta, P. N. Sorption of moisture by wood within a limited range of relative humidities. In *Wood and Fiber Science*.1995.27 (3). p. 250-257. ISSN 0735-6161

[5] Time, B. *Hygroscopic Moisture Transfer in Wood, PhD Thesis 1998:20,* Dept. ofBuilding and Construction Eng. Trondheim, Norvegian University of Science and Technology, 1998.

[6] Koronthályová, O. – Matiašovský, P. Thermal Conductivity of Fibre Reinforced Porous Calcium Silicate hydrate-based Composites. In *Journal of Thermal Envelope and Building Science.* 2003. 26 (4). p. 71-89. ISSN 1744-2591

[7] EN ISO 12572:2001 *Hygrothermal performance of building materials and products - Determination of water vapour transmission properties.*

[8] EN ISO 12571:2000 *Hygrothermal performance of building materials and products - Determination of hygroscopic sorption properties.*

Fly-ash influence on the thermal diffusivity of ceramic samples

Jozef Kováč[1], Anton Trník[1,2], Igor Medveď[1,2]

[1]Department of Physics, Constantine the PhilosopherUniversity, 94974 Nitra, Slovakiaemail: jozef.kovac@ukf.sk
[2]Department of Materials Engineering and Chemistry, CzechTechnicalUniversity, 16629 Prague, Czech Republic

Abstract: *At present the importance of using secondary raw materials in several types of composite materials has become a challenging task. The topic of this paper is the study of the fly-ash influence on the thermal diffusivity of ceramic materials. The measurements were carried out by the flash method. The temperature dependencies of the thermal diffusivity up to 600°C were obtained, and their discussion is provided.*

Keywords: *thermal diffusivity, fly-ash, flash method.*

1. Introduction

Increasing living standards of people is a cause of a growing consumption of materials and energy.The consequence is an increased growth of industrial production and energy. It causes the problem concerninga necessarily increasing amount of waste.One possibility is to use waste produced as a source of secondary raw materials. One of these materials is the fly-ash that is created in the combustion process (for example, in power plantsduring coal burning).An addition of the fly-ash into ceramic materials is one of the possible solutions of its use. However, the fly-ash can change some properties of materials, and it is of great importance to study to what extent the fly ash can be added as to not to decrease the desired final material properties from the thermal or mechanical point of view. In this paper, we focus on its effect on the thermal diffusivity of a kaolin-based ceramic material.

2. Theory of the flash method

To measure the thermal diffusivity of a material, we used the standard flash method. This method is based on the measurementof a thermal response of the material, a part of which is heated by a short heat-pulse. The impulse energy is absorbed in the material only within a thin layer of width ε, while the rest of it remains (at the very beginning) thermally unaffected. The theoretical description is based on an approximation given by the one-dimensional heat equation. One assumes thatthere is no thermal flux through the material ends. In the limit of a very small ε, the time evolution of the temperature at the end of the sample that is not subject to the impulse is given as [1]

$$T(t) = T(e,t) = \frac{Q}{\rho c e}\left[1 + 2\sum_{n=1}^{\infty}(-1)^n \exp\left(-n^2\pi^2 \frac{a\,t}{e^2}\right)\right], \qquad (1)$$

where Q is the pulse energy per unit area, ϱ is density, c is the heat capacity, e is the thickness of the sample. After a sufficient time period (in the limit t→∞) and under the assumption that no heat losses occur, the temperature becomes stationary at a value Tlim. The ratio of the temperature rise and the final temperature limit is [2, 3]

$$\frac{T(e,t)}{T_{\lim}} = \left[1 + 2\sum_{n=1}^{\infty}(-1)^n \exp\left(-n^2\pi^2\omega\right)\right], \tag{2}$$

where ω is the dimensionless time defined as

$$\omega = ate^{-2}. \tag{3}$$

The development of the relative temperature rise depending on the dimensionless time ω is shown in Figure 1.

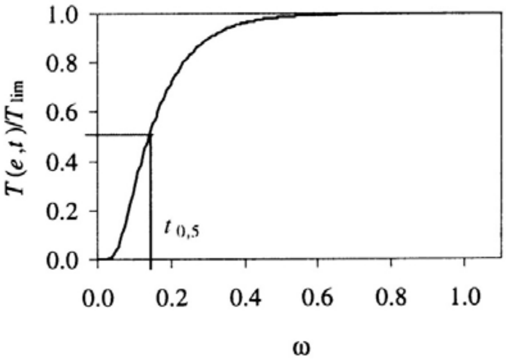

Figure 1: The relative temperature rise depending on the dimensionless time ω.

A simple way to calculate the thermal conductivity was introduced by Parker et al. [2]. It is based on identifying a characteristic point on the temperature curve which corresponds to the half of the maximal temperature rise. Then ω attains the values around 0.1388 and the thermal conductivity can be calculated from the simple relation [2]

$$a = 0.1388\frac{e^2}{t_{0,5}}, \tag{4}$$

where $t_{0.5}$ is the actual time when the temperature rise is equal to the half ofthe final temperature limit.

3. Measurement apparatus

The basic part of the measurement apparatus is a source of radiation. We used a xenon flash lamp. The radiation source has an adjustable flash duration. The pulse length is governed by a software unit impulse. An iris was placed between the lamp and the sample to achieve a more uniform distribution of the heat pulse on the sample surface. A thermocouple is attached to the other end of the measured sample (i.e., to the end not exposed to the pulse). The thermocouple measures the time dependence of the temperature response to the pulse. The apparatus contains a reference sample which is not exposed to direct pulse. The temperature of the reference sample is also measured by a thermocouple. Both thermocouples are connected differentially and actually measure the temperature difference between the two samples. In addition to increasing the sensitivity of the apparatus,this arrangementeliminates the adverse effects on the measurements becausethey have the same impact both samples. The difference of the thermocouples voltages is measured by a digital device that transfers the data to a computer. In order to measure the dependence of the thermal diffusivity on the temperature, the measurement apparatus was placed in a furnace. The furnace temperature is regulated by an adjustable voltage source.

Samples
We analyzed two materials denoted as A and D. The material A was composed of clay(60%) and an opening material (40%). The opening material was made of clay firing to 1000°C at theheating rate 10°C/min and lasting 90 minutes at the maximal temperature. The clay is an essential part in the production of tiles, enamels, electroporcelain, chimney liners, and utility ceramics. The material D contained 60% clay, 20% opening material, and 20% fly-ash from Hodonin power plant in the Czech Republic. The fly-ash contained SiO2 (29.1%), CaO (25.9%), Al2O3 (17.7%), Fe2O3 (2.7%), MgO (2.6 %), and other components. The samples for the measurement of the thermal diffusivity were made from these two materials. The samples had the cylindrical shape with the diameter of12 mm and the thickness of1.3 mm.

4. Experimental results

Experimental results concerning the temperature dependence of thermal diffusivity of sample A are shown in Figure 2. It shows that the thermal diffusivity decreases with an increasing temperature. The first rapid decrease is evident at the temperatures below 100 °C, and itcorresponds to the evaporation of physically bound water in the sample. The second rapid decrease is evident at about 350°C. In this case dehydroxylation occurs in the sample when kaolinite undergoes a structural transformation into metakaolin. The basic structure of kaolinite consists of tetrahedral layers $[Si_2O_5]^{2-}$ and octahedral layers $[Al_2(OH)_4]^{2+}$ [4].The chemical reaction of dehydroxylation can be formally described by the equation $Al_2O_3.2SiO_2.2H_2O \rightarrow Al_2O_3.2SiO_2 + 2H_2O$ [4]. During this reaction water (which was previously bound) is released. According to the measurements, dehydroxylation occurs at about 420° C. However, the structure of kaolinite has defects in real crystals, and this affects the temperature at which dehydroxylation takes place.

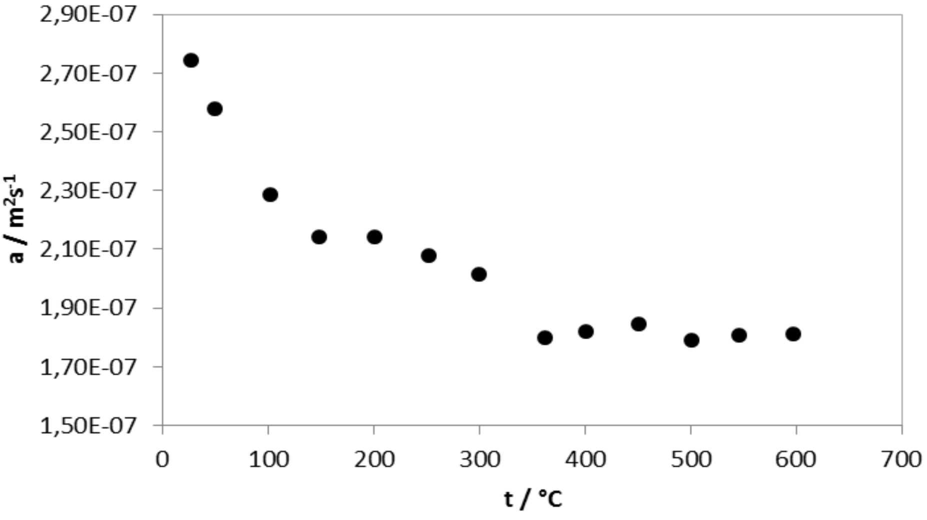

Figure 2: The thermal diffusivity in dependence on the temperature of sample A.

A larger amount of defects caused by instability of a crystalcauses that dehydroxylation occurs at lower temperatures.According to our measurements we may conclude that the sample containedrather many defects.

The temperature dependence of the thermal diffusivity of sample D is in Figure3. In this case it is also apparent that the thermal diffusivity decreases with an increasing temperature. The first significant decrease at 100°C corresponds again to the evaporation of physically bound water from the sample. However, dehydroxylation is apparent at about 450°C, wherea notable decrease of the thermal diffusivityis obvious.

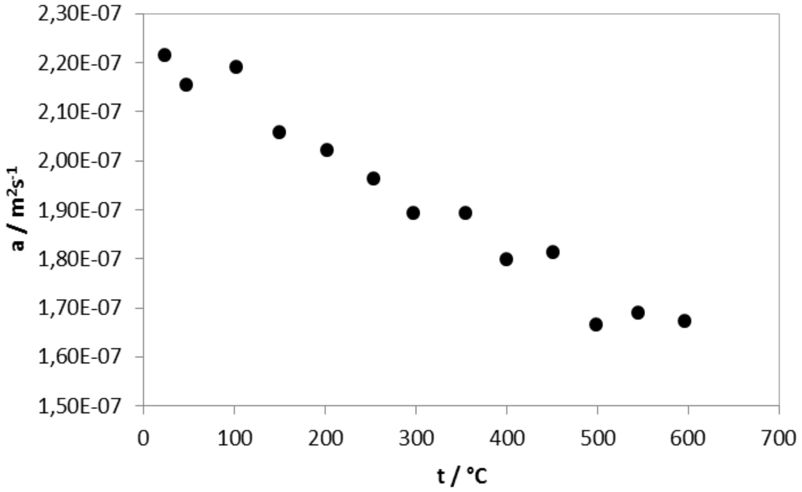

Figure 3: The thermal diffusivity in dependence on the temperature of sample D.

5. Conclusion

Comparing the Figs. 2 and 3, we observe that the addition of fly ash in ceramic samples rather decreases the thermal diffusivity, especially at lower temperatures. Indeed, the most significant difference is betweenthe room temperature and about 100°C. At higher temperatures the difference is smaller, until it becomes rather insignificant above about 500°C. The measurement results show that the addition of fly ash in ceramic samples leads to a positive effect on the thermal diffusivity of ceramic material in the temperature range from the room temperature to 100°C. Therefore, this method is suitable for the production of ceramic products which are not exposed to high temperatures. It would be appropriate to focus on the change of properties of samples after firing ceramics in different temperature regimes in other measurements. It would also be appropriate to focus on measuring the changes of mechanical properties of ceramic samples which may affect the practical applicability of ceramic materials containing fly ash.

Acknowledgements

This research was supported by grants VEGA 1/0302/09, APVV SK-CZ-0004-09 and the Ministry of Education, Youth and Sports of the Czech Republic, under the project No. MSM: 6840770031.

References

[1] VOZÁR, L. Flash method for thermal diffusivity measurement. Theory and praxis. CPU, Nitra, ISBN 80-8050-362-1, 2001.

[2] PARKER, W.J. – JENKINS, R.J. – BUTLER, C.P. – ABBOTT, G.L. Thermal Diffusivity Measurement Using the Flash Technique. In J. Appl. Phys. 32. p. 1679-1684. 1961.

[3] O.Y. Troitsky, V.I. Ryazanov, In-situ measurement of thermophysical properties by means of the flash technique. In High Temperatures – High Pressures 32. p. 389-392. 1991.

[4] ŠTUBŇA, I. – TRNÍK, A. – VARGA, G. Dehydroxylácia kaolinitu – krátky prehľad. In Silikátnik 2006, Slovenská silikátová vedecko-technická spoločnosť 2006.

Sorption hysteresis of lightweight carbonate plasters

Peter Mihalka, Peter Matiasovsky, Bozena Vasilkovova

Institute of Construction and Architecture, Slovak Academy of Sciences, Dubravska cesta 9, 845 03 Bratislava, Slovakia

Abstract: *The main water vapour adsorption – desorption curves and the scanning curves in the hygroscopic range were determined for lightweight carbonate plaster by a vacuum dessicator method. Simultaneously the sorption isotherms and pore size distribution curve of the material were determined by the BET nitrogen adsorption/desorption tests, together with the pore size distribution by the Mercury Intrusion Porosimetry (MIP) technique. The sorption of the analysed material has a hysteretic character. Various models of the hysteresis were developed until now. The determined water sorption curves were approximated on the basis of BET sorption and MIP data with use of capillary condensation model. The approach simultaneously enabled an analysis of the scanning curves.*

Keywords: *Sorption, hysteresis, pore structure*

1. Introduction

A pore structure of the lightweight carbonate interior plaster was analysed by the sorption and intrusion techniques. A comparison of the water vapour and nitrogen sorption isotherms and the mercury and nitrogen pore size distribution curves gives complex information on the material pore structure parameters.

A previous comparison of the nitrogen and water sorption data for plasters with the mercury intrusion data confirmed that the nitrogen sorption as well as the mercury intrusion cannot be used directly to predict the water vapour sorption capacity (Matiasovsky and Bagel, 2009). The plasters are characterised by a lower sorption capacity for the nitrogen than for the water vapour. The MIP technique gives information about only a part of the pore system. Nevertheless the results of both methods can be applied indirectly for modelling the water vapour sorption of some materials. According to Lowell et al. (2004) in general three approaches to the sorption hysteresis modeling were defined: the independent pore model, the network model and the disordered porous material model. The first approach was applied for modelling the lightweight carbonate water vapour sorption.

2. Measurements

For selected lightweight carbonate plaster the measurements of the water vapour and nitrogen sorption were carried out. The analysed material had the bulk density of 580 kg/m3 and its open porosity was 67 %. Simultaneously the mercury intrusion porosimetry of the material was made. From the results of the measurements the sorption isotherms, the pore size distributions and the specific surface areas were determined.

The water vapour and nitrogen sorption experiments belong to the BET sorption techniques. The determination of pore size distribution is the intrusion technique. In both (water and nitrogen) sorption tests the amount of mono-layer adsorbate can be determined by fitting the sorption isotherm to the BET (Brunauer, Emmett & Teller 1938) equation.

2.1 Water vapour sorption

The water sorption measurement gives information about the equilibrium moisture content in the range of ca 0 – 98 % relative humidity.

The BET specific surface area in (m^2/g) can be determined from water vapour adsorption data, using the equation based of the amount of a monolayer adsorbate,expressed in (g/g), completely covering the specific surface of a material:

$$SSA_{H_2O} = u_m \cdot 3610 \tag{1}$$

The water vapour sorption isotherms at 20°C temperature were measured by the static dessicator method. The samples were placed in sealed dessicators containing saturated solutions of the salts: $LiCl.H_2O$, $MgCl_2.6H_2O$, NH_4NO_3, NaCl, NH_4Cl, KCl, KNO_3, and $CuSO_4$+ $2H_2O$, maintaining the atmospheres of 11.5 %, 33 %,64 %, 75.4 %, 79.5 %, 84.7 %, 94 %, 98 % relative humidities respectively, 53 % relative humidity were maintained in the climate chamber. The equilibrium moisture content was determined by the gravimetric method.

2.2 Nitrogen sorption

The nitrogen sorption measurement gives the equilibrium amount of monolayer adsorbate, expressed in (cm^3/g), in the same range of relative pressures as in case of the water vapour sorption. The BET specific surface area can be determined using the equation:

$$SSA_N = v_m \cdot 4.35 \tag{2}$$

Besides the adsorption and desorption curves, additional information about the pore size distribution of analysed material was determined from the nitrogen desorption isotherm in the range of pores with the radii of 1 – 89 nm, using the BJH model (Barret, Joyner, Halenda1951).

Nitrogen adsorption-desorption isotherms of nitrogen gas at liquid nitrogen temperature were obtained with Quantachrome Autosorb iQ Station 1 instrument. The isotherms were obtained for the 0.01 – 0.98 relative pressure range.

2.3 Mercury intrusion porosimetry

The mercury intrusion porosimetry is based on the premise that a non-wetting liquid (one having a contact angle greater than 90°) will only intrude capillaries under pressure. The relationship between the pressure and capillary diameter is described by Washburn (1921).

The relative pressure-volume data were determined by the 2002 mercury intrusion porosimeter and the micropore unit 120 of ERBA Science, enabling the determination of pores with radii from 3.7 nm up to 0.06 mm. The pore size distribution is determined from the volume intruded at each pressure increment. The total porosity is determined from the total volume intruded. The specific surface area of pores is calculated from the pore radii and the pore volumes.

3. Results and analysis

According to IUPAC classification (Sing et al., 1985) the measured water and nitrogen sorption isotherms of lightweight carbonate plaster belong to type IV isotherms and type H1 hysteresis, typical for porous materials containing well defined cylindrical-like pores (Figure 1). For the hysteresis type H1 the independent pore model is suitable (Lowell et al., 2004).

From the comparison of the lightweight carbonate sorption results a lower sorption capacity for the nitrogen than for the water vapour is evident. The specific surface areas ratio determined for water and nitrogen A_{water}/A_Nequals ca 3. The similar ratio was found for the adsorbates volumes at 95 % relative pressure V_{water}/V_N. The differences between nitrogen and water vapour sorption was discussed in detail by Delmelle et al. (2005) presenting the values of specific surface areas ratio for the volcanic ashes within interval 1.4 - 3.8 and the ratios of the adsorbates volumes at 95 % relative pressure within interval 1.1 - 4.2.Matiasovsky and Bagel (2009) presented the ratios 1.32 - 10.38 and 0.54 - 2.43 respectively for plasters. In most of the mentioned cases the ratios of specific surface areas and adsorbed volumes are close as it is presented in Figure 2. For a majority of the analysed materials the V_{water}/V_N ratios represent the 0.78 portion of the A_{water}/A_N ratios.This result is can be explained if we suppose that the thickness of the adsorbate layer $t(p/p_o)$ on the adsorbate relative pressure p/p_o is expressed in (nm) by Halsey equation:

$$t = \tau \left[\frac{5}{\ln(p_0 / p)} \right]^{1/n} \tag{3}$$

where τ is the effective diameter of sorbate molecule equal to 0.277 nm for water and 0.354 nm for nitrogen, n = 4 at adsorption and 3 at desorption.Then thisvalueis identical with the ratio of effective diameters of water and nitrogen molecules. This relationship means that both adsorption and desorption isotherms are functions of the specific surface area. Only a few materials not satisfy it and they belong to cement based plasters characterised by a significantly higher sorption capacity for the water than for the nitrogen, given by the presence of gel pores accessible to water only.

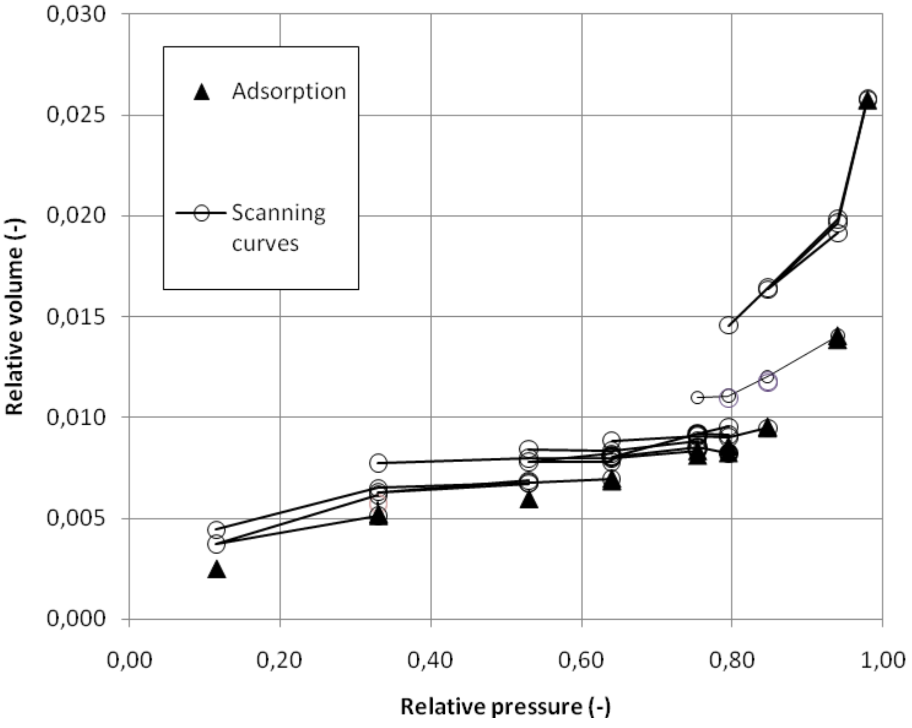

Figure 1: Water vapour sorption isotherms of lightweight carbonate plaster

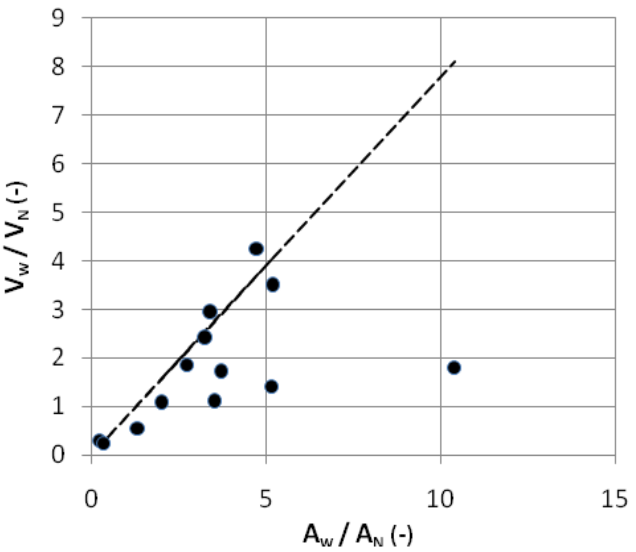

Figure 2: Similarity between ratio of specific surface areas (A_{water}/A_N) and ratio of sorbate volumes at 95% rel. pressure (V_{water}/V_N), ----equality reduced by ratio of effective diameters of water and nitrogen molecules

In Figure 3 there is shown a relationship between specific surface areas and the adsorbates volumes at 95 % relative pressure already without the cement based plasters. The obtained correlations expressed for water and nitrogen give the regression coefficients corresponding, after the recalculation, with the statistical thicknesses of water (1 nm) and nitrogen (1.63 nm) adsorbatefilms at given relative pressure, calculated by Equation (3). The fact that the volume of both adsorbatesat 95 % is proportional to the specific surface areas suggests that the multilayer adsorption on the pore surfaces is the dominant process and the results of nitrogen sorption, multiplied by A_{water}/A_Nratio, can be applied at the water sorption modelling. In Figure 4 there is the application for lightweight carbonate plaster where the nitrogen sorption isotherms multiplied by the factor of 3 are compared with the water wapour sorption isotherms.

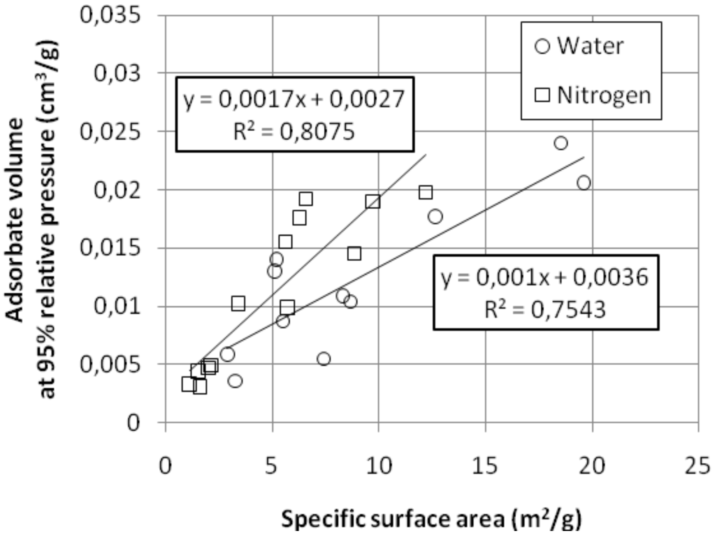

Figure 3: Dependence of sorbate volume at 95% rel. pressure on specific surface area

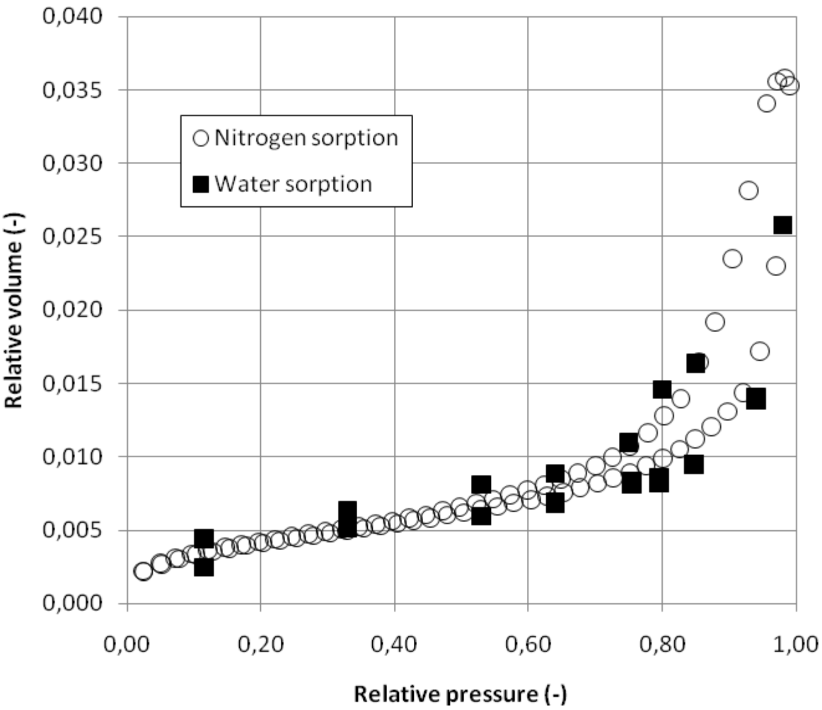

Figure 4: Sorption isotherms of lightweight carbonate plaster for nitrogen (increased by the factor of 3) and water

For modelling of the sorption hysteresis form pore structure parameters it is necessary to have information about the pore size distribution in the whole range of relative pressures.

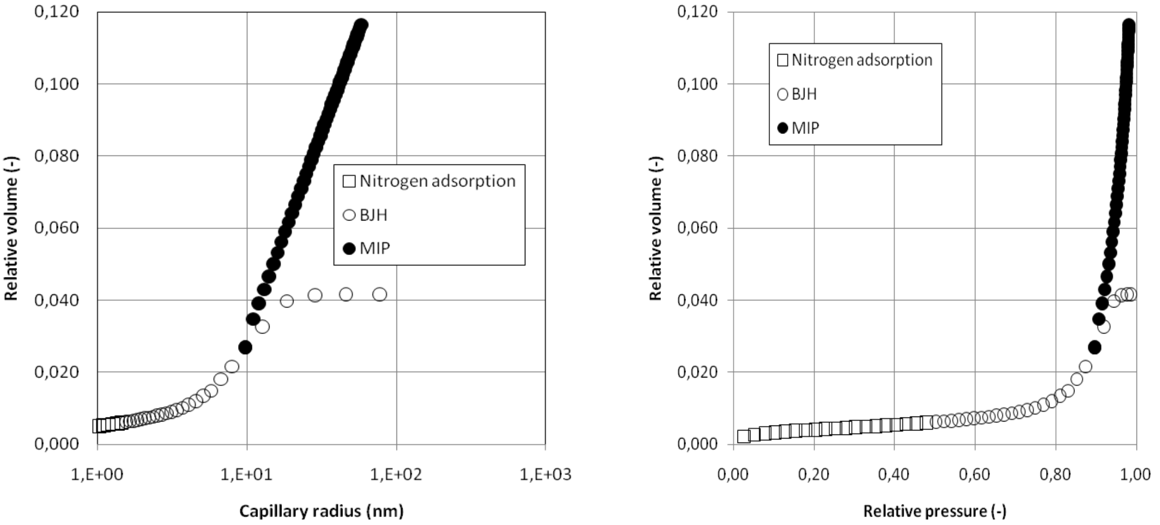

Figure 5: Pore size distribution of lightweight carbonate plaster (on left) recalculated into equilibrium condensed water contents (on right)

In Figure 5 there is the pore size distribution (on left) for the lightweight carbonate plaster recalculated into the condensed water contents at relative pressures (on right) with the use of theclassical Kelvin equation for water in the cylindrical pore:

$$\ln(p / p_0) = -\frac{k \cdot 0.535}{r_p} \tag{4}$$

where r_p is the pore radius in (nm) and k = 1 at adsorption and 2 at desorption. The curvesin Figure 5 consist of three sections: the nitrogen adsorption in 0 – 50 % relative pressure interval, the pore size distribution from BJH model in 50 – 75 % relative pressure interval and the pore size distribution from MIP test for relative pressures higher than 75 %.

4. Modelling

The knowledge on the pore sizedistribution enables to model the sorption hysteresis with the use of BJH model. A detailed description of the model is for example in (Lowell et al., 2004). The model is based on the calculation of pore volume from the relative pressure and liquid adsorbate datameasured during the nitrogen desorption. Using this model the reverse procedure enables the sorption modelling from information on pore volume data.

4.1 Main sorption isotherms

The classical Kelvin equation does not take into consideration the existence of an adsorbed multilayer film prior to a pore condensation. In BJH model this fact is taken into accountby the modified Kelvin equation where the pore radius r_p is replaced by the Kelvin radius r_k expressed in Equation (5), where the capillary pore radius is given by the sum of the Kelvin radius and statistical thickness of the adsorbate film:

$$r_p = r_k + t \tag{5}$$

The BJH modelling procedure is based on a calculation of Kelvin radii and liquid adsorbate changes ΔV_lbetween successive relative pressures from the couples of relative pressure and liquid adsorbate datameasured during desorption. Simultaneously there are calculated the changes in film statistical thickness Δt obtained from the Halsey equation (3). Then the mean values of Kelvin and capillary pore radii in each change of successive entries are calculated. At the end the pore volume changes are calculated from mean pore and capillary radii, changes of liquid adsorbate, changes of film thickness and adsorbed film surface area$A$:

$$\Delta V_p = \left(\frac{\vec{r}_p}{\vec{r}_k} \right)^2 (\Delta V_l - \Delta t \sum A) \tag{6}$$

The total specific surface area of pore walls is obtained by the summation of its increments according to relationship:

$$\Delta A = \frac{2 \Delta V_p}{\vec{r}_p} \tag{7}$$

The above presented BJH model was implemented to the lightweight carbonate sorption hysteresis modelling by the following way: The adsorption isotherm was calculated from the statistical film thicknessobtained by Equation (3) and multiplied by the calculated specific surface area A. Its values are assigned to the relative pressures calculated by Equation (3) for k =

1. The desorption isotherm was calculated by a summation of pore volume changes, arranging Equation (6) into the form:

$$\Delta V_l = \Delta V_p \left(\frac{\vec{r}_k}{\vec{r}_p} \right)^2 + \Delta t \sum A \tag{8}$$

The calculated values are assigned to the relative pressures calculated by Equation (3) for $k = 2$.

4.2 Scanning curves

The modelling of scanning curves issued from an assumption that when during the adsorption process the film thickness reaches the critical value, a capillary condensation occurs. The adsorption isotherm is then composed of two parts: the part representing the condensed adsorbate (the film reached the critical thickness) and the part representing the adsorbate film (the film thickness is smaller than critical).

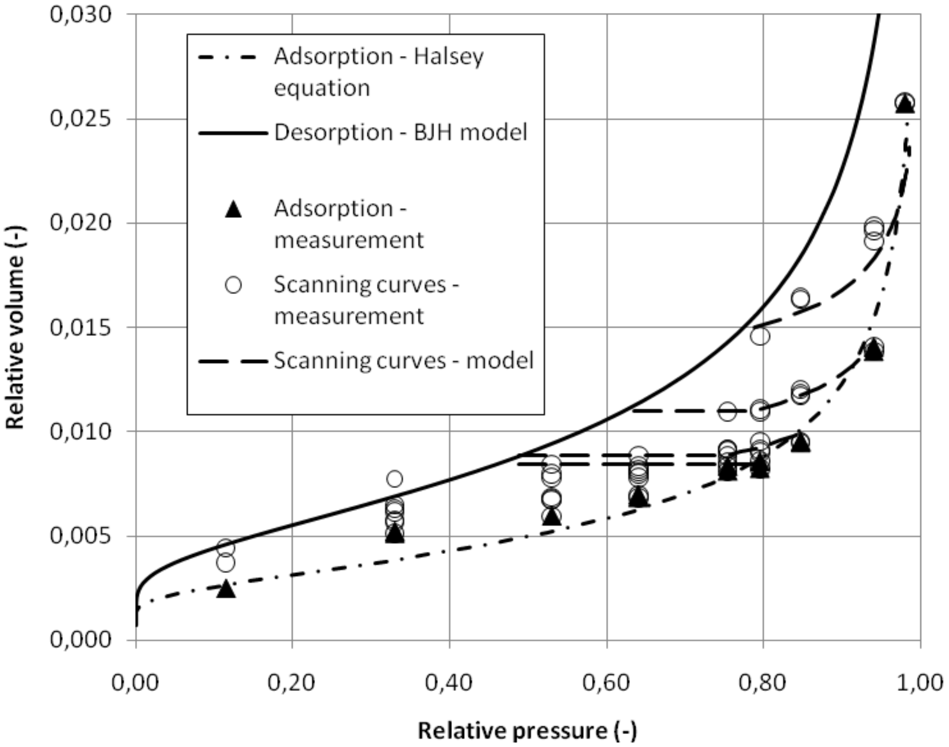

Figure 6: Comparison of measured and modelled water vapour sorption isotherms and scanning curves

In a case of capillary condensation the spontaneous creating of the hemispherical meniscus is characteristic and the transition between adsorption and desorption isotherm is flat independently on a relative humidity. In a case of the lightweight carbonate plaster the capillary condensation occurs at relative humidities (RH) smaller than 80 % (Figure 1). These values correspond to the film thickness representing the 20 % of capillary radius.

If the adsorption isotherm is represented by adsorbate film the transition between adsorption and desorption isotherms is caused only by the change of film thickness on the pore surface area reduced by the capillary surface area of the capillaries filled in with the condensate. And the values of scanning curves are assigned to the RH calculated by Equation (3) for $k = 1$.

In Figure 6four modelled scanning curves compared with the measured data are depicted: At the curve between 80 and 98 % RH the change of film thickness is performing. In the case of the curves between 75 and 94 % RH and between 64 and 85 % RH when the RH is smaller than 80 % the flat transition between evaporation and condensation takes place. At RH bigger than 80 % the film thickness change takes place. At the curve between 53 and 80 % RH only the transition between evaporation and condensation is possible.

5. Conclusions

The analysis of results of the water vapour and nitrogen sorption in combination with the results of MIP for the lightweight carbonate plaster proved the compatibility of the used methods in water vapour sorption modelling, the possibility to identify the pore structure and to model the sorption hysteresis with the use of BJH model of capillary condensation. The approach is applicable for the type IV isotherms and type H1 hysteresis, typical for porous materials containing well defined cylindrical-like pores.

Acknowledgements

This article has been produced with the financial assistance of the European Regional Development Fund (ERDF) under the Operational Programme Research and Development/Measure 4.1 Support of networks of excellence in research and development as the pillars of regional development and support to international cooperation in the Bratislava region/Project No. 26240120020 Building the centre of excellence for research and development of structural composite materials – 2nd stage.

References

[1] ISHIDA, T. - MAEKAWA, K. - KISHI, T. Enhanced modeling of moisture equilibrium and transport in cementitious materials under arbitrary temperature and relative humidity history, In *Cement and Concrete Research*, vol. 37, 2007,p p. 565-578. ISBN 978-2-35158-060-8

[2] LOWELL. S. - SHIELDS, J.E. - THOMAS, M.A. - THOMMES, M.:*Characterization of porous solids and powders: surface area, pore size and density*, Kluwer, Dordrecht, 2004. pp. 101-126,ISBN 1-4020-2302-2

[3] MATIAŠOVSKÝ, P. - BÁGEĽ, Ľ.Compatibility of BET nitrogen and water adsorption/desorption isotherms of interior plasters. In *Energy Efficiency and New Approaches : proceedings of the fourth international building physics conference.* 2009,pp. 11-16. ISBN 978-975-561-350-5.

[4] GREGG S.J. - SING K.S.W. *Adsorption, Surface Area and Porosity,* LondonAcademic Press, London, 1982. ISBN 10: 0123009561

[5] DELMELLE P. - VILLIERAS F. - PELLETIER M. Surface area, porosity and water adsorption properties of fine volcanic ash particles. In *Bulletin of Volcanology*vol. 67, 2005, pp. 160-169. ISSN 0258-8900

[6] NEIMARK, A.V. - RAVIKOVITCH P. I.Capillary condensation im MMS and pore structure characterization, In *Microporous and mesoporous materials*vol. 45-46, 2001, pp.696-707. ISSN 1387-1811

[7] BARRET E.P. - JOYNER L.G. - HALENDA P.H. Determination of pore volumes and area distributions in porous substances. I. Computation from nitrogen isotherms, In.*Journal of American Chemical Sociery,* Vol. 73,. 1951, pp. 373 – 380. ISSN 00027863

[8] BRUNAUER S. - EMMETT P.H. - TELLER E. Adsorption of Gases in Multimolecular Layers, In*Journal of the American Chemical Society*, vol. 60, 1938, pp. 309-319. ISSN 00027863

[9] Washburn E.W. The dynamics of capillary flow.In. *Physical Review,* vol.17, 1921, pp. 273-283.

[10] Sing K.S.W., Everett D.H., Haul P.A.W., Moscou L., Pierotti R.A., Rouquerol J. and Siemieniewska T. IUPAC Recommendations, In *Pure Applied Chemistry* 57,603.

Isothermal dilatometric study of sintering in electroceramics

Jana Moravčíková[1], Ján Ondruška[1], Anton Trník[1,2], Igor Medveď[1,2]

[1]Department of Physics, Constantine the Philosopher University, A. Hlinku 1, 949 74 Nitra, Slovakia, E-mail:atrnik@ukf.sk

[2]Department of Materials Engineering and Chemistry, Czech Technical University, 16629 Prague, Czech Republic

Abstract: *Solid-state sintering was studied in ceramic samples by dilatometric measurements. The samples were preheated at 490 °C for 24 hrs to reach a complete transformation of kaolinite into metakaolinite because dehydroxylation and the solid-state sintering run simultaneously. The samples were studied in an isothermal regime at the temperatures 500, 600, 700, 800, 900, 1000 and 1050 °C when no liquid phase is created. The relative expansion was measured for a period of 8 hrs. For the temperatures below 800 °C only a small contraction (0.15 – 0.20 %) was observed and after 4 hrs the samples became stabilized. For the temperatures above 1000 °C the contraction continued all the time and reached 2.5 %. We also determine which diffusion mechanism is dominant for the sintering process at a given temperature.*

Keywords*: solid-state sintering, ceramics, thermodilatometry, lattice diffusion, grain boundaries diffusion*

1. Introduction

An understanding of behavior of ceramics can provide insights into firing processes, the influence of additives and raw materials, e.g., the densification and sintering process, the reaction kinetics, phase transitions, glaze development. Thermodilatometric analysis (TDA) is very suitable method for investigation of such processes in ceramics and is commonly used.

Sintering is a technique of consolidating powder compacts by use of thermal energy. This process is widely used to fabricate bulk ceramic components [1, 2]. Sintering is a high-temperature technological process that transforms individual ceramic particles into a compact polycrystalline body. The driving force of the sintering process is an excess of the free energy associated with the large free surface of an agglomerate of fine powder particles. During solid-state sintering powder particles are welded to their neighbors, junctions between them are gradually increased with time, and the internal free surface of the powder compact is decreased [2, 3].

Sintering is accompanied by the vanishing of the porosity, which is connected with shrinkage of the sample measurable by dilatometer. Sintering processes can be divided into two types: solid state sintering and liquid phase sintering. For traditional kaolin-based ceramics, solid state sintering occurs when the powder compact is densified wholly in a solid state at the sintering temperature 600 - 1000 °C, while liquid phase sintering occurs when a liquid phase is present in the powder compact during sintering at temperature higher than 1000 °C[1, 2]. Thermodilatometric behavior of a kaolin-base ceramic sample during heating above 450 °C is determined primarily by dehydroxylation process in the kaolinite crystals. The elastic behavior is determined mainly by improving the contacts between crystals as a consequence of the solid state sintering [2, 4]. Dehydroxylation plays a minor role, except at a short temperature interval 550 – 620 °C. The thermal expansion after completing of dehydroxylation terminates at the temperature ~900 °C, when the collapse of the metakaolinite lattice accompanied by rapid shrinkage appears. Identically, there is a steep increase of some mechanical properties (modulus of elasticity, mechanical strength) as the response to a faster solid state sintering and on the new structure rather than the defect and microporous metakaolinite [5].

In order to interpret our results from the microscopic point of view, we shall employ the standard two-spherical-particle model of initial stages of sintering introduced in [6]. Out of several possible sintering mechanisms, only two contribute to the shrinkage: lattice (volume) diffusion of molecules from grain boundaries and grain boundary diffusion of molecules from grain boundaries.Their dependencies on time are given as [1]

$$\left(\frac{\Delta l}{l}\right)_{lat} = -At^{1/2}, \qquad \left(\frac{\Delta l}{l}\right)_{gb} = -Bt^{1/3}, \tag{1}$$

respectively, with

$$A = \left(\frac{D_l \gamma_s \Omega}{kTa^3}\right)^{1/2}, \qquad B = \left(\frac{3D_b \delta_b \gamma_s \Omega}{4kTa^4}\right)^{1/3}, \tag{2}$$

where D_l and D_b is the lattice and grain boundary diffusivity, respectively, δ_b is the grain boundary diffusion thickness, γ_s is the specific surface energy, Ω is the atomic (molecular) volume, k is the Boltzmann constant, T is the thermodynamic temperature, and a is the particle (grain) radius. The temperature dependence of the diffusivities usually satisfies the Arrhenius law,

$$D_l = D_{l0} \exp\left(\frac{-E_l}{RT}\right), \qquad D_b = D_{b0} \exp\left(\frac{-E_b}{RT}\right), \tag{3}$$

where the exponential pre-factors D_{l0} and D_{b0} are independent of temperature (they coincide with the corresponding diffusivities at infinite temperature) and E_l and E_b is the activation energy of lattice and grain boundary diffusion, respectively.

The aim of the contribution is to observe the sintering with the help of the TDA (thermodilatometric analysis) during isothermal heating at different temperatures and to employ the standard two-spherical-particle model of initial stages of sintering to fit our experimental data.

2. Sample and measurement method

Green electroceramic samples were made from a mixture of kaolin (35.5 wt. %), Al_2O_3 (35 wt. %), and feldspar (29.5 wt. %). The mixture was ground and sieved on a 100 mesh/mm^2 sieve and then a plastic material was prepared from this mixture. The cylindrical samples ∅12×50 mm were made with the laboratory extruder.

Since solid-state sintering and dehydroxylation run simultaneously over ~600 °C, the samples were preheated at 490 °C for 44 hrs to reach a complete transformation of kaolinite into metakaolinite. This temperature is inside the dehydroxylation region but under the solid-state sintering region. Completeness of dehydroxylation in the preheated samples was tested by thermogravimetry. No changes of weight were observed above 400 °C. After 44 hrs the samples lost 5.1 % of their weight, which corresponds to an amount of constituent water in the green mixture.

Preheated samples were studied by thermodilatometry in isothermal regime at the temperatures 500, 600, 700, 800, 900, 1000 and 1050 °C. The value of the highest temperature (1050 °C) ensures no creation of the liquid phase in the samples.

In this research, a push rod alumina dilatometer was used [7] for investigation of the low temperature stage of the sintering. The temperature in the dilatometer was increased linearly with the rate of 20 °C/min up to the temperature of the isothermal heating. The relative expansion of the sample was measured during 8 hrs. The measurements were repeated with fresh samples to confirm measured results.

3. Results and discussion

The results of thermodilatometry at the linear heating are depicted in Figure 1. It is generally accepted that dehydroxylation in the green ceramic sample begins at the temperature 420 – 450 °C. This process is accompanied by a sample contraction above 500 °C, which is a consequence of the transform of kaolinite into metakaolinite. In the case of the pure kaolinite, the contraction continues up to 1050 °C[8]. The thermodilatometric curve of the green sample shows the contraction only up to 800 °C. The main reason of the expansion above 800 °C is that the pure kaolin is not used, but 65 wt.% of the sample are expanding constituents (alumina and feldspar). In fact, the thermodilatometric curve is a sum of three curves, for feldspars, kaolin and alumina. At 850 – 950 °C metakaolinite is replaced by a spinel phase [9]. The spinel phase then transforms into mullite above 1075 °C [10, 11].

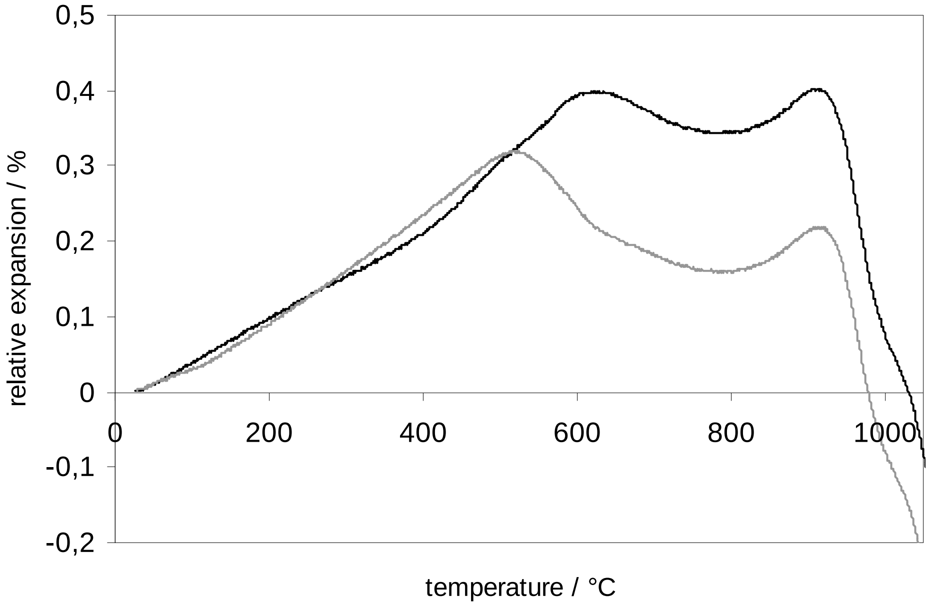

Figure 1: Thermodilatometric curves of the dehydroxylated sample (black) and green sample (grey) with linear heating 5 °C/min

Figure 1 show also the thermodilatometric curve of the sample which was thermally treated during 44 hrs at 490 °C (the black curve). As thermogravimetry confirmed, the sample does not contain constituent water. So, the contraction starting above 600 °C cannot be attributed to dehydroxylation. We supposed a solid-state sintering as a cause of the contraction. Similarly as for the green sample, two competing mechanisms take place in the sample. One of them is solid-state sintering, which leads to the contraction, and the other is thermal expansion of metakaolinite, feldspar, and alumina.The steep contraction starting at ~900 °C is due to change of metakaolinite into spinel and mullite.

Figure 2 depicts thermodilatometric curve from the room temperature to a given temperature of the isothermal heating 1050 °C. A section 0-S responds to the linear heating (as shown in Figure 1) with the heating rate 20 °C/min. The isothermal heating started after 52 min.

The results of thermodilatometry in the isothermal regime are presented in Figs. 3, 4, and 5. The time t = 0 corresponds to the point S in Figure 2. The results of thermodilatometric curves for isothermal heating at 500 – 800 °C (see Figs. 3 and 4) do not prove the rule that the higher the temperature, the bigger the final contraction. The result of sintering of the sample fired at 800 °C is too small because of the expansion the ceramic components (alumina and feldspar).

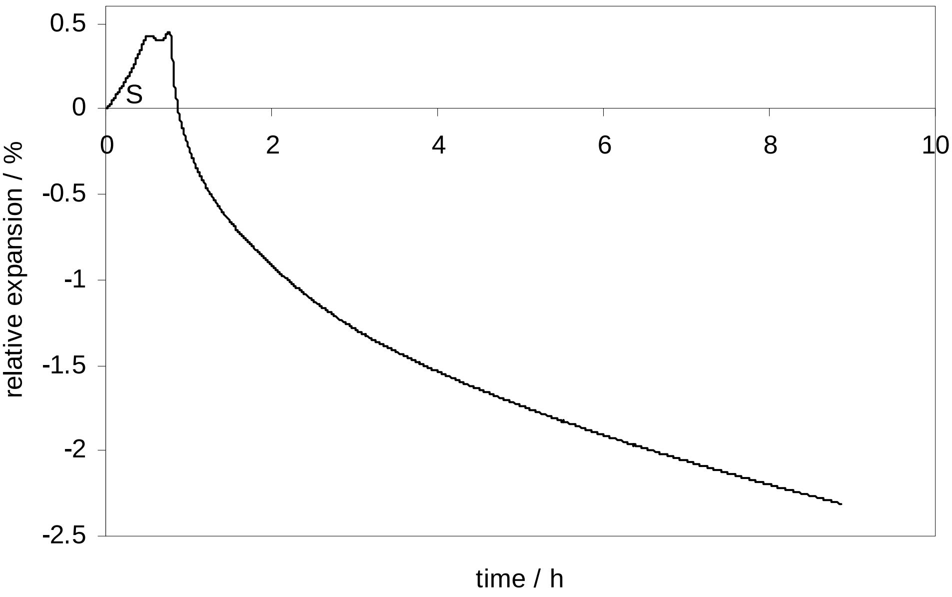

Figure 2: Thermodilatometric curve for 1050 °C

The results of fired samples at temperatures 900, 1000, and 1050 °C show that the higher the temperature, the bigger the contraction of the sample. For temperatures higher than 1000 °C the contraction continued all the time and reached 2.5 %.

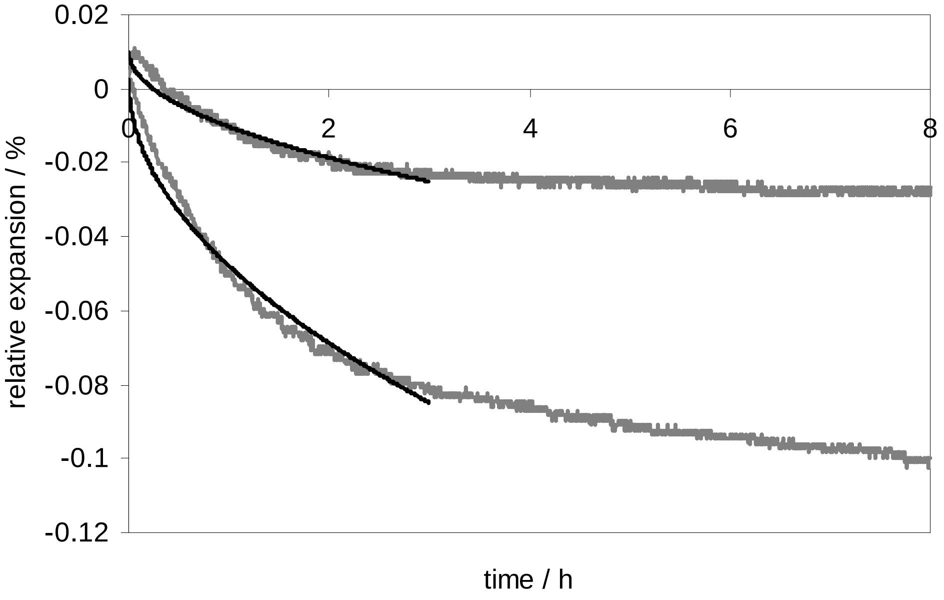

Figure 3: Thermodilatometric curves for isothermal heatings at 500 °C, 600 °C and the corresponding theoretical fits.

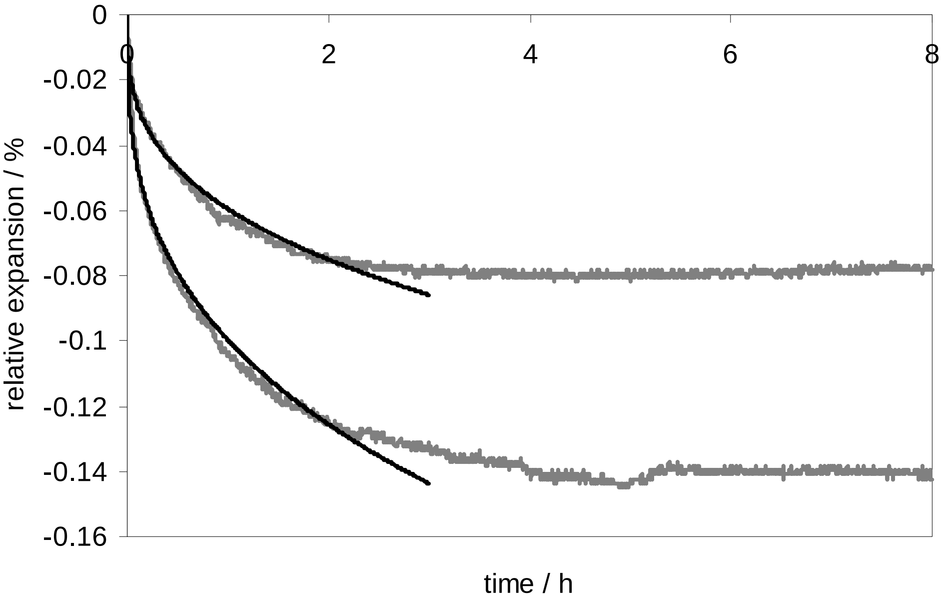

Figure 4: Thermodilatometric curves for isothermal heatings at 700 °C, 800 °C and the corresponding theoretical fits.

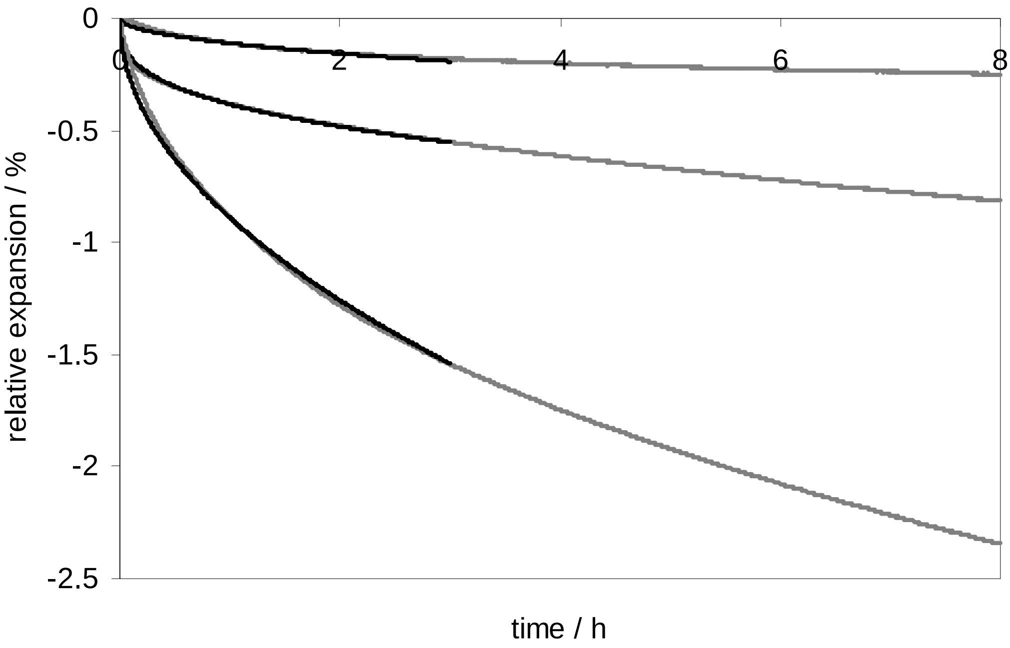

Figure 5: Thermodilatometric curves for isothermal heatings at 900 °C, 1000 °C, 1050 °C and the corresponding theoretical fits.

We will now use the relations from Eq. (1) to find the best fits to the measured experimental data. Subsequently, using thus obtained values of A and/or B for the studied temperatures, we will apply Eq. (3) to find the activation energies, E_l and E_b, and exponential pre-factors, D_{l0} and D_{b0}.

However, we shall first use the general formula

$$\left(\frac{\Delta l}{l}\right) = -C t^{\nu} \tag{4}$$

to estimate the power $\nu > 0$ that best fits the experimental data on shrinkage. This will allow us to conclude which of the two sintering mechanisms causing shrinkage is dominant or whether both mechanisms are significant and must be considered together. The results are given in Table 1. One may observe that the power ν is either very close to 1/2 (for the temperatures 500 °C, 600 °C, 900 °C, and 1050 °C) or to 1/3 (for the temperatures 700 °C, 800 °C, and 1000 °C). Thus, it follows that one of the sintering mechanisms is always dominant as far as shrinkage is concerned, while the other mechanism is insignificant. Namely, lattice diffusion is dominant for the first set of temperatures and grain boundary diffusion is dominant for the second set of temperatures. Therefore, when fitting the shrinkage experimental data by applying the relations from Eq. (1), it is sufficient to consider only the dominant mechanism and use only the corresponding relation, and it is not necessary to use the sum of two relations from Eq. (1). As a matter of fact, since ν lies either above 1/2 or below 1/3, the fitting procedure using the sum of the two relations cannot yield meaningful results because either A or B would be found to be negative, which is physically inappropriate.

Table 1: The values of the parameters from Eq. (4) obtained from the fitting procedure.

	ν		C / 10^{-6} $s^{-\nu}$		R^2
	Value	Standard error	Value	Standard error	
500 °C	0.589	0.004	1.133	0.044	0.9959
600 °C	0.543	0.005	5.743	0.238	0.9974
700 °C	0.304	0.002	83.51	1.612	0.9990
800 °C	0.310	0.003	47.46	1.112	0.9986
900 °C	0.557	0.004	11.36	0.415	0.9984
1000 °C	0.327	0.001	264.9	1.759	0.9999
1050 °C	0.509	0.001	136.3	1.780	0.9996

Let us now use the relations from Eq. (1) and obtain the best fits to the experimental data on shrinkage. As argued above, for the temperatures 500 °C, 600 °C, 900 °C, and 1050 °C it is meaningful to employ the first relation in Eq. (1), whereas for the temperatures 700 °C, 800 °C, and 1000 °C it is meaningful to employ the second relation in Eq. (1). The results are summarized in Table 2 and the fitting curves are shown in Figs. 3, 4, and 5. As should be expected, for a given temperature the value of the fitting parameter *A* or *B* is close to the value of the parameter *C* given for that temperature in Table 1.

Table 2: The values of the parameters from Eq. (1) obtained from the fitting procedure.

	Dominant mechanism	Relation used to fit the shrinkage	A / 10^{-6} $s^{-1/2}$ B/ 10^{-6} $s^{-1/3}$		R^2
			Value	Standard error	
500 °C	Lattice diffusion	$-At^{1/2}$	3.374	0.006	0.9965
600 °C	Lattice diffusion	$-At^{1/2}$	8.402	0.023	0.9963
700 °C	Grain boundary diffusion	$-Bt^{1/3}$	65.03	0.105	0.9987
800 °C	Grain boundary diffusion	$-Bt^{1/3}$	38.86	0.070	0.9984
900 °C	Lattice diffusion	$-At^{1/2}$	18.47	0.048	0.9973
1000 °C	Grain boundary diffusion	$-Bt^{1/3}$	250.0	0.118	0.9998
1050 °C	Lattice diffusion	$-At^{1/2}$	148.3	0.109	0.9996

The reason why different dominant sintering mechanism is associated with different temperatures should be attributed to the fact that the studied material contains several components that behave differently in dependence on the temperature so that they have different size variations with the temperature, thus causing different overall effects on the sample as a whole. Therefore, depending on the physical-chemical processed occurring in the material (see above), a different sintering mechanism may turn out to be dominant.

4. Conclusions

Thermodilatometric analysis of fully dehydroxylated samples was used for the studying the solid-state sintering of the ceramic material used for industrial production of the high-voltage insulators. The results showed the solid-state sintering above 500 °C does not lead unambiguously to a rule „the higher the temperature, the bigger the final contraction" mainly at the lower temperatures. It is an outcome of the complexity of the tested material and processes in it. For temperatures 500, 600, 700, 800 °C only a small contraction (0.15 – 0.20 %) was observed and after 4 hrs the samples became stabilized. For temperatures higher than 1000 °C contraction continued all the time and reached 2.5 %.

Using our experimental data, we found that a different sintering mechanism is dominant (as far as shrinkage is concerned) for different temperatures. For 500, 600, 900, and 1050 °C the dominant mechanism is lattice (volume) diffusion of molecules from grain boundaries (the shrinkage vs. time curve behaves as $t^{1/2}$), while for 700, 800, and 1000 °C it is grain boundary diffusion of molecules from grain boundaries (the shrinkage vs. time curve behaves as $t^{1/3}$).

Acknowledgements

This work was supported by the grants VEGA 1/0302/09, VEGA 1/0216/09 and by the Ministry of Education, Youth and Sports of the Czech Republic, under the project No. MSM: 6840770031. Authors wish to thank the ceramic plant PPC Čab for providing samples.

References

[1] S.L. Kang, Sintering. (Elsevier Oxford, 2005)

[2] K. Traore, T.S. Kabre, P. Blanchart, Ceramics International. 27, 875 (2001)

[3] E.A. Olevsky, A. Maximenko, O. Biest, International journal of mechanical sciences. 44, 755 (2002)

[4] K. Winkelmann, O. Gobel, A.P. Nikkila, P. Vuorinen, T. Mantyla, E. Zschech, Metall. 48, 382 (1994)

[5] I. Štubňa, A. Trník, L. Vozár, Ceramics International. 35, 1181 (2009)

[6] W.D. Kingery, M. Berg, J. Appl. Phys. 26, 1205 (1955)

[7] I. Štubňa, A. Vážanová, G. Varga, D. Hrubý, In: Proc. Conf. Research and Teaching of Physics on the Context of UniversityEducation. (SPU Nitra, Nitra 2007), pp. 69-74

[8] G. Varga, A. Trník, In: Proc. VII. Scientific conference of PhD students and young researchers. (Constantine the PhilosopherUniversity, Nitra, 2006) pp. 612-616

[9] Y.F. Liu, X.Q. Liu, et al., Ceramics International. 28, 479 (2002)

[10] C.Y. CHen, W.H. Tuan, Ceramics International. 27, 795 (2001)

[11] G.W. Brindley, M. Nakahira, J of the Amer. Ceramic Soc. 42, 314 (1959)

Effective permittivity modelling of lime-cement perlite plaster

T. Palszegi[1] **and M. Holubek**[2]

[1]Faculty of Chemical and Food Technology, Slovak University of Technology in Bratislava, Radlinského 9, 812 37 Bratislava, SLOVAK REPUBLIC

[2]Faculty of Civil Engineering, Slovak University of Technology in Bratislava, Radlinského 11, 813 68 Bratislava, SLOVAK REPUBLIC

Abstract: *The effective permittivity (ε_{eff}) of lime-cement perlite plaster has been theoretically modelled on the basis of fractal pore-size distribution (FPD) function of the corresponding solid-air-water (S-A-W) heterogeneous material. The method of Friedman [1] has been applied in FPD related calculations of the ε_{eff} of AWS, SWA three-phase composite spheres andof a water content/porosity ratio weighted sum of SWA and ASW composite spheres, corresponding to the assumed, dielectric signal dominating heterogeneous structures. Good correspondence has been obtained between the theoretical dependence of ε_{eff} on the volumetric water content - in the case ofmodel, based on SWA composite spheres - and the experimental one, measured for the lime-cement perlite plaster probe [2] using time domain reflectometry (TDR) technique.*

Introduction

Understanding theoretically the relation between the effective dielectric constant (relative permittivity - ε_{eff}) of soils and their volumetric water content θ is very useful for interpretation of e.g. time domain reflectometry (TDR) measurements of ε_{eff} . The dielectric properties of these three phase heterogeneous (porous) - i.e. solid-air-water (S-A-W) - systems, are depending on not only the dielectric property and volume fraction of each phase, but also the geometrical shapes and arrangements of the inclusions. Most popular theoretical models for ε_{eff} of porous media are based on networks of parallel and series modes or introducing the morphology effects of a porous structure by some empirical parameters – short review see e.g. in [3].

An attempt to determine analytically the ε_{eff} of S-A-W composed soils has been given in [1] taking into account the geometrical shapes and arrangements of the inclusions on the basis of six different three-phase composite spheres, i.e. WSA, SWA, ASW, SAW, AWS and WAS spheres embedded into a homogeneous matrix of permittivity ε_{eff} . In [1] has been shown, that a water content/porosity ratio related weighted sum of SWA and ASW composite spheres determined permittivity gave the best correspondence with experimental ε_{eff} . The reason for this is in the fact, which the real configuration of the S, W and A phases in soil varies with the saturation degree [1]. For low moisture contents it is reasonable to assume that the A phase is continuous and surrounding the S and W phases – this gives the SWA composite spheres. As the W content increases, the A phase develops discontinuities, and a better description is that of a continuous W phase surrounding the S and A phases, resulting in the ASW composite spheres.

In present article in the calculation of ε_{eff} of a special lime-cement perlite plaster probe the formation of SWA and ASW composite spheres will be related to the fractal distribution of pores. After the fractal analysis of experimental pore distribution of lime-cement perlite plaster, based on fractal pore-size distribution (FPD), the ε_{eff} of AWS, SWA three-phase composite spheres and of their saturation degree related weighted sum will be calculated. The theoretical ε_{eff} will be compared with the experimental one, measured for the lime-cement perlite plaster probeusing TDR technique [2].

Modelling of $\varepsilon_{\mathrm{eff}}$ for lime-cement perlite plaster

The fractal analysis of experimental pore-size distribution of lime-cement perlite plaster is based on FPD $W(r)$, given as follows (see e.g. in [4]):

$$W(r) = \frac{3-D_p}{r_m^{3-D_p}} r^{-1-D_p} \tag{1}$$

where r is the radius of a pore, D_p is the fractal dimension of pores and r_m is the maximum pore radius. D_p is given by the expression

$$D_p = \frac{\log(1-\phi)}{\log\left(\frac{r_0}{r_m}\right)} \tag{2}$$

where ϕ represents the total pore fraction (porosity) and r_0 the minimal pore radius. Theporosity is given by the equation

$$\phi = \frac{3-D_p}{r_m^{3-D_p}} \int_{r_0}^{r_m} r^3 r^{-1-D_p} dr \tag{3}$$

and the porosity fraction ϕ_x corresponding to the maximum pore radius r_x is given byintegral analogical toEq.(3), but for the upper integration border equal to r_x .

The experimental pore-size distribution function of a probe of lime-cement perlite plaster is shown in Figure1, taken from [2].

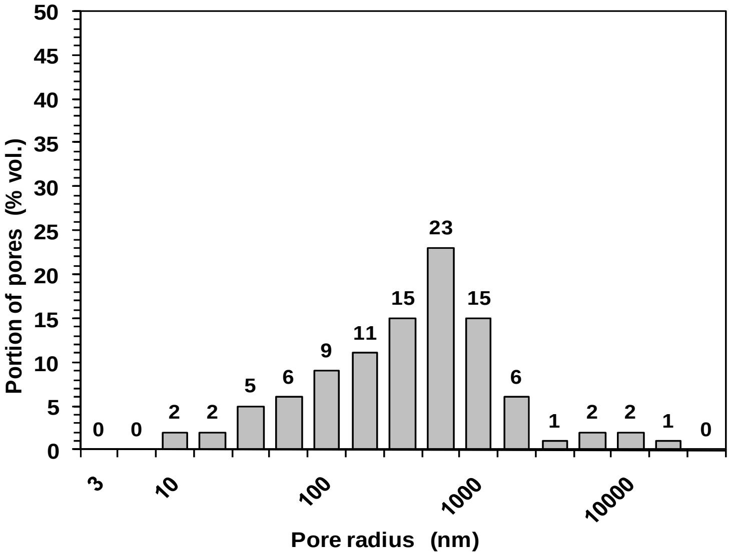

Figure 1: Experimental pore-size distribution function of lime-cement perlite plaster.

For distribution in Figure1 the smallest and largest pore radius, r_0 and r_m, are taken to be equal 10 nm and 10000 nm. Then, the calculated FPD and cumulative FPD functions are shown on Figs. 2a and 1b on real and log-log scales, respectively.

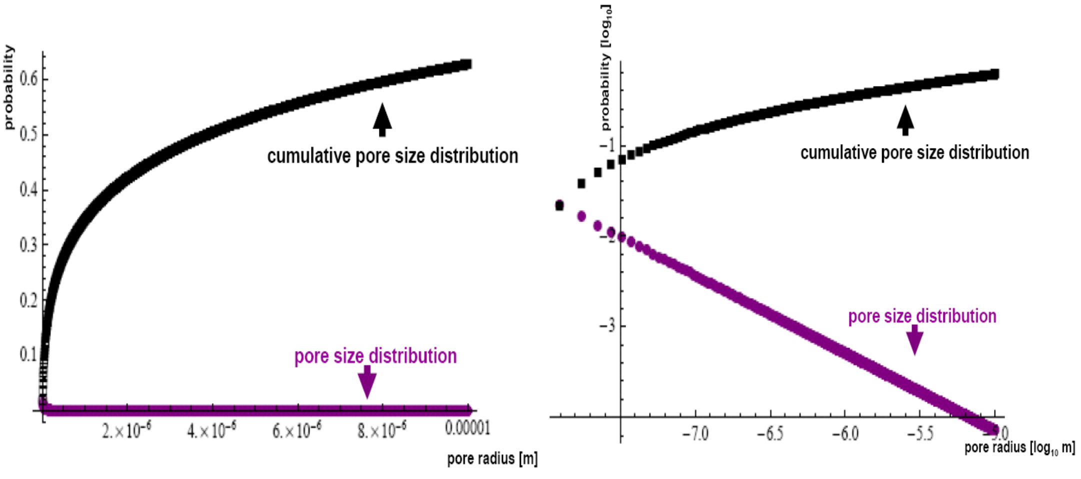

a) **b)**

Figure 2: FPD and cumulative FPD functions, calculated for the formula of $w(r)$ given by Eq.(1), on real – Figure 2a - and log-log scale - Figure2b -for lime-cement perlite plaster given by Figure 1.

In Figure3 is shown that the experimental and theoretical pore-size distributions correspond well each to other.

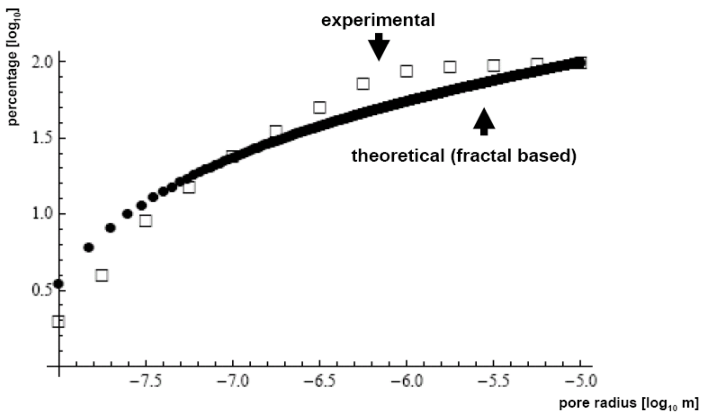

Figure 3: Experimental and theoretical – which is FPD function based – pore-size distributions of lime-cement perlite plaster.

To model ε_{eff} of the lime-cement perlite plaster under study, composite spheres SWA and ASW are assumed to be formed in analogy with the assumptions of paper [1]. The ε_{eff} of these composite spheres are calculated by the formula, taken from [1], as follows:

$$\begin{aligned}\varepsilon_{eff} &= \varepsilon_1 + (\{3[(\phi_3 + \phi_2)(\varepsilon_2 - \varepsilon_1)(2\varepsilon_2 + \varepsilon_3) - \phi_3(\varepsilon_2 - \varepsilon_3)(2\varepsilon_2 + \varepsilon_1)]\varepsilon_1\} / \\ &[(2\varepsilon_2 + \varepsilon_1)(2\varepsilon_1 + \varepsilon_1) - 2\tfrac{\phi_3}{\phi_3 + \phi_2}(\varepsilon_2 - \varepsilon_1)(\varepsilon_2 - \varepsilon_3) - (\phi_3 + \phi_2)(\varepsilon_2 - \varepsilon_1) \\ &(2\varepsilon_2 + \varepsilon_3) + \phi_3(\varepsilon_2 - \varepsilon_3)(2\varepsilon_2 + \varepsilon_1)\end{aligned} \tag{4}$$

where the volumetric fractions of the three phases, ϕ_i, refer to the radii of the spheres, R_i, according to $\phi_1 = \frac{R_1^3 - R_2^3}{R_1^3}$, $\phi_2 = \frac{R_2^3 - R_3^3}{R_1^3}$ and $\phi_3 = \frac{R_3^3}{R_1^3}$.

The calculations of permittivity as a function of water content, θ, and porosity $\varphi = n$ - using notation of [1] - i.e. $\varepsilon_{eff}(\theta, n)$ have given the results collected in Figure4. The dependences of $\varepsilon_{eff}(\theta, n)$ have been calculated as functions of maximum radius of water containing pores – corresponding to values of θ, assuming that all pores are full with moisture under a maximum volume one - taken for porosity the value $n = 0.63$. Formula $\varepsilon_{eff}(\theta, n) = f_W^{SWA}\varepsilon_{eff}(\theta, n, SWA) + f_W^{ASW}\varepsilon_{eff}(\theta, n, ASW)$ [1] has been used for the water content/porosity ratio related weighted sum of SWA and ASW composite spheres - $f_W^{SWA} = 1 - \frac{\theta}{n}$ and $f_W^{ASW} = \frac{\theta}{n}$ – giving the green colour "line" (details for weights see in [1], especially Eq.(7) and text there).

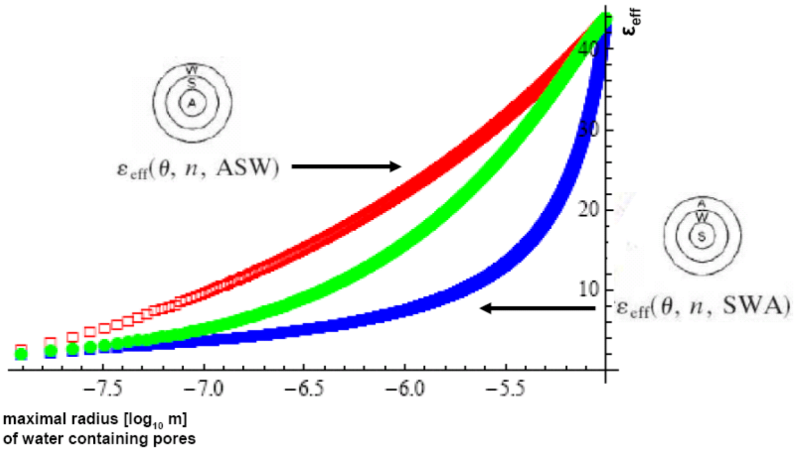

Figure 4: $\varepsilon_{eff}(\theta, n)$ *for* $n = 0.63$ *of AWS (red contour squares), SWA (blue full squares) three-phase composite spheres and of their weighted sum (green full circles) – given by* $\varepsilon_{eff}(\theta, n) = f_W^{SWA}\varepsilon_{eff}(\theta, n, SWA) + f_W^{ASW}\varepsilon_{eff}(\theta, n, ASW)$ *– as function of maximum radius of full of water pores.*

In Figure 5 are compared the experimental and theoretical dependences of $\varepsilon_{eff}(\theta, n)$. The experimental values – shown in Figure5 by black contour squares – have been obtained by TDR [2].Good correspondence has been obtained between the model calculation - based on SWA composite spheres - and of the experimental one.

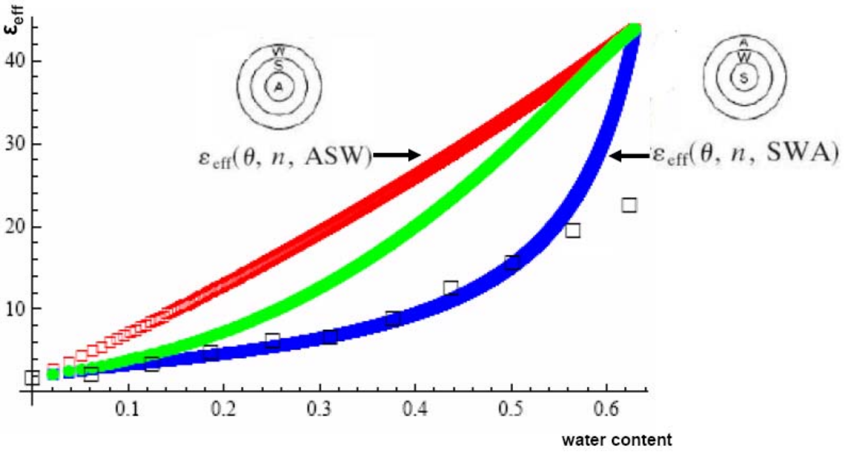

Figure 5: $\varepsilon_{eff}(\theta, n)$ *for* $n = 0.63$ *of AWS (red contour squares), SWA (blue full squares) three-phase composite spheres and of their weighted sum (green full circles) – given by* $\varepsilon_{eff}(\theta, n) = f_W^{SWA}\varepsilon_{eff}(\theta, n, SWA) + f_W^{ASW}\varepsilon_{eff}(\theta, n, ASW)$ *- and of the experimental values (black contour squares).*

Conclusions

The theoretical modelling of effective permittivity ε_{eff} of lime-cement perlite plaster on the basis of the FPDfunction extended method of Friedman [1] has given a good correspondence with the experimental; TDR measured one for SWA composite spheres model. The SWA composite spheres represent not the most physically sound arrangement of the inclusion of phases. The AWS composite spheres, together with the SWA arrangements should represent the most natural choice in the case, if the W phase would form films on the inner walls of the pores, as well as on the outer walls of the grains. A study of a fractal analysis based model for such a case of arrangement of phases is in progress.

Acknowledgments

This work was supported by grant VEGA 1/0591/10.

References

[1] S.P.FRIEDMAN, Water Res. Res. **34** (1998), 2949

[2] P. MIHALKA, P. MATIASOVSKY and M. HOLUBEK, *Determination of liquid water diffusivity of lime-cement perlite plaster at cyclic wetting and drying regimes*, In Thermophysics2010 - Proceedings, 3. – 5.11. Valtice, Czech Republic (2010), 200

[3] M.WANG and N. PAN, J.Appl.Phys. **101** (2007), 114102

[4] A.HUNT and R.EWING, *Porous media primer for physicists*, Lect. Notes Phys. **771**(2009), 57

Dilatometer used for Measurements in Building Materials Testing

Ivan Christov[2], Gabriela Pavlendová[1], Juraj Veselský[1]

[1]Department of Physics, Faculty of CE, SlovakUniversity of Technology,

Radlinského 11, 813 68 Bratislava, SlovakRepublic

[2]METRODAT s.r.o., Beblavého 8, 811 01 Bratislava

Abstract: *Dimensional change of building materials as a function of temperature and moisture is important characteristic that needs to be monitored. In cooperation of the Department of Physics at STU and company METRODAT the dilatometer for measurement of thermal and moisture expansion coefficient was produced. Measuring systems using LVDT sensor located into ZERODUR closed loop measurement frame provide the maximum precision, repeatability and accuracy in temperature range from -15°C to 105°C and from 10 % to 100 % relative air humidity. The sample holder is made from stainless steel and allows to work with samples from 10 mm to 160 mm of initial lengths. The measurement process is PC controlled.*

Keywords: *thermal expansion, moisture expansion, dilatometer*

1. Introduction

Knowledge of the material characteristics of building materials is very important not only in terms of their primary functions (as an element of construction work), but also in terms of their mutual compatibility. Nowadays, this knowledge must be understood in a broader scale. It is necessary to understand linking of material properties dependence on their composition, temperature and humidity with connection to their function in the construction work. Such a complex view at the construction materials appears all the more necessary in terms of replacement, respectively reconstruction of historic buildings using contemporary materials. Part of any restoration project on historic buildings is the replacement, respectively refilling of damaged areas using new construction materials. In terms of heritage conservation requirements in practice are often used inappropriate, incompatible, materials. Construction companies aggressively promote "modern" and for historical monuments often inappropriate building materials. Very often the results are houses that lost their “spirit”, without the patina of age, authentic materials, structures, details of construction and the interior. [1]. Many times, due to inappropriate composition of the material used in reconstruction, damage to the original material and irreversible decline occurs where the original and new material are in contact.

The basic characteristics of construction materials are mechanical properties (density, strength, modulus of elasticity) and thermal properties (coefficient of thermal conductivity, thermal diffusivity, mass, respectively. volumetric heat capacity). Equally important are the thermal and moisture expansion coefficients of materials.

An expansion of a material is measured by an apparatus called a dilatometer. As far as we know, the market offers only dilatometers for measuring coefficient of thermal expansion. Therefore in cooperation of the Department of Physics at FCE STU and company METRODAT, within project Slovak Grant Agency VEGA No. 1/0591/10, was developed and produced the dilatometer for measurement of thermal and moisture expansion coefficient.In the following parts of our paper its construction is described.

2. Design characteristics of the device

The measuring setconsists of three separatedandinterrelatedsubsystems with software control system:

- The measuring chamber
- Control system – an externalchiller
- Operating software

2.1 The measuring chamber

The measuring chamber is used for tempering of measured sample in the range of (-10° C to +105° C) and also its exposing to moisture from 10 % to 90 % RH. The sample is placed on a removable stainless steel grate, which allows shaping forced air flow in its immediate vicinity. Heat and humidity transfer to the sample is provided by forced air circulation, which is tempered to the desired temperature by passing through two aluminum heat exchangers with extremely large surface contact area. Internal air circulation ensures axial fan located in between the aluminum heat exchangers. Axial fan EG&G AXIMAX1 [2] used in the configuration is designed for continuous operation under extreme conditions (-40° C to +125° C). Fan speed during the measurement is controlled by YASKAWA frequency inverter in the range 6.000 ÷ 23.000 sp/min. The desired value of aluminum heat exchangers temperature during the measurements is provided by power Peltier thermoelectric cooler (TEC) (2x545W) [3] placed between the aluminum heat exchangers and water tempered copper block. The temperature of water in the copper block is controlled by external chiller COHERENT T251 [4] so that the temperature difference in TEC does not exceed 20° C to secure their optimal working conditions.

Working temperature of TEC is scanned by platinum resistance thermometer and controlled by temperature controller (thermostat) OMRON E5CK [5] in cooperation with SORENSEN [6] power supply according to required proceeding of measuring cycle.

Part of the measuring chamber is micro dosing syringe pump GRASEBY [7] that dispenses the required amount of water into a fabric wick. The wick is placed in the path of circulating air between the aluminum heat exchangers. Moisture is drifted by air circulating which transfers the moisture into the measured sample. The temperature of the sample is measured by miniature thin-film platinum resistance thermometer indirectly through the air temperature, which tempers the sample by forced circulation. Minimum thermometer dimensions provide low thermal inertia and therefore a high response rate to temperature changes. Moisture is continuously monitored by humidity sensor SHT 15 produced by SENSIRION. This sensor contains a built-in semiconductor thermometer by which the relative humidity is continuously adjusted to the current temperature. As a result, the sensor provides an accurate indication of the current relative humidity (RH) without the necessity of its subsequent correction in the control computer. The sensor is equipped with the datalogger, which routinely stores measured RH values and then provides them for further processing in a form of a table or chart together with the data on dew point.

An important part of the measuring chamber is a measuring frame, which ensures accurate scanning of dimensional changes of measured samples depending on temperature and humidity changes. The measuring frame, in terms of design and materials, was designed so that its properties affect the measurement results in the smallest possible measure (degree). With respect to this requirement was the frame itself placed outside the measuring chamber so that its substantial part is not exposed to changes in temperature and humidity along with the measured sample. The material chosen for the measuring frame was a glass-ceramic material ZERODUR [8], whose own thermal expansion is about two decimal orders of magnitude lower than the one of the measured samples. The properties of this material, in particular, changes in mechanical dimensions depending on changes in temperature and humidity in presented application allow neglecting of their impact on the accuracy of the measurement process. The measuring frame is closed, located along both sides of the measuring chamber. Individual parts of the frame are firmly connected together using diffusion welding technology to eliminate the negative and also difficult to define impact of possible adhesives on thermal expansion properties of whole measuring frame. From the shorter sides of the measuring frame two touch fingers (rods) enter the measuring chamber. Shorter – reference finger is firmly connected with the measuring frame and forms a solid stop, where measured sample is based on. Longer – measuringfinger is moving, driven in guides.

It is long enough to allow compensation for the actual sample sizes in the range from 10 mm to 160mm. After forcing the finger to the measured sample and setting the desired thrust it is firmly connected by clamping mechanism to linear variable differential transformer LVDT MACRO SENSORS SBP 375040 [9]. The reason for using this type of LVDT was that it allows measuring linear changes in length in the range of 3 mm with a resolution of 0.1 μm. These parameters correspond exactly with the desired properties of the measuring system.

The clamping mechanism allows for setting the zero position of the sensor, depending on initial conditions and anticipated course of the measurement cycle.

2.2 Control system

Its task is to create conditions for the automated course of measuring process according to the requirements specified by operator. It consists of several separate devices located in a common cabinet:

- LVDT conditioner DAYTRONIC 4032 [10] – its role in cooperation with the LVDT sensor is to record and evaluate changes in linear dimension of measured sample. In the configuration with the selected type of linear variable differential transformer enables recording the changes in size in the order of 10^{-7} m (0.1 μm) within ±1.5 mm. These parameters correspond with properties of measured building materials. Regulation of the conditioner functions and transmission of measured data to the control computer is provided by RS232 interface.

- Frequency inverter YASKAWA VS Mini [11] – its role is to control speed of axial blower EG&G AXIMAX1 during the measurement cycle as required by the control computer. Communication with the computer is provided through a digital potentiometer X9C503S [12] controlled by serial interface RS232.

- Temperature controller OMRON E5CK [5] – ensures controlling of the aluminum heat exchangers temperature, which determines the temperature of the air circulating in the measuring chamber and the temperature of the measured samples. Current temperature of aluminum heat exchangers is scanned by platinum resistance thermometer. The signal from the temperature controller is led to the power amplifier from which Peltier cells are powered by, so that circulating air temperature reaches the value desired by control computer in accordance with the required course of the measurement cycle.

- Power supply SORENSEN [6] – usedto power the Peltier TEC cells with DC in the range 0 to 16A (0 ÷ 32V). For the proper operation of cells the minimum current ripple of power supply is necessary.

- Auxiliary, power and communication circuits – their role is to provide power to individual devices in the control system, adjustment of analog signals to digital processing and secure transmission of commands and data between the computer and individual devices of the control system.

There is a connector **USB II** located on the front panel of the control system for connecting with **control computer**. Standard IBM compatible personal computer (desktop or laptop) where **control software** is installed can be used to control the whole process of measurement. There are also controls and displays of individual devices displayed there to enable their respective manual control as well as direct reading of operating values. Connectors for interconnection of the control system with measuring chamber and chillers are located on the back of the cabinet control system.

2.3 External chiller

External chiller COHERENT T251 is a separate device, whose task is to temper copper exchanger block mechanically linked to Peltier cells on such a temperature, depending on the course of the measuring cycle, so that the temperature difference between the sides of Peltier cells does not exceed 20° C. This means that at low temperature of measured sample chiller keeps the temperature of the copper block about 20° C higher than the actual sample temperature and at high temperature of measured sample chiller keeps the temperature of the copper block about 20° C lower than the actual temperature of the sample. Chiller has separate double heat exchanger, water – Peltier cells – air, as well as complete supply, control and communication circuits. Chiller is electrically connected to control system and the water circuit is connected directly to the copper block of the measuring chamber.

2.4 Control software

Control software is installed in a standard personal computer and allows the operator to enter the desired parameters of measuring cycle, the desired course, the density of measurement points, the number of measurement cycles and also the approximate size of the sample. Based on these input data control software sets the parameters of individual devices in the measuring system, controls their function and downloads operating and measured values. Continuously evaluates downloaded data and according to their analysis coordinates activity of the individual devices so as to achieve the desired objective measurement. Measured data are stored in memory and after the measurement cycle according to operator requirements will be provided for further processing or processed into tables and graphs.

Acknowledgments

This work has been supported by the Slovak Grant Agency VEGA, under Grant No. 1/0591/10.

References

[1] Vošková, K.: Pamäť tradičného stavebného remesla. http://www.obnova.sk/. (In Slovak)

[2] www.ametekaerodefense.com

[3] Thermal Enterprises, 2 Shady Lane, Kendall Park, NJ08824, USA

[4] www.thermotekusa.com

[5] www.omron.com

[6] www.sorensen.com

[7] www.graseby.com

[8] www.schott.com

[9] www.macrosensors.com

[10] www.daytronic.com

[11] www.yaskawa.com

[12] www.littlediode.com

Application of the Domain Reflectometry in Identification of Moisture Transport Parameters of Building Materials

Zbyšek Pavlík, Jan Mihulka, Milena Pavlíková, Lukáš Fiala, Robert Černý

Department of Materials Engineering and Chemistry, Faculty of Civil Engineering, Czech
Technical University in Prague, Thákruova 7, CZ-166 29 Prague 6, Czech Republic

e-mail: pavlikz@fsv.cvut.cz

***Abstract**: The moisture diffusivity determined as function of moisture content represents an important information for the application of building materials in building industry. The knowledge of this parameter can be used with advantage in the practical design of buildings using computational analysis of hygrothermal performance and subsequent service life analysis. In this paper, the time domain reflectometry method is used for monitoring moisture profiles in building materials with the main aim to identify the moisture dependent moisture diffusivity.The experiments revealthat the empirical experimental calibration of the time domain reflectometry method for moisture measurement in specific building materials is a necessary condition for obtaining sufficiently accurate moisture diffusivity in inverse analysis.*

***Keywords:** moisture diffusivity, time domain reflectometry, inverse analysis*

1. Introduction

Moisture present in porous building materials and structures is generally considered as highly significant factor accelerating material and structural degradation.In some specific cases, for instance in combination with frost action, the high moisture content can lead even to serious negative events like buildings' damage and total failure. In addition to this mechanically induced damage, the presence of moisture has been in several studies related to the negative health effects [1]. On that account, the water must be removed from damp residential, administrative and public buildings to prevent deterioration of their indoor quality due to the biological growth, ranging from bacteria, algae and fungi to moss [2], [3]. The action of micro-organisms causes buildings' damage also by producing acid secretions such as oxalic acid, whereas plants can create mechanical stresses by sending roots into crevices.

Because of the harmful moisture action described above, there is necessary to design and build such buildings that will prevent water ingress into their structures, materials, and inner space. Specific attention must be paid especially to applied materials that strictly define and limit structures' functionality and performance from the point of view of water transport and storage. Since water accumulation in building materials assumes water intake into their inner structure, the liquid water transport properties are the most decisive parameters that characterize the possibility of porous materials to absorb and transport water.

The simplest way how to characterize the ability of porous material to absorb water and transport it by capillary forces is the use of water sorptivity concept based on the simple free water intake experiment [4]. In [5] the authors analysed this approach for description of liquid water transport and proved that the free water intake experiment basically can be used as means of material characterization but its strong and weak points should always be considered if conclusions on the behaviour of a particular material are to be drawn. The main advantage of sorptivity concept according to original work by Hall [4] is its experimental simplicity. If the required degree of precision is ascertained [6], the results can serve well for the basic assumption of water transport capabilities of analyzed material. However, one should always take into account that the obtained results have only relative value and cannot be applied for example for precise calculations of moisture transport. However, within the buildings' design, there is a need of knowledge of hygrothermal performance of engineered buildings for example using computational simulations, where the material parameters are used as input data. Therefore, more precise and advanced methods must be applied for determination of material parameters characterizing the liquid water transport.

In building research and design practise, the water transport is modelled by common methods of irreversible thermodynamics, and using just one generalized thermodynamic force. Two approaches are mostly employed, where either the gradient of partial density of water or gradient of hydraulic head are accounted for [7]. In this way, the transport of liquid water is described either by moisture diffusivity or hydraulic conductivity. The concept of hydraulic conductivity is often used for example in soil science, whereas the moisture diffusivity is more often applied in building science. Probably the only reason for the frequent application of moisture diffusivity concept in investigation of moisture transport properties of building materials is simplicity of required moisture distribution measurement in comparison with capillary pressure measurement necessary for hydraulic conductivity calculation.

In the presented work we applied the moisture diffusivity concept for description of the ability of AAC material to transport liquid moisture. As it was given above, for determination of moisture diffusivity as function of moisture content, there is necessary to assess moisture distribution in specific time and position in the studied sample, i.e., measurement of moisture profiles. These experimental data are then submitted to inverse analysis procedure and the moisture dependent moisture diffusivity function is calculated. It is quite obvious that for moisture profiles measurement, non-destructive continuous technique of moisture content measurement are preferable. In this paper, we present TDR (Time Domain Reflectometry) method as suitable technique for such measurements. We first introduce calibration procedure of TDR technique for studied AAC using several different methods. Then, the moisture profiles are measured within the 1-D vertical uptake experiment and the obtained data are submitted to inverse analysis using Matano method. Finally, the moisture dependent moisture diffusivity of AAC is calculated and plotted.

2. Experimental

2.1 Experimental setups

For the TDR measurements in this paper, the cable tester TDR/MUX/mts produced by Easy Test was used. This device has working frequency 1.8 GHz and allows continuous monitoring of relative permittivity values on TDR principle. The determination of moisture content using the measured permittivity values is then based on the fact that the static relative permittivity of pure water is equal to approximately 80 at 20°C, while for most dry building materials it ranges from 2 to 6. All the performed experiments were realised using two-rod laboratory sensors

LP/ms also developed by Polish company Easy Test. The sensorsare made of two 53 mm long parallel stainless steel rods, having 0.8 mm in diameter and separated by 5 mm. The sphere of sensors' influence was determined with the help of a simple experiment. The sensor was fixed in the beaker and during the measurement, there was added water step by step. From the measured data (relative permittivity in dependence on water level) there was found out that the sphere of influence creates the cylinder having diameter about 7 mm and height about 60 mm, circumference around the rods of sensor. The accuracy of moisture content reading given by producer is ± 2% of displayed water content. Details on TDR technique, measurement principles and applications can be found in [8] – [12].

At first, calibration experiment was done in order to determine the calibration curve of TDR method for measured material. The calibration was done on 25 samples having dimensions of 40 x 40 x 100 mm. Two parallel holes having the same dimensions as the sensor rods were bored into each sample. Then, the sensors were placed into the samples and sealed by silicon gel. The samples were partially saturated by water and insulated to prevent water evaporation. The relative permittivity of wet samples was then continuously monitored until the measured values reached the constant value. Then, the experiment was interrupted, sensors removed from the samples and moisture content in the samples was determined using gravimetric method. In this way, empirical calibration curve of TDR technique for studied AAC was obtained. Since experimental calibration of TDR technique is very time consuming, application of empirical conversion functions and dielectric mixing models was tested to improve and shorten calibration process (see Section 3).

In the second experiment, the measurement of moisture profiles was done. This experiment was done on rod-shaped sample of dimensions 50 x 100 x 250 mm that was vertically oriented and its lower face was exposed to water penetration. The lateral sides of the sample were water-proof insulated by epoxy resin because of simplified 1-D water transport. Into the sample, 8 TDR sensors were horizontally placed at specific positions along the sample length. The sensors' installation was the same as in the calibration experiment. The moisture propagation in the sample was continuously monitored, and after specific time interval, the experiment was stopped, and moisture profiles were determined.

2.2 Studied material

The experiments were done on AAC material produced by company Xella International Inc. in order to evaluate its ability to transport liquid water in case of vertical suction. The trade name of this material is Ytong P4 – 500. As the application of homogenization techniques and empirical functions for evaluation of moisture content from measured relative permittivity assumes the knowledge of some material properties, the measurement of porosity, bulk density and matrix density were carried out as well. The measurements were done on the vacuum saturation principle[13]. The results are given in Table 1.

Table 1: *Basic properties of Ytong P4 – 500*

Total open porosity [%]	68
Bulk density [kg/m^3]	509
Matrix density [kg/m^3]	1587

3. Determination of moisture content from measured relative permittivity

Three basic approaches to the determination of moisture content from measured relative permittivity are usually used in building physics. The first possibility is utilization of empirical conversion functions generalized for a certain class of materials. The second possibility is application of dielectric mixing models, which require knowledge of the relative permittivities of the material matrix, water, air and other parameters, that cannot be measured directly, but have to be determined by empirical calibration of the model.The third method consists in empirical calibration for the particular material using a reference method, such as the gravimetric method. This method is the most reliable until now, but the most time consuming one [14].In this work, the empirical calibration was done by gravimetric method as described in the previous section. The empirical calibration curve was then used for the validation of two other empirical conversion functions originally designed for soils' moisture assessment and of different three and four phase dielectric mixing models.

3.1 Empirical conversion functions

Empirical conversion functions represent an effective tool for estimation of moisture content from relative permittivity values measured by TDR. They are based on experimental measurement of a number of calibration curves for similar materials [15]. For example, the third-order polynomial relation proposed by Topp and his colleagues [16] was for many years considered to be the ideal solution for the determination of moisture content of soils using TDR measurement. Since Topp's relation was applied by several researchers also for other types of materials, we tested its validity for AAC as well. This relation is expressed as

$$\theta = -5.3\cdot 10^{-2} + 2.92\cdot 10^{-2}\cdot\varepsilon_{eff} - 5.5\cdot 10^{-4}\cdot{\varepsilon_{eff}}^{2} + 4.3\cdot 10^{-6}\cdot{\varepsilon_{eff}}^{3}, \tag{1}$$

where $\varepsilon_{\varepsilon\phi\phi}$[-] is the effective relative permittivity, and θ [m^3/m^3] the moisture content in the porous body.

In this work we have tested also the applicability of Malicki's formula [17] that was successfully used also in building materials research. It is expressed in equation

$$\theta = \frac{\sqrt{\varepsilon_{eff}} - 0.819 - 0.168 * \rho - 0.159 * \rho^{2}}{7.17 + 1.18 * \rho}. \tag{2}$$

Here, ρ [kg/m^3] is bulk density of measured material, in our case of AAC.

3.2 Dielectric mixing models

In this work, dielectric mixing models based on homogenization theory of effective media were tested as well. In terms of homogenization, a porous material is considered as a mixture of three phases, namely solid, liquid and gaseous phase. In specific cases, the four phase representing the bound water properties can be added. For AAC, the solid phase is formed by fine-grained siliceous sand, burned lime, cement and aluminium powder. Liquid phase is represented by water and gaseous phase by air. In case of the dry material, only the solid and gaseous phases are considered. The volumetric fraction of air in porous body is given by the measured total open porosity. In case of penetration of water, part of the porous space is filled by water. For application of mixing models and evaluation of relative permittivity of the whole material ε_{eff}, the permittivities of particular constituents forming the total porous body have to be known.

Since relative permittivities of water ε_w and air ε_a are listed in common sources, the relative permittivity of porous matrix ε_s remains the only unknown input parameter for dielectric mixing models. For its determination we used value of relative permittivity measured for AAC in the dry state, where only permittivity of solid matrix and air contributed to the total effective permittivity of studied material. Using Rayleigh formula [14] we than calculated ε_s.

The second step within the homogenization procedure represents determination of relative permittivity of the whole material, where the mixing is performed for solid matrix, air, and water. Within these calculations, one must take into account that the effective relative permittivity of a multi-phase composite cannot exceed the bounds given by the relative permittivities and volumetric fractions of its constituents. These bounds are usually called Wiener's bounds, according to the Wiener's original work [18] and can be expressed by the following simple relations

$$\varepsilon_{eff} = \frac{1}{\frac{f_1}{\varepsilon_1} + \frac{f_2}{\varepsilon_2} + \frac{f_3}{\varepsilon_3}}, \tag{3}$$

$$\varepsilon_{eff} = f_1\varepsilon_1 + f_2\varepsilon_2 + f_3\varepsilon_3. \tag{4}$$

Equation (3) represents the lower limit and equation (4) the upper limit of the effective relative permittivity, whereas f_j is the volumetric fraction of the particular phase, and ε_j its relative permittivity.

For verification and certain limitation of the effective relative permittivity values we have used also the Hashin-Shtrikman's bounds [19], which were originally derived for the theoretical determination of the effective magnetic permeability of macroscopically homogeneous and isotropic multiphase materials. Since these bounds were originally proposed for two-phase mixtures only, we derived their three-phase expressions

$$\varepsilon_{lower} = \varepsilon_1 + \frac{3\varepsilon_1}{\frac{1}{\sum_{i=2}^{n} f_i \frac{\varepsilon_i - \varepsilon_1}{2\varepsilon_1 + \varepsilon_i}} - 1} \tag{5}$$

$$\varepsilon_{upper} = \varepsilon_n + \frac{3\varepsilon_n}{\frac{1}{\sum_{i=1}^{n-1} f_i \frac{\varepsilon_i - \varepsilon_n}{2\varepsilon_n + \varepsilon_i}} - 1}, \tag{6}$$

where $f_1 – f_n$ are the volumetric fractions of the particular phase ($f_1 + f_2 + ... + f_n = 1$), and $\varepsilon_1 – \varepsilon_n$ are their relative permittivities, whereas $\varepsilon_1 < \varepsilon_2 < \varepsilon_n$.

For mixing of phases forming the total porous body resulting in moisture dependent relative permittivity function matching the limitations of Wiener's and Hashin-Shtrikman's bounds, several dielectric models can be used. In this work, Lichtenecker's equation, Polder and van Santen's models and four phase de Loor's model were tested to get basic information on the applicability of dielectric mixing models for building materials, especially for AAC. Since all these models were closely described in [14], we will introduce here only their basic equations and necessary explanation.

Lichtencker's equation is given by formula

$$\varepsilon_{eff}{}^{k} = f_1\varepsilon_1{}^{k} + f_2\varepsilon_2{}^{k} + f_3\varepsilon_3{}^{k}, \tag{7}$$

where the parameter k varies within the [-1,1] range. Thus, the extreme values of k correspond to the Wiener's boundary values. In this work, we have used parameter k as the fitting parameter and tried to find the acceptable agreement between measured and calculated results.

Three different types of Polder and van Santen's models derived for specific shape of inclusions forming the porous materials are expressed in equations

$$\varepsilon_{eff} = \varepsilon_s + \sum f_j(\varepsilon_j - \varepsilon_s)\cdot\frac{3\varepsilon_{eff}}{2\varepsilon_{eff} + \varepsilon_j}, \tag{8}$$

$$\varepsilon_{eff} = \varepsilon_s + \sum f_j(\varepsilon_j - \varepsilon_s)\cdot\frac{5\varepsilon_{eff} + \varepsilon_j}{3\varepsilon_{eff} + 3\varepsilon_j}, \tag{9}$$

$$\varepsilon_{eff} = \varepsilon_s + \sum f_j(\lambda_j - \lambda_M)\cdot\frac{2\varepsilon_j + \varepsilon_{eff}}{3\varepsilon_j}. \tag{10}$$

Here, f_j is the volumetric fraction of air or water, ε_j is the relative permittivity of air or water. Equation (8) is valid for spherical inclusions, equation (9) assumes acicular orientation of inclusions and the equation (10) was derived for their disc orientation.

Finally, we tested also applicability of four phase models that take into account also the effect of permittivity of bound water that is completely different from permittivity of free water in capillary system of porous materials. The effect of bound water is consider in de Loor's model as

$$\theta = \frac{3(\varepsilon_s - \varepsilon_{eff}) + 2\theta_{bw}(\varepsilon_{bw} - \varepsilon_{fw}) + 2\psi(\varepsilon_a - \varepsilon_s)}{\varepsilon_{eff}(\frac{\varepsilon_s}{\varepsilon_{fw}} - \frac{\varepsilon_s}{\varepsilon_a}) + 2(\varepsilon_a - \varepsilon_{fw})} + \frac{\varepsilon_{eff}\theta_{bw}(\frac{\varepsilon_s}{\varepsilon_{fw}} - \frac{\varepsilon_s}{\varepsilon_{bw}}) - \varepsilon_{eff}\psi(\frac{\varepsilon_s}{\varepsilon_a} - 1)}{\varepsilon_{eff}(\frac{\varepsilon_s}{\varepsilon_{fw}} - \frac{\varepsilon_s}{\varepsilon_a}) + 2(\varepsilon_a - \varepsilon_{fw})}. \tag{11}$$

In equation (11) ε_{eff} is the measured value of effective relative permittivity of the porous medium; θ the moisture content in the porous body [m^3/m^3]; θ_{bw} the amount of water bonded on porous walls; ε_{bw} the relative permittivity of bonded water (3.1); ε_{fw} the relative permittivity of free water (79 at 20°C), ε_a the relative permittivity of air, ψ the total open porosity (0.68 m^3/m^3) determined using vacuum water saturation test and α is an empirical parameter.

4. Inverse analysis of moisture profiles

Determination of moisture diffusivity as function of moisture content requires inverse analysis of experimentally measured moisture profiles. Inverse analysis depends on assumed mode of moisture transport. In this paper we have assumed non-linear diffusion equation for description of liquid moisture transport and simplification of this transport to 1-D case. Within our calculation we have applied Boltmann-Matano [20] treatment taking into account the real situation of performed water suction experiment, where constant initial conditions and

Dirichlet boundary conditions on both ends of the specimen were maintained. Since the inverse analysis procedure based on application of Matano method was already published by many authors, we introduce only final formula for calculation of moisture diffusivity function from measured moisture profiles

$$\kappa(u_x) = \frac{1}{2t_0 \left(\frac{du}{dx}\right)_{x_0}} \int_{x_0}^{\infty} x \frac{du}{dx} dx \qquad (12)$$

wheret_0 =*const.* is a given time where the moisture field $w(z,t_0)$ is known and z is the space variable. The details on the inverse analysis procedure can be found e.g. in [21], [22].

5. Results and discussion

The empirical calibration curve of applied TDR device for moisture content monitoring in studied AAC is presented in Figure 1.Here, Wiener's and Hashin-Shtrikman's bounds are also presented. One can see that Wiener's bounds validated the measured data quite well. However, for higher moisture content the measured data exceeded the upper Hashin-Shtrikman's bound. These data were also not in agreement with our previous similar measurements and calculations performed for different types of AAC [14].

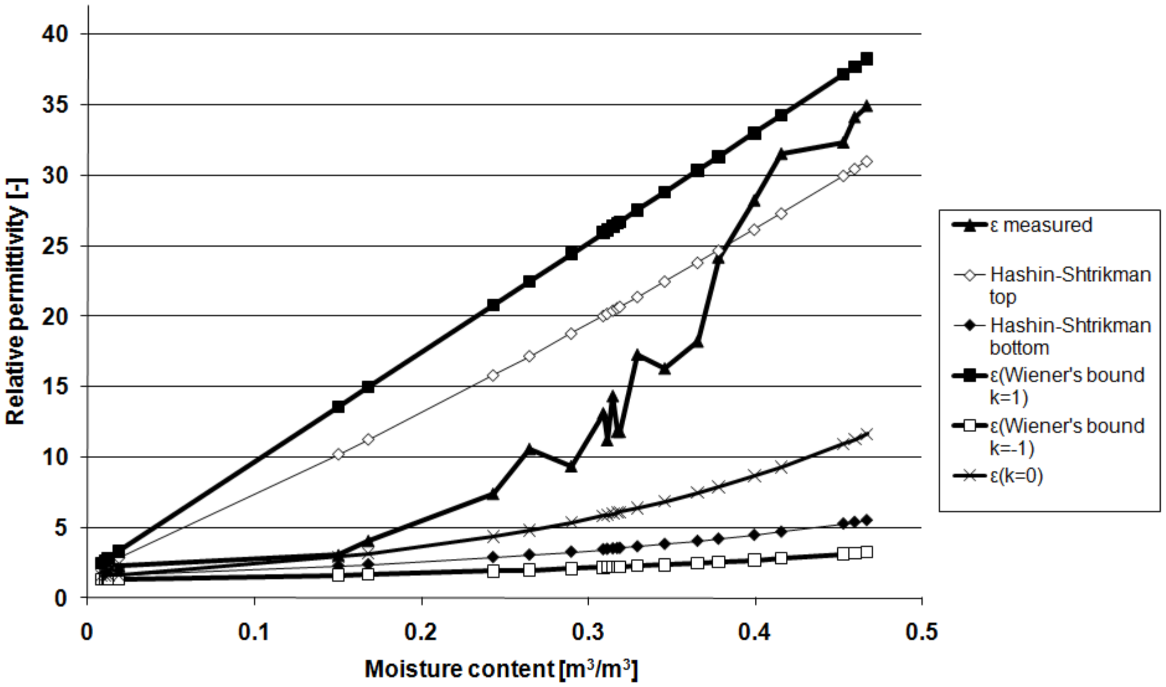

Figure 1: Relative permittivity of AAC as function of moisture content – empirical calibration curve

The results of validity testing of chosen empirical formulas coming from soil science are presented in Figure 2. We can see that results of Topp's curve are mostly higher than those measured. Relatively good agreement is observed for Malicki's function in lower moisture content, typicallyup to 0.32 m^3/m^3. For higher moisture content, the Malicki's function failed as well. This is, however, not very surprising result. The empirical and semi-empirical formulas for evaluation of moisture content from measured relative permittivity designed for application in soil science cannot be universal, especially for building materials having different texture and structure of porous space.

The results obtained by Lichtenecker's equation are given in Figure 3. It is quite obvious that the Lichtenecker's equation is for the studied material inapplicable in the whole range of studied moistures.

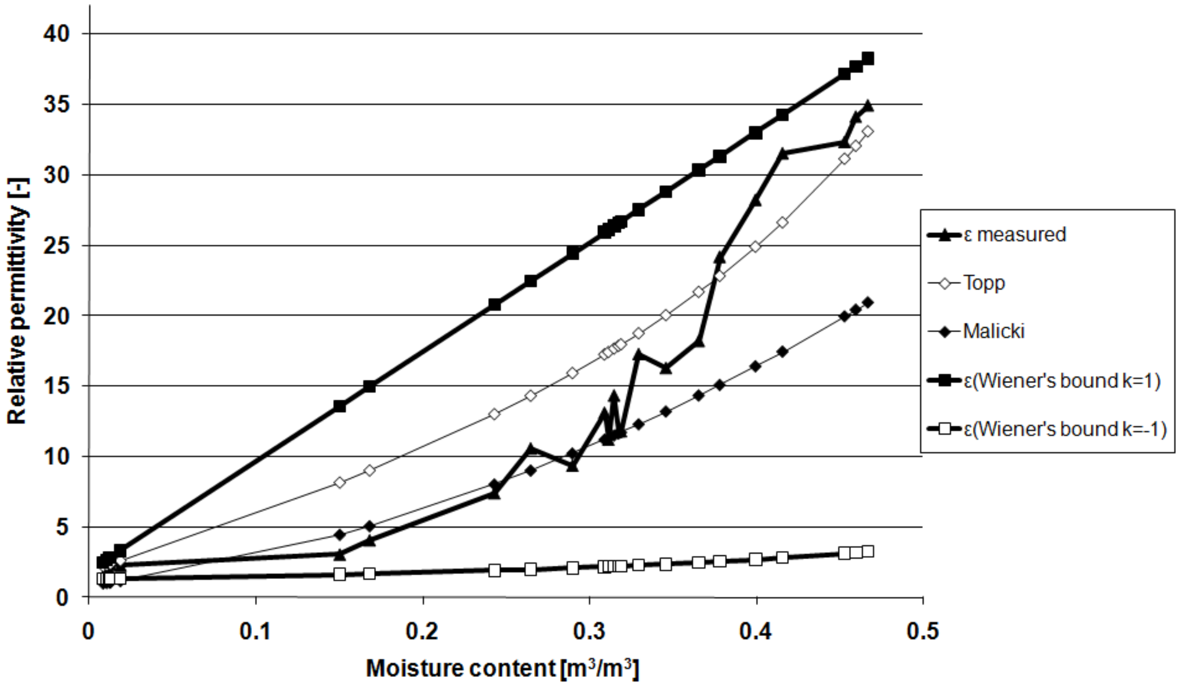

Figure 2: Relative permittivity of AAC as function of moisture content - empirical models

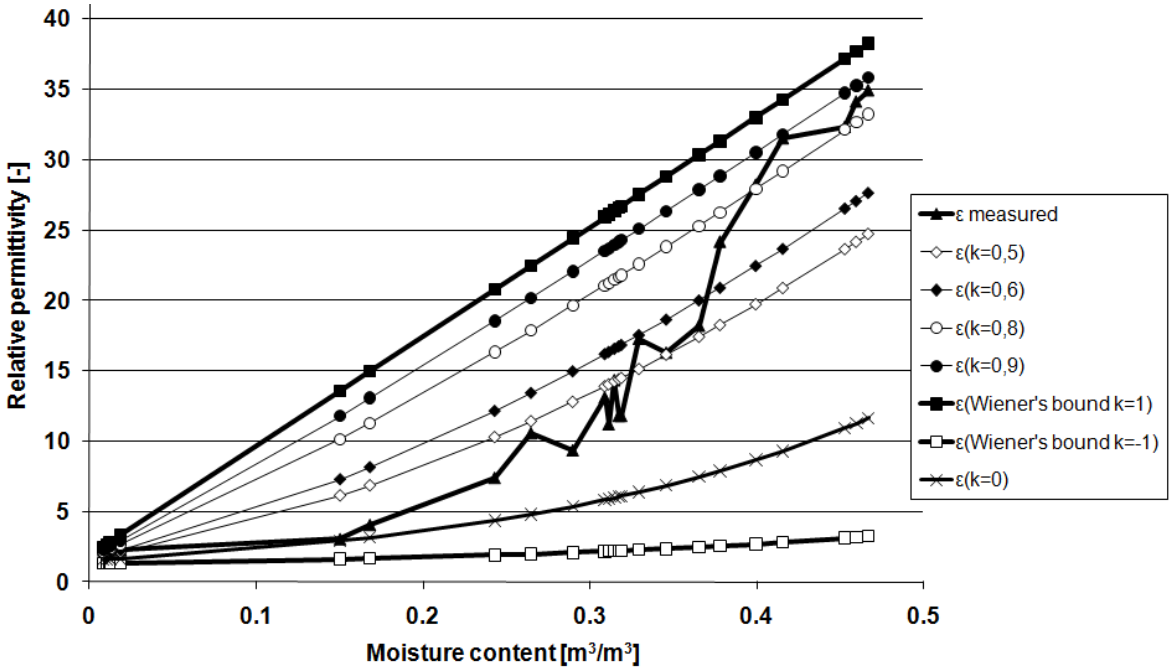

Figure 3: Moisture dependent relative permittivity function calculated using Lichtenecker's formula for specific values of k parameter

The effect of the shape of inclusions was studied using three Polder and Van Santen's mixing formulas. The results are given in Figure4. In this case, a partial agreement of measured and calculated results was obtained for spherical inclusions only, typically in moisture range up to 0.18 m³/m³. Other studied models completely failed.

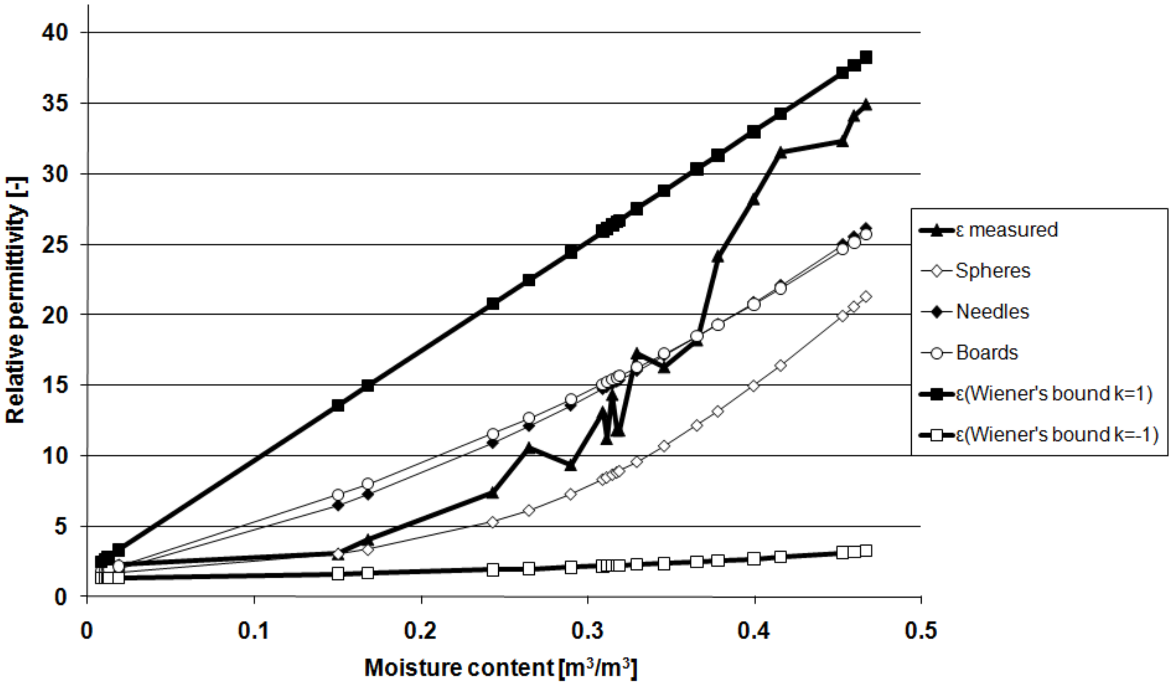

Figure 4: Results of application of Polder and van Santen's models for specific inclusions' shape

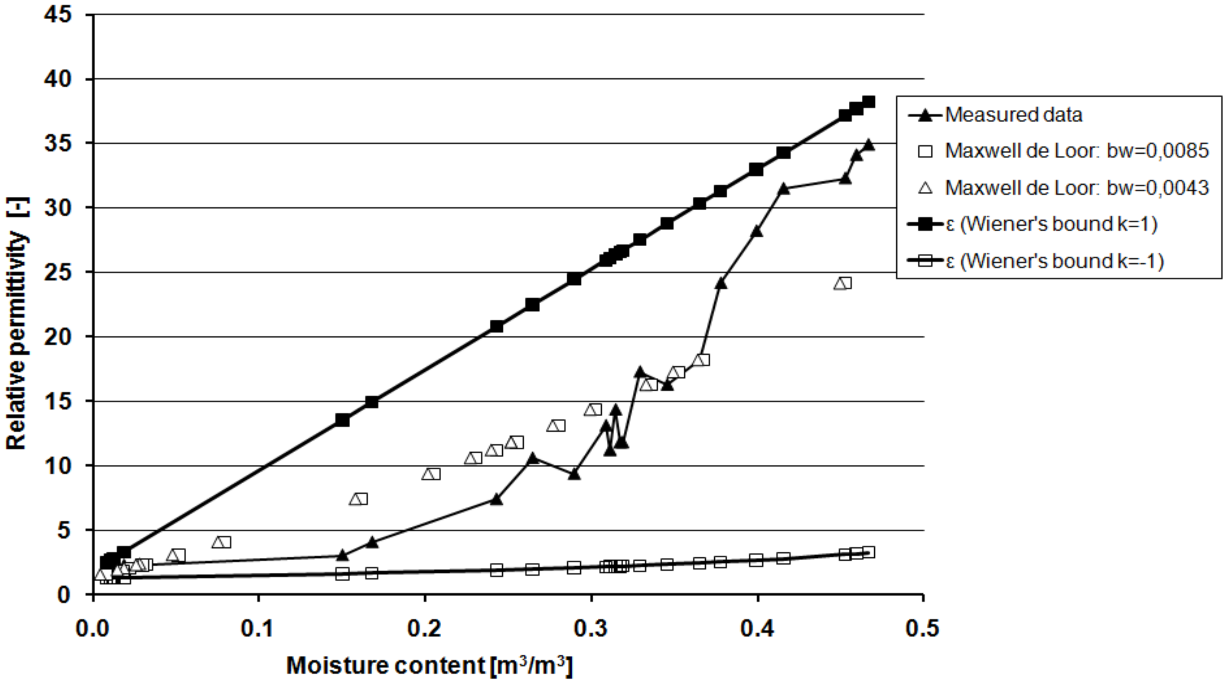

Figure 5: Moisture dependent relative permittivity calculated by de Loor's 4-phase model

Results obtained using four-phase de Loor's model given in Figure 5 are not very promising from the point of view of model's applicability, since the shape of the calculated curves does not correspond to the experimental calibration curve. Although the amount of bound water and empirical parameter α can be improved and used for optimization of the model, the general usage of this model for different types of building materials without previous experimental verification remains an open question.

The measured moisture profiles evaluated using above given empirical calibration curve are presented in Figs. 6. Looking at the results we can observe that the initial moisture transport was very fast. Then, the water transport was decelerated, probably because of the gravity effect on vertical moisture uptake. This feature we observed already in previous works, where the moisture transport driven by capillary forces was significantly reduced because of the predominant effect of gravity force in the big capillary pores. Since AAC is highly porous material containing some big diameter capillary pores, the same effect can be assumed also here.

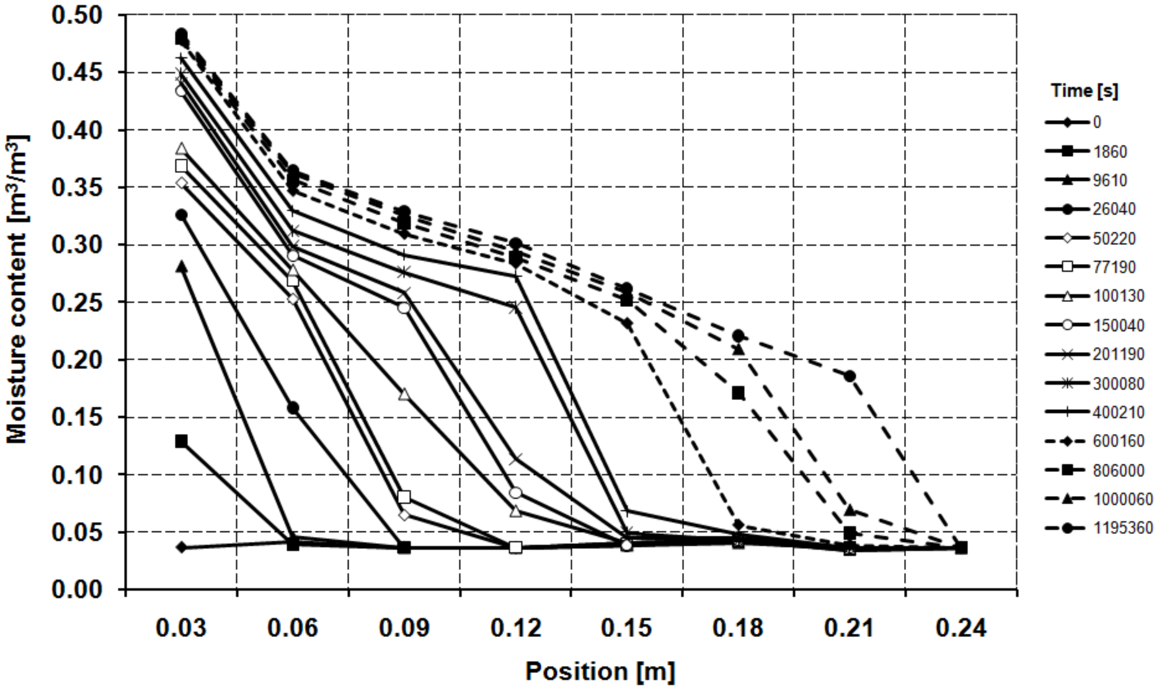

Figure 6: Moisture profiles for AAC measured by TDR

The moisture dependent moisture diffusivity is presented in Figure 7. Looking at the data in Figure 7, the moisture diffusivity varies within the range of three orders of magnitude. On that account, there is evident the necessity to determine moisture diffusivity as function of moisture content and not as a single apparent value what is often done by some researchers. From the quantitative point of view, the values of moisture diffusivity are relatively high, especially in higher moisture range, and explain the rapid moisture transport in the inner structure of AAC.

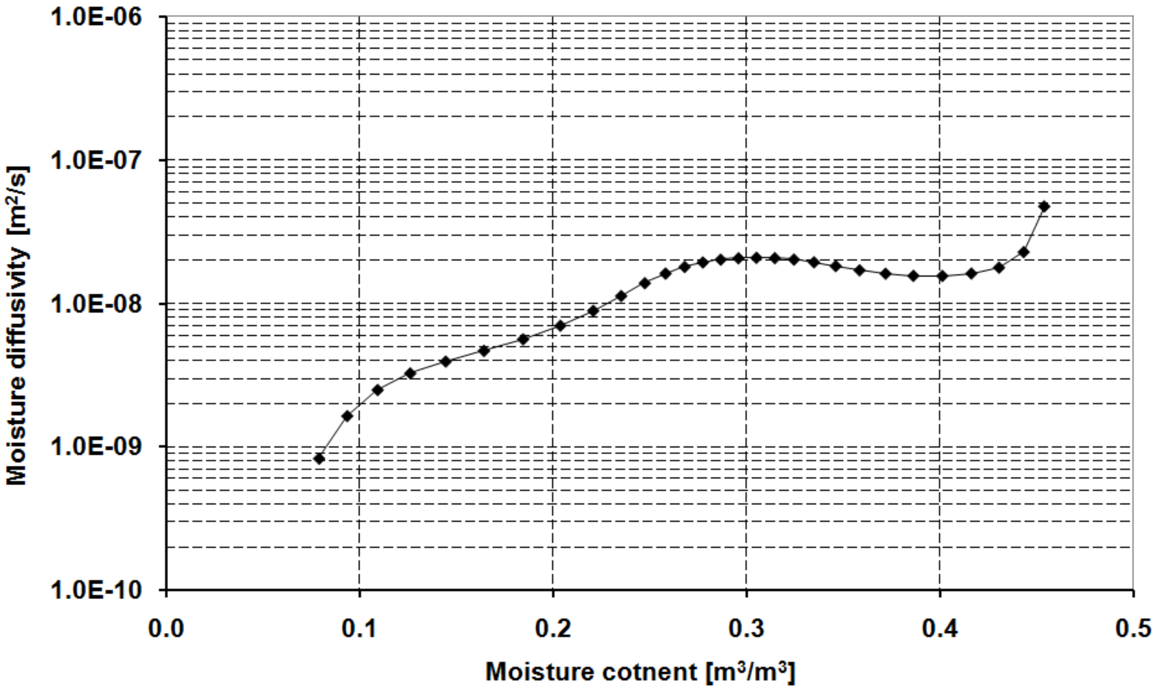

Figure 7: Moisture diffusivity of AAC as function of moisture content

6. Conclusions

The experiments and calculations presented in this paper proved the necessity of empirical experimental calibration of TDR method for moisture measurement in specific building materials. The obtained empirical calibration curve of AAC revealed one important fact. It could not be expressed by a unique function in whole the studied range of moisture content, but two different parts of relative permittivity-moisture content functions could be distinguished. In the moisture content range of 0 – 35%, a roughly exponential shape could be observed. Then, the calibration curve increased more rapidly for not exactly known reasons. This unusual shape of the calibration curve was the main reason why all the studied dielectric mixing models failed. If these models were applied on the two different parts of calibration curve separately, we might possibly succeed but this would certainly not be a pure solution from the theoretical point of view.

The determination of moisture diffusivity as function of moisture content represents an important information for the application of studied AAC in building industry, where the advantage of this knowledge can be used in the practical design of buildings using computational analysis of hygrothermal performance and subsequent service life analysis.

Acknowledgments

This research has been supported by the Czech Ministry of Education, Youth and Sports, under project No.MEB 051004.

References

[1] Bornehag, C. G., Blomquist, F., Gyntelberg, F., Jaervholm, B., Malmberg, P., Nordwall, L., Nielsen, A., Pershagen, G. J., Sundell, G. J., Dampness in Building and Health Nordic

Interdisciplinary Review of the Scientific Evidence on Associations between Exposure to "Dampness" in Buildings and Health Effects (NORDDAMP). Indoor Air, Vol. 11, 72-86.

[2] Fog Nielsen, K., Mould growth on building materials, secondary matebolits, mycotoxines and biomarkers. The Mycology group, Biocentrum – DTU, Technical Univesity Denmark, Lyngby, 2002.

[3] Adan, O. C. G., On the fungal defacement of interior finishes, Ph.D. Thesis, Eindhoven University of Technology, Eindhoven, 1994.

[4] Hall, C., Water Sorptivity of Mortars and Concretes: A Review. M. Conc. Res., 1989, Vol. 41, 51–61.

[5] Vejmelková, E., Pavlíková, M., Jerman, M., Černý, R. Free Water Intake as Means of Material Characterization. J. Build. Phys., 2009, Vol. 33, 29-44.

[6] Bomberg, M., Pazera, M. and Plagge, R., Analysis of Selected Water Absorption Coefficient Measurements. J. Therm. Env. Build. Sci., 2005, Vol. 28, 227–243.

[7] Černý, R., Rovnaníková, P., Transport Processes in Concrete, 1st ed., London, Spon Press, 2002, 379-380.

[8] Malicki, M. A., Skierucha, W., A manually controlled TDR soil moisture meter operating with 300 ps rise-time needle pulse. Irrig. Sci., 1989, Vol. 10(2), 153-163.

[9] W. Skierucha, Accuracy of soil moisture measurement by TDR technique. Int. Agrophys., 2000, Vol. 14, 417-426.

[10] Pavlík, Z., Mihulka, J., Pavlíková, M., Černý, R., Monitoring Coupled Moisture and Salt Transport Using Single Vertical Suction experiment. Fourteenth International Conference on Computational Methods and Experimental Measurements. Algarve, Portugal, 2009, Wessex, WIT PRESS, 157-167.

[11] Pavlík, Z., Fiala, L., Černý, R., Sobczuk, H., Suchorab, Z., Effect of particle shape on the accuracy of dielectric mixing models applied for determination of moisture content of building materials. Energy Efficiency and New Approaches.Fourth International Building Physics Conference. Topkapi, Istanbul, Beysan Matbaacilik ve Reklamcilik, 2009, 33-39.

[12] Skierucha, W., Wilczek, A., Alokhina, O., Calibration of TDR probe for low soil water content measurements. Sensors and Actuators A: Physical, 2008, Vol. 147, 544-552.

[13] Jiřičková, M., Application of TDR Microprobes, Minitensiometry and Minihygrometry to the Determination of Moisture Transport and Moisture Storage Parameters of Building Materials, Prague: Czech Technical University, 2004.

[14] Pavlík, Z., Fiala, L., Černý, R., Sobczuk, H., Suchorab, Z., Effect of particle shape on the accuracy of dielectric mixing models applied for determination of moisture content of building materials. Energy Efficiency and New Approaches.Fourth International Building Physics Conference. Topkapi, Istanbul, Beysan Matbaacilik ve Reklamcilik, 2009, 33-39.

[15] Robinson, D. A., Jones, S. B., Blonquist Jr. J. M., Friedman, S. P., A Physically Derived Water Content/Permittivity Calibration Model for Coarse-Textured, Layered Soils. Soil Sci. Soc. Am. J., 2005, Vol. 69, 1372-1378.

[16] Topp, G. C., Davis, J. L., Annan, A. P., Electromagnetic determination of soil watercontent: Measurements in coaxial transmission lines. Water Resources Research, 1980, Vol. 16, 574-582.

[17] Malicki, M. A., Plagge, R., Roth, C. H., Improving the calibration of dielectric TDR soil moisture determination taking into account the solid soil. European J. Soil Sci., 1996, Vol. 47, 357-366.

[18] Wiener, O., Die Theorie des Mischkorpers fur das Feld der stationaren Stromung. Abhandlungen der Mathemati-schen-Physischen Klasse der Königlichen Sächsischen Gesellschaft der Wissenschaften, 1912, Vol. 32, 509-604.

[19] Hashin, Z., Shtrikman, S., A Variational Approach to the Theory of the Effective Magnetic Permeability of Mul-tiphase Materials. J. Appl. Phys., 1962, Vol. 33, 3125.

[20] Matano, C., On the relation between the diffusion coefficient and concentration of solid metals. Jap. J. Phys., 1933, Vol. 8, 109-115.

[21] Pavlík, Z., Michálek, P., Pavlíková, M., Kopecká, I., Maxová, I., Černý, R., Water and Salt Transport and Storage Properties of Mšené Sandstone. Constr. Build. Mat., 2008, Vol. 22(8), 1736-1748.

[22] Pavlík, Z., Jiřičková, M., Fiala, L., Černý, R., Inverse Modelling of Salt Diffusion and Advection in Building Materials. Research in Building Physics and Building Engineering, 2006, London, Taylor and Francis, 155-160.

Comparison of mechanical and thermal properties of fire protection boards

Jan Toman, Tomáš Korecký, Miroslava Lapková, Robert Černý

Czech Technical University in Prague, Faculty of Civil Engineering, Department of Materials Engineering and Chemistry, Thákurova 7, CZ-166 29 Prague 6, CZECH REPUBLIC

Abstract: *Usage of board materials for protecting the construction against external harmful effects, both mechanical and chemical, is nowadays very frequent and profitable. In this paper measurement of mechanical (modulus of elasticity) and thermal properties (thermal conductivity, thermal diffusivity, specific heat capacity) on 4 selected materials is presented. Two kinds of them were cement composite materials and other two were made on gypsum base. Each of the observed properties was measured on samples which had been previously loaded by high temperature. The dependence of measured properties on temperature of heating is assessed.*

Key words: *mechanical properties, thermal properties, composite materials, high temperature*

1. Introduction

Nowadays board materials are very often used as lining of building structures.

This solution brings two fundamental effects:

- Structure protection against harmful external effects which could be, for example mechanical, chemical and physical. As standard procedure in the building industry veneer board is often used for increasing fire protection.
- Aesthetic arrangement of the building is interior surfaces.

Composite materials are often used to improve mechanical properties. In order to consider the quality of fire protection it was decided to observe their mechanical and thermal material parameters [1].

2. Materials samples description

Observed board samples were delivered from VÚSTAH Brno. The samples were from four types of board material:

PROMATECT – white material, board thickness 3 cm

FIREBOARD – grey material, board thickness 2.5 cm

RIGIBS – pink material, board thickness 1.2 cm

FERMACELL – white material, board thickness 1.2 cm

The first two materials had been tested and the results of this had been presented [7]. So in this paper we presented only results of properties of materials Rigibs and Fermacell.

These materials are made for commercial purposes and their composition has been kept secret by the firm. For this reason we don´t know the exact composition of the materials.

For measuring we prepared 16 pieces of samples from the delivered boards. To find out thermal technical properties of the materials boards were cut into squares of size 7 x 7 cm from all materials.

To determine the mechanical qualities 16 beams were cut into size 3 x 18 (or 15) cm x board thickness.

3. Methodology of measurement

Thermal properties of heat stability were measured on boards from given materials by apparatus IZOMET 2114, which determined the heat conductivity and volumetric heat capacity (product of specific heat capacity and specific density). [2]

The measurement of heat stability of mechanical properties was executed by a non-destructive method on prepared samples by ultrasound apparatus DIO 526, with which it is possible to measure speed of wave spreading by sonic method or resonant method base frequency and then is possible to calculate dynamic modulus of elasticity from dimensions [3].

The parameters were observed in different temperature shocks because it is possible to presume that they depend on temperature [1], [4].

Individual limits of temperature stress were set in reference (consideration) to theoretical temperatures of stability of concrete, i.e. decomposition of calciumhydroxid circa 470 °C and decomposition of hydrates circa 680 °C [5]. Measurement was realized on samples stressed with the following temperatures:

- normal temperature 25 °C
- drying 110 °C
- medium heating 250 °C
- higher heating - below the first critical temperature 450 °C
- higher heating - between the first and the second critical tem. 650 °C
- high heating – over the second critical temperature 750 °C
- maximal temperature stress 1000 °C

4. The experiment

We created a bunch of samples in order to be able to examine the influence on gradual temperature increases. It means the comparison of repeated temperature stress and direct heating on high temperature (thermal shock). Each sample was stressed in a different way, which is documented in the enclosed table, where there colour-indicated temperature stress at particular samples.

The difference was also in the default conditions created before temperature stress. Samples 1 to 8 had been dried before at 110 °C (or 70 °C in case materials based on gypsum) for 7 days to equilibrium weight. Samples 9 to 16 hadn´t been dried and thus maintained equilibrium moisture; these samples were stressed by temperature. [6]

For each temperature stress the defined bunch of samples was always placed to an electrical kiln. The kiln was heated by constant rising to a particular temperature. Then the rising of temperature was stopped and the kiln was kept at the set temperature for 3 hours. After that heating was switch off and the tested samples cooled down to normal temperature.

Thermal qualities were measured in normal temperature around 25 °C.

5. Results of experiment

All measured values were analysed in EXCEL editor. In to these tables there were plotted all values for each observed material in dependence on burn temperature. It means weight of sample, relative loss in weight, samples dimensions, volume, bulk density, heat capacity, thermal diffusivity, volume heat capacity, time of wave pass, speed of wave spreading, dynamic modulus of elasticity, frequency of resonance and dynamic modulus of elasticity determined by resonance method.

By this way we created tables only for materials Rigibs and Fermacell because for materials Promatect and Fireboard we created in the past and presented last year [7].

All changes in measured values – i.e. relative decrement of weight, thermal conductivity and volumetric heat capacity, measured on particular samples were plotted into figures depended on burn temperature. On these samples are good visible permanent changes in each value caused by temperature stress on all materials.

On the other graphs relative loss of weight during burn, volumetric specific heat capacity and thermal diffusivity are shown.

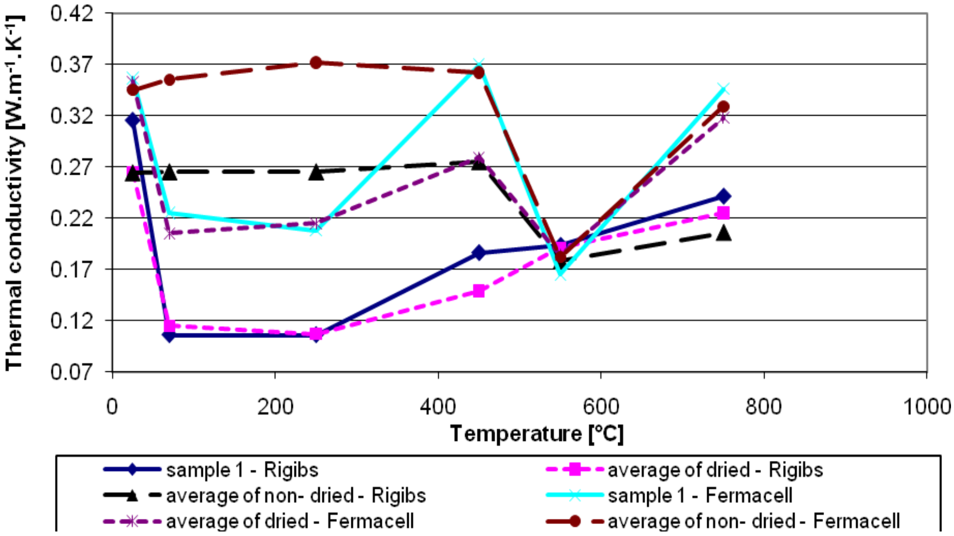

Figure 1: Thermal conductivity dependence on temperature – FERMACELL and RIGIBS

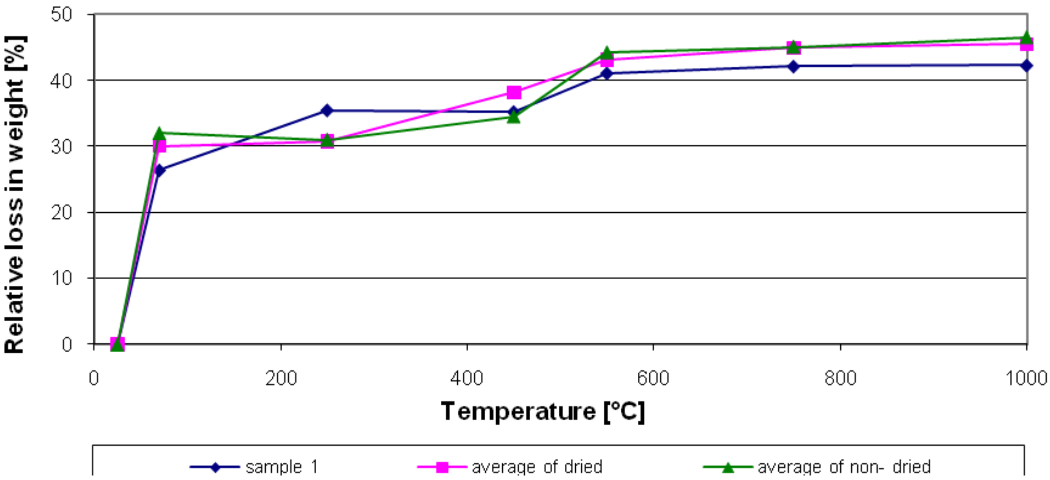

Figure 2: Relative loss in weight dependence on temperature – RIGIBS

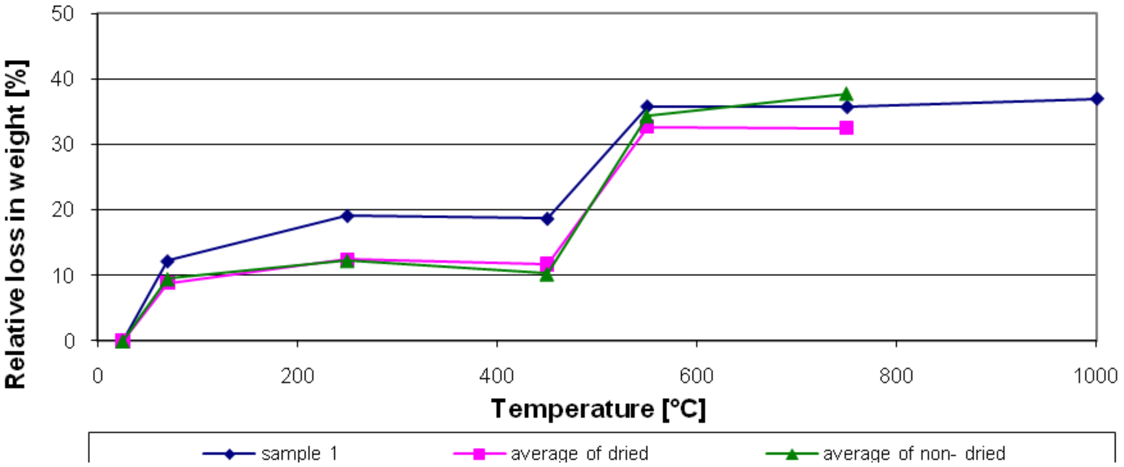

Figure 3: Relative loss in weight dependence on temperature – FERMACELL

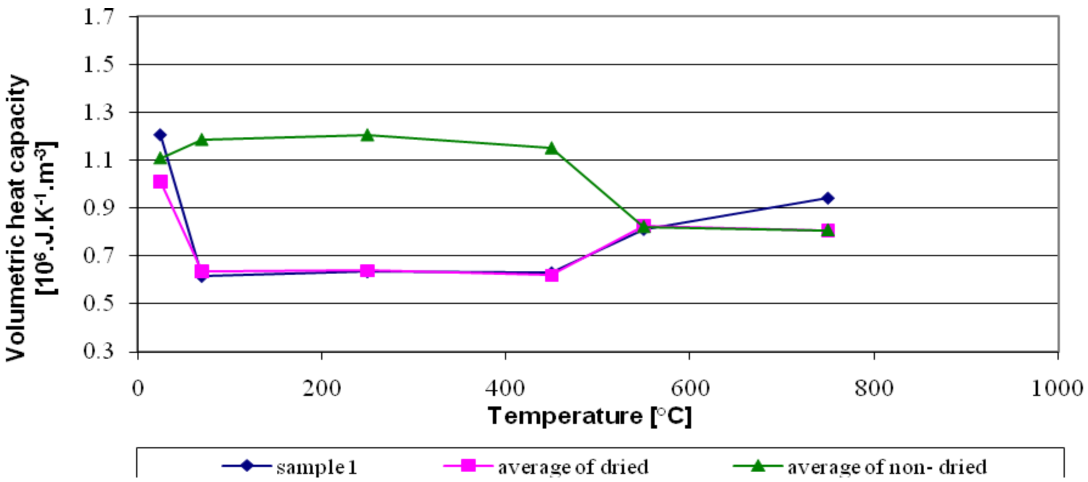

Figure 4: Volumetric thermal capacity dependence on temperature – RIGIBS

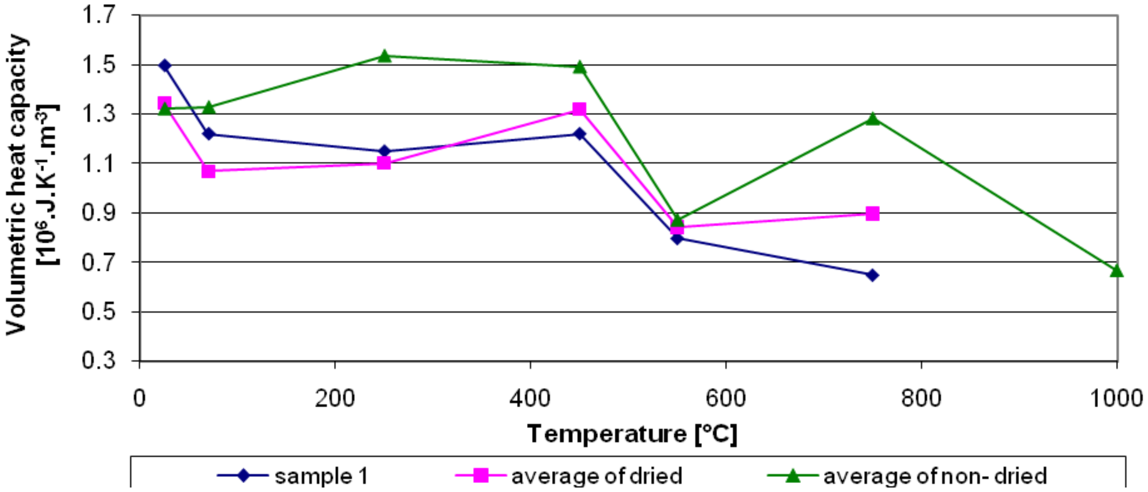

Figure 5: Volumetric thermal capacity dependence on temperature – FERMACELL

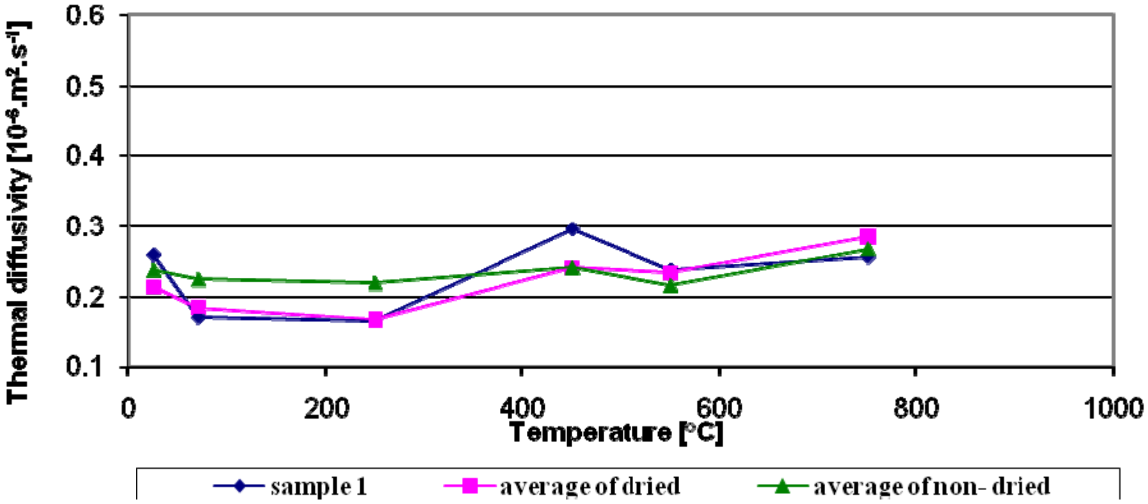

Figure 6: Thermal diffusivity dependence on temperature – RIGIBS

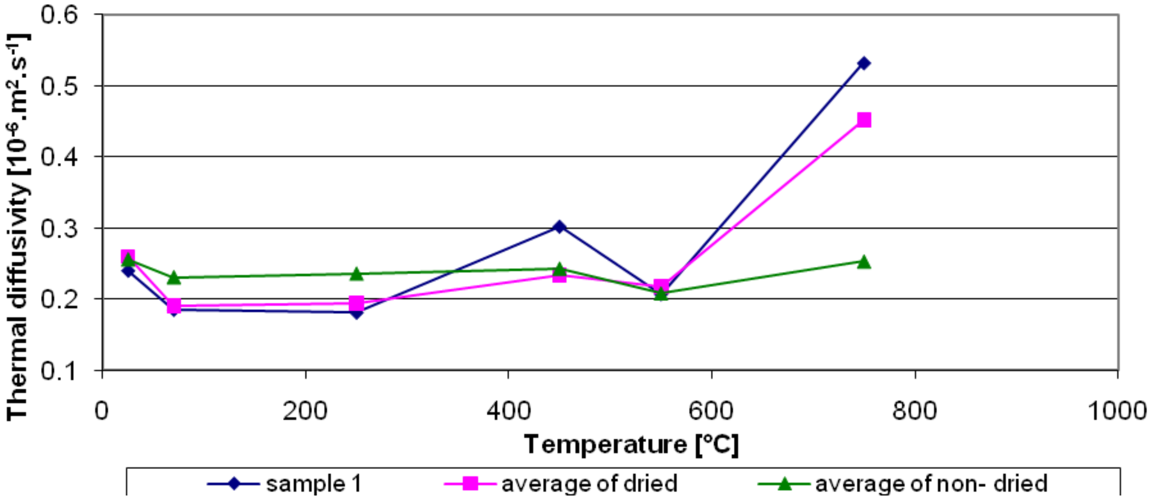

Figure 7: Thermal diffusivity dependence on temperature – FERMACELL

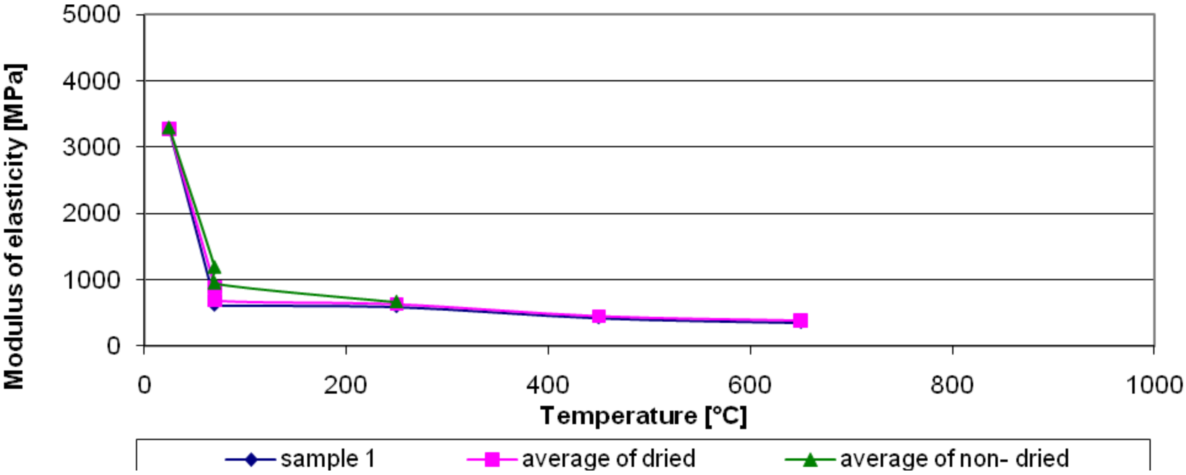

Figure 8: Modulus of elasticity dependence on temperature – RIGIBS

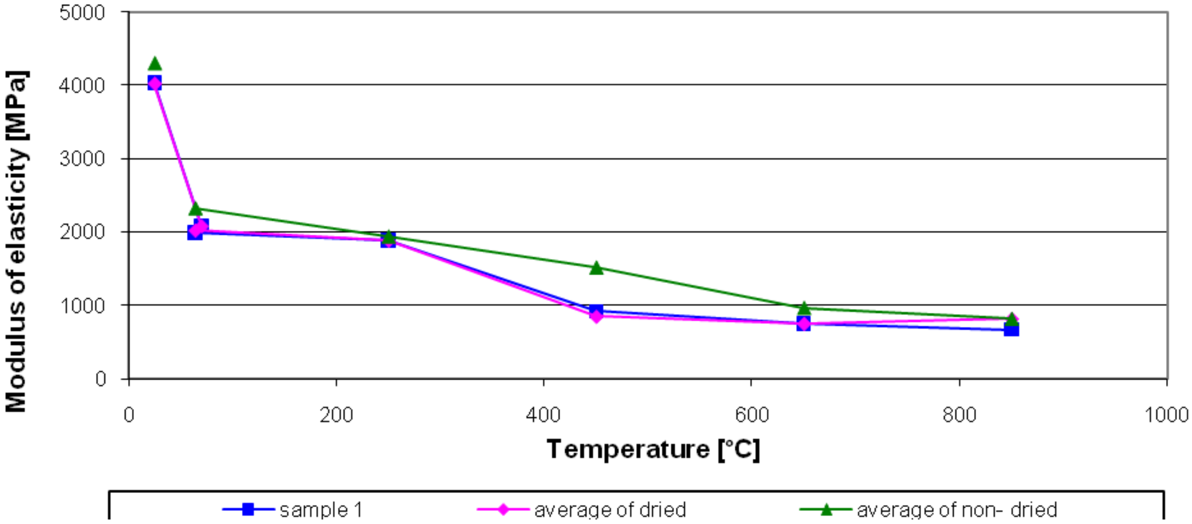

Figure 9: Modulus of elasticity dependence on temperature – FERMACELL

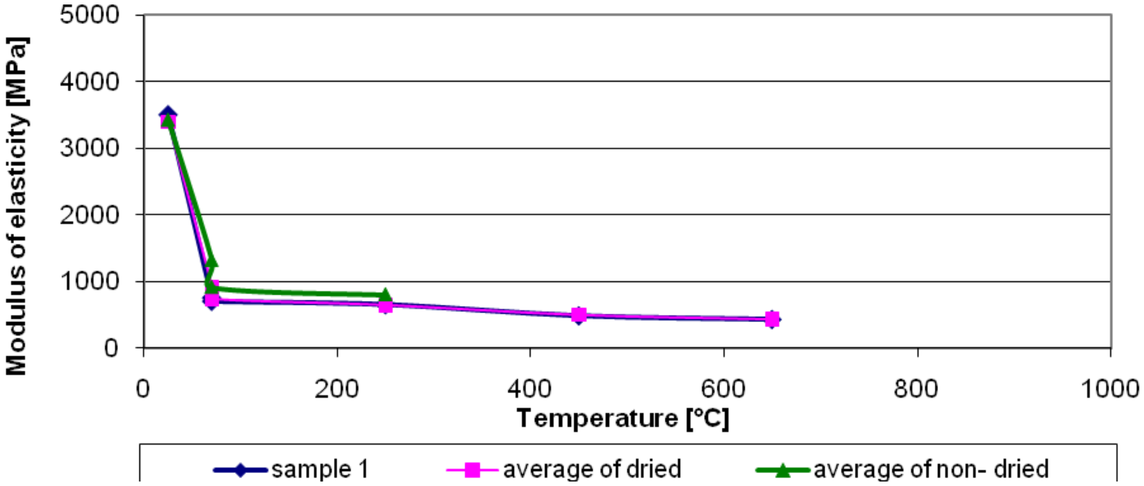

Figure 10: Modulus of elasticity dependence on temperature – resonant method – RIGIBS

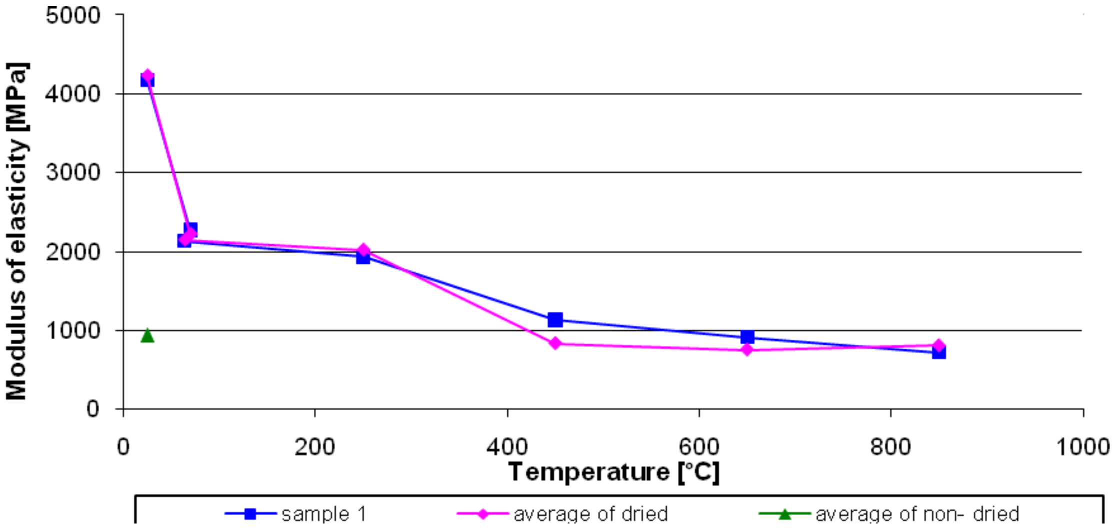

Figure 11: Modulus of elasticity dependence on temperature – resonant method – FERMACELL

6. Discussion

In case of evaluation of modulus of elasticity it is possible to claim that measurements executed by resonant method and by method based on measuring speed of wave spreading don´t show important differences. By this we can consider both methods comparable and results usable.

Further we found out the expected result, that modulus of elasticity of PROMATECT and FIREBOARD is more temperature stable than at materials based on gypsum it means RIGIMBS and FERMACELL. This was expected, because gypsum, as dihydrate, change by temperature to hemihydrates and at high temperatures even to anhydrite. It was confirmed also by measuring the relative loss in weight.

By comparing the obtained figures it is possible to claim that the heat conductivity of PROMATECT material is relatively stable with a slightly decreasing trend. Differences in values in dependence on primary conditions which material was observed aren´t important.

On the contrary, the FIREBOARD material has a stronger tendency to an increase in the heat conductivity dependent upon burn temperature. There is also the apparent bigger influence of previous drying, it meaning the influence of moisture on non-dried samples on thermal conductivity.

Quite on cue the experiment proved that board materials based on gypsum RIGIBS and FERMACELL don´t have enough structural stability under high temperatures (the samples broken at temperatures around 800 °C). Therefore although on lower temperature values of thermal properties are suitable, from the point of view of fire protection composite boards PROMATECT and FIREBOARD are more suitable.

Using figures comparing the relative decrement of weight of the PROMATECT material it is possible to claim that for lower temperatures (up to 500°C) the values are not changed much (maximal change 7%). But higher temperatures caused bigger changes of values (circa 30%). In contrast, the FIREBOARD material is affected by more significant changes already of lower temperatures (below 500 °C) and with higher temperatures values get more fixed.

From figures of thermal diffusivity and volumetric heat capacity of all materials it is evident that the important break point happens again at around 500 °C. The material PROMATECT has a decreasing trend of volumetric heat capacity while on the material FIREBOARD it is possible to observe a gentle increase.

It was explicitly documented that on all samples which had been dried before, the dispersion of observed values is smaller than the dispersion of non-dried.

7. Conclusions

In conclusion it is possible to claim that all thermal parameters are comparable for all materials. Perhaps only the fact that the thermal conductivity of the material PROMATECT wasmeasured slightly lower and also the total structural stability was found better.Therefore boards made of this material are more suitable as fire protection lining.

The advantage of the material PROMATECT is that it has smaller bulk density, and therefore better thermal isolation properties, than the material FIREBOARD.

By this it is possible to claim that the observed composite materials are suitable for use as thermal insulation at lower temperature (up to 300 °C). As fire protection the most suitableboards are PROMATECT, the FIREBOARD also has relatively good stability at high temperatures.

Acknowledgements

This work has been financially supported by the Ministry of Education, Youth and Sports of Czech Republic, under project No MSM: 6840770031 and by the Ministry of Industry and Trade of Czech republic, under project No MPO FR – TI 1/216.

References

[1] Toman J.: Temperature and moisture influence on physicals parameters of buildings materials (in Czech), dissertation thesis DrSc. CVUT in Prague 1992.

[2] Carslaw, Jaeger : Conduction of heat in solids.Oxford.1959.

[3] Toman J., Semerák P.: Physic 10 – Practical lessons (in Czech), CVUT Prague 2001.

[4] Krempaský J.: Measuring of thermo-physical values (in Slovak), SAV Bratislava 1969.

[5] Concrete – source book of technologist, advertisement studio ARTIS, 2005.

[6] Michalko O., Bažantová Z. and.: Mechanicalproperties..., Slovak and Czech

International Calorimetric Seminar, University of Pardubic 2010, p 73

[7] Toman J., Korecky T., Frank M., Cerny R.: High temperature stability of board composites, THERMOPHYSICS, Brno University of Technology, 2010

Theoretical Analysis of Sensitivity of Heat Flow Sensor in Isothermal Calorimeter

Vratislav Tydlitát, Jan Zakoutský, Robert Černý

Department of Materials Engineering and Chemistry, Faculty of Civil Engineering,
CzechTechnicalUniversity in Prague, Thákruova 7, CZ-166 29 Prague 6, Czech Republic, e-mail:
tydlitat@fsv.cvut.cz

Abstract: *The calibration constant of an isothermal heat flow calorimeter is derived in a theoretical analysis of steady-state heat transport, using equivalent thickness of heat-conducting metallic layer on the surface of the pair of ribs used as heat flow sensor and its equivalent thermal conductivity. The sensitivity of the heat flow sensor on the values of heat transfer coefficient from the surface of the rib and thickness of electroplated copper on the surface of the constantan wire, which are not exactly known, is then analyzed theoretically within their uncertainty range. A comparison of theoretical and experimentally measured calibration constants makes possible to identify the correct values of the two unknown parameters.*

Keywords: *isothermal heat flow calorimeter, calibration constant, theoretical analysis, steady-state heat flow*

1. Introduction

Heat flow calorimeters are applied for isothermal or near isothermal measurement of reaction heat. Most devices do not measure directly heat but heat power, so that they are able to monitor heat flow. The heat flow sensors are in principle either contact or contactless. The contact principle has been used by Calvet and Prat [1], Kuzel [2], Lemke [3], Evju [4] and others. The contactless sensing of heat flow in conduction calorimeters has been described by Mtschedlov-Petrossjan et al [5], Oliew and Wieker [6], Tydlitát et al. [7].

Contactless transfer of heat by convection, conduction and radiation in an isothermal heat flow calorimeter can be measured using a thermopile rib.In this paper we present the relation between the sensitivity of the heat flow sensor and the thermoelectric voltage of the copper/constantan thermopile of the isothermal heat flow calorimeter designed in [7].

2. Theoretical derivation of the calibration constant of the heat flow calorimeter

The isothermal heat flow calorimeter KC01 [7] was developed for the measurement of hydration heat of cement, lime and gypsum. The design of its thermopile rib is shown in Figure 1.

It consists of synthetic resin laminate sheet (pertinax), on whose surface constantan wire is densely wound, two turns per mm, and connected on upper and lower ends. The diameter of the constantan wire is 0.1 and 0.127 mm. On one side of the rib the constantan wire surface is electroplated with copper. Both the edges of the rib form the junctions of copper/constantan thermocouples. The thermocouples are fixed with a thin layer of varnish.

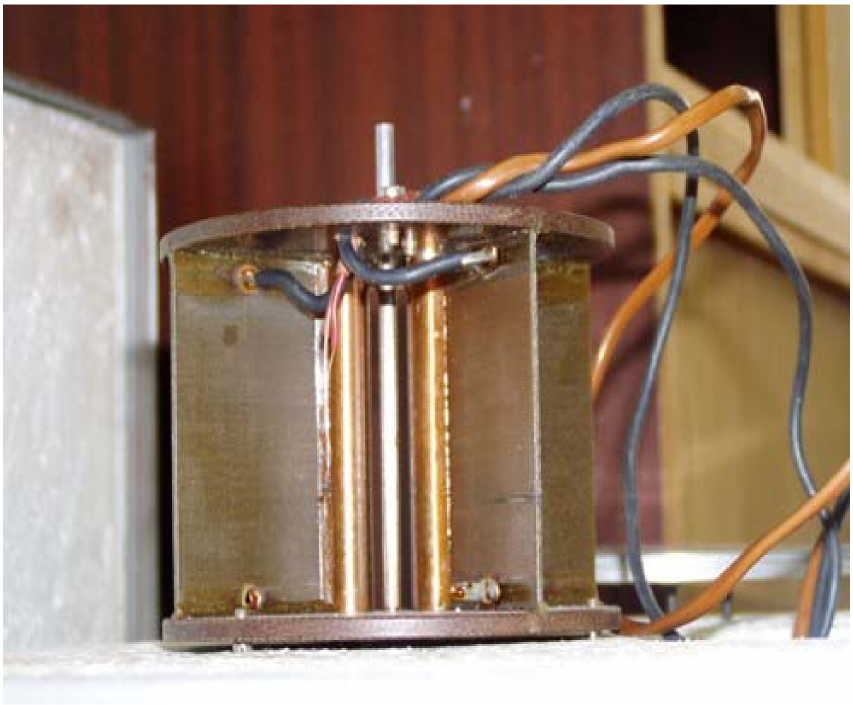

Figure 1 Measuring part of the calorimeter KC01, the „core".

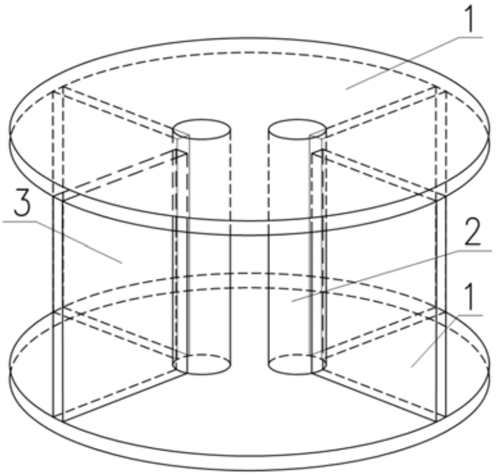

Figure 2 Measuring part of the calorimeter KC01. 1 - upper and lower base (textite), 2 - copper tubes for samples, 3 – the textite (bakelite/paper) rib with wound thermopiles glued to tube.

One edge of the rib with thermocouple junctions is glued to a copper tube, the other one is free. The design of the core of the KC01 calorimeter is drawn on Figure2.We can see two ribs on each of the measuring and reference tubes.We will describe the function of the rib as a sensor of heat flow from the copper tube to the cylindrical coat surrounding the calorimetric core. The surrounding aluminum coat is 6 mm thick and has constant temperature t_w.

The constantan and copper-plated constantan wires on the surface of the rib transfer most of the heat from the source (copper tube, see Figure 1, 2.). The thermal conductivity of the laminate part is so low that it can be neglected. On each 0.5 mm of the rib height there is a loop, with one half constantan (of 0.1 or 0.127 mm diameter) and one half of constantan electroplated with copper. The thickness *d* of the electroplating is not exactly known and we estimate it to be between 0.01 and 0.04 mm. For simplification of the heat transport theory we introduce the equivalent thermal conductivity λ and equivalent thickness *u* of the layer of unit length, conducting the heat on the surface of the rib. The equivalent thickness *u* was calculated using the diameters of the constantan wire *g* and copper-plated constantan with diameter $g_c$wound in two turns per millimeter,

$$u = \frac{\pi}{4}\left[4g^2 + 2\left(g_c^{\ 2} - g^2\right)\right]. \tag{1}$$

The equivalent thermal conductivity λ can be expressed as

$$\lambda = \frac{\pi}{4u}\left[4g^2\lambda_{co} + 2\left(g_c^{\ 2} - g^2\right)\lambda_{Cu}\right] \tag{2}$$

where λ_{Cu} is the thermal conductivity of copper and λ_{co} the thermal conductivity of constantan.

Using the heat balance in every cross-section of the rib of thickness *dx* (Figure 3) we can write

$$q(x) = 2q_1(x) + 2q_2(x) + q(x+dx) \tag{3}$$

$$q(x) = -\lambda ub\frac{dt(x)}{dx} \tag{4}$$

$$q_1(x) = 2\alpha u\left(t(x) - t_w\right)dx \tag{5}$$

$$q_2(x) = 2\alpha b\left(t(x) - t_w\right)dx \tag{6}$$

$$q(x+dx) = -\lambda ub\frac{dt(x+dx)}{dx} \tag{7}$$

where α is the coefficient of heat transfer from the surface of the rib, the other parameters are explained in Figure 3.

After inserting (4)-(7) into (3) and rearranging we obtain the second-order differential equation

$$-\frac{d^2t(x)}{dx^2} + \frac{\alpha}{\lambda}\frac{2(u+b)}{ub}t(x) = \frac{\alpha}{\lambda}\frac{2(u+b)}{ub}t_w \tag{8}$$

A particular solution of equation (8) is

$$t(x) = t_w \tag{9}$$

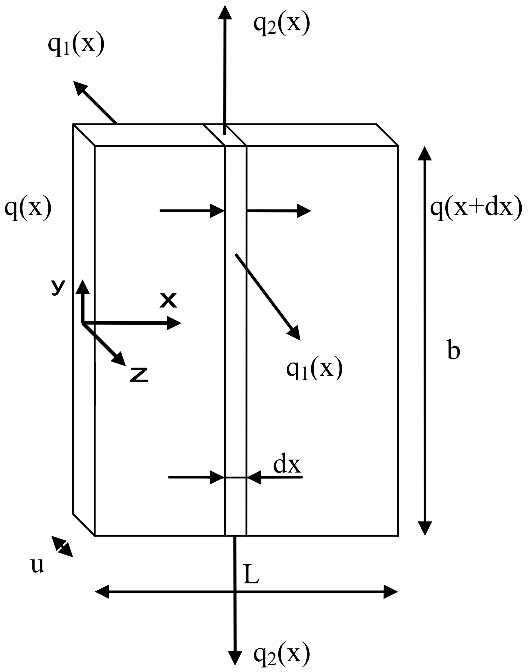

Figure 3: The rib cross section at x and x+dx, with height b, width L and thickness u. Heat flows in direction x are q(x) and q(x+dx), heat flows q1(x) are in direction z and –z, heat flows q2(x) are in direction y and -y.

The complete solution of equation (8) is then the sum of a particular solution and the solution of the homogenous equation (10)

$$-\frac{d^2t}{dx^2}+c^2t=0,\; c^2=\frac{\alpha}{\lambda}\frac{2(u+b)}{ub}, \tag{10}$$

$$t(x)=t_w+A_1e^{cx}+A_2e^{-cx} \tag{11}$$

The boundary conditionscan be expressed as

$$t(0)=t_w+A_1+A_2 \tag{12}$$

$$q(0)=\int_0^L q_1(x)dx+\int_0^L q_2(x)dx+\left[t(L)-t_w\right]\alpha ub \tag{13}$$

For one-dimensional heat flow in solids the following holds:

$$q(0)=-\lambda\left(\frac{dt}{dx}\right)_{x=0}ub \tag{14}$$

Using (12) - (14), we obtain

$$A_1=(t(0)-t_w)\times\frac{(1-\alpha/\lambda c)\exp(-cL)}{\left[(1+\alpha/\lambda c)\exp(cL)+(1-\alpha/\lambda c)\exp(-cL)\right]} \tag{15}$$

$$A_2=(t(0)-t_w)\times\frac{(1+\alpha/\lambda c)\exp(cL)}{\left[(1+\alpha/\lambda c)\exp(cL)+(1-\alpha/\lambda c)\exp(-cL)\right]} \tag{16}$$

As mentioned earlier, one hundred copper/constantan thermocouples on the rib compose the thermopile. Each of its thermocouples produces voltage of e = 40 μV per Kelvin of temperature difference between the junctions. The total voltage U on two thermopiles (see Figs. 1 and 2) conducting the heat from one copper tube can be calculated using the expression (17) from the difference of the thermocouple junction temperatures $t(0)$ - $t(L)$, and the number n of thermocouples in a thermopile for the two ribs:

$$U = 2n\left(t(0) - t(L)\right)e \tag{17}$$

For the heat flow in the thermopile from the copper tube (at x=0) we obtain from (14)and (11)

$$q(0) = \lambda\left(A_2 - A_1\right)cub \tag{18}$$

The heat flow sensitivity of the pair of ribs then simply is

$$f = \frac{q(0)}{U} \tag{19}$$

In other words, f is the theoretically derived value of the calibration constant of the KC01 calorimeter.

3. Results and discussion

Using the theoretical analysis of steady-state heat flow with equivalent thickness u of heat-conducting metallic layer and its equivalent thermal conductivity λ presented in the previous section we can calculate the theoretical sensitivity of the pair of ribs used in KC01 conducting calorimeter as heat flow sensor.

Some parameters could not be measured. The first was the heat transfer coefficient α from the surface of the rib to the surrounding air and to the surface of the aluminum coat. The second quantity known only in the range of 2 to 4 hundredths of millimeter was the thickness d of electroplated copper on the surface of the constantan wire.

The directly measured quantity was the calibration constant of KC01 calorimeter with 0.127 mm wire, 17.8 mW mV^{-1}. The calibration method used was based on Joule heat generated by direct current.

In Table 1 we present the equivalent thickness u and equivalent thermal conductivity λ used in the steady-state heat flow analysis for different values of the thickness d of copper coating on the constantan wire.

Table 1 Equivalent quantities for the steady-state heat flow analysis

Thickness **d** [mm] of copper coatingon the constantan wire	0.01	0.02	0.03	0.04
Equivalent thickness **u** [mm] for constantan 0.1 mm	0.153	0.185	0.224	0.266
Equivalent thickness **u** [mm] for constantan 0.127 mm	0.237	0.277	0.321	0.371
Equivalent thermal conductivity**λ** [Wm^{-1}K^{-1}] for constantan 0.1mm	88.1	140.1	181.2	213.7
Equivalent thermal conductivity **λ** [Wm^{-1}K^{-1}] for constantan 0.127 mm	75.4	119.4	156.1	186.5

Table 2 Calculation of sensitivity f for ribs with constantan wire 0.1 mm

u,λTable 1, ***b*** 0.05 m, ***L*** 0.035 m, ***g*** 0.1 mm								
d	[mm]	**0.01**	**0.02**	**0.03**	**0.04**	**0.01**	**0.04**	**0.04**
c	[m^{-1}]	34.506	24.832	19.913	16.841	38.578	18.829	23.061
α	[Wm^{-2}K^{-1}]	8	8	8	8	10	10	15
x	[m]	t(x)-t$_w$ [K]	t(x)-t$_w$ [K]	t(x)-t$_w$ [K]	t(x)-t$_w$ [K]	t(x)-t$_w$ [K]	t(x)-t$_w$ [K]	t(x)-t$_w$ [K]
0		1	1	1	1	1	1	1
0.005		0.8698	0.9203	0.9447	0.9588	0.8489	0.9498	0.9293
0.01		0.7656	0.8549	0.8989	0.9243	0.7294	0.9080	0.8709
0.015		0.6843	0.8026	0.8619	0.8965	0.6372	0.8743	0.8241
0.02		0.6233	0.7627	0.8335	0.8750	0.5688	0.8484	0.7883
0.025		0.5810	0.7346	0.8133	0.8597	0.5215	0.8299	0.7630
0.03		0.5560	0.7178	0.8012	0.8505	0.4938	0.8189	0.7478
0.035		0.5475	0.7121	0.7971	0.8473	0.4845	0.8151	0.7426
q(0)	[W]	0.0136	0.0159	0.0171	0.0178	0.0159	0.0217	0.0307
U	[μV]	3620	2303	1623	1222	4124	1479	2059
f	[mW/mV]	3.8	6.9	10.5	**14.5**	3.9	**14.6**	**14.9**

Table 3 Calculation of sensitivity f for ribs with constantan wire 0.127 mm

u, λ Table 1, ***b*** 0.05 m, ***L*** 0.035 m, ***g*** 0.127 mm								
d	[mm]	**0.01**	**0.02**	**0.03**	**0.04**	**0.01**	**0.04**	**0.04**
c	[m^{-1}]	29.982	22.0682	17.92478	15.26966	33.52089	17.072	17.90527
α	[Wm^{-2}K^{-1}]	8	8	8	8	10	10	11
x	[m]	t(x)-t$_w$ [K]	t(x)-t$_w$ [K]	t(x)-t$_w$ [K]	t(x)-t$_w$ [K]	t(x)-t$_w$ [K]	t(x)-t$_w$ [K]	t(x)-t$_w$ [K]
0		1	1	1	1	1	1	1
0.005		0.8934	0.9342	0.9539	0.9654	0.8749	0.9577	0.9540
0.01		0.8070	0.8798	0.9155	0.9364	0.7744	0.9224	0.9156
0.015		0.7387	0.8362	0.8845	0.9129	0.6958	0.8938	0.8846
0.02		0.6871	0.8027	0.8605	0.8947	0.6367	0.8717	0.8607

0.025		0.6509	0.7790	0.8435	0.8818	0.5955	0.8560	0.8437
0.03		0.6294	0.7648	0.8333	0.8739	0.5711	0.8466	0.8334
0.035		0.6221	0.7599	0.8297	0.8712	0.5628	0.8433	0.8298
q(0)	[W]	0.0147	0.0166	0.0176	0.0181	0.0173	0.0222	0.0242
U	[μV]	3023.1	1921.0	1362.4	1030.2	3497.2	1254.0	1361.4
f	[mW/mV]	4.9	8.6	12.9	**17.6**	5.0	**17.7**	**17.8**

Tables 2, 3 show the calculations of sensitivity f, performed using equation (11) with different values of the free parameters α and d. In Table 2 we can see in the first four columns that the heat flow$q(0)$ in the rib grows with increasing thickness d of the copper coating on constantan wire. The thermoelectric voltage U decreases. The sensibility f grows to values near to 15 mW mV^{-1}. With the increase of the heat transfer coefficient α from 8 to 15 Wm^{-2}K^{-1}the sensitivity f remains near 15 mW mV^{-1}. For thermoelectric voltage e of the 0.1 mm constantan such values have not been measured. It should be noted, however, that the value of the sensitivity of copper/constantan thermocouple e used for calculation here was only estimated as 40 μV K^{-1} but in the reality it may be lower. The first four columns of Table 3 show that$q(0$ and f grow with increasing thickness d of copper coating, similarly as in Table 2. However, only small influence of varying α is evidenced and the calculated sensitivity of the calorimeter f is very close to the measured calibration constant of 17.76 mW.mV^{-1} for constantan wire 0.127 mm with known sensitivity e = 40 μVK^{-1}.

4. Conclusions

A theoretical analysis of steady-state heat flow in the heat-conducting metallic layer on the surface of the pair of ribs used as heat flow sensor in the KC01 isothermal heat flow calorimeter was presented, which made possible to calculate the theoretical value of calibration constant of the calorimeter and to perform sensitivity analysis of the heat flow sensor to various parameters. Using a comparison of theoretical and experimentally measured calibration constants, the correct values of the unknown parameters were identified.

Acknowledgements

This research has been supported by the Ministry of Education, Youth and Sports of the CzechRepublic, under project No MSM: 6840770031.

References

[1] Calvet, E., Prat, H. *Recent progress in microcalorimetry*. Pergamon Press, Oxford,1963

[2] Kuzel, H.-J., Ein leistungsfähiges Wärmeleitungskalorimeter. *TIZ-Fachberichte*, Vol. **108** No.1, 1984, pp. 46-51

[3] Lemke, T. *TAM Air.An Eight Channel Isothermal Heat Flow Calorimeter.* Edition: C3 Prozess undAnalyzentechnik GmbH Dr Thomas Lemke, Haar beiMünchen, DBR 2007

[4] Evju, C. Initial hydration of cementitious systeme using a simple isothermalcalorimeter and dynamic correction. *J. Therm. Anal. Calorim*.,Vol. **71,** 2003, pp. 829-840

[5] Mtchedlow-Petrssjan, O.P., Sen, A., Uscherow-Marschak, A. Zur Untersuchungder Hydratation von Bindemittels nach der methode der Differential-Mikrokalorimetrie. *Silikattechnik,* Vol. 29, 1969, pp. 229-231

[6] Oliew, G., Wieker, W. Aufbau und Einsatzmöglichkeiten eines Differentialkalorimeters. *Silikattechnik,*Vol. 31, 1981, No.3, pp. 152-154

[7] Tydlitát, V., Tesárek, P., Černý R. Calorimeter for the Measurement of Hydration Heat of Mortars. *Utility model* No. 18347, Industrial Property Office, Prague 2008.

Energy demand for building objects with controlled interior temperature

Stanislav Šťastník[1], Jiří Vala[1], Karel Trojan[2]

[1]Faculty of Civil Engineering, Brno University of Technology, Veveří 95, CZ-602 00 Brno, Czech Republic, email: stastnik.s@fce.vutbr.cz, vala.j@fce.vutbr.cz

[2]MG-RING Ltd., Dykova 21, CZ-636 00 Brno, Czech Republic, email: karel.trojan@volny.cz

Abstract: *Building objects with controlled interior temperature, namely the cooling and freezing plants containing both freezer rooms and offices, are great energy consumers, thus the optimization of their energy demand is needed. The technical standards give some recommendations only for the design of new objects; for the majority of existing and operated objects only the common requirements to the energy audit (under strong physical, geometrical, etc. simplifications, coming from the one-dimensional heat conduction) is available. However, practical experience shows, thanks to high temperature differences between interior temperature and environmental one, the significant influence of additional physical processes, as surface heat radiation and moisture-driven deterioration of insulation layers. This paper presents possible improvements in computational modelling of such objects, with the aim of reduction of energy expenses.*

Keywords: *Building objects with controlled interior temperature, building materials, heat and mass transfer, computational modelling.*

1. Introduction

The world energy consumption is still increasing, regardless all attempts to exploit energy sources in an effective way and to boost energy reduction, even at the international level, as organized namely in the European Union. Design, construction methods and operation of building objects, especially industrial ones, has a substantial and long-lasting environmental impact. The requirements to material inputs from building objects are often excessive, accompanied by high energy consumption, especially for heating, ventilation and air-conditioning. Additional energy consumption must be taken into account for special technologies, as in the case of freezer rooms in cooling and freezing plants.

The needed interior temperature is higher than 0°C in cooling plants (usually between -4°C and +11 °C), lower in freezing plants (typically between –5 °C and –40 °C). The interior temperature is determined by a set of hygienic standards, due to the proposed exploitation, mostly for food storage, as discussed in [3] and [6]; other standards are related e.g. to building and rooms for medical (or other special) exploitation. The basic Czech technical standard for the design of cooling and freezing plants [11] is partially obsolete, incompatible with the standards related to thermal protection and performance of buildings [12] and [13], bringing the requirement of energy audit for existing and operated objects, though under strong physical, geometrical, etc.

simplifications, coming from the one-dimensional heat conduction; for the deeper analysis see [5] and [8]. Although the difference between the temperature values at various building surfaces in summer may be greater than 100 K, no exact energy classes and evaluation criteria are available.

From the constructive point of view, the following requirement must be respected:

- All rooms must be protected against the heat and moisture sources.
- All applied materials must be temperature- and moisture-resistant under operating conditions; moreover, any influence on stored goods (especially in the case of foods) is strictly forbidden.
- The whole interior surface of cooling and freezing rooms must be provided by a complete vapour-tight insulation, joined to pervasive constructions.
- The composition of all insulation layers must satisfy hygienic demands, especially the cleaning and disinfection of the floor must be facilitated.

The evaluation of wall, ceiling and floor constructions should come from [12] where 6 temperature ranges, denoted as A-F, are distinguished, due to operating temperature: A-B for cooling rooms and C-F for freezing ones, together with prescribed values of the minimal thermal resistance. The methodology of so-called energetic labels, used for traditional heated buildings, works with the basic shape parameter A/V where V denotes the total volume of a building and A the sum of relevant surfaces; such approach can be extended to cooling and freezing plants naturally.However, the thermal resistance, introduced as h/λ where h denoted the layer thickness and λ the thermal conductivity, in the case of more layers the sum of such values, gives certain information to the insulation ability, but nothing to the accumulation ability. Clearly two steps of generalization for better computational tools are useful:

- consideration of non-stationary phenomena in heat conduction, including heat transfer properties of all material interfaces,
- including other non-negligible physical processes, as moisture redistribution or radiation fluxes from the environment.

2. Computational approaches

The simplest computational approach, supported by technical standards, is based on the stationary evaluation of above mentioned thermal resistances of all parts of a building. Nevertheless, in this paper we shall work (in general) in the non-stationary formulations, thus we have to introduce also the thermal capacity (related to a mass unit) c, the material density ρ and for simplicity of notation $\kappa = c\rho$, too (in the stationary case, to neglect time derivatives of the temperature, $\kappa = 0$ can be considered formally).

Following the conception of the building as a thermal system by [10], let us assume that thebuilding, namely the whole cooling or freezing plant, occupying (geometrically) certain domain Ω in the 3-dimensional Euclidean space R^3, supplied by the system of Cartesian coordinates $x=(x_1,x_2,x_3)$, is composed from a finite number n of disjoint elements (open sets) Ω_i with $i\in\{1,2,...n\}$, i.e. the closure of the union of all such Ω_i is identical with the closure of Ω in R^3. (The possible reduction to 2- or even 1-dimensional simplified models is obvious and can be left to the reader.) The interfaces between such elements can be introduces as intersections Γ_{ij} of closures of Ω_i and Ω_j with $i\in\{1,2,...n\}$ and $j\in\{i+1,i+2,...n\}$. Defining Ω_0 as the whole space R^3 except the closure of Ω, we are able to extend the introduction of Γ_{ij} to the case $i=0$, too. Moreover, we shall consider the time t from certain time interval $I=[0,t_*]$ with a positive length t_*; the dot symbol will be reserved for partial derivatives with respect to t.

Let us now study the time development an unknown temperature field $T(x,t)$ on all $I\times\Omega_i$ with $i\in\{1,2,...n\}$ and an unknown interface thermal flux field $q(x,t)$ on all non-empty $I\times\Gamma_{ij}$ with $i\in\{1,2,...n\}$ and $j\in\{i+1,i+2,...,n\}$. In particular, let us pay attention to an arbitrary element Ω_i with $i\in\{1,2,...n\}$. The basic equation of heat conduction (if no internal heat sources are present) is then

$$\kappa\dot{T}-\nabla(\lambda\nabla T)=q\ ; \tag{1}$$

the first symbol ∇ (applied to a vector field) means the divergence, the second one (applied to a scalar field) means the gradient. The boundary condition (of the Neumann type) related to certain part of the boundary of Ω_i, namely to Γ_{ij} with $i\in\{0,1,...,n\}$ and $j\in\{i+1,i+2,...,n\}$, is

$$\lambda\nabla T\cdot\nu=\varepsilon q \tag{2}$$

with $\varepsilon=1$ where $\nu=(\nu_1,\nu_2,\nu_3)$ is the local unit normal, whose formal orientation is from Ω_i to Ω_j; similarly (2) holds with $\varepsilon=-1$ on Γ_{ij} with $i\in\{0,1,...,n\}$ and $j\in\{0,1,...,i-1\}$. Taking into account the positive interface heat transfer factor γ (assuming that its value are a priori known for all above discussed interfaces), we can complete (2) and (3) by the additional relations

$$\gamma\varepsilon\delta T=q\ ; \tag{3}$$

Using the standard notation of Lebesgue and Sobolev spaces, let us suppose that both time-independent material characteristics λ and κ belong to the Cartesian product of all spaces $L^\infty(\Omega_i)$ with $i\in\{1,2,...,n\}$, whereas the similar characteristic γ is included in the Cartesian product of all spaces $L^\infty(\Gamma_{ij})$ with $i\in\{0,1,...,n\}$ and $j\in\{i+1,i+2,...,n\}$ (having the same values on Γ_{ij} and Γ_{ji}, empty Γ_{ij} are ignored). We need to know the environmental temperature $T(x,t)$ for all $t \in I$, at least for all points x on the outer boundary of Ω. Assuming that all initial values $T(x,0)$ and $q(x,0)$ are prescribed (with the above specified admissible x), being not in contradiction with (1), (2) and (3) (some stationary initial status is available), we have to find T in the Bochner space

$$V = L^2(I,W^{1,2}(\Omega_1)) \times L^2(I,W^{1,2}(\Omega_2)) \times ... \times L^2(I,W^{1,2}(\Omega_n))$$

and q (thanks to the trace theorem) in the space

$$S = L^2(I \times \Gamma_{01}) \times L^2(I \times \Gamma_{02}) \times ... \times L^2(I \times \Gamma_{n-1n})$$

where only the spaces with non-zero sets in their arguments are considered. The Green-Ostrogradskiĭ theorem converts (1), (2) and (3) for any $i \in \{0,1,...,n\}$ to the more compact form

$$(\varphi,\kappa\dot{T})_i + (\nabla\varphi,\lambda\nabla T)_i = <\varphi,q>_{0i} + <\varphi,q>_{1i} + ... + <\varphi,q>_{i-1i} - <\varphi,q>_{i+1i} - ... - <\varphi,q>_{ni}$$

for any $i \in \{1,2,...,n\}$, (4)

$<\psi,\gamma^{-1}q>_{ij} = <\psi,T_i - T_j>_{ij}$ for any $i \in \{0,1,...,n\}$ and $j \in \{i+1,i+2,...,n\}$;

arbitrary test functions $\varphi \in V$ and $\psi \in S$ occur here and the **indices** of T distinguish the traces from Ω_i and Ω_j (because the continuity of T cannot be guaranteed).

Let us notice the special structure of (4). Introducing the brief notations of particular bilinear forms

$$B_i(\varphi,T) = (\varphi,\kappa\dot{T})_i + (\nabla\varphi,\lambda\nabla T)_i \ ,$$

$$F_{ij}(\varphi,q) = <\varphi_i,q>_{ij} \ ,$$

$$G_{ij}(\psi,T) = <\psi,T_i>_{ij}$$

$$A_{ij}(\psi,q) = <\psi,\gamma^{-1}q>_{ij}$$

(the indices of φ and T for the identification of traces are utilized again), we are able to rewrite (4) as

$$B_i(\varphi,T) - F_{0i}(\varphi,q) - F_{1i}(\varphi,q) - ... - F_{i-1i}(\varphi,q) + F_{i+1i}(\varphi,q) + ... + F_{ni}(\varphi,q) = 0 \ ,$$
$$A_{ij}(\psi,q)_{ij} - G_{ij}(\psi,T) + G_{ji}(\psi,T) = 0 \ .$$

This shows the symmetrical sparse structure of the system of evolution generated by (4), respecting the carefully introduces interface orientations. For illustration, omitting all arguments in forms B, F, G, A with corresponding indices for simplicity, in particular for $m = 3$ (if all contacts of 3 particular elements of a building are non-empty, as well as their contacts with the environment) we receive

$$
\begin{aligned}
&B_1 - F_{10} + F_{12} + F_{13} = 0 \ , \\
&B_2 - F_{20} - F_{21} + F_{23} = 0 \ , \\
&B_3 - F_{30} - F_{31} - F_{32} = 0 \ , \\
&\qquad G_{10} + A_{01} = G_{01} \ , \\
&\qquad G_{20} + A_{02} = G_{02} \ , \\
&\qquad G_{30} + A_{12} = G_{03} \ , \\
&-\ G_{12} + G_{21} + A_{12} = 0 \ , \\
&-\ G_{13} + G_{31} + A_{13} = 0 \ , \\
&-\ G_{23} + G_{32} + A_{23} = 0 \ .
\end{aligned}
$$

All left-hand-side terms here contain some unknown variables, namely T on Ω_1, Ω_2 and Ω_3 and q on Γ_{01}, Γ_{02}, Γ_{03}, Γ_{12}, Γ_{13} and Γ_{23}. The right-hand-side terms are a priori known, thanks to the prescribed development of the environmental temperature.

To handle more complicated configurations, some results from the graph theory are useful. The existence and uniqueness of the solution of (4) can be then verified using the method of discretization in time, based on the properties of Rothe sequences, and the Lax-Milgram theorem. The same approach can be applied to the convergence of sequences of approximate solutions from finite-dimensional subspaces of V and S (as in the finite element, finite volume or finite difference methods).

The technical practice, namely in our case with great temperature differences, forces the analysis of

- the special thermal phenomena in rooms,
- the real influence of moisture in pores of particular layers,
- the contribution of the thermal radiation, especially on the outer surface, being in contact with climatic changes.
- still other effects, as mentioned later.

Such phenomena are seemingly not involved in (4); however, we shall demonstrate that (under rather strong simplifications) they can be included into our model.

The proper analysis of heat transfer in rooms belongs to the rather complicated research area, based on the classical thermodynamic principles of mass, (linear and angular) inertia and energy (or enthalpy). Usually air flow is dominating, thus the models based on pure heat conduction are not acceptable. Since such considerations bring serious complications into the system of evolution, namely the equations of Navier-Stokes type, whose solvability is not transparent, all computational tools, as Chap. 5 in [1] and [4], incorporate some physical and geometrical simplifications to couple the thermal calculations with the approaches of computational fluid dynamics. Fortunately, in freezing and cooling plants the temperature in rooms is strictly prescribed by technical standards, thus their energy audit can be performed using constant values temperature in particular rooms (the prefect air mixing is considered).

The influence of moisture could be also neglected with the reference to corresponding technical standards, but it has been really observed in practice in many cases. Especially the slow (not completely reversible) time development of moisture in porous insulation layers causes the deterioration of their thermal properties, namely the substantial increase of their thermal conductivity. The complete computational model like [2] needs the additional information on the material porous structure and multi-scale considerations; however, to our simulations some observed moisture contents can be inserted to modify all material characteristics, considered as functions of x and T , at least in the most important case of λ .

The influence of thermal radiation is not involved in (4) directly, but following [1], Chap. 6, with respect to [7] it can be inserted, at least at the outer surface, affected by quasi-periodic (day and year) climatic processes, using the additional heat fluxes

$$\tilde{q} = \sigma(T_i^4 - T_0^{\,4}) \tag{5}$$

with $i \in \{1, 2, ...n\}$ where σ denotes the Stefan constant;the modifications of (5) respecting the material emissivity, absorptivity and reflexivity, as well as the radiation view fctors (for generallyinclined surfaces , are available. However, the nonlinearity of (5) brings technical complications into the mathematical existence theory and forces some artificial additional assumptions, not discussed in this paper.

The computational tool should evaluate all potential heat fluxes inside a building, as well as those between a building and its environment. Thus for all incorporated building elements the thermal losses from infiltration and ventilation, the thermal contributions from solar radiations, human activities and various electrical devices are relevant. The energy audit accounts the energy consumption for all installed equipments, namely for heating, freezing, ventilations systems, etc.Regardless the stochastic character of climatic data and above discussed simplifications, the computational simulations could then generate results closer to the reality than the rather trivial stationary calculations.

3. Software implementation and practical example

The software package SIM_Stabil has been developed at the Faculty of Civil Engineering of the Brno University of Technology to handle most non-stationary thermal simulations based on (4) and some its improvements like (5). The complex simulations of buildings with heating, freezing and ventilations systems and a priori defined operation strategies, depending on day or year cycles, is available. Its modular structure, open to various extensions and additional functions,enables to study e.g. parameters connected with the exploitation of passive solar heat or with the location, size and orientation of widows. The output information is consequently able to be applied to the analysis how both the existing old and recently designed buildings could respect the changes in particular requirements of technical standards that are frequently mixtures of technical and political considerations and decisions.

As a typical example of requirement from technical practice, let us study a building with the lowest interior temperature -24 °C; this room is adjacent (through its envelope) to external environment. The contribution to the thermal behaviour from solar radiation is non-negligible. All computations have been done for 1 climatic year with 365 days; their outputs are the values of the year energy consumption.

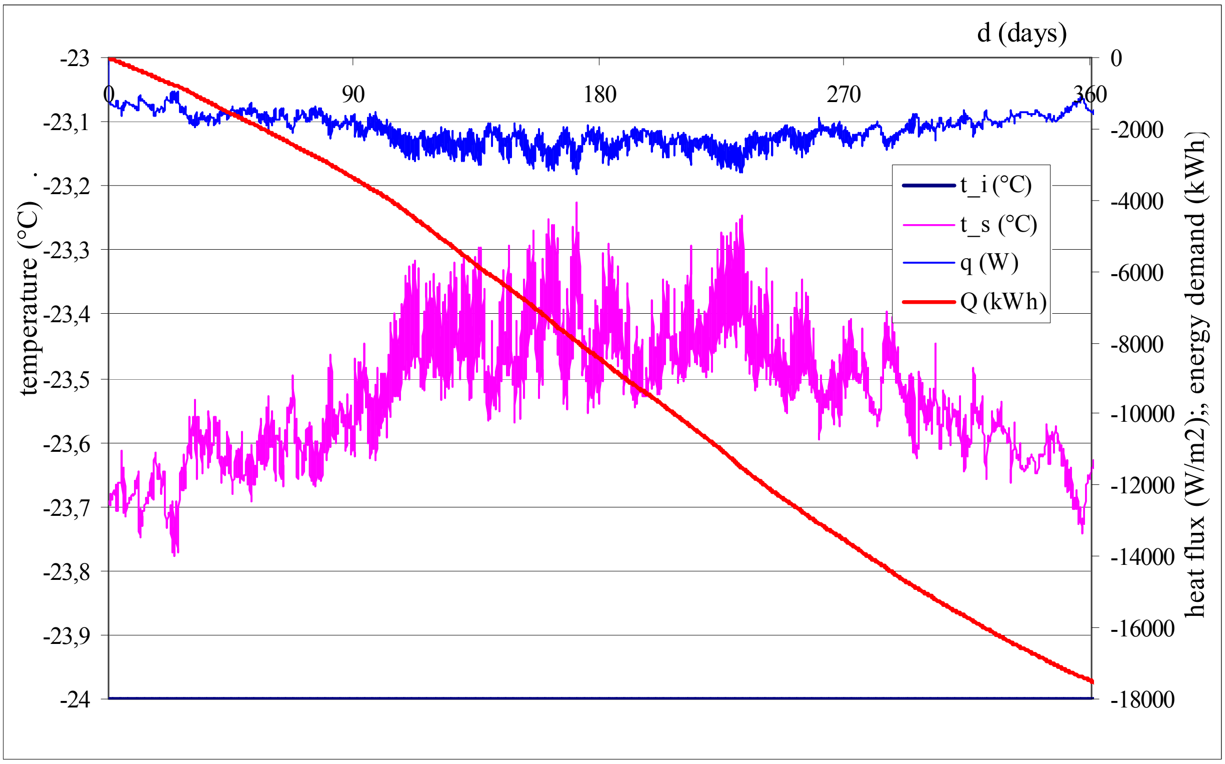

Figure 1: Results of numerical simulations for a simple freezing plant

Figure 1 demonstrates the time development of the selected values of some quantities, coming from the SIM_Stabil-based simulations. Here t_i refers to the temperature of air in the freezer room, t_s to the mean value of the temperature of all interior surfaces, q (unlike the notation in the preceding section) the thermal wattage needed for the conservation of the interior temperature and Q the energy consumption, zero at the year begin.

4. Conclusions

The traditional stationary computational approach to the evaluation of energy demand of building objects gives not very reasonable results. The non-stationary approach, suggested in this paper, involving (under a set of simplifications) the activity of selected additional physical processes, whose consequences have been observed in practice, seems to remove most errors of the previous approach. The original software package SIM_Stabil has been prepared to support such simulations.

The computational simulations for 3 types of building objects have been performed – those with the shape parameters $A/V = 0.73$ for a freezing plant with the size 10 x 10 x 6 m (which is comparable with the common size of a family house), those with $A/V = 0.40$ and those with $A/V = 0.12$ (which corresponds to the size of a real industrial plant). The detailed extensive results should be published in the Ph.D. thesis of the 3rd author; the conversion of the selection of most important results to recommendations to the design of cooling and freezing plants and their energy audits is in progress.

Acknowledgements

This research is supported by the by the project of specific research of the Brno University of Technology, Reg. No. FAST-S-11-47, by the Ministry of Education, Youth and Sports of Czech Republic, Reg. No. MSM 0021630511, and by the OP Education for Competitiveness, Reg.No. CZ.1.07/2.2.00/07.0410.

References

[1] DAVIES, M.G.*Building Heat Transfer*. John Wiley & Sons, Hoboken, 2004. ISBN 0-470-84731-2.

[2] DEFRAYE, T.; BLOCKEN, B.; CARMELIET, J. Computational modelling of convective heat and moisture transfer at exterior building surfaces.In *7th International Conference on Urban Climate* in Yokohama(Japan), 2009, 4 p.

[3] DELGADO, A. E., SUN, D.-W. Heat and mass transfer models for predicting freezing processes – a review. In *Journal of Food Engineering* 47 (2001), p. 157-174.

[4] FENGZHI, L.; YI, L., YINGXI, L.; ZHONGXUAN, L. Numerical simulation of coupled and mass transfer in hygroscopic porous materials considering the influence of atmospheric pressure. In *Numerical Heat Transfer (Part B)* 45 (2004), p. 249-262.

[5] KRARTI, M. *Energy Audit of Building Systems – An Engineering Approach*. CRC Press, New York, 2000.

[6] PHAM, Q. T.; Modelling of freezing processes. In *Frozen Food Science and Technology* (EVANS, J.; ed.), Blackwell, Oxford, 2008, p. 51-80.

[7] SAFARIPOUR, M. H.; MEHRABIAN, M. A. Predicting the direct, diffuse and global solar radiation on a horizontal surface and comparing with real data.In *Heat and Mass Transfer* 49 (2011), in print, 15 p.

[8] SHAPIRO, I. Energy audit in large commercial office buildings.In *ASHRAE Journal* 51 (2009), p. 19-27.

[9] SIWIŃSKA, A.; GRABALIŃSKA, H. Thermal conductivity coefficient of cement-based mortars as air relative humidity function. In *Heat and Mass Transfer* 49 (2011), p. 1077-1087.

[10] VALA, J. ;ŠŤASTNÍK, S.On the thermal stability in dwelling structures. In *Building Research Journal* 52 (2004), p. 31-55.

[11] ČSN 14 8102 *Thermal insulation of cooling and freezing plants*.ČNI,Prague, 1993.

[12] ČSN 73 0540-2*Thermal protection of buildings – Part 2: Requirements*. ČNI, Prague, 2007.EN ISO 13789 *Thermal performance of buildings –Transmission and ventilation heat transfer coefficients - Calculation method*.ČNI, Prague, 2007.

Thermal Properties of Self-compacting Concrete

Tereza Kulovaná, Eva Vejmelková, Robert Černý

Department of Materials Engineering and Chemistry, Faculty of Civil Engineering, Czech Technical University in Prague, Thákurova 7, 166 29 Prague 6, Czech Republic

Abstract: *Effect of high temperatures on the properties of self-compacting concrete containing blast furnace slag as partial replacement of Portland cement is studied. Open porosity, bulk density, matrix density, thermal conductivity,and specific heat capacity are the investigated parameters. Experimental results show that the analyzed material resists well to elevated temperatures up to 600°C.*

Keywords: *self compacting concrete, basic physical parameters, thermal properties*

1. Introduction

Concrete belongs to the materials which are often used in harsh environments. It can be exposed for instance to high temperatures, high mechanical loads or salt attack. In such conditions, even concretes with superior mechanical properties in normal conditions can be significantly damaged and their further use after surviving the effect of such environments is not clear.

Portland or blended cement as traditional binder in concrete is the most universal binder to date, although it has a number of disadvantages, such as high energetic demand for its production, low resistance against aggressive substances and instability at high temperatures. At the end of 20th century there appeared a trend of low-energy binders based on the utilization of secondary raw materials. Development in self-compacting concrete(SCC) technology was possible due to the development of new generation of superplasticizers. Now the investigation mainly concentrated on the description of different microfillers influence on the properties of fresh mixture and hardened SCC in normal laboratory conditions. In this respect, slag is one of the possibilities how to expand the range of concrete and mortars by other materials that meet the requirements to binders and in many aspects have better properties than classical Portland cement especially at high temperature conditions.

In this paper, effect of high temperatures on basic physical and thermal properties of SCC containing ground granulated blast furnace slag is studied. Determination of these properties will make possible a more effective application of the material, which issupposed to be able to resist to high temperatures, in the practice.

2. Materials

To elaborate the self compacting concrete mixture composition, the design principles established by Okamura and Ozawa [1]have been applied. Blastfurnace cement CEM III/A 42.5N HSR/NA, containing ca. 57% blast furnace slag with a specific surface area 460

m^2/kg (Blaine) was used. Thechemical composition of the cement is presented in Table 1. The composition of concrete mixtures is given in Table 2.Basalt crushed aggregate of continuous grading was applied, characterized by density of 2820 kg/m^3. The maximum grain size was 8 mm. The volume ratio of coarse aggregate to sand was assumed 2/3.

Table 1: Chemical composition of cement

Component	% by mass
SiO_2	29.9
Fe_2O_3	2.2
Al_2O_3	6.3
CaO	54.3
MgO	3.8
SO_3	2.6
NaO	0.3
K_2O	0.6

Table 2. Composition of the studied SCC

Component	Unit	Amount
Cement CEM III 42.5N HSR/NA	kg m^{-3}	589
Superplasticizer	% by mass	1.7
Aggregates0/2 mm	kg m^{-3}	998
Aggregates2/8 mm	kg m^{-3}	670
Water	kg m^{-3}	154

The specimens were heated to 600°C (denoted as SCC-600) and to 1000°C (denoted as SCC-1000) with the heating rate of 10 °C/min, then left at the final temperature for two hours and finally slowly cooled. After completing the loading procedure, their basic physical and thermal properties were measured and compared with the data obtained for reference specimens (denoted as SCC-ref), which did not undergo any thermal load.

3. Experimental methods

Among the basic properties, the bulk density ρ[kgm^{-3}], matrix density ρ_{mat}[kg m^{-3}] and open porosity ψ_0 [%] were measured by the water vacuum saturation method [2]. Each sample was dried in a drier to remove majority of the physically bound water. After that the samples were placed into a desiccator with deaired water. During three hours air was evacuated with vacuum pump (Figure 1) from the desiccator. The specimen was then kept under water not less than 24 hours. From the mass of water saturated sample m_w [kg] and mass of the immersed water saturated sample m_a [kg], the volume V of the sample was determined from the equation

$$V = \frac{m_w - m_a}{\rho_l} \tag{1}$$

where ρ_l is the density of water.The basic physical parameters were calculated according to the equations

$$\psi_0 = \frac{m_w - m_d}{V\rho_l} \tag{2}$$

$$\rho = \frac{m_d}{V} \tag{3}$$

$$\rho_{mat} = \frac{m_w}{V(1-\Psi_0)} \tag{4}$$

where$m_d$is the mass of the dry sample [kg].

The samples for determination of basic properties were cut from the standard prisms; their size was 40 x 40 x 20 mm.

Figure 1. Vacuum pump with desiccator

The thermal conductivity λ ($W \cdot m^{-1} K^{-1}$) as the main parameter of heat transport and the specific heat capacity c ($J\ kg^{-1}\ K^{-1}$) as the main parameter of heat storage were measured using the commercial device ISOMET 2104 (Applied Precision, Ltd.). ISOMET 2104 (Figure 2) is equipped with various types of optional probes, needle probes are for porous, fibrous or soft materials, and surface probes are suitable for hard materials. The measurement is based on the analysis of the temperature response of the analyzed material to heat flow impulses. The heat flow is induced by electrical heating using a resistor heater having a direct thermal contact with the surface of the sample. The measurements in this paper were done in dependence on moisture content. The samples for determination of thermal properties had a size of 70 x 70 x 70 mm.

Figure 2. ISOMET 2104

4. Experimental results and discussion

Table 3 shows basic parameters of the studied material SCC. The matrix density increased with the thermal load due to dehydration of initially hydrated phases which is accompanied with densifying of structure. On the other hand, the decrease of bulk density is in agreement with increase of porosity. The most important change in porosity occurred between the loading temperature of 600°C state and the loading temperature of 1000°C where the increase of porosity was as high as 65 %. The porosity changes between unloaded state and the loading temperature of 600°C were lower than 10 %.

In the degradation of cementitious materials containing Portland cement due to thermal load the decomposition of $Ca(OH)_2$ which is taking place at about 480 °C is the most important factor [3]. The studied samples were prepared using cement containing slag which is thermally more stable and its degradation is supposed to take place at higher temperatures. This was confirmed by the measurements of basic physical parameters in this paper.

Table 3: Basic physical properties

	ρ [kg m^{-3}]	ρ_{mat} [kgm^{-3}]	Ψ [-]
SCC-ref	2484	2814	11.7
SCC-600	2470	2820	12.4
SCC-1000	2366	2976	20.5

Tables 4 and 5 show a remarkable increase of thermal conductivity of studied SCC with increasing moisture content for all thermal-loading states. Its values in water saturated state were up to two times higher than values in dry state. The highest thermal conductivity in dry state achievedthe reference materialSCC-ref whilethe lowest was obtained for the material SCC-1000 loaded to 1000°C. This corresponds with the porosity in Table 3.The values of specific heat capacity significantly increased with increasing moisture, as a consequence of the added water with high specific heat capacity. In all thermal-loading states the analyzed SCC achieved similar values of specific heat capacity in dry state. The differences were only up to 5%.

Table 4. Thermal properties in dry state

	λ [$Wm^{-1}K^{-1}$]	χ [$J\ kg^{-1}\ K^{-1}$]
SCC-ref	1.433	680
SCC-600	1.223	681
SCC-1000	1.003	656

Table 5. Thermal properties in water saturated state

	u [$kgkg^{-1}$]	λ [$Wm^{-1}K^{-1}$]	c [$Jkg^{-1}K^{-1}$]
SCC-ref	0.0369	1.933	804
SCC-600	0.0692	1.953	907
SCC-1000	0.0721	2.047	892

5. Conclusions

The results of measurement of basic physical and the thermal properties of SCC produced with cement containing blast furnace slag in this paper showed that the effect of slag was positive in a long term view. The main results can be summarized as follows. The most substantial changes in pore volume were observed between 600°C and 1000°C, where the porosity increase was about 65%. The highest value of thermal conductivity in dry state achievedthe reference material SCC-ref, which was not exposed tothermal load, while the lowest value was observed for thematerial SCC-1000 loaded to 1000°C. Based on the obtained results it can be concluded that the main benefit of using cement containing slag is the increase of concrete thermal stability in comparison with ordinary Portland cement.

Acknowledgements

This research has been supported by the Ministry of Education, Youth and Sports of the Czech Republic, under project No. MEB 051028 and SGS10/232/OHK1/3T/11.

References

[1] Ozawa K., Kunishima M., Maekawa K., Development of high performance concrete based on the durability design of concrete structures. Proceedings of the second East-Asia and Pacific Conference on Structural Engineering and Construction (EASEC-2), Vol. 1, 1989, p. 445-450.

[2] Roels, S., Carmeliet, J., Hens, H., Adan, O., Brocken, H., Černý, R., Pavlík, Z., Hall, C.,Kumaran, K., Pel, L,, Plagge, R., Interlaboratory Comparison of Hygric Properties of PorousBuilding Materials. Journal of Thermal Envelope and Building Science, Vol. 27, 2004,p. 307-325.

[3] Černý R, Rovnaníková P., 2002. Transport Processes in Concrete. Spon Press, London.

Using of multi-parametric non-linear regression method based on step wise measurements for determining of thermal parameters of phase change materials

Oldrich Zmeskal, Lenka Dohnalova, Pavla Stefkova

Faculty of Chemistry, Brno University of Technology, Purkynova 118, CZ-612 00 Brno, Czech Republic, email: zmeskal@fch.vutbr.cz

Abstract: *The contribution deals with a study on the properties of a system consisting of laminated solar cells on PCM (phase change material) backsheet board. The aim of this study is to evaluate an ability of PCM board to decrease a working temperature of solar cells and related increase of its efficiency. Crystalline silicon solar cells were used in this study. The laboratory measurement was performed during a heating process caused by external voltage source applied to the solar cell. The diameter of PCM samples with square solar cells (25 × 25 mm) was 30 mm. The measurement was realized in a temperature interval of 20 – 40 °C. Cooling was performed by Micronal® PCM (BASF) with the phase change temperature of 25°C.*

Keywords: *PCM, specific heat, solar cells, thermal fractal systems, thermal conductivity, thermal diffusivity*

1. Theory

The fractal theory of the thermo-physical properties description is derived, in general, from the field theory. It can describe the dependence of a temperature change on the heat supplied to material. The trend of this change can be expressed by the parameter K (so called fractal measure) and the parameter D (so called fractal dimension). The fractal dimension can describe the average change of temperature in the whole material (it has a global character). The results for the special cases (point, linear and planar heat source – Dirac pulse) and a homogeneous infinite material were derived from a system of differential equations [1 – 3]. The fractal dimension expresses the character (dimension) of the heat source (D = 1, 2, 3) for the ideal experiment, see Fig. 1.

But the fractal dimension gives generally the information about the properties of a real heat source (immediately after heating) and about the heat drain from the material to the surroundings. The fractal dimension will be upper for a planar heat source and cylindrical sample ($D > 2$) or less ($D < 2$) then for an ideal heat source.

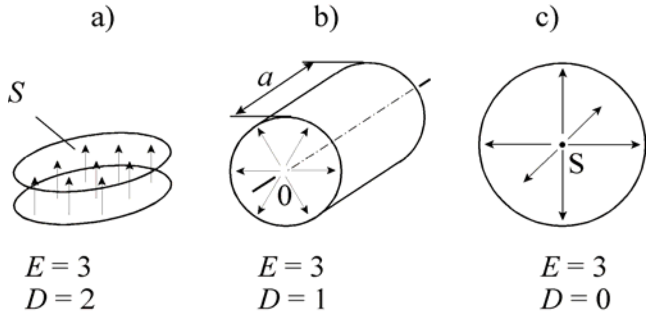

Figure 1: Heat flow geometry for (a) plane-parallel, (b) cylindrical, and (c) spherical coordinate Euclidean

2.1. General fractal model of heat transport

The model will be derived from the fractal theory of physical field published by authors in [4]. The dependence of temperature ΔT on radius r of space-time for the thermal field [5] can be written for this model as

$$\Delta T(r) = -\frac{\hbar c}{k_{\mathrm{B}}} \frac{K\, r^{D-E+2}}{D(D-E+2)}, \tag{a}$$

where $\hbar$ is modified Planck constant, c is speed of heat propagation, k_{B} is Boltzmann constant, and E, D, K are Euclidean and fractal dimension and fractal measure, respectively.

If a size of space-time vector is rewritten as $r^2 = r_T^2 - c^2(t-t_0)^2 = r_T^2 - c^2t^2 + 4a_0t - c^2t_0^2$, where r_{T} is radius of topological space, t_0 is the time response delay, $a_0 = c^2t_0/2$ is maximal value of thermal diffusivity (for $E = D$) can be equation (1) rewritten to

$$\Delta T_r(t) = -\frac{K\hbar c}{k_{\mathrm{B}}} \frac{(4a_0t)^{(D-E+2)/2}}{D(D-E-2)} \left(-\frac{c^2t_0^2 - r_T^2}{4a_0t} - \frac{c^2t}{4a_0} + 1 \right)^{(D-E+2)/2}. \tag{b}$$

When $h^2 = c^2t_0^2 - r_{\mathrm{T}}^2$ is square of corrected sample size and the terms in parenthesis represent main part of exponential function ($1 - x \approx \mathrm{e}^{-x}$) we can write

$$\Delta T_r(t) = -\frac{K\hbar c}{k_{\mathrm{B}}} \frac{(4a_0t)^{(D-E+2)/2}}{D(E-D-2)} \exp\left[-\frac{D-E+2}{2} \left(\frac{h^2}{4a_0t} + \frac{c^2t}{4a_0} \right) \right]. \tag{c}$$

When the thermal diffusivity is written as $a = 2a_0/(D-E+2)$, and heat losses parameter as $R = 4a/c$ we can then write

$$\Delta T_r(t) = \frac{K\hbar c}{2\pi k_{\mathrm{B}}} \frac{1}{D} \left(\frac{D-E+2}{2\pi} \right)^{(D-E)/2} (4\pi at)^{(D-E+2)/2} \exp\left[-\left(\frac{h^2}{4at} + \frac{4at}{R^2} \right) \right]. \tag{d}$$

And finally, if we define the heat source quality parameter as $s = (E-D)/2 = (a-a_0)/a$ and the power of heat source in relation to thermal conductivity of real sample (characterized by fractal dimension D) as

$$\frac{P}{2\lambda} = \frac{K\hbar c}{k_{\mathrm{B}}} \frac{1}{D} \left(\frac{D-E+2}{2\pi} \right)^{(D-E)/2}. \tag{e}$$

we can finally write for dependence of change of temperature on time by equation

$$\Delta T(t) = \frac{P(4\pi at)^{1-s}}{2\pi\lambda} \exp\left[-\left(\frac{h^2}{4at} + \frac{4at}{R^2} \right) \right], \tag{f}$$

The thermal conductivity of real material can be written as $\lambda = c_{\mathrm{p}}\rho a$, where ρ is its mass density and c_{P} is specific heat.

2.2. *Multi-parametric non-linear regression method for evaluation of transient measurement*

The described method can be used for the determination of the real fractal model parameters (f) using regression method applied to equation

$$y(t) = \ln \Delta T(t) = \ln\left(\frac{P(4\pi a)^{1-s}}{2\pi\lambda}\right) + (1-s)\ln t - \frac{h^2}{4at} - \frac{4at}{R^2} = a_0 + a_1 x_1 + a_2 x_2 + a_3 x_3 \quad \text{(g)}$$

,

where $x_1 = \ln t$, $x_2 = 1/t$ and $x_3 = t$. From the parameters a_0, a_1, a_2 and a_3 respectively can be calculated thermophysical and other parameters of measured system: the heat source quality parameter $s = (E-D)/2 = 1 - a_0$ (or fractal dimension D of heat source in 3D space, $E = 3$), the heat losses parameter proportional to measured sample diameter $R = h/\sqrt{a_2 a_3}$, thermal diffusivity $a = -h^2/4a_2$, and thermal conductivity $\lambda = (P/2\pi)\cdot(-\pi h^2/a_2)^{a_1}\cdot \mathrm{e}^{-a_0}$. From the last two parameters finally for the known mass density ρ the specific heat $c_\mathrm{p} = \lambda/\rho a$.

2. Experimental

2.1. *Thermal measurement of PMMA*

The measured sample of PMMA was disc-shaped with a radius $R = 15$ mm and thickness $h = 6$ mm. Its density was $\rho = 1184$ kg·m^{-3}, the table thermal diffusivity $a = 1.12\times10^{-7}$ m^2·s^{-1}, the table specific heat $c_\mathrm{P} = 1450$ J·kg^{-1}·K^{-1}, and the table thermal conductivity of the sample was $\lambda = 0.193$ W·m^{-1}·K^{-1}.

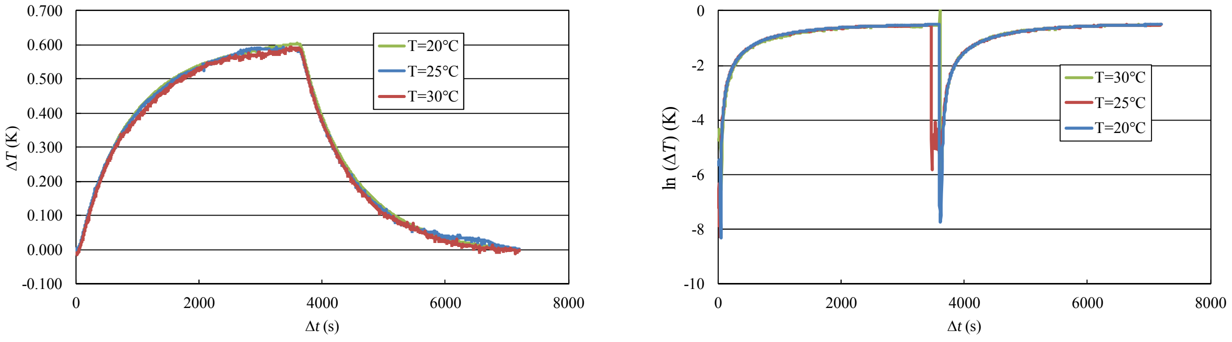

Figure 2: Transient response of temperature after a step-wise heating $\Delta T = f(\Delta t)$ (left graph) and its logarithm $y(\Delta t, \Delta T)$, see to Eq. (7) for the determination of heat system parameters of PMMA.

The dependences for step wise measurement on PMMA (1 hour heating and 1 hour cooling) for the three different temperatures are presented at the Figure 2 (left). It is evident that the dependences are similar the same. The logarithmic dependences of these responses what were used for the calculation of thermal parameters (7) are presented at the Figure 2 (right). From these dependences were calculated with using of multi-parametric nonlinear regression the thermal diffusivity, thermal conductivity, specific heat, heat source quality parameters and heat losses parameters (see Table 1).

Table 1 Thermal parameters calculated from measured characteristics of PMMA
(h = 0.006 m, ρ = 1184 kg.m^{-3})

PMMA	D (-)	P (W)	T_0 (°C)	$a\times10^7$ (m^2.s^{-1})	R (m)	λ (W.m^{-1}.K^{-1})	c_p (J.kg^{-1}.K^{-1})
20 °C	2.145	0.041	19.87	0.626	0.041	0.276	3779
25 °C	2.195	0.041	24.90	0.693	0.035	0.247	3129
30 °C	2.160	0.040	29.63	0.632	0.037	0.261	3560
average values	2.167	0.041	---	0.650	0.038	0.261	3489
tabulated values	2.000	---	---	1.120	0.015	0.193	1450

2.1. Thermal measurement of PCM

The measured sample of PCM (Micronal® in drywall) was disc-shaped with a diameter R = 15 mm and thickness h = 14 mm. Its density was ρ = 693 kg m^{-3}, the thermal diffusivity a = 1.28×10^{-7} m^{2}s^{-1}, the thermal conductivity was ρ = 0.176 W m^{-1}K^{-1}, the specific heat c_p = 1983 J kg^{-1}K^{-1}, and heat losses parameter R = 44 mm and heat source quality parameter s = 0.86 (D = 2.73). For the temperature near the phase change temperature (T = 25°C) are these parameters diametrically different: the thermal diffusivity a = 1.20×10^{-6} m^2/s and heat losses parameter R = 129 mm and heat source quality parameter s = 1.55 (D = 4.11).

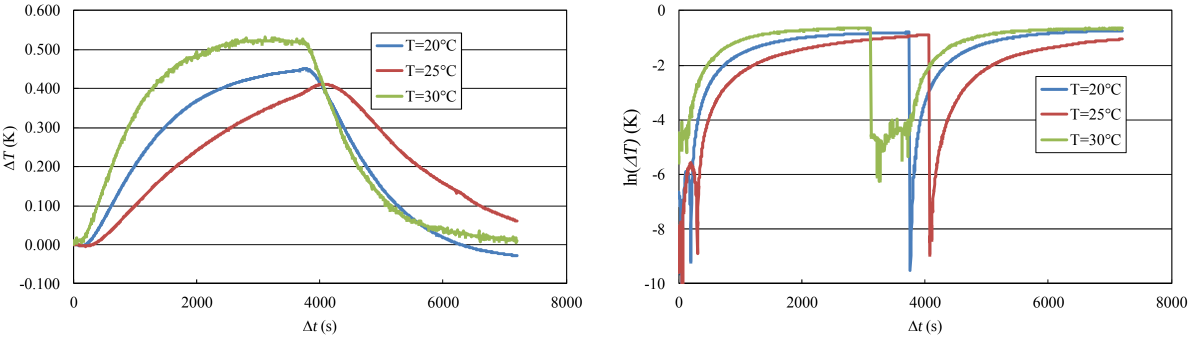

Figure 3: Transient response of temperature after a step-wise heating $\Delta T = f(\Delta t)$ (left graph) and its logarithmus $y(\Delta t, \Delta T)$, see to Eq. (7) for the determination of heat system parameters of PCM.

The dependences for step wise measurement on PCM (1 hour heating and 1 hour cooling) for the three different temperatures are presented at the Figure 3 (left). There are evident differences between the dependences. These differences are caused by different thermal parameters in solid (bellow 25 °C) and liquid phase (under 25 °C). The logarithmic dependences of these responses what were used for the calculation of thermal parameters (7) are presented at the Figure 3 (right). From these dependences were calculated with using of multi-parametric non-linear regression the thermal diffusivity, thermal conductivity, specific heat, heat source quality parameters and heat losses parameters (see Table 2). These parameters are different for liquid and solid phase. Near the phase change temperature the parameters can not be calculated due to chemical processes what are occurs in the material.

Table 2 Thermal parameters calculated from measured characteristics of PCM
($h = 0.014$ m, $\rho = 693$ kg.m^{-3})

PCM	D (-)	P (W)	T_0 (°C)	$a\times10^7$ (m^2.s^{-1})	R (m)	λ (W.m^{-1}.K^{-1})	c_p (J.kg^{-1}.K^{-1})
20 °C	2.431	0.067	20.01	0.683	0.051	0.172	3633
25 °C	5.426	0.051	24.83	-2.110	0.155	0.012	-82
30 °C	1.800	0.067	29.30	0.761	0.032	0.453	8589
tabulated values (wax) $\rho = 980$ kg.m^{-3}	---			1.530	---	0.180	1200
tabulated values (gypsum) $\rho = 2300$ kg.m^{-3}	---			0.970	---	0.190	850

3. Conclusion

In this article, the method of transient responses analysis of different kind of dependences is described. This method was applied to thermal responses after step-wise initiations (supply of heat). The functionality of proposed method was confirmed by the agreement of tabulated and measured results for PMMA [5 – 8]. In addition, the method can be used for getting other parameters such as losses, the phase change reason parameters and for determining of properties near the phase change temperature of PCM (Micronal®).

Acknowledgements

This work was supported by the project "Centre for Materials Research at FCH BUT" No. CZ.1.05/2.1.00/01.0012 from ERDF and by grant FR-TI1/144 from the Ministry of Industry and Trade of the Czech Republic

References

[1] CARSLAW, H. S., JAEGER, J. C. *Conduction of Heat in Solids*. Clarendon Press London, 1959.

[2] KUBICAR, L. *Pulse method of measuring basic thermophysical parameters*. Elsevier, Amsterdam, Tokyo, Oxford, New York. 1990.

[3] BOHAC, V., DIESKA, P., KUBICAR, L. 2007 The Heat Loss Effect at the Measurements by Transient Pulse Method. in *Measurement Science Review*. 7: p. 24-27

[4] ZMESKAL, O., BUCHNICEK, M., VALA, M. Thermal properties of bodies in fractal and Cantorian physics. *Chaos, Solitons & Fractals*. 2005. 25(5): p. 941-954. ISSN 0960-0779.

[5] ZMESKAL, O., VALA, M., WEITER, M., STEFKOVA, P. Fractal-Cantorian geometry of space-time. *Chaos, Solitons & Fractals*. 2009. 42(3): p. 1878-1892. ISSN 0960-0779.

[6] ZMESKAL O., HREBENOVA, L., STEFKOVA, P. A New Differential Method for the Evaluation of Step Wise and Pulse Transient Measurements, in 9th *Asian Thermophysical Properties Conference*. Beijing, China, China National Convention Center. 2010. p. 19 - 22.

[7] ZMESKAL, O., STEFKOVA, P., HREBENOVÁ, L., BARINKA R. Pulse Transient Method as a Tool for the Study of Thermal Properties of Solar Cell Laminating Films. *International Journal of Thermophysics*. 2009. 30(6): p. 1891-1901. ISSN 0195-928X

[8] ZMESKAL, O., HREBENOVA L., STEFKOVA P. Determination of Thermal and Moisture Parameters from the Transient Responses, in *Thermophysics 2010*, O. Zmeskal, ed. Valtice Chateau, Czech Republic, 2010. p. 338 - 344 (2010), ISBN-978-80-214-4166-8

Monitoring of temperature-moisture regime of rock massive at SpisCastle

Ľudovít Kubičár[1], Danica Fidriková[1], Viliam Vretenár[1], Ján Vlčko[2], Vladimír Greif[2], Martin Brček[2], Ivana Šimková[2]

[1]Institute of Physics SAS, Dubravska cesta 9, 845 11 Bratislava, Slovakia, kubicar@savba.sk,

[2]ComeniusUniversity, Faculty of Natural Science, Department of Geological Engineering, Ilkovičová 3, 81219 Bratislava, Slovakia

Abstract: *Deterioration of rock massive is strongly influenced by moisture that in combination with temperature, salt and various biofactors, have high correlation with geographical location, microclimate and with the local hydrological conditions. Innovative hot ball sensor for measuring thermal conductivity in connection with the RTM instrument is used for monitoring of local temperature and thermal conductivity. As thermal conductivity of porous structure is a function of the pores distribution and its content, this system can be used for monitoring of the water content in rock massive. This paper presents results obtained by monitoring of the temperature-moisture regime of the rock massive at the SpisCastle in the period of September 2008 to June 2011. Hot-ball sensors were inserted into different depth of the rock massive. Data on temperature and moisture variation were recorded that correspond to annual and diurnal cycles. Meteorological data are correlated to the measured results.*

Keywords: *monitoring of moisture, hot-ball method, thermophysical sensor, rock massive*

1. Introduction

Deterioration of rock massive is strongly influenced by moisture that in combination with temperature, salts and various biofactors, have high correlation with geographical location, microclimate and with the local hydrological conditions. Fissures, cracks and pores can be accessible for water depending on transport path in rock massive. Porous structure of the rocks, water and gas transport and freezing and thawing effects in pores influence the structural stability of the rocks. In long-term process changes in rocks can be found concerning mineralogical and petrographical composition as well as physical-technical properties. Therefore information regarding moisture-thermal regime of the rocks represent a basic assumption to understand the rock deterioration processes.

Innovative transient methods have been used for measuring specific heat, thermal diffusivity and thermal conductivity. Moisture effects, drying, freezing and thawing processes were studied for water saturated rock specimens. Recently water transport in sandstone has been studied [1]. Degradation was studied by measuring specific heat, thermal diffusivity and thermal conductivity of the water saturated specimen due to freeze/thaw cycle. All above mentioned experiments were performed in laboratory. The experiments have shown that thermal conductivity changes reflect the listed processes.

Improvements in methodology of the transient methods and the application of latest electronic elements make possible the construction of monitoring systems which significantly simplify its operation. Recently a hot ball sensor for measuring local thermal conductivity in connection with the RTM monitoring system has been presented [2].

This paper presents results obtained by monitoring of the temperature-moisture regime of the rock massive at the Spis Castle in the period from September 2008 to June 2011. Hot-ball sensors were inserted into different depths of the rock massive. Data on temperature and moisture variation were recorded that correspond to annual and diurnal cycles within period from September 2008 to June 2011. Results are correlated with the meteorological data.

2. Characteristics of the rock massive and sensor body

The bedrock upon which Spis Castle stands is built of a travertine mound that is underlain by Palaeogene soft rocks formed by claystone and sandstone strata (flysch-like formation). The travertine body reaches more than 52 metres (Figure 1a) in thickness. The travertines are white to yellow in color, micro- to macroporous with fluidal structure, slightly weathered along the joints, strongly karstified. Joints, cracks and pores are accessible for percolating water depending on natural transport path within travertine rock body [3]. Figure 1a shows rock massive on which the Spis Castle is situated. Holes in diameter of 25 mm to different depths were drilled into the rock massive. Body of moisture sensor was constructed from the core drill (i.e. from the same material like rock mass) with cylindrical shape and length of 40 mm. A hole in diameter of 2 mm was bored into the axis of the body cylinder. Thermal conductivity sensor in a form of a ball in diameter up to 2 mm was fixed in the centre of the moisture sensor. Figure 1b shows moisture sensor in which the thermal conductivity sensor is fixed together with a view on the bored hole into the rock massive. Figure 1c shows body of the moisture sensor covered by sealing material that made contact for heat and moisture transport. Figure 1d shows overall arrangement of the sensors on the rock wall of the travertine rock body.

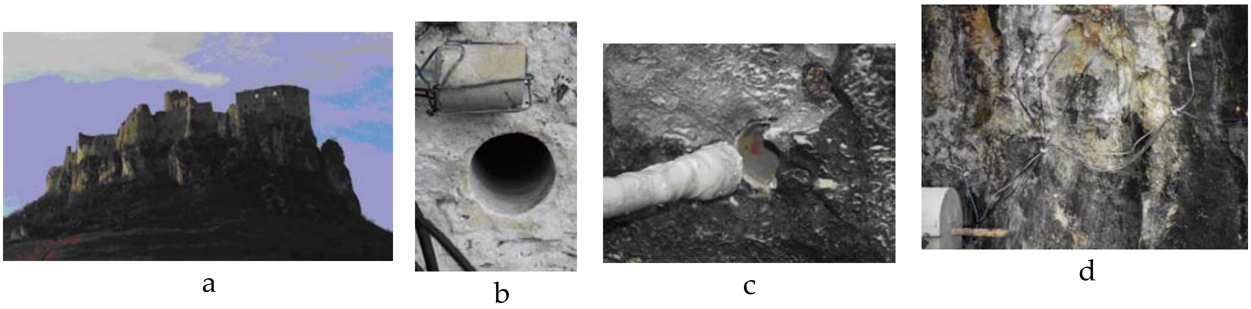

Figure 1.: a – view of the Spissky hrad situated on the rock massive, b – body of the moisture sensor and a hole in the rock massive, c – sensor body covered by sealing material, d – positioning of the moisture sensors on the rock massive.

3. Principle of the sensor

The principle of the hot ball sensor is based on a model that assumes a constant heat flux q from the empty sphere of radius r_b into the infinitive medium that starts to be delivered for times $t > 0$

Figure 2. Model of the hot ball (left), its realization (middle) and moisture sensor (right)

(see Figure 2 left). Then the temperature distribution within the medium is characterized by a function [2]

$$T(r,t)=\frac{q}{4\pi\lambda r^{2}}\left\{\sqrt{\frac{at}{\pi}}\left(1-e^{\frac{-r^{2}}{at}}\right)+r\cdot erfc\left(\frac{r}{\sqrt{at}}\right)\right\} \tag{1}$$

where erfc(x) is the error function defined by $erfc(x)=\frac{2}{\pi}\int_{0}^{x}\exp\left(-\zeta^{2}\right)d\zeta$ and λ and a are thermal conductivity and thermal diffusivity of the surrounding medium, respectively. Function (1) gives a working equation of the measuring method based on the hot ball for long time approximation

$$T_m=\frac{q}{4\pi r_0\lambda}\,. \tag{2}$$

Rearranging the latter equation yields the working equation of the hot-ball sensor

$$\lambda=\frac{q}{4\pi r_0 T_m}\,. \tag{3}$$

where Tm is stabilized value of the temperature response that is reached in the long time limit at the surface of the empty sphere with the radius rb. During stabilization time the heat produced by ball penetrates into a surrounding material in a depth that corresponds to a sphere with diameter about 20 mm providing the hot-ball sensor in diameter of 2 mm is used. The criterion of penetration depth for construction of the body of moisture sensor is used.

A sensor body is constructed from material to be tested in a form of cylinder in diameter and heigth that corresponds to penetration depth. Then hot-ball is fixed into the centre of the cylinder body. Such sensor body can be easily placed into appropriate hole of the rock massive providing the contact for heat and water transport between the sensor body and surrounding rock massive. Thermal conductivity of the pore material is a function of the pore content [1].

Therefore the moisture sensor can by used for the determination of the water content in the rocks when calibration is caried out prior to the installation of the sensor. A calibration of the moisture sensor is performed in dry and water saturated stage considering its weigth. Then simple relation between the water content in sensor body and the sensor signal is used.

The RTM 1.01 instrument was constructed that can work in the regime of the monitoring regime in connection with the hot ball sensor (6). The scheme of the instrument is shown in Figure 2. A stabilized voltage was used for driving the heating element. The RTM instrument is based on data logger in connection with the appropriate microcomputer. Suitable software has been compiled that allows simple instrument operation and data transmission through USB port.

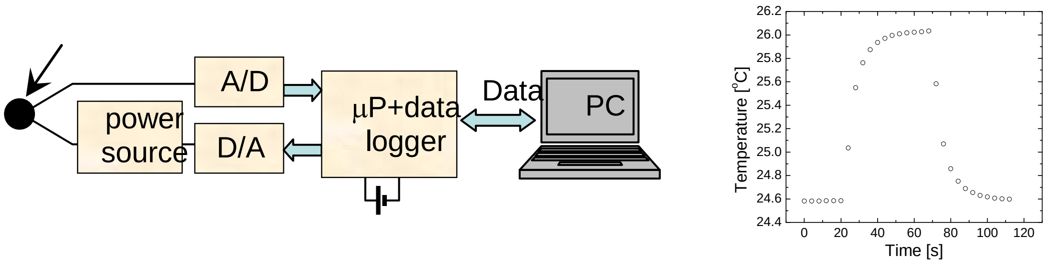

Figure 3.: Scheme of the RTM1.01 instrument (left), signal of the sensor (right)

Typical measurement signal is shown in Figure 3 right. The measuring procedure consists of the specimen temperature measurement (base line), switching on the heating and simultaneously scanning the ball temperature. When the ball temperature stabilizes, the heating is interrupted and a period of the temperature equilibration follows. When the temperature is equilibrated the next measurement may be realized.

4. Results and discussion

Moisture sensors were inserted into the rock massive in 5 different depths, namely 100 mm, 400 mm, 800 mm 1000 mm and 1500 mm. However sensor stability was poor therefore we present data taken from 3 different depths, namely 100 mm, 400 mm, and 1500 mm. Data are presented in Table 1 together with relevant meteorological data. Clear winter – summer cycle can be recognized in temperature for all three depths. The amplitude of the temperature cycle as a function of depth is given in Table 2. Instead of thermal conductivity, data on the parameter q/Tm (see equation (2)) are shown. The reason is in calibration deficiency and hot-ball construction. Water penetrated into the hot-ball sensor structure and this influenced the electrical isolation. As a result the signal of the hot ball was influenced by content of water in hot ball instrument. Thus sensitivity of the hot-ball to the variations of the moisturelowers. This can be recognized in all three moisture sensors. The hot-balls have high sensitivity at the beginning of the monitoring. However the signal sensitivity considering moisture changes started to diminish during monitoring period. Small variation of measured parameter q/Tm can be found in latter period of monitoring. Nevertheless a clear correlation can be found between the precipitation, humidity, and temperature and q/Tm parameter. Variation of q/Tm parameter corresponds to variations of the night – day temperature [4].

There is clear correlation between data on precipitation and the surrounding humidity. When the precipitation comes, then the surrounding humidity is growing.Parameter q/Tm characterizing the moisture in rock massive at 100 mm depth is going to lower values in dry period (26.7.2009 – 1.8.2009). The amplitude of q/Tm cycling depends on size of temperature variation and on the surrounding humidity. Feature of the q/Tm due to day – night cycle has similarity to summer – winter cycle (see Table 1.), i.e. growth of temperature causes always growth of local moisture providing that a source of moisture exists.

Table 1: Data on temperature, parameter q/Tm, precipitation and humidity collected during period September 2008 to June 2011

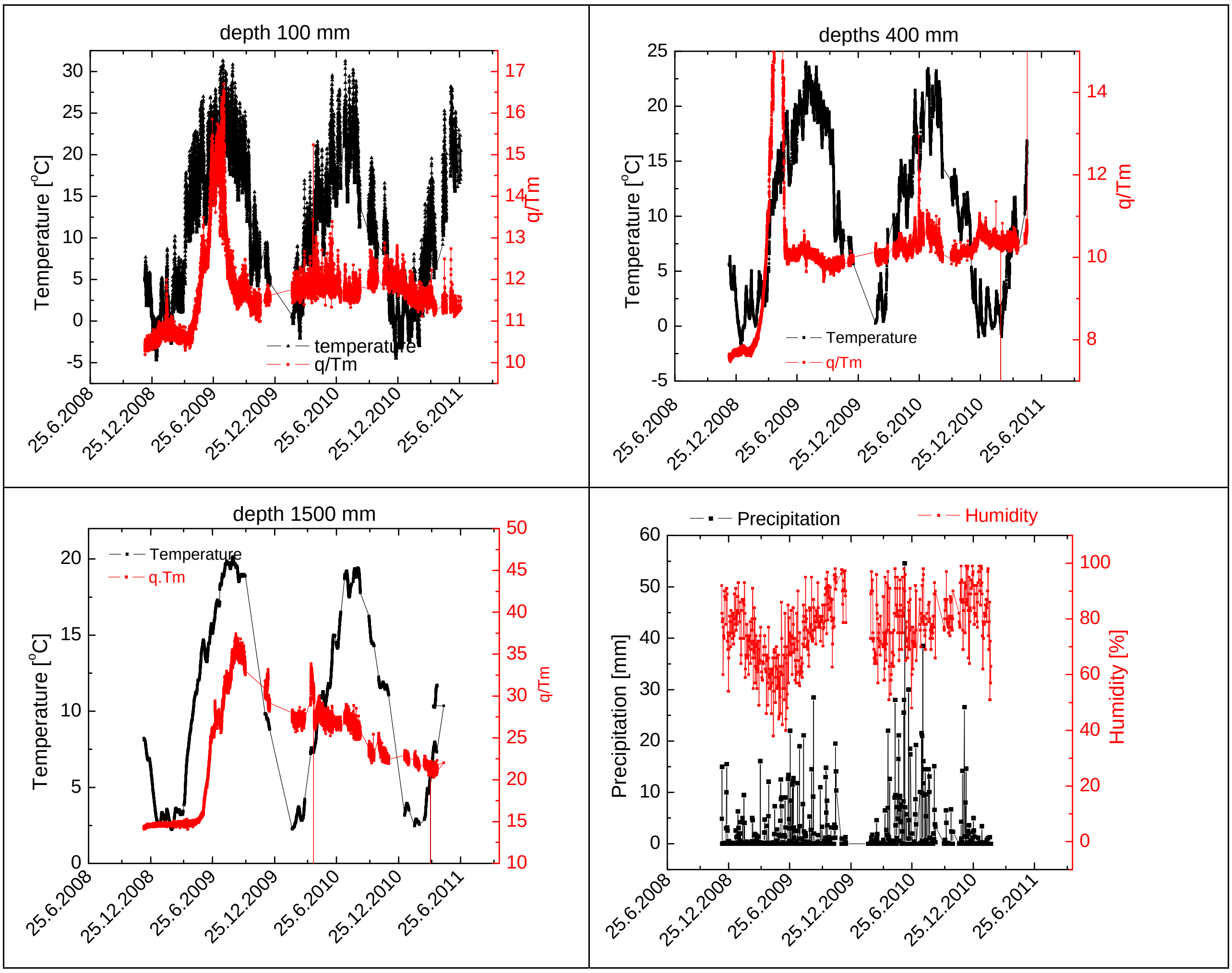

Figure 4.: Fine structure of data on temperature, parameter q/Tm, precipitation and humidity collected during period from July 23 to August 10, 2009.

Table 2: Amplitude of the temperature changes and the corresponding mean temperatures during monitored period September 2008 to June 2011.

Depth [mm]	Amplitude of temperature changes [°C]	Mean temperature during period of January [°C]
100	35	0.44
400	25	0.72
1500	15.5	3.4

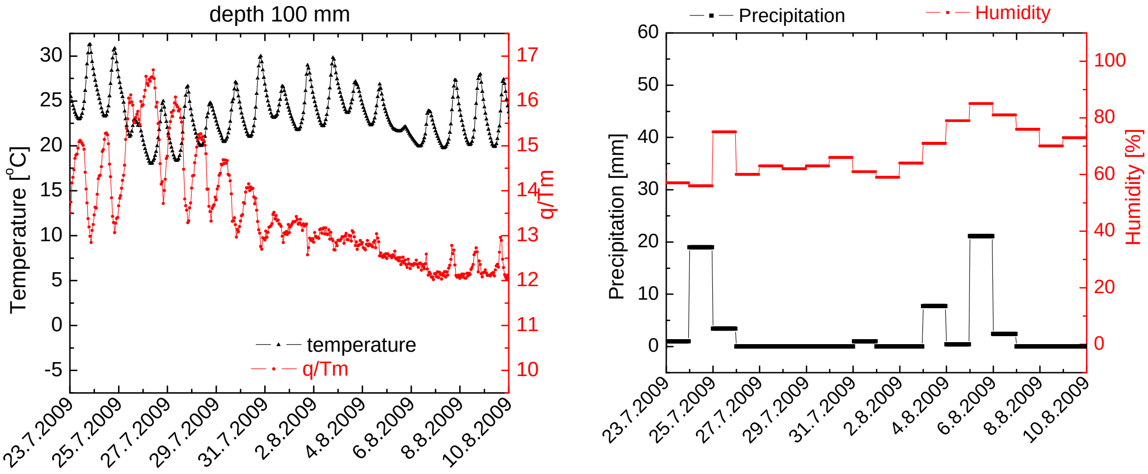

Figure 5: Fine structure of data on temperature, parameter q/Tm, precipitation and humidity collected during period from July 23 to August 10, 2009

Conclusion

Paper presents data on temperature, q/Tm parameter corresponding to local moisture, precipitation and the surrounding humidity that were collected in travertine massive and to the surrounding atmosphere at Spis Castle location. The monitoring was realized at 100 mm, 400 mm and 1500 mm depths in period from September 2008 to June 2011. Two kind of data cycle were found, namely annual and a diurnal. Temperature was changing periodically within these cycles. Depending on surrounding humidity variation in q/Tm parameter was found that corresponds to temperature variations. Short characteristic of the rock massive on which the Spis Castle is built is given. Moisture sensor that utilizes the hot-ball method for measuring local thermal conductivity is described. Sensor body has form of cylinder 20 mm in diameter and in length. Hot ball sensor is fixed in the centre of the cylinder. The sensor body is constructed of core material that was obtained during the drilling of a hole into the rock massive. Sensor functionality was limited by penetration of the water into the ball construction. The water protection has to be improved for long – time monitoring regime.

Acknowledgements

Authors would like to express thanks to Dr Stofanik and Mr Markovic and Mr Peller for technical assistance. The works was supported by APVV grant LPP-0442-09 and APVV 0641-10.

References

[1] Kubičár, Ľ., Vretenár, V., Boháč, V., and Tiano P., 2006, Thermophysical Analysis of Sandstone by Pulse Transient Method, Int. J. of Thermophysics, 27, 220 - 234

[2] Kubičár, Ľ., Vretenár, V., Boháč, V., and Tiano P., 2006, Thermophysical Analysis of Sandstone by Pulse Transient Method, Int. J. of Thermophysics, 27, 220 – 234

[3] Brček M., Vlčko J., Kubičár Ľ., Boháč V., Adamcová R., 2009, Vlhkosť - negatívny faktor deteriorácie horninového masívu, Acta Geologica Slovaca, 1, 1-8

[4] Kubičár, Ľ., Vretenár, V., Štofanik V., Boháč, V., and Tiano P., 2008, Monitoring of thermal-moisture regime of cultural objects, Proc. of conference: In situ Monitoring of Monumental Surfaces - SMW08, Florence p. 53 – 62

Pulse transient model for finite size of cuboid samples tested on stone materials

Vlastimil Boháč[1], Peter Dieška[2], [1]Ľ. Kubičár, [1]V.Vretenár

[1]Institute of Physics, Slovak Academy of Sciences, Bratislava, Slovakia

[2] Department of Physics, FEI - STU, Ilkovičova 3, Bratislava, Slovakia

Email: bohac@savba.sk

Abstract: *The pulse transient technique is recently used for testing thermophysical properties of many types of materials. The proper model accounting different disturbance effects help to improve accuracy of the measurements. The specimen shape has the same level of importance, because of different heat dissipation in symmetrical as well as non-symmetrical arrangements. The solution for square cross section of the specimen of different length has to assume heat penetration in three dimensions. The discussed model assumes asymmetrical arrangement of specimen in a form of finite cuboids of different length, and the plane heat source that have zero thermal capacity placed in between cuboidal specimen with ideal thermal contacts. The model was tested on stone material.*

Keywords: *testing of model, pulse transeint method, stone materials*

1. Introduction

Quality of natural stone used as building construction material is tested usually by classical methods, measuring basic physical and mechanical parameter like volume density, water absorption uniaxial compressive strength, flexural strength, coefficient of the linear thermal expansion, frost and wear resistance and similar one are determined in standard way. Values of stated properties are determined from aside the rock genesis, mineral composition and structure [1, 2]. Recently, methods for investigation of the thermophysical properties, namely the thermal conductivity, thermal diffusivity and specific heat are going to be promoted as next useful methods for quality test as these properties are strongly connected with the change of thermodynamical state of the material structure or atomic structure arrangement, arrangement of crystalline components and consideration on material defects created in time that are responsible for further development of structure degradation. Process of deterioration of stone or it's state and quality comparing it's basic or initial state should be monitored by continuous measurements (monitoring) of thermophysical properties [3, 4]

Thus, the thermophysical properties can serve as next criteria for distinguishing in between different stone quality or level of their deterioration and thus quantification of material quality.

The physical models are usually based on infinitively large specimen size. The problems connected with deficiency in a large amount of testing material cause some problems in data evaluation according an ideal model. The finite geometry of the specimen cause additional effects that influence the accuracy of the measured data.

In our case the pulse transient method was used for measurement of thermophysical parameters, e.g. the thermal diffusivity, specific heat and thermal conductivity of natural stone. For the data evaluation it was used a model for square cross section of cuboid specimens with finite length. Model accounts heat sink temperature at both ends of specimen set and includes also the effect of heat losses from the sample surface. Model was tested for evaluation of thermophysical parameters of stone material.

2. Principle of Pulse transient method

The principle of the Pulse transient method is to record the temperature transient response to the heat pulse generated by a plane heat source and to calculate the thermophysical parameters from the characteristic features of the measured curve of the temperature response (Fig. 1. right).

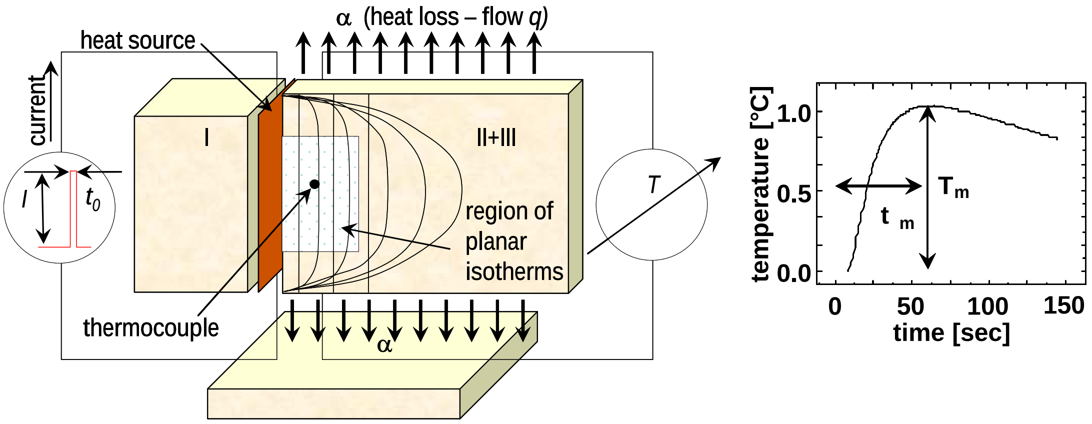

Figure 1. The principle of the pulse transient method is drawn. Sample parts II+III were drawn in sections to illustrate the planar isotherms in the middle plain of cutting. Specimen set is drawn with heat flow paths when drawn deformed isotherms are influence by heat loss effect (left). An example of the temperature response is on the right.

Transient temperature response measured at the distance *h* from the heat source is calculated according temperature function $T(x, t\text{-}t_0)$ providing that the model (Eq. 1.) is valid [5]. The ideal model assumes that the planar heat flow in infinitively large samples is not deformed as it penetrates into the depth of the specimen bulk (white-dotted area in the Fig. 1). The problem is that the temperature isotherms are not planar over the radial cross section of the specimen but they are deformed at the edges. This effect is caused by the heat losses from the sample surface in a case of large distances from the heat source, e.g. the thicknesses of material bigger than the optimal value [1, 2, 3, 4]. In previous experiments just a correction to the ideal model considering the real pulse width was applied to ideal model [5]. The model is characterized by temperature function (Eq. 1)

$$T(h,t) = \frac{2\cdot Q}{c\rho\sqrt{\kappa}}\left[\sqrt{t}\cdot i\Phi^*\left(\frac{h}{2\sqrt{\kappa t}}\right) - \sqrt{t-t_0}\cdot i\Phi^*\left(\frac{h}{2\sqrt{\kappa(t-t_0)}}\right)\right] \qquad (1)$$

where $i\Phi^* = \frac{e^{-x^2}}{\sqrt{\pi}} - x\cdot erfc(x)$. Here the meanings of used symbols are the following: Q - heat flow density at source, c - specific heat, κ - thermal diffusivity, ρ - density, t - time, t_0 - heat pulse duration, *erfc* - error function, *h* - the specimen thickness. Equation 1 should be used for data evaluation by fitting procedure also.

2.1 One-point evaluation procedure

At the standard experiment due to fast calculations we use simple relations for the evaluation of thermal diffusivity, specific heat and thermal conductivity. These relations were derived for the maximum of temperature response on Fig.1. (One-point evaluation procedure). Then, the thermal diffusivity is calculated according to the equation

$$\kappa = h^2 \cdot f_\kappa / 2t_m \tag{2}$$

and the specific heat

$$c = Q \cdot f_c / \sqrt{2\pi e}\rho h T_m \tag{3}$$

where f_κ and f_c are correction factors [6]. Maximum temperature of the transient response found at time t_m is T_m (Fig. 1.) Thermal conductivity is given by data consistency relation

$$\lambda = \kappa\rho\, c = h \cdot Q \cdot f_\kappa \cdot f_c / 2\sqrt{2\pi e}\ t_m T_m \tag{4}$$

2.2 Model for cuboid shape samples

A previous explanation of a heat loss effect was solved in a new model developed for cuboid samples. According Fig.2 there were defined initial and boundary conditions for the basic heat transport equation.

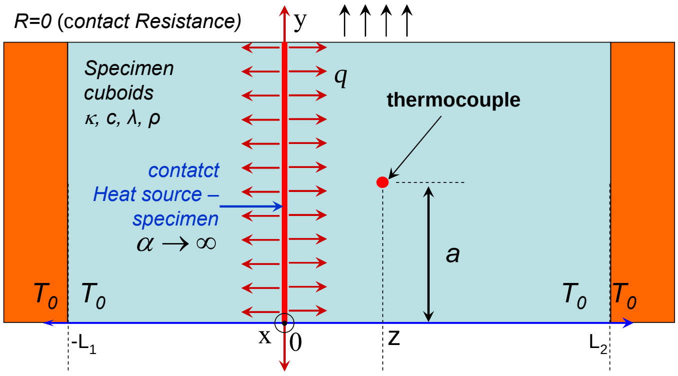

Figure 2. Model of the measurement – Sample parts I is of L1 thickness and II+III of L2 thickness. The grooves could be made at different distances between the heat source and thermocouple to investigate influence of heat loss effect from the sample surface.

The new model assumes heat source placed in between symmetric arrangement of the specimens in the shape of semi-infinitive cuboid blocks having squared cross section. Heat source is of zero heat capacity and is in ideal heat contact with the specimen (thermal contact resistance is zero).The solution of the heat equation is a temperature function in the form

$$T_{11}(t,x,y,z) = T_0 \frac{w}{2} \sum_{n=1}^{\infty} \sum_{m=1}^{\infty} \frac{b_n b_m}{v_{nm}} \varphi_n(\frac{x}{a}) \varphi_m(\frac{y}{a}) \sum_{j=-\infty}^{\infty} \left[F(u_{1j}, v_{nm}) - F(u_{2j}, v_{nm}) \right] \tag{5}$$

where $\varphi_n(s) = \sqrt{\dfrac{2\beta}{\beta + \sin^2 \mu_n}} \cos(\mu_n s)$, $F_n(u,v) = e^{-2uv} \Phi^*(u-v) - e^{2uv} \Phi^*(u+v)$

$$T_0 = \frac{qa}{\lambda},\ \beta = \frac{a\alpha}{\lambda},\ v_{nm} = w\sqrt{\mu_n^2 + \mu_m^n},\ w = \frac{\sqrt{\kappa t}}{a},\ b_n = \varphi_n(0)\frac{\sin(\mu_n)}{\mu_n}$$

$$u_{1j} = \frac{|z + 4Lj|}{2\sqrt{kt}}, \; u_{1j} = \frac{\left||z| + 4L_j + 2L_1\right|}{2\sqrt{kt}}$$

The meaning of variables:

T temperature field in specimen body, **t** time, **z** axial space coordinate, **L_1** length of the sample on the left, **L_2** length of the sample on the right, **x,y** transversal space coordinates, **$2a$** transversal size of the sample, **q** heat flow density at source, **λ** thermal conductivity, **κ** thermal diffusivity, **α** heat transfer coefficient for sample - ambient interface, **$\Phi^*(u)$** is the complementary error function, μ_n are the roots of equation $\beta \cos \mu - \mu \sin \mu = 0$

The relation (5) characterizes the step-wise measuring regime. After the duration of the heat pulse t_0, the temperature is expressed by the relation

$$T^*(t, x, y, z) = T(t, x, y, z) - T(t - t_o, x, y, z) \tag{6}$$

where $T(t, x, y, z)$ and $T(t - t_0, x, y, z)$ are given by the relation (5). The relation (6) characterizes the pulse transient regime.

3. Experiment

The experimental details were described in [6]. Thermophysical parameters were evaluated by one-point evaluation procedure (Eq. 2 and 3.) derived from ideal model. In the past the use of the ideal model and the one-point evaluation procedure led to a problem with the heat loss disturbance effects shown in Fig. 1 for an illustration. This effect was described and finally avoided by optimization of specimen geometry [5, 7].

The sandstone specimen set was in a form of cuboids having finite length. The dimensions of parts I in Fig.1 were 50x50x25 and two parts 50x50x25mm cut longitudinally. The volume density of used samples were 2190 and 2614.8 kg m^{-3} and porosity measured by weighting dry and water saturated specimen was 27.5%. Heat source meander was etched of Ni foil and insulated by kapton foil. Its dimensions were 50x50mm. Measurements were performed in RTB 1.02 measurement chamber [8]. The heat pulse parameters e.g the current and pulse duration were optimized to get temperature response of about 1°C. The heat source resistance was about 2 ohms. Before the measurements the specimens of sandstone were dried in oven at 70°C till no changes in weight at three subsequent measurements in reasonable time.

The experimental details were described in [6]. Thermophysical parameters were evaluated by one-point evaluation procedure (Eq. 2 and 3.) derived from ideal model. In the past the use of the ideal model and the one-point evaluation procedure led to a problem with the heat loss disturbance effects shown in Fig. 1 for an illustration. This effect was described and finally avoided by optimization of specimen geometry [5, 9]. In practice this limit resulted in limits of the specimen thickness between 6 – 8mm for a class of homogeneous materials and between 18 - 22 mm for strongly non-homogeneous materials. The model for cuboid samples (Eq. 5) accounts heat losses from the sample surface via heat transfer coefficient in between the sample surface and surroundings and assumes temperature of heat sinks at both ends of specimen set. New model is able to answer the question if optimal geometry was used for measurements.

4. Results

The measured data plotted for different sample thicknesses show influence of heat loss effect during measurements. The figure 3 shows measured thermophysical parameters for different thicknesses Parameters calculated by one-point evaluation procedure that do not account heat losses from the sample surface are shifted from data stability region for bigger thicknesses. Evaluation by fitting procedure using new model push the data in one strip with small scattering around constant values represented by drawed blue line. The result of this analysis should confirm that ideal thickness for one-point evaluation procedure is between 15 to 20mm.

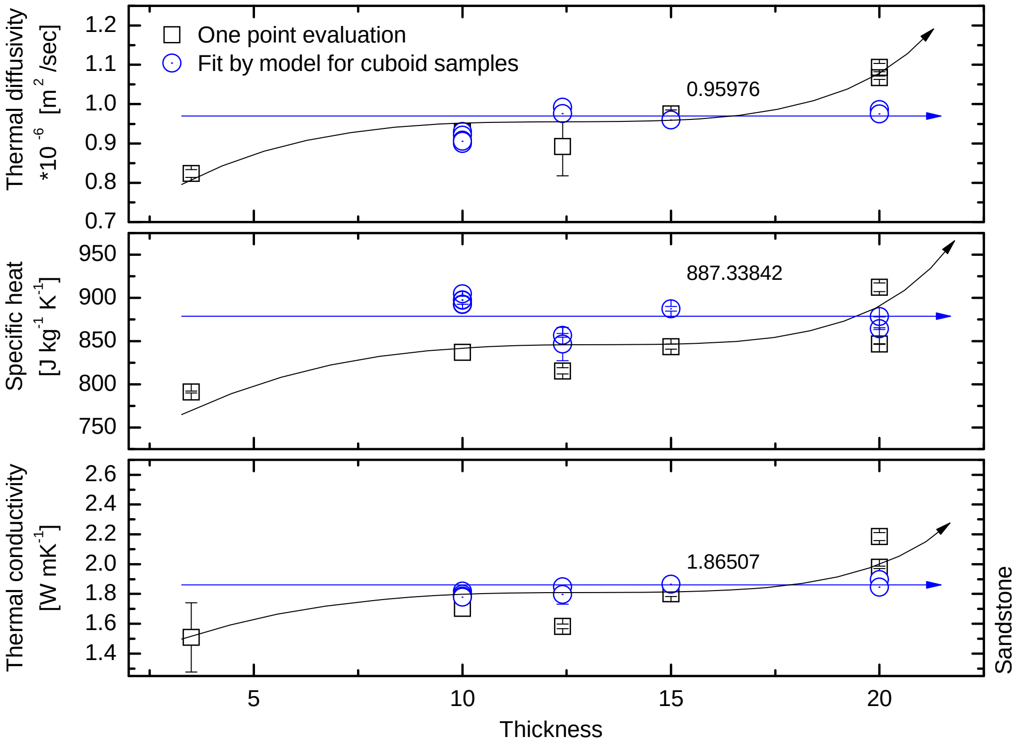

Figure 3. Data of thermal diffusivity, specific heat and thermal conductivity plotted for different sample thickness. Data evaluated by one-point procedure show shift from data stability region for small and large thicknesses due to heat loss effect.

The data from one-point evaluation procedure are drawn in temperature dependency in figure 4. Here the problem of different thicknesses is evident. For smaller thicknesses than ideal the data are underestimated and for 20 mm overestimated. In this graph there were added values of data evaluated by fitting procedure by new model for cuboid samples marked in blue circles. These data were obtained at different temperatures as well at different sample thicknesses and additionally in two temperature analyses regimes. The first one was temperature ramp during heating and freezing and the second one measured in isothermal regime. In figure 4 there is evident influence of ramp on data precision. Mathematically the maximum of the temperature responses were increased at heating and decreased at cooling as some small value of temperature was superposed on temperature response as it could be measured in isothermal regime. The data values measured in isothermal regime are in between these two data sets.

The heat transfer coefficient calculated for the data for small thicknesses were not able to estimate unambiguously and has physible values 10 and 18 W m^{-2} K^{-1} just for thickness 15 and 20 mm respectively.

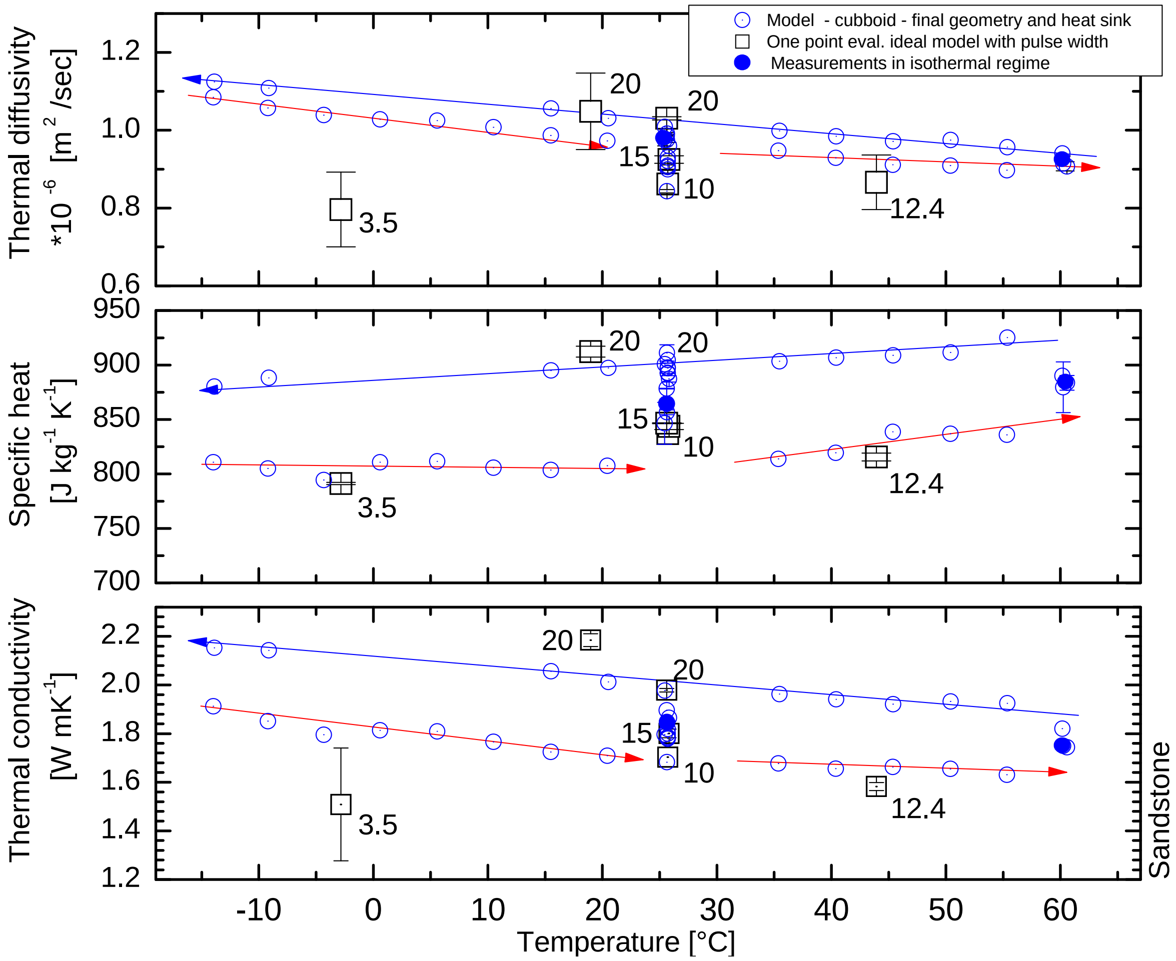

Figure 4. Temperature dependency of thermal diffusivity, specific heat and thermal conductivity with marked temperature and vacuum history evaluated by one-point procedure and by fitting with cuboid model. Numbers at for one point evaluated data denotes sample thicknesses.

The model for cuboid samples (Eq. 5 and 6) fits next free parameters: thermal diffusivity, thermal conductivity and heat transfer coefficient. The problem is that the sensitivity coefficient for this parameter is increasing in time of measurement, so for samples with bigger thicknesses we use longer pulse duration and thus longer time for recording of temperature response. The longer measurements result in better accuracy for this parameter evaluation.

Conclusions

The thermophysical properties of sandstone were investigated by pulse transient method for dry state of stone. The data were evaluated by two methods – the one pint evaluation procedure and by fitting procedure using a new model for cuboid samples that accounts heat losses from the sample surface. The new model corrected values of all parameters and is less sensitive for variability of sample thickness.

The measurements were done in the temperature range from -15 up to 60°C. The slope of temperature dependence of transport parameters is positive, while the slope for specific heat is negative. The heat transfer coefficient from the sample surface to the surrounding is temperature dependent and its value is greater for higher temperatures.

Comparing all new results with the previous one measured on two sets of Sander sandstone samples [10] found, that the new model is able to fix the problem with heat loss effect from the sample surface.

Acknowledgments

This research was supported by Slovak Research and Development Agency under the contract No. APVV-0641-10, „Study of rocks properties and investigation of structural and textural characteristic in correlation with thermophysical and physico-mechanical properties". Data used for model testing were obtained in MCDUR project [10].

References

[1] VLČKO J., JEZNÝ M., PAGÁČOVÁ Z., 2006, Influence of Thermal expansion on slope displacements. In: *Landslides, Risk analysis and sustainable disaster management.* Proc. 1. General assembly ICL, Washington, Springer, ch. 7, 71-74

[2] KÜHNEL R.A. 2002, Driving forces for rock degradation, *Protection and Conservation of the Cultural Heritage of the Mediterranean Cities,* Galán and Zezza (eds). Swets& Zeitlinger, Lisse, ISBN 90 5809 253 4, pp11-18

[3] BOHÁČ V., HARCEK M., KUBIČÁR L., VRETENÁR V., 2005, Thermophysical properties of new electrotechnical ceramics measured by pulse transient technique, *Proc of the TERMANAL 2005*. 12th conference on thermal analysis and calorimetry, Ed. E.Klein, Dept. of Physical Chemistry, I9SBN 80-227-2285-5

[4] VRETENÁR V., KUBIČÁR Ľ., BOHÁČ V. and TIANO P., 2007, Thermophysical analysis of Gioia marble in dry and water-saturated states by pulse transient method. *Int. J of Thermophysics* 28, pp. 1522-1535.

[5] BOHÁČ V. et all. Methodology of parameter estimation of pulse transient method. *Proc. TEMPMEKO 2004*, 22 - 25 June 2004 Dubrovník, Croatia

[6] Kubičár Ľ., 1990, Pulse Method of Measuring Basic Thermophysical Parameters in *Comprehensive Analytical Chemistry* Vol. XII Thermal Analysis Part E Ed Svehla G, Amsterdam, Oxford, New York, Tokyo: Elsevier, pp 350.

[7] BOHÁČ V., Dieška P., Kubičár Ľ. *MEASUREMENT SCIENCE REVIEW,* Volume 7, Section 3, No. 2, 2007

[8] Institute of Physics, SAS, Dúbravská cesta 9, Slovakia, http://thermophys.savba.sk

[9] BOHÁČ V., DIEŠKA P., KUBIČÁR Ľ. *MEASUREMENT SCIENCE REVIEW,* Volume 7, Section 3, No. 2, 2007

[10] KUBIČÁR Ľ., VRETENÁR V., BOHÁČ V., Tiano, P., 2006: Thermophysical analysis of sandstone by pulse transient method, Int. J. Thermophysics 27 (1), 220-234

New Hot ring method for thermophysical parameters measurement: preliminary results and analysis

Viliam Vretenár[1], Ľudovít Kubičár[1], Vlastimil Boháč[1] and Peter Dieška[2]

[1]Institute of Physics SAS, Dúbravská cesta 9, 845 11 Bratislava, Slovakia

[2] Faculty of Electrical Engineering and Information Technology, STU, Ilkovičova 3, 812 19 Bratislava, Slovakia

Abstract: *New method for measuring thermal conductivity, thermal diffusivity and specific heat of solids is presented. The plane sensor, in the form of hot ring, generates the heat flux and simultaneously measures the temperature response. An analytical solution of the temperature function has been derived for an ideal model and used for data calculation. Reliability of the method is inspected by measurement on standard reference sample PMMA, whereas for heterogeneous materials, comparison tests with the Pulse transient method have been realized. Appropriate design of the sensor is chosen in accordance with the finite element method analysis and experimentally verified by infrared camera pictures. Accuracy of the method together with possible source of errors (disturbing effects) is discussed.*

Keywords: *Hot ring method, thermophysical properties, thermal conductivity, thermal diffusivity, specific heat*

Introduction

Over the last decades the transient methods [1] have started to be widely used for measurements of thermophysical parameters. A lot of different types of thermophysical sensors operating in transient mode have spread into research laboratories as well as in industry. The most frequently used thermophysical sensors or their variations can be summarized in the following techniques, the hot wire [2], transient plane source [3], hot strip [4], hot bridge [5] and hot-ball [6] technique. Depending on sensor geometry and measuring regime, the thermal conductivity, thermal diffusivity and specific heat can be determined simultaneously. Principal differences between classical and transient methods lie in varieties of specimen sizes, measuring time, and number of measured parameters. Transient methods need significantly shorter time for a measurement than classical ones, and moreover, some of them can be used to determine the specific heat, thermal diffusivity and thermal conductivity within a single measurement.

The present paper deals with new Hot ring method for thermophysical properties measurement of solid materials. The working function of the method is derived according to properly chosen model. Effect of various sensor structures together with disturbing factors is analyzed and discussed. Finally, accuracy of the method is roughly estimated by comparison measurements and by measurement on reference sample.

Principle of the Hot ring method

The ideal model of the method is shown in Fig. 1. The model assumes non-limited specimen body inside which an ideal circle of radius R is placed as a heat source. The temperature of the specimen is uniform and stabilized. Then the heat source starts to delivery constant heat flow into the specimen, generating a transient temperature field around it. Using an appropriate working function upon measured temperature response, the thermophysical parameters can be calculated.

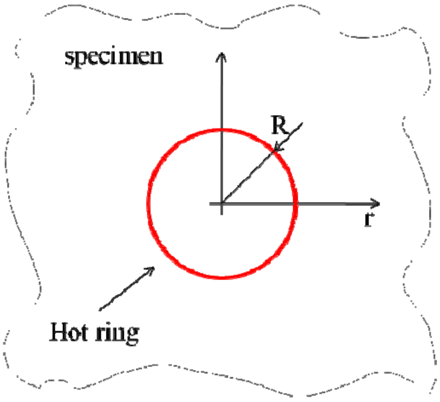

Figure 1: Ideal model of the Hot ring method

Working function of the method is derived from a solution of equation of heat conduction considering initial and boundary conditions of the ideal model. Then the temperature field inside the specimen can be ascribed by the working function

$$T(t,r) = T_0 F(u,v) \tag{1}$$

$$T_0 = \frac{P}{4\pi\lambda R} \qquad F(u,v) = \frac{1}{\pi}\int_0^{\pi} \frac{\Phi^*\left(v\sqrt{1+u^2+2u\cos\phi}\right)}{\sqrt{1+u^2+2u\cos\phi}}\,d\phi \tag{2}$$

$$u = \frac{r}{R} \qquad v = \frac{R}{2\sqrt{at}} \tag{3}$$

where *R* is Hot ring radius, *r* is location of temperature measurement, *a* represents thermal diffusivity, *λ* stands for thermal conductivity and *P* is the overall heat flow.

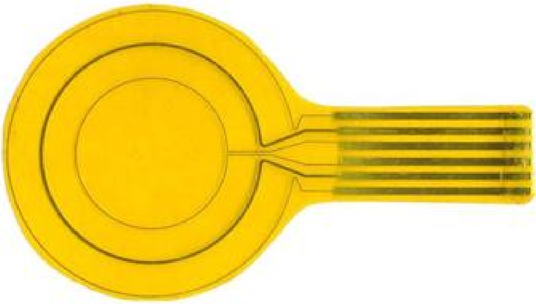

Figure 2: Hot ring sensor – first simple design

Real construction of Hot ring sensor is depicted in Fig. 2, where the first version of simple design has been chosen. The sensor is constructed by etching process on Nickel foil having thickness of 10 μm. Etched Nickel patterns are then fixed between two Kapton foils, each of 25 μm of thickness. Middle wide ring serves as a heating element, whereas narrow inner and outer rings are used for temperature response measurement. Typical radius of hot ring is around 10 mm. Such planar sensor is clamped between two parallel faces of specimen. Characteristic temperature response along with fitted ideal function (eq. 1) is presented in Fig. 3. The dimension of sensor elements and actual value of used heat flow during measurement are written in the graph. Working function was fitted using Levenberg-Marquardt algorithm. Evidently good agreement between model and experiment has been achieved.

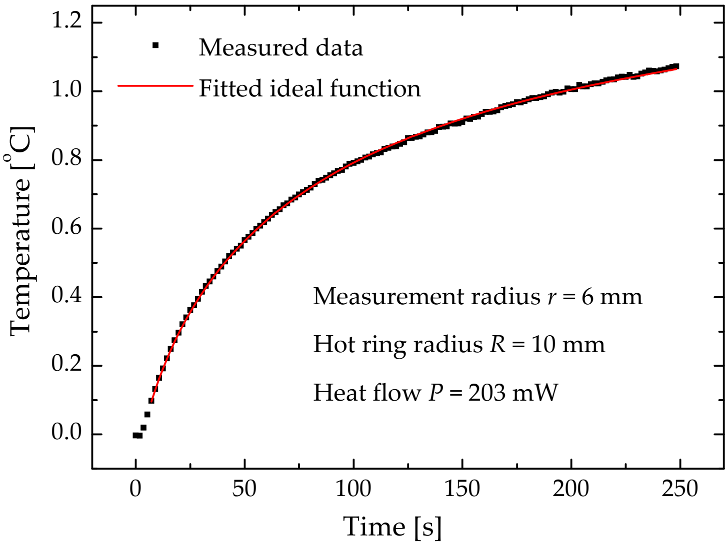

Figure 3: Typical temperature response of the method

Experimental apparatus

All measurements have been carried out by laboratory system for the thermophysical sensors testing (Fig. 4). Specimens were temperature stabilized in measuring chamber RT1.02 (Transient MS) and controlled by thermostat Lauda RP845 having accuracy of ±0.01°C and temperature range from -40 to 170 °C. For heat flow generated in the hot ring the precise source meter Keithley 2400 (up to 1 A and 200 V) was employed. Highly sensitive digital multimeter Keitley 2010 was taken for measuring the temperature response. PC with custom software developed in our laboratory (TMS ver. 1.4) controls all units.

Figure 4: Picture of the laboratory measurement system for thermophysical properties of solids and liquids in temperature range from -40 to 170 °C

Impact of sensor structure

Effect of sensor structure is analyzed by the means of the influence of electrical leads connecting hot ring with power source. Analysis is performed by numerical calculation using finite element method (Comsol MultiPhysics 3.2) and experimentally verified by thermal imaging camera, where the pictures of real sensors during the heating were taken.

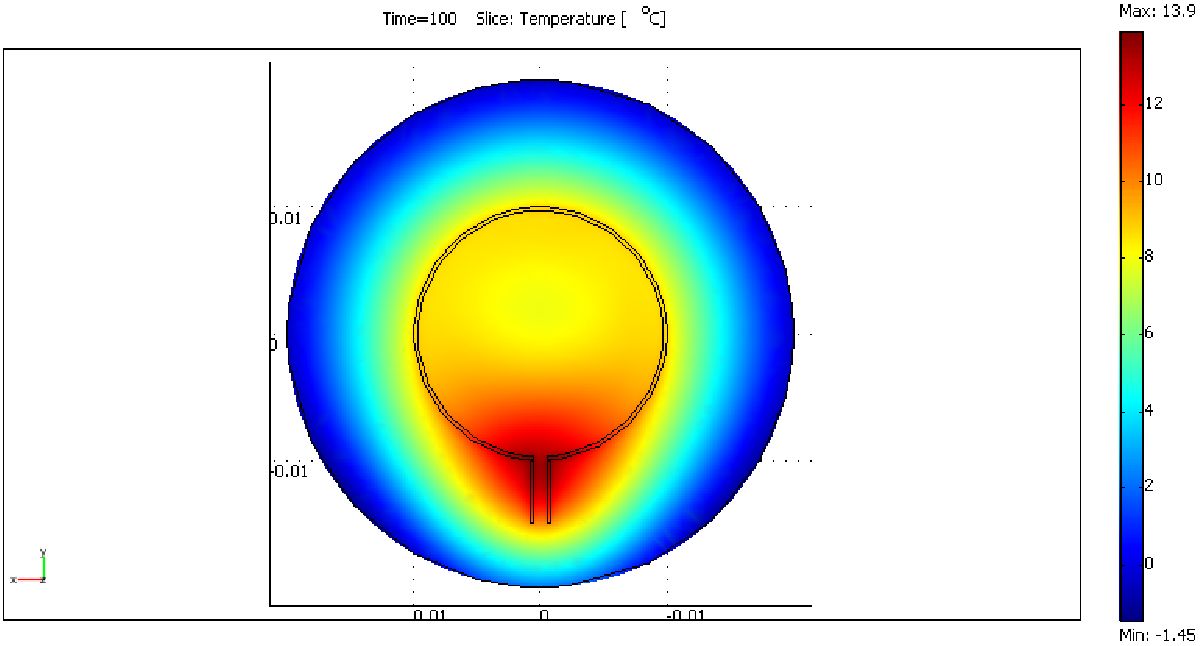

Figure 5: Numerical analysis of simple hot ring design

Numerical analysis of simple sensor design confirmed the effect of non-ideal circular shape of real constructed hot ring. Overheated area in Fig. 5 is clearly visible. Design of hot ring sensor is depicted by black line. The temperature field around connecting wires (two parallel lines) is deformed and circular symmetry is broken.

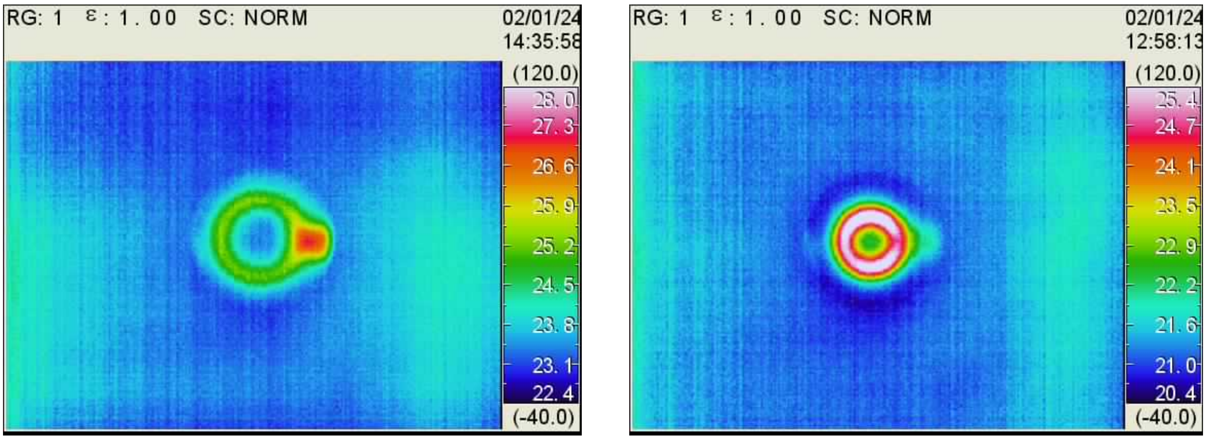

Figure 6: Real thermal patterns of simple (left) and properly designed (right) sensor

Similar to numerical analysis, the thermal picture of simple sensor (left) revealed both the heat accumulation and temperature deformation around connecting wires (red area). Proper design of sensor (right) must be taken in order to suppress non-uniform heat generation and to eliminate even small potential deformation of temperature field. Unfortunately, the actual design of hot ring sensor is currently patent pending.

Experiment and preliminary results

Functionality and reliability of the proposed method has been tested by measurements on several kinds of samples with thermal conductivities up to 1 $Wm^{-1}K^{-1}$. As representative result, the standard reference sample PMMA (Table 1) for homogenous material and Vicenza natural stone (Table 2) for heterogeneous one are presented here. In the case of PMMA (reference sample), the difference between measured and published data [7, 8] is quite below 5%. For heterogeneous Vicenza stone, the difference from data, which were measured by Pulse transient method, is less than 7%. Surprisingly, no differences in measurements using and not using thermally conductive paste between the sample and sensor have been observed for all tested materials.

Table 1: PMMA – reference specimen

Thermophysical parameter	Measured	Reference*	Diff.
Thermal diffusivity [mm^2s^{-1}]	0.124	0.119	+4.2%
Thermal conductivity [$Wm^{-1}K^{-1}$]	0.193	0.192	+0.5%
Specific heat [$Jkg^{-1}K^{-1}$]	1315	1363	-3.5%

* Published data [7, 8]

Table 2: Vicenza – natural stone

Thermophysical parameter	Measured	Reference*	Diff.
Thermal diffusivity [mm^2s^{-1}]	0.707	0.668	+5.9%
Thermal conductivity [$Wm^{-1}K^{-1}$]	1.089	1.099	-0.9%
Specific heat [$Jkg^{-1}K^{-1}$]	823.0	878.7	-6.3%

* Measured by the Pulse transient method

Conclusions

A new Hot ring method for measuring the thermal conductivity, thermal diffusivity and specific heat of solids has been presented. Numerical as well as experimental analysis of the disturbing effects on the measuring process, i.e. the real shape of the hot ring element and its thermal contact with specimen has been performed. For low conductive materials (λ<1 $Wm^{-1}K^{-1}$) satisfactory accuracy of measurement (around 5%) was found. But considering good thermally conductive materials, the reliability of the method is still a question, which needs to be examined. Besides measuring all three thermophysical parameters the main advantage of this simple one probe method is in nearly no requirements on sample geometry, just sufficiently flat two faces. In addition, despite small area of sensing element (one narrow ring) even heterogeneous materials appear to be measured precisely (suitable for building materials excepting materials of high porosity or big pore sizes). Finally, proper design of the sensor is an ultimate key factor eliminating the disturbing effects and governing thus accuracy of measurements.

Acknowledgements

This work was supported by the Slovak Research and Development Agency under the contract No. APVV-0641-10 and by the European Micro and Nano Technology (MNT) support programme - project MAFINCO.

References

[1] Kubičár, Ľ., Boháč, V.: *Review of several dynamic methods of measuring thermophysical parameters.* in "Proc. of 24th Int. Conf. on Thermal Conductivity / 12th Int. Thermal Expansion Symposium", ed. P.S. Gaal, D.E. Apostolescu, Lancaster: Technomic Publishing Company (1999), p. 135-149

[2] Davis, W., R.: *Hot-Wire Method for the Measurement of the Thermal Conductivity of Refractory Materials,* in Maglić K D, Cezairliyan A, Peletsky V E, (Eds.) Compendium of Thermophysical Property Measurement Methods, Vol. 1 Survey of Measurement Techniques, 1984, New York, London, Plenum Press, p. 161

[3] Gustafsson, S., E.: *Transient plane source technique for thermal conductivity and thermal diffusivity measurements of solid materials,* Rev. Sci. Instrum., Vol. 62, 1991, p. 797-804

[4] Gustafsson, S., E., Karawacki, E., Khan, M., N.: *Transient hot-strip method for simultaneously measuring thermal-conductivity and thermal-diffusivity of solids and fluids,* J. Phys. D.: Appl. Phys., Vol. 12, Iss. 9, 1979, p. 1411-1421

[5] Hammerschmidt, U., Meier, V.: *New Transient Hot-Bridge Sensor to Measure Thermal Conductivity, Thermal Diffusivity, and Volumetric Specific Heat,* Int. J. Thermophys., Vol. 27, No. 3, 2006, p. 840

[6] Kubičár, Ľ., Vretenár, V., Štofanik, V., Boháč, V.: *Hot-ball method for measuring thermal conductivity*, Int. J. Thermophys., Vol. 31, No. 10, 2010, p. 1904-1918

[7] Assael, M., J., Antoniadis, K., D., Jiangtao Wu: *New Measurements of the Thermal Conductivity of PMMA, BK7, and Pyrex 7740 up to 450K,* Int. J. Thermophys., Vol. 29, No. 4, 2008, p. 1257-1266

[8] Boháč, V., Kubičár, Ľ., Vretenár, V.: *Methodology of parameter estimation of pulse transient method and the use of PMMA as standard reference material,* in Proc. of TEMPMEKO 2004, ed. by D. Zvizdic, L.G. Bermanec, T. Veliki, T. Stasic, (LPM/FSB Zagreb, 2004), p. 1299–1306

Preliminary heat transfer investigations in thermally activated battery

Piotr Koniorczyk, Janusz Zmywaczyk, Bogdan Machowski, Mariusz Kastek

Department of Mechatronics, Military University of Technology, Kaliskiego 2, 00-908
Warsaw, Poland, email: piotr.koniorczyk@wat.edu.pl

Abstract: *Thermally activated batteries belong to chemical sources of electric current. They are used to supply special devices in the army [1]. They have activated time from 0.1 s to several seconds and their working time amount to dozens of minutes. The heat being generated during their work inside the battery causes a temperature increase up to 600 K. In the frame of this work a preliminary investigations of temperature distribution on the outer surface of the thermally activated battery BTR-03 as well as the heat flux distribution were carried out [8]. Comparing the temperature dependence as a function of time at several points on the outer surface of the battery BTR-03, obtained from experiment and calculated numerically allowed an initial validation of the model of heat transfer in the battery. Thus calculations of various structural variants of thermal insulation of the battery BTR-03 inside specific device are possible thanks to the heat transfer model.*

Keywords: *measurement of temperature, thermally activated battery*

1 Introduction

Thermally activated batteries are characterized by high mechanical strength, reliability over a wide temperature range, freedom from maintenance during storage and long shelf life. The values of voltage and current are adjusted to the requirements of the user [1, 2]. In the case of battery BTR-03 it was assumed that battery life does not exceed 11 minutes (660 s) [1, 2]. Structure of the thermal battery BTR-03 is based on the electrochemical system $Ca/LiCl,KCl/PbSO_4$ [1, 2, 8]. Anodic reaction mechanism is presented in the paper of Nissen [3]. The battery consists of multiple cells connected in series. The individual elements forming the basic component, a single cell, are made in the form of flat rings arranged in the following way: calcium anode, an electrolyte layer which is a mixture of salts $LiCl$ and KCl and the cathode is made of z $PbSO_4$. Individual cells are separated by the pyrotechnic heat tablets - Figure 1 [1]. In the temperature range from (-)50 °C to (+)50 °C electrolyte is solid, showing no ionic conductivity. Activation of the thermal battery occurs after melting of the electrolyte salt, which is realized as follows. Startup of the impact igniter mounted in the lid of the battery initiates an exothermic reaction of the pyrotechnic heat tablets. Generated heat energy raises the temperature of individual elements of the battery to about 600 K, melts the electrolyte and initiates redox reaction, that causes the emergence of voltage in each of the cells. Completion of the battery life occurs in the case of complete reaction of the respective electrode materials, or in the case of the solidification of the electrolyte. To prevent premature crystallization of the electrolyte, thermal insulation is placed inside the battery [1]. The battery BTR-03 is cylindrical in shape with a diameter of 56 mm, height 74 mm and a weight not exceeding 450 g [1, 2].

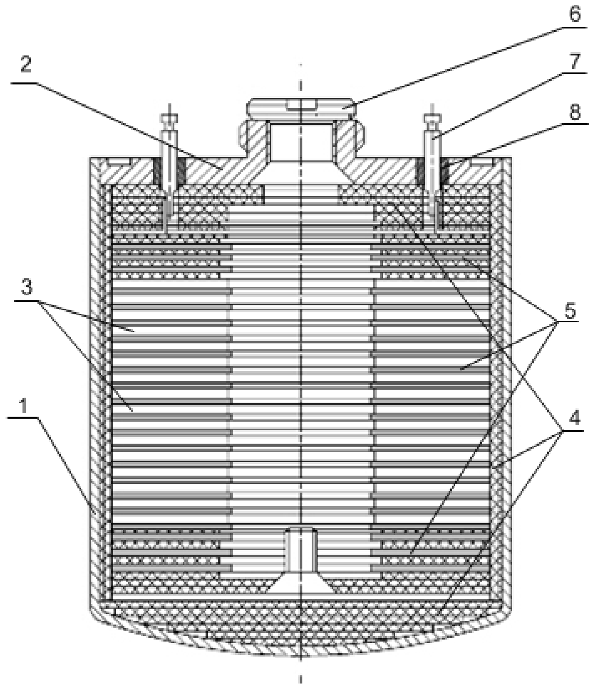

Figure 1: Cross section view of thermal battery BTR-03: 1 – cup, 2 – lid, 3 – cell, 4 – battery thermal insulation elements, 5 – heat tablet, 6 – impact igniter, 7 – battery pole, 8 – pole insulation.

2 Battery activation

When impact igniter of the battery BTR-03 initiates its activity, the flame fills the space inside the cylinder of the battery. Initiation of all 28 heat tablets occurs exactly at the same time. As a result of consultation with the manufacturer of the BTR-03 it was assumed that the linear velocity of burning of the pyrotechnic heat tablet material is 5 cm/s and in 1 s all heat tablets are burned [8]. All of the 22 heat tablets are connected with 22 cells and located in the middle of the battery BTR-03. Three heat tablets are placed above a pile of 22 sets: tablet-cell and the other 3 tablets are placed under the pile. Additional tablets are separated from one another only by the thermal insulation layers of cardboard and they constitute of thermal protection of cell pile from the top and from the bottom. This prevents premature crystallization of the electrolyte due to its cooling. A single tablet weighs about 1.8 g and occupies a volume of $1.154 \cdot 10^{-6}$ m^3. Manufacturer of battery BTR raises the calorific value of a single heat tablet in subsequent series. Initially its value was about 1600 J/g, followed by 1850 J/g. There is no current data on the calorific value of heat tablet of the battery BTR-03. In our case, the single heat tablet calorific value of 2600 J/g and BTR-03 battery activation time of 0.1 s [1, 2,] were assumed. As a result a total heat flux of 130 kW is obtained from the battery during one second. Dividing this value by the volume of 28 heat tablets, we get the maximum value of single tablet heat source equals $4 \cdot 10^9$ W/m^3. Calculations of heat transfer in the battery BTR-03 were carried out within time interval of 700 s which exceeds the burn time of tablets by 700 times. Therefore a constant value of volumetric heat source density in time of 1 s was assumed. Finally, in heat transfer model the volumetric heat source density as a function of $\dot{q}_v(t)$ – Figure 2 with its maximal value equals $4 \cdot 10^9$ W/m^3 was assumed for doing calculation.

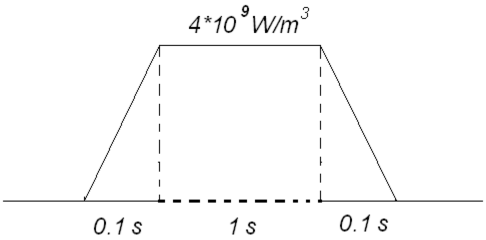

Figure 2: Time-dependence of volumetric heat source density $\dot{q}_v(t)$ *for the battery BTR-03 single heat tablet.*

3 Experimental arrangements

Temperature measurements in 6 points on outer surface of the battery BTR-03 were performed using coated thermocouples type K 0.5 mm in coat diameter by company Omega (USA). Location of thermocouples on the outer surface of the battery cup is shown in Figure 4. Thermocouples were glued with high temperature silicone glue (temp. max 600 K) *Red Hi-Temp RTV* (USA) and affixed to the outer surface of battery cup using clips in the form of strips of duralumin – Figure 3. The battery was activated by a needle puncture of the impact igniter with a trigger. The trigger was activated with a direct voltage signal of 27 V. A set consisting of base unit NIcDAQ 9172 and measuring card NI 9213 (National Instruments, USA) was used to measure temperature versus time *T(t)* at selected points on the outer surface of the battery BTR-03: a_0, a_1, a_2, a_3, a_4, a_5 (Figure 4). Results of measurements are shown in Figures 7÷12. The temperature measurements illustrated in Figures 7÷12 were carried out also using a thermal imaging camera FLIR SC5600. At present this IR camera involves NUC (non-uniform correlation) for temperature measuring range only up to 383 K as a result of our financial limitation.

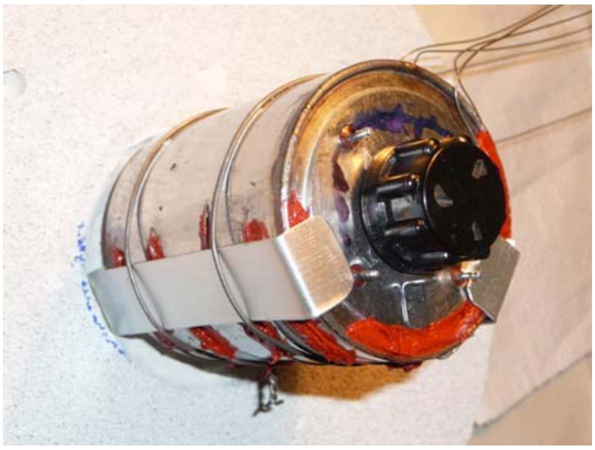	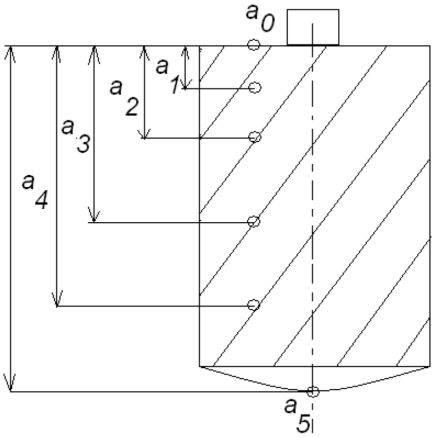
Figure 3: View of the battery BTR-03 with mounted coated thermocouples which are used to measure the temperature on the outer surface of the battery cup.	*Figure 4: Distribution of thermocouples along the length of the battery BTR-03:* a_0 *– 0 mm,* a_1 *– 10 mm,* a_2 *– 24 mm,* a_3 *– 45 mm,* a_4 *– 62 mm,* a_5 *– 74 mm.*

The results *T(t)* obtained with the use of IR camera FLIR SC5600 (Figures 7÷12) are closer to the numerical results than the measurements obtained with the use of thermocouples.

4 Numerical evaluations and experimental results

Due to the high cost of the battery BTR-03 (about 1000 EU per unit) it is not possible to check the structural variants of thermal insulation of thermal battery, which is located in a special device. Thus, preliminary numerical model of heat transfer in the battery BTR-03 suspended in the air was created, based on the performed experiment. Numerical calculations were carried out by means of COSMOS/M commercial software package. Four-sided mesh of 2320 elements and 2742 nodes was applied – Figure 6. The results of calculations using finite volume method were given in the form of the distribution of isotherms cross-section of the battery in successive time intervals – Figures 13÷17. Also the results of calculations of the temperature dependence and heat flux density as a function of time in the chosen nodes of the mesh elements compatible with the measuring points $a_0 \div a_5$, i.e. $T_i(t)$ and $\dot{q}_i(t)$ were shown in Figures 7÷12 and 18÷19. The initial-boundary value problem, i.e. non-stationary heat transfer equation with internal heat sources (heat tablets) and boundary conditions of the third kind was solved. It was assumed that the battery life does not exceeded 700 s. The problem was treated as a two-dimensional due to the axial symmetry of the battery BTR-03. The results of calculations of the temperature dependence as a function of time $T(t)$ at the points: a_0, a_1, a_2, a_3, a_4, a_5 (Figure 4) were compared with the experimental data and illustrated in Figures 7÷12. Constant thermophysical properties of materials used to build the battery BTR-03 were assumed for numerical calculations – Table 1 and Figure 5. Battery cup was made of the alloy steel 1H18N9T with a thickness of 1 mm – Figure 5. Cylindrical cup thermal insulation consists of three layers: the outer layer – insulation paper prespan with a thickness of 0.3 mm, the middle layer – micanite with a thickness of 0.15 mm, the inner layer – cardboard with a thickness of 1.5 mm. 22 sets: heat tablet and cell are located inside the battery cup. Additional three heat tablets are located above the pile of 22 sets and an additional three are located below the pile of 22 sets.

Table 1: Average values of material thermal properties adopted for numerical calculations: c_p – specific heat, k – thermal conductivity, ρ - density

material	**c_p, J/(kg·K)**	**k, W/(m·K)**	**ρ, kg/m^3**
1H18N9T [7]	460	26	8900
micanite [7]	880	0.52	3000
cardboard [7]	1340	0.20	500
substitute cell material: calcium anode+electrolyte+cathode* [6]	800	k_r=50 (along the radius of battery) k_z=4 (along the axis of battery)	5000
heat tablet [6]	800	1	2000
battery interior gas* [6]	1110	6	0.40

(* [6] – based on the data of electrolytes)

Additional heat tablets are separated only by the thermal insulation layers of cardboard and are a thermal protection of the cell pile from the top and from the bottom. This is necessary to prevent premature crystallization of the electrolyte due to its cooling. Each heat tablet has a ring shape with a thickness of 0.7 mm, outer diameter is 50 mm, inner diameter is 19.5 mm. Each cell also has a ring shape with a thickness of 1.3 mm, outer diameter is 50 mm, inner diameter is 20 mm. The space above and below the cell pile is filled with thermal insulation cardboard – Figure 5. The temperature and the heat flux density distribution, i.e. $T_i(t)$ and $\dot{q}_i(t)$ on the outer surface of the cup battery BTR-03 was obtained on the basis of solution of initial-boundary value problem, described by the equation of heat transfer with a source term in cylindrical coordinates [3, 4, 7]:

$$\frac{\partial T}{\partial t}=\frac{k}{\rho\cdot c_p}\left[\frac{\partial^2 T}{\partial r^2}+\frac{1}{r}\frac{\partial T}{\partial r}+\frac{\partial^2 T}{\partial z^2}\right]+\frac{\dot{q}_v}{\rho\cdot c_p},$$

where: T – temperature at a given point on the outer surface of the battery cup, t – the time from the initial moment, r, z – cylindrical coordinates of the point, k, ρ, c_p – thermophysical properties of materials of the battery BTR-03, $\dot{q}_v$ - volumetric heat source,

Ambient temperature was assumed as an initial condition $T_{ambient}=293\ K$. On the outer surface of the battery cup BTR-03 the heat transfer by convection and the boundary condition in the form $\dot{q}=\alpha\cdot\left(T_{ambient}-T_{battery\ cup\ surface}\right)$ were established. Assumed value of coefficient of heat transfer is $\alpha=15\ \mathrm{W/\left(m^2\cdot K\right)}$. This is an overall coefficient, which was created as the sum of two components $\alpha=\alpha_{convection}+\alpha_{radiation}$, i.e. the coefficient of heat transfer for air and the coefficient of heat transfer associated with the heat transfer by radiation $\alpha_{radiation}=5\div 6\ \mathrm{W/\left(m^2\cdot K\right)}$. In free space inside the battery BTR-03 there are mainly emissions from heat tablets. It was assumed that a heat transfer inside the battery takes place only through conduction of heat. We do not include convection and heat transfer by radiation. In the cylinder of battery axis gas properties were assumed as for air at 700 K and in accordance with what was said above, the heat transfer was assumed through conduction only. In the numerical calculations of heat flux density on the outer surface of the battery cup BTR-03 changes of heat flux density were shown as a function of time along the radius $\dot{q}_r(t)$ at points: a_1, a_2, a_3, a_4 (Figure 18) and along the height $\dot{q}_z(t)$ at points a_0, a_5 (Figure 19), i.e. on the surface of the upper and lower lids of the battery cup BTR-03.

5 Conclusions

The temperature distribution measurements on the outer surface of the battery cup BTR-03 at selected points along the length of the battery and the preliminary numerical calculations carried out on a currently available limited material data, helped to validate the model of heat transfer in the battery. Due to the high cost of battery it is not possible to take temperature distribution measurements of the battery cup inside the special device. Hence the design of thermal insulation of the battery BTR-03 can be done only by numerical simulation.

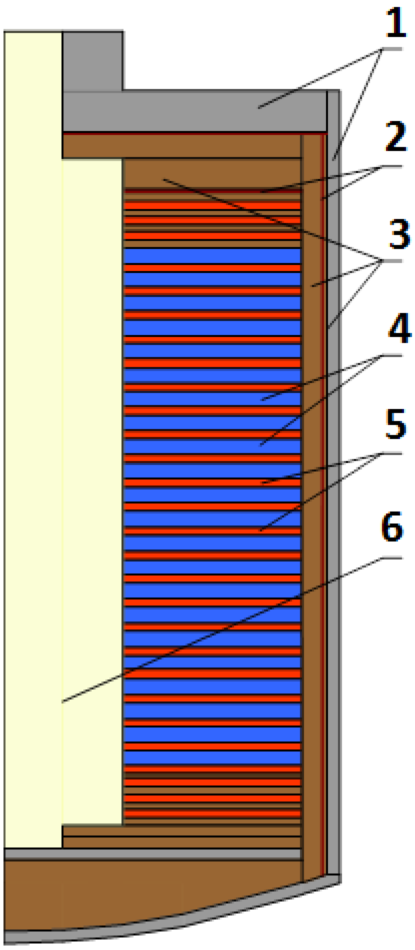

Figure 5: Section of battery BTR-03: 1 – 1H18N9T, 2 – micanite, 3 – cardboard, 4 – substitute cell material, 5 – heat tablet material, 6 – battery interior gas.

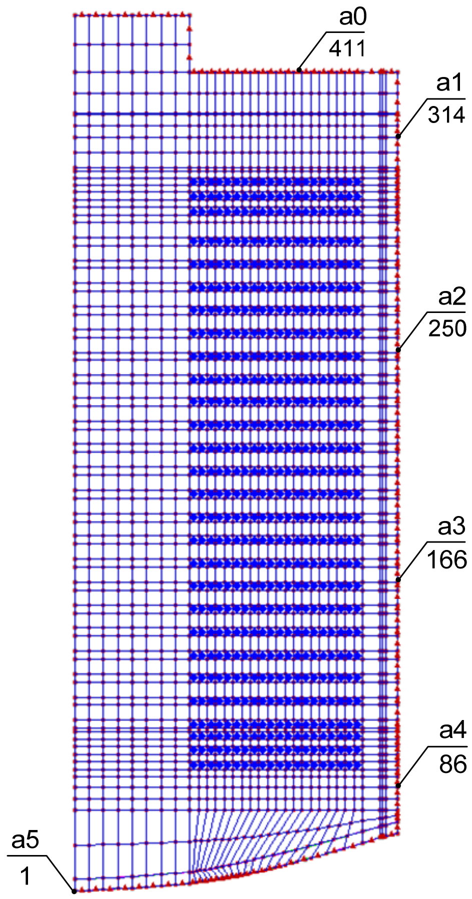

Figure 6: Four-sided mesh of 2320 elements and 2742 nodes: blue dots – volumetric heat source, red dots – boundary conditions (replacement coefficient of heat transfer). Selected points: a_1, a_2, a_3, a_4 and the corresponding node numbers.

The enormous power of all 28 pyrotechnic heat tablets determines the heat transfer in the battery BTR-03. Hence, constant thermophysical coefficients adopted at the present stage of development of numerical model of heat transfer in the battery BTR-03: thermal conductivity, thermal diffusivity and specific heat (Table 1) are not – in authors opinion – too simplistic. The authors see an opportunity to develop a numerical model of heat transfer in the battery BTR-03. At first results of heat transfer in a singular set, composed of the electrolyte, anode, cathode and the pyrotechnic heat tablet have to be obtained. The model should take into account the heat of melting of the electrolyte. Research on thermophysical properties of electrolyte as a function of temperature is also needed.

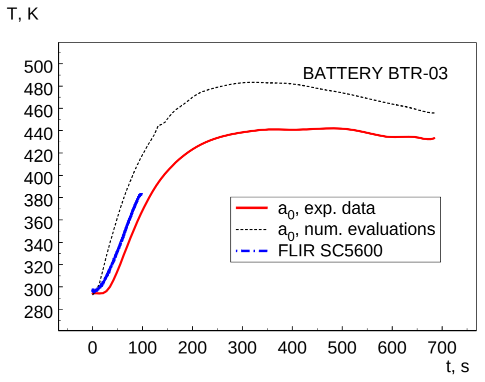

Figure 7: Temp. distribution at point a_0

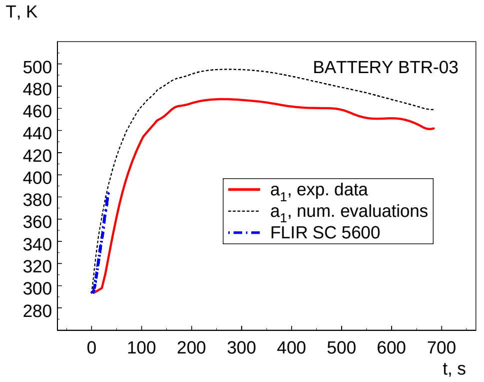

Figure 8: Temp. distribution at point a_1.

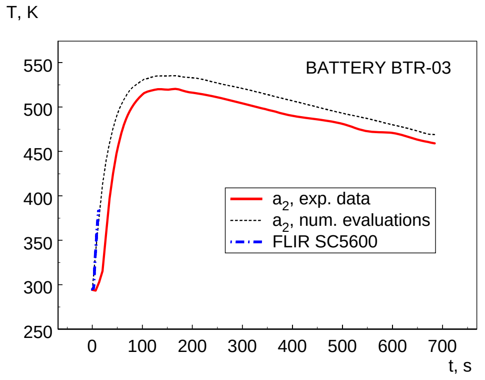

Figure 9: Temp. distribution at point a_2.

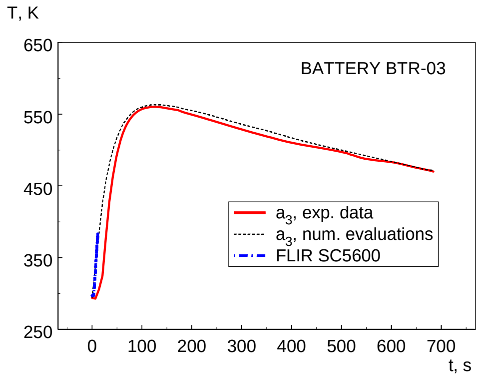

Figure 10: Temp. distribution at point a_3.

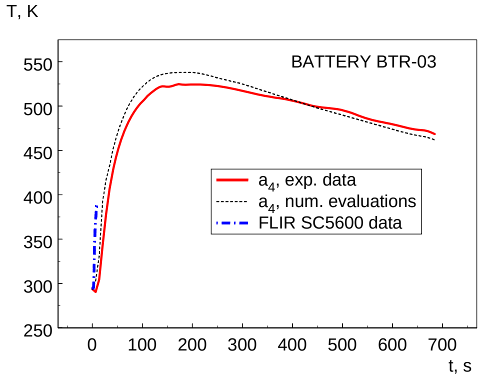

Figure 11: Temp. distribution at point a_4.

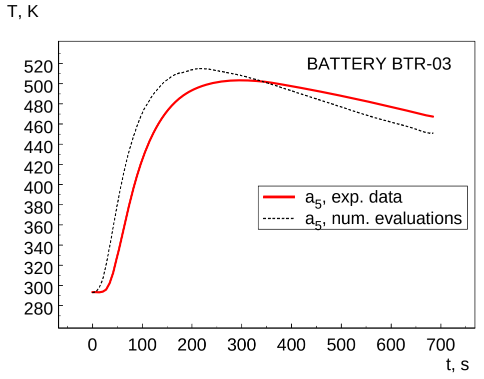

Figure 12: Temp. distribution at point a_5.

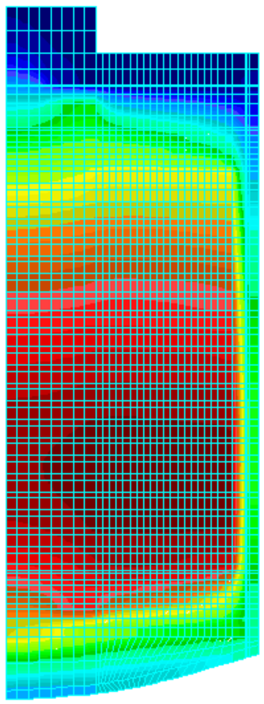

Figure 13: Temp. distribution for t=120 s.

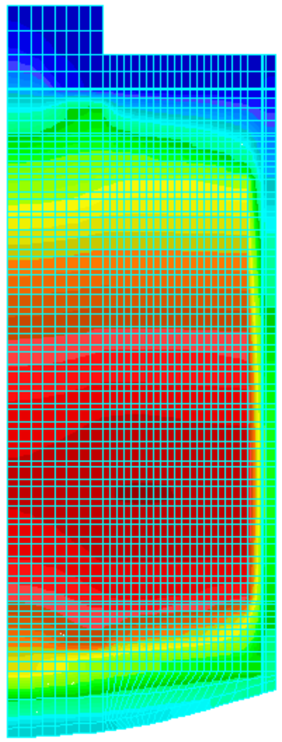

Figure 14: Temp. distribution for t=140 s.

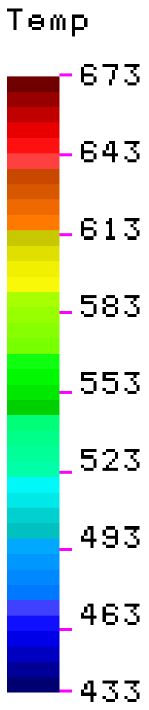

Temperature scale (Temp. in K).

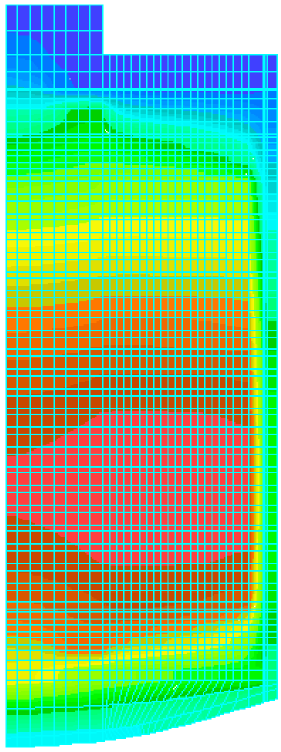

Figure 15: Temp. distribution for t=180 s.

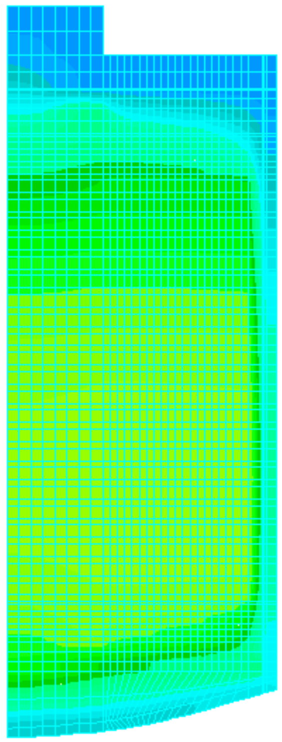

Figure 16: Temp. distribution for t=360 s.

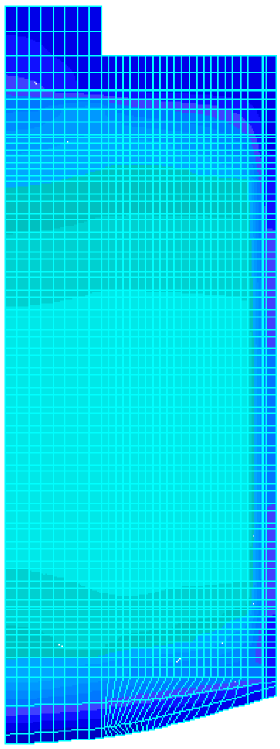

Figure 17: Temp. distribution for t=700 s.

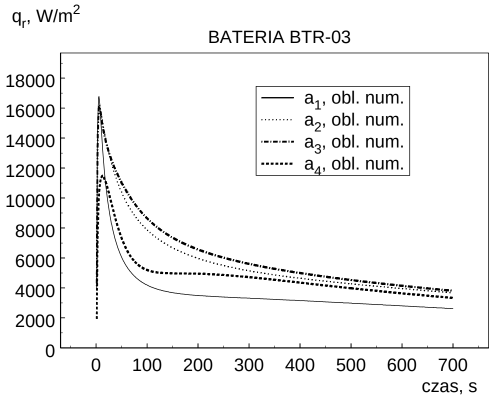

Figure 18: Dependencies of heat flux density as a function of time along the radius $\dot{q}_r(t)$ on the cup surface at the points a_1, a_2, a_3, a_4.

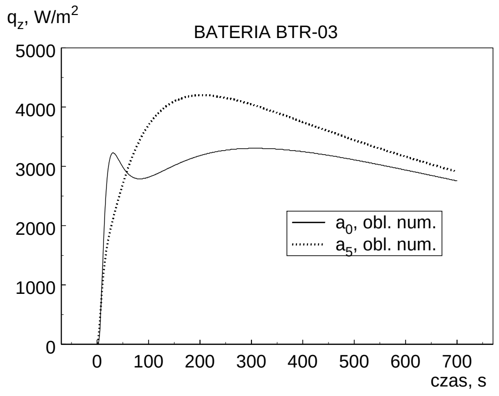

Figure 19: Dependencies of heat flux density as a function of time along the height $\dot{q}_z(t)$ on the upper and lower lids at the points a_0 *and* a_5.

The interior of the battery BTR-03 reaches a maximum temperature of 672 K after about 2 minutes after initiation. At that time, the outer surface of the cup reaches the maximum temperature of 583 K (Figure 7÷12 and Figure 13). The battery BTR-03 does not heat up symmetrically – Figure 7÷12 and Figure 13÷17. Therefore, the amount of additional heat tablets above the pile of 22 cells should be increased from 3 units to 4 units. Heat dissipation through the lid of battery cup is larger than through the bottom of the battery cup. – Figure 7 and Figure 12. According to the authors in order to maintain the battery electrolyte in the liquid state for longer period than currently the numerical calculations with more additional heat tablets above and below the 22 cell pile should be carried out. Analysis of changes of heat flux density as a function of time $\dot{q}_r(t)$ on the outer surface of the battery BTR-03 cup at the points a_1, a_2, a_3, a_4 (Figure 8÷11) confirms data from the manufacturer that the full power of the pyrotechnic heat tablets is available already in the first second. Analysis of changes of heat flux density as a function of time $\dot{q}_r(t)$ on the upper and lower lids of the battery BTR-03 cup $\dot{q}_z(t)$ leads to the conclusion that the heat flux density at these sites remains virtually constant since the initiation of the battery until the end of its work. The numerical calculations of heat transfer in the battery BTR-03 presented in this paper allow the analysis of the battery as a heat source. Location of the battery in the special device has no longer significance, because the shape and the type of thermal insulation of the battery BTR-03 can be designed without expensive experimental studies.

Acknowledgement

This work was supported by grant OR00003208 from the Ministry of Science and Higher Education of Poland (PBR/15-196/2009/WAT). The authors would like to express their gratitude to Dr. M. Preiskorn from MUT for his help in doing calculations.

References

[1] TABAT S., STYCZYNSKI S., ZIOŁKOWSKI Z., KAMINSKI R., SZŁAPKA R., CZAJKA B. Characterization of thermally activated battery BTR-05, www.witu.mil.pl/www/biuletyn/zeszyty/20060097s/241.pdf (in Polish)

[2] STYCZYNSKI S., CZAJKA B., TABAT S., SZCZESNIAK B., CISZEWSKI A., WACHOWSKI L., SOŁOPA W., RYDZYNSKA B., Model of thermally activated reserve battery with a basis of $Li/KCl\text{-}LiCl\text{-}RbCl\text{-}LiF/FeS_2$, www.witu.mil.pl/www/biuletyn/zeszyty/20060097s/233.pdf (in Polish)

[3] KOZLOW W.P. Two-dimensions axial non-stationary heat transfer problems, *Science and Technology*, Minsk 1986, in Russian

[4] ABRAMOWITZ M., STEGUN I.A. Handbook of Mathematical Functions with Formulas, Graphs and Mathematical Tables, *Dover Publications*, Inc, New York, 1965

[5] NISSEN D.A., *J. Electrochem. Soc.*, 1979, 2, 176

[6] Material Property Database MPDG v.7.08, JAHM Software, Inc. USA, 2009

[7] WIŚNIEWSKI S., Heat transfer, *WNT*, Warsaw 2000 (in Polish)

[8] Central Laboratory of Batteries and Cells – Poland, www.claio.poznan.pl

Simultaneous monitoring of moisture and salt concentration using the time domain reflectrometry method

Zbyšek Pavlík[1], Jan Mihulka[1], Milena Pavlíková[1], Lukáš Fiala[1], Robert Černý[1]

[1] Department of Materials Engineering and Chemistry, Faculty of Civil Engineering,
Czech Technical University in Prague, Thákurova 7, CZ-166 29, Prague 6, CZECH REPUBLIC

Abstract: *Simultaneous monitoring of moisture and chloride concentration in porous building materials using the time domain reflectrometry method is presented. The experiments for determination of moisture and chloride transport properties are performed in the conditions of one-sided water and 0.1M NaCl solution uptake. The obtained results can find use in computational modelling of moisture and chloride ions transport in porous building materials, what can be useful for example for their damage assessment by means of salt action.*

Keywords: *moisture, chloride concentration, TDR, building materials*

1. Introduction

Moisture and water soluble salts in porous building materials represent an important issue in building science. Typically, the significant deterioration of buildings' functionality and materials' integrity can be observed in historical buildings, where horizontal water-proofing insulation is missing or damaged. Here, the frost induced damage and salt crystallization, hydration and high hygroscopic absorption take place. In case of materials of historical masonry, the moisture and salt related problems represent very actual topics especially from the point of view of their conservation and reconstruction. Since many historical buildings in Central European territory were built from different kinds of stones, among them argillite, sandstone, granite and limestone were most often used, there is a need to study these materials with a view to their ability to transport and accumulate water. Performance of these materials with regard to water and salt solution imbibition represents basic information for estimation of their durability and service life not only as raw masonry materials, but also in relation to structure, where they are already inbuilt.

For the determination of moisture and salt transport properties of porous materials, there is necessary to measure liquid water and salt concentration in specific position and time in studied material sample. It in fact means measurement of moisture and salt concentration fields. On this account, there is necessary to find sufficiently accurate and reliable method for moisture and salt concentration measurement. Since the presence of water in inner structure of porous media highly affects its properties, several moisture measurement methods were developed and advanced until now [1]. However, the reliability of the most of the moisture measurement methods is negatively influenced by presence of salt ions dissolved in water that change water conductivity [2], [3]. Typical examples are resistance moisture meters although they are often used in building practice even in materials containing salts. For materials with a high amount of salts, the resistance moisture meters are practically inapplicable, because the errors rapidly increase with the increasing moisture content. Therefore, specific attention must be paid while choosing the proper method for monitoring of salt solution propagation. In general, high frequency microwave methods of moisture measurement are considered to have universal applicability even in the case of high salt concentration in water [3].

In this work, TDR method is chosen as suitable for planned experiments. This method represents a specific methodology among the microwave impulse techniques, and in our previous work [4] we reported about its applicability for moisture measurement in building materials containing salts. Since we have applied combined TDR/electrical conductivity sensors, not only moisture content, but also chloride concentration was measured using one experimental apparatus. The experiments for determination of moisture and chloride transport properties were performed in the conditions of one-sided water and 0.1M NaCl solution uptake. On the basis of measured moisture and chloride concentration fields, moisture diffusivity and chloride diffusion coefficient of studied sandstone were calculated.

2. TDR (Time Domain Reflectometry) Method – Fundamental Principles

TDR method was introduced in early eighties [5], and since that time its applicability for moisture measurement was intensively investigated and improved. Now, it is widely accepted method to measure volumetric water content in both laboratory and field conditions, whereas the most of applications can be observed especially in soil science. On the other hand, application of TDR method for moisture measurement in hard building materials is not often, because of several problems with invasive TDR sensors installation.

The principle of TDR device consists in measuring the travel time of launched electromagnetic pulses along a waveguide (sensors) of exactly known length [6]. Time/velocity of pulse propagation depends on the apparent relative permittivity of the porous material where the waveguide is placed in, which can be expressed as

$$\varepsilon_r = \left(\frac{c t_p}{2L} \right)^2 , \tag{1}$$

where t_p [s] is pulse travel time, L [m] is the length of waveguide, c [m/s] is velocity of light in free space (2.9979 x 10^8), ε_r [-] is the material apparent dielectric permittivity. The value of the apparent ε_r measured by TDR probe represents the real part of the complex dielectric permittivity ε whereas its imaginary part ε_i is neglected and the measurement is performed in the frequency range 0.5 to 1 GHz [7], [8]. In this frequency range, the dielectric loss caused by polarization and conduction is supposed to be negligible.

Evaluation of moisture content θ [m^3/m^3] is based on fact that the presence of moisture modifies pulse travel time t_p and in this way also the dielectric permittivity. Therefore, using the measurement of apparent dielectric permittivity values, one can simply evaluate also actual moisture content in material, where the TDR waveguide (sensor) is placed. The relation $\theta = f(\varepsilon_r)$ represents calibration curve of specific TDR sensors for particular material. It can be result of empirical calibrations [6], [9] or modelling on the base of three or four phase dielectric mixing models based on effective media theory [10], [11], [12].

3. Experimental

Within the experimental part of the paper, measurement of moisture and chloride concentration profiles was done using TDR sensors placed into the studied sandstone sample. Diffusion-advection model used for inverse analysis of measured concentration profiles takes into account not only diffusion and advection of salt ions, but also the partial chloride ions binding in inner structure of materials. On this account, the measurement of chloride binding isotherm was performed as well.

3.1 Studied material

The suction experiment was realised on sandstone sample. It is fine grained silicious material and was chosen as a typical representative of stone masonry materials in the Central European territory. The studied material comes from quarry Mšené, Czech Republic and its properties we closely analysed in [13].

3.2 Measurement of moisture and chloride concentration profiles

The experiment for determination of moisture and salt concentration profiles was done in the conditions of one-sided 0.1 M NaCl solution vertical uptake into the rod-shaped sandstone sample. The sample size was 50/100/250 mm and all the lateral sides of the sample were vapour proof insulated by epoxy resin to ensure 1-D moisture and salt solution transport. The measuring technology was as follows. At first, the sensors were placed into the sample and sealed by silicone gel. Since sandstone is hard material, there was not possible to install TDR sensors by simple impress. Therefore, the particular sensors were placed into the before bored two parallel holes having the same dimensions as the sensor rod. For good contact of sensor with material, the bored powder of the studied material was partially placed back into the bored holes. Into the studied sample, 8 two-rod TDR miniprobes were placed for the monitoring of complex relative permittivity and electrical conductivity. Then, the sample was put into a vessel containing 0.1 M NaCl water solution and the suction has started. The complex relative permittivity and electrical conductivity were continuously monitored and stored in computer. After specific time interval, the experiment was interrupted and the sample was cut to eight separate pieces containing particular sensors. Finally, the sensors were removed and in each piece the moisture content and chloride concentration were measured by reference method. The moisture content was accessed by gravimetric method and chloride concentration by ion selective electrode (device pH/ION 340i) applied on leaches from particular sample pieces. In this way, the empirical calibration curve of TDR method for sandstone was determined.

3.3 Applied TDR device and sensors

For the TDR measurements in this paper, the cable tester TDR/MUX/mts produced by Easy Test was used. The working frequency of this device is 1.8 GHz for the relative permittivity measurement. This apparatus was developed in the Institute of Agrophysics PAS, Lublin, Poland that is active in the design and development of TDR technique for last twenty years (see for example [8], [14], [15]). The main distinctive feature of the applied device different to commonly used step pulse systems originated in Tektronix cable tester is usage of $\sin^2$-like needle pulse for feeding the two rods parallel waveguide sensor. The shape of the needle pulse resembles the shape of Gaussian curves with the rise and fall times (time distance between 10% and 90% of the signal amplitude) equal to 0.25ns. The reflectogram by needle pulse is much simple to interpret in the calculation of time distances between respective reflections [6].

Several TDR sensors were developed and used in practical measurements until now [16]. In our experiment, two rods waveguide sensors LP/ms by Easy Test were applied. The sensors are made of two 53 mm long parallel stainless steel rods, having 0.8 mm in diameter and separated by 5 mm. These sensors allow simultaneous measurement of apparent dielectric permittivity and electrical conductivity. In this way, both moisture content and salt concentration can be evaluated at the one time and position in studied sample.

3.4 Measurement of chloride binding isotherms

Chloride binding isotherm describes dependence of amount of bound chloride ions C_b [kgm^{-3}] in material sample on concentration of chlorides ions in surrounding salt solution C_f [kgm^{-3}]. For measurement of chloride binding isotherm of sandstone, equilibrium adsorption method was used [17]. Within the measurement, the samples were put into water-chloride solution of specific known concentration and the solution concentration was monitored until equilibrium concentration was reached. Then, the salt concentration in particular sample was measured using ion selective electrode and point wise function $C_b=C_b(C_f)$ was determined.

4. Inverse analysis of moisture and chloride concentration profiles

For the determination of moisture dependent moisture diffusivity and concentration dependent chloride diffusion coefficient, inverse analysis of moisture and chloride concentration profiles was performed. For inverse analysis, there is crucial to formulate model of moisture and chloride transport. Here, the diffusion-advection mechanism of chloride ions transport was assumed. In this way, the salt solution transport is described by system of two parabolic equations, whereas one of them describes the salt mass balance and the second one water mass balance (for details see [18], [19]).

Since we have assumed for the simplicity of the studied problem only 1-D salt solution transport, the system of two parabolic equations could be subjected to an inverse analysis in a similar way as for one parabolic equation, provided the initial and boundary conditions were simple enough, and the material parameters D (salt diffusion coefficient) and κ (moisture diffusivity) can be identified as functions of water content and salt concentration. The simplest possibility of such an inverse analysis is an extension of the Boltzmann-Matano treatment under the same assumptions of constant initial conditions and Dirichlet boundary conditions on both ends of the specimen for both moisture content and salt concentration where one of the Dirichlet boundary conditions is equal to the initial condition. After applying Boltzmann transformation and performing some straightforward algebraic operations, we arrive at the following formula for the determination of salt diffusion coefficient D

$$D(z_0) = -\frac{C_f(z_0)\kappa(z_0)\left(\frac{dw}{dz}\right)}{w(z_0)(\frac{dCf}{dz})_{z_0}} + \frac{\int_{z_0}^{\infty} z(\frac{d(wC_f)}{dz} + \frac{dC_b}{dC_f}\frac{dC_f}{dz})}{2t_0 \cdot w(z_0)\cdot(\frac{dC_f}{dz})_{z_0}}, \tag{2}$$

where z is the space variable, t_0 the time corresponding to the chosen moisture and concentration profiles $w = w(z,t_0)$, $C_f = C_f(z,t_0)$, the chosen values of moisture and concentration are $w_0 = w(z_0, t_0)$, $C_{f0} = C_f(z_0, t_0)$, the corresponding moisture diffusivity and salt diffusion coefficient $\kappa(z_0) = \kappa(w_0, C_{f0})$, $D(z_0) = D(w_0, C_{f0})$ and $C_b = f(C_f)$ is the ion binding isotherm.

The diffusion mechanism of moisture transport where the dependence of moisture diffusivity κ on moisture w is taken into account was assumed in the first case of calculation of moisture diffusivity. For the inverse analysis of experimentally determined moisture profiles $w(x, t)$, Matano method was employed. Its application leads to the following solution for moisture diffusivity

$$\kappa(w_0) = \frac{1}{2t_0\left(\frac{dw}{dz}\right)_{z=z_0}} \int_{z_0}^{\infty} z\frac{dw}{dz}dz\,, \tag{3}$$

where t_0 =*const.* is a given time where the moisture field $w(z,t_0)$ is known and z is the space variable. The details on the inverse analysis procedure can be found in [19].

5. Results

The calibration curves of applied TDR technique for moisture and chloride concentration measurement are given in Figs. 1, 2. The measured data show the dependences of relative permittivity on moisture content and electrical conductivity on chloride concentration. Interesting is especially behaviour of electrical conductivity, which highly increases at chloride concentrations lower than 0.002 g/g, whereas at higher concentrations, the increase of electrical conductivity is much lower. Determination of these calibration curves represents necessary knowledge for the applicability of TDR technique for salt solution transport monitoring. For practical evaluation of moisture content and chloride concentration, the experimental data were smoothed by simple polynomial relations with high reliability.

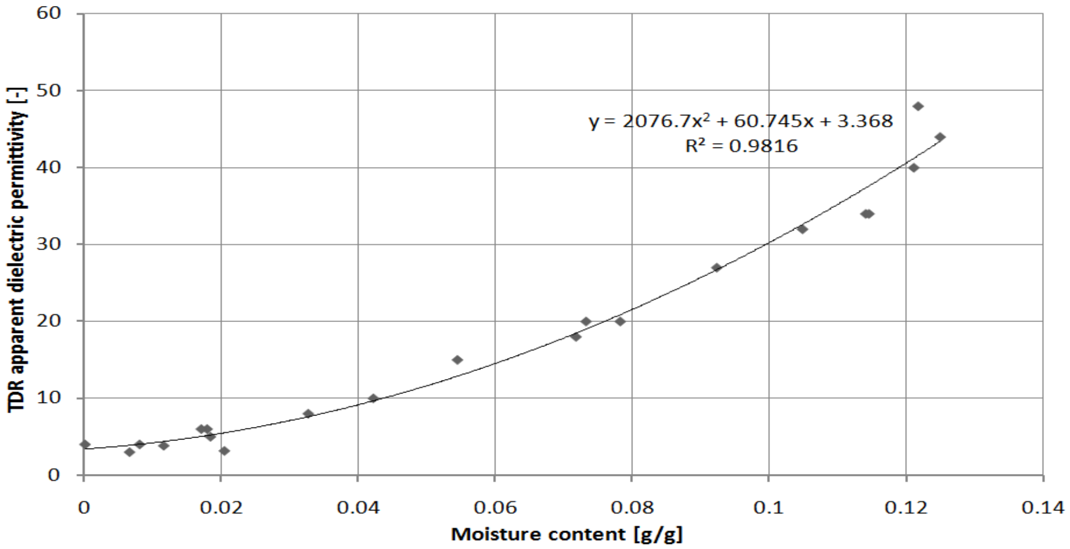

Fig. 1: Apparent dielectric permittivity of sandstone as function of moisture content

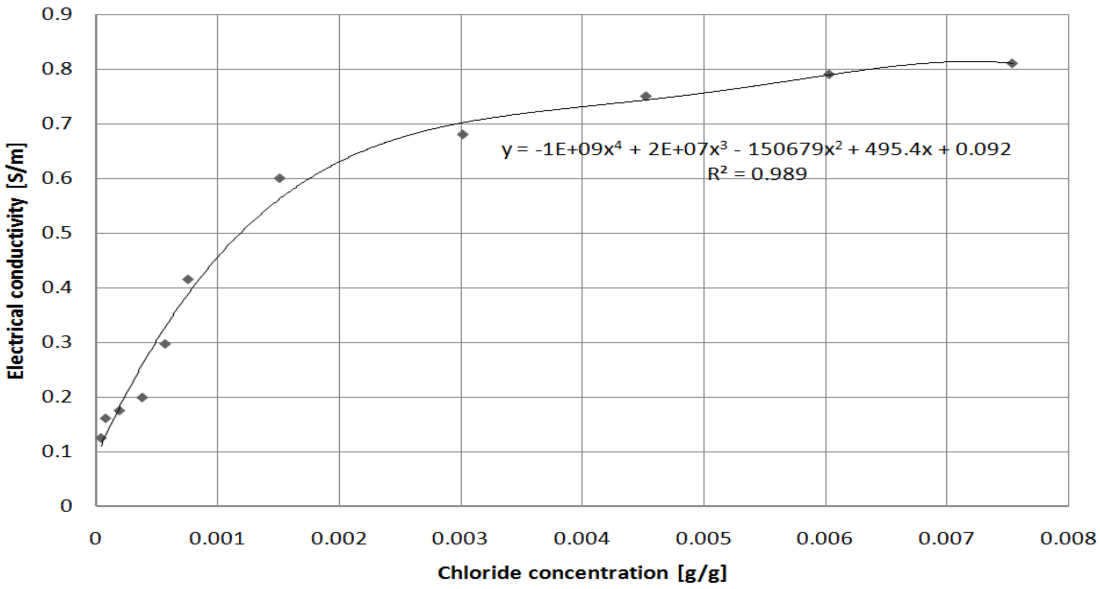

Fig. 2: Electrical conductivity of sandstone as function of chloride concentration

The measured moisture and chloride concentration profiles evaluated using above given empirical calibration curves are presented in Figs. 3, 4. Looking at the results we can observe fast moisture transport into the studied material. The moisture front reached within the time interval shorter than 2 hours distance 190 mm from penetrated surface.

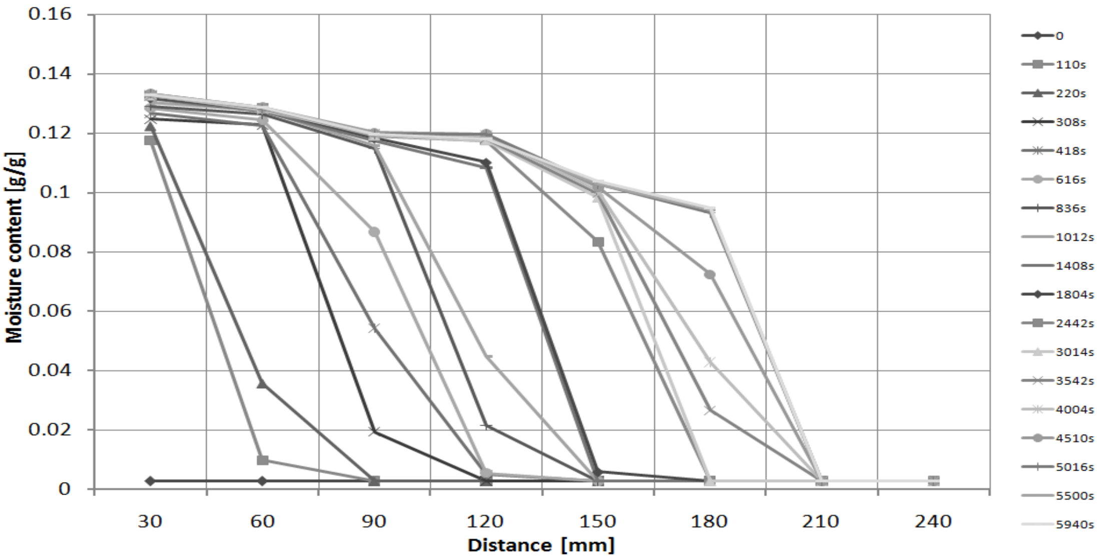

Fig. 3: Moisture profiles for sandstone measured by TDR

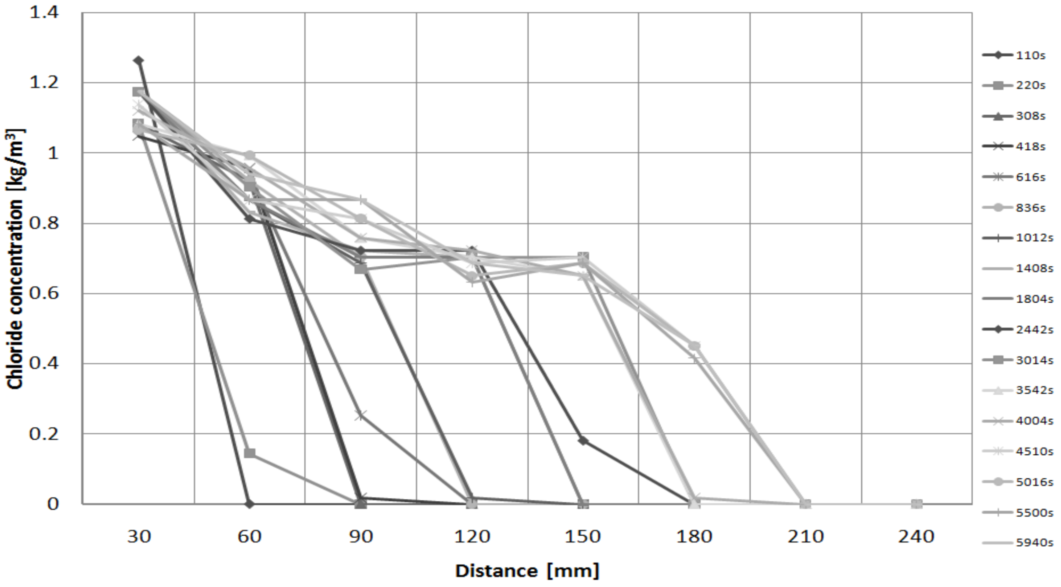

Fig. 4: Chloride concentration profiles for sandstone measured by TDR

The moisture dependent moisture diffusivity and concentration dependent chloride diffusion coefficient are presented in Figs. 5, 6. Looking at the data in Fig. 6, the moisture diffusivity varies within the range of three orders of magnitude. A similar trend is found also for concentration dependent chloride diffusion coefficient, where the results vary in the range of two orders of magnitude.

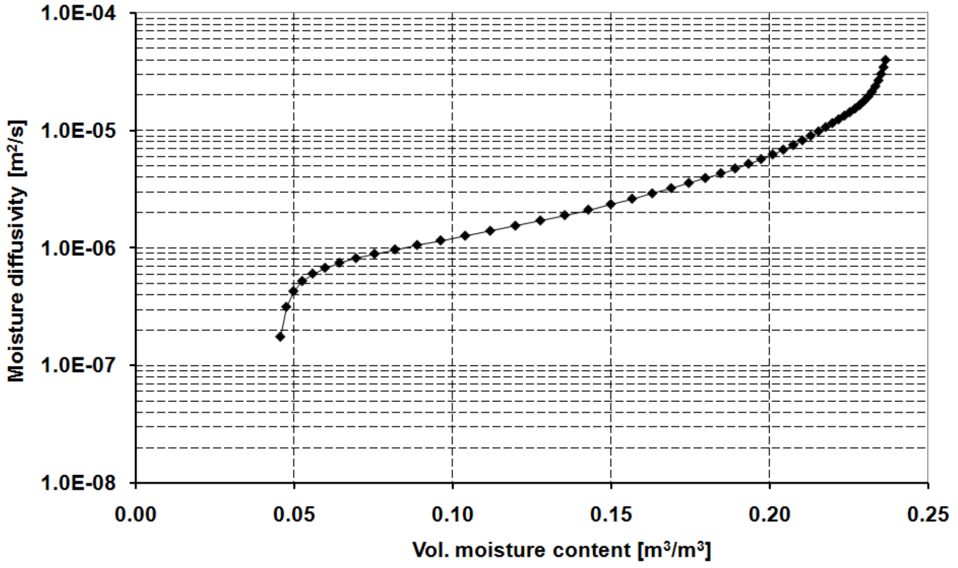

Fig. 5: Moisture diffusivity of studied sandstone

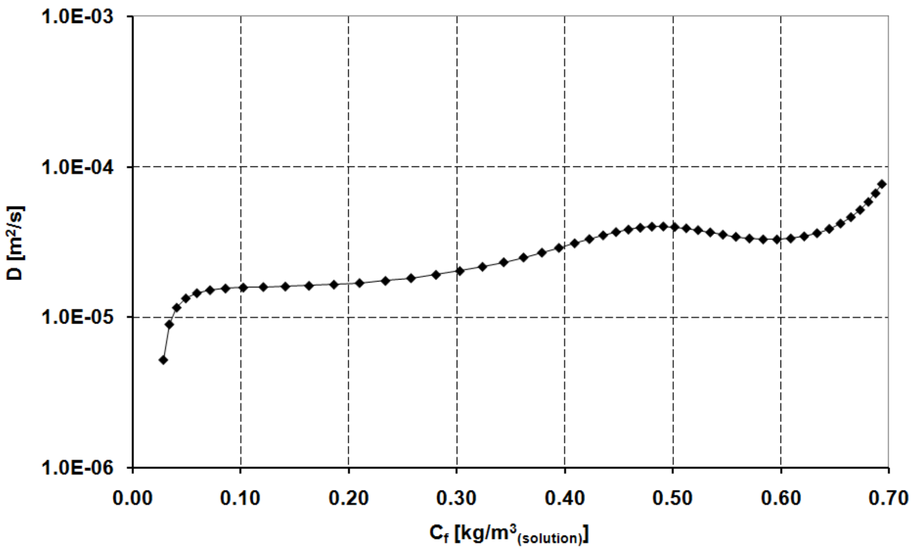

Fig. 6: Chloride diffusion coefficient of studied sandstone

6 Conclusions

The assessment of chloride diffusion coefficient and moisture diffusivity represents important information for application of studied sandstone for reconstruction of historical masonry and monuments. The knowledge of these material properties can be used in practical design of buildings with respect to possible moisture and salt transport. The results of the presented work can also find use in computational modelling of moisture and chloride ions transport in sandstone, what can be useful for example for its damage assessment by means of salt action.

The suction experiment presented in this paper has proven the capability of TDR combined sensors for simultaneous monitoring of moisture and salt concentration in porous building materials. This finding is very perspective for future work, especially for building practice that requires complex, precise and reliable methods for moisture and salt concentration measurement.

Acknowledgment

This research has been supported by the Czech Ministry of Education, Youth and Sports, under project No MEB 051027.

References

[1] Černý, R., Rovnaníková, P., Transport Processes in Concrete, 1st ed., London, Spon Press, 2002, 311-312.

[2] Pavlík, Z., Mihulka, J., Pavlíková, M., Černý, R., Monitoring Coupled Moisture and Salt Transport Using Single Vertical Suction experiment. Fourteenth International Conference on Computational Methods and Experimental Measurements. Algarve, Portugal, 2009, Wessex, WIT PRESS, 157-167.

[3] Pavlík. Z., Methods for Determination of Moisture Content of Porous Building Materials, Česká technika – nakladatelství ČVUT, 2010.

[4] Pavlík. Z., Mihulka, J., Pavlíková, M., Effect of Salt Concentration on the Applicability of TDR Method for Moisture Content Measurement in Porous Materials. 8th International Conference on Electromagnetic Wave Interaction with Water and Moist Substances, ISEMA 2009. Helsinki, Finland, 2009, Helsinki University of Technology, 372-376.

[5] Topp, G. C., Davis, J. L., Anna, A. P., Electromagnetic determination of soil water content: measurements in coaxial transmission lines. Water Resour. Res., 1980, Vol. 10, 542-582.

[6] Skierucha, W., Wilczek, A., Alokhina, O., Calibration of TDR probe for low soil water content measurements. Sensors and Actuators A: Physical, 2008, Vol. 147, 544-552.

[7] Skierucha, W., Wilczek, A., Horyński, M., Sumorek, A., Determination of Electromechanical Properties of Dusts Obtained from Cereal Grain. Transactions of the ASABE, Vol. 51(1), 177-184.

[8] Malicki, M. A., Skierucha, W., A manually controlled TDR soil moisture meter operating with 300 ps rise-time needle pulse. Irrig. Sci., 1989, Vol. 10(2), 153-163.

[9] Roth, C. H., Malicki, M. A., Plagge, R., Empirical evaluation of the relationship between soil dielectric constant and volumetric water content as the basis for calibrating soil moisture measurements by TDR. J. Soil Sci., 1992, Vol. 43, 1-13.

[10] Sihvola, A., Electromagnetic mixing formulas and applications, IEEE Electromagnetic Waves Series No. 47, 1999, Stevenage, Hertz, UK

[11] Pavlík, Z., Fiala, L., Černý, R., Sobczuk, H., Suchorab, Z., Effect of particle shape on the accuracy of dielectric mixing models applied for determination of moisture content of building materials. Energy Efficiency and New Approaches. Fourth International Building Physics Conference. Topkapi, Istanbul, Beysan Matbaacilik ve Reklamcilik, 2009, 33-39.

[12] Robinson, D. A., Jones, S. B., Blonquist Jr., J. M., Friedman, S. P., A Physically Derived Water Content/Permittivity Calibration Model for Coarse-Textured, Layered Soils. Soil Sci. Soc. Am., 2005, Vol. 69, 1372-1378.

[13] Pavlík, Z., Michálek, P., Pavlíková, M., Kopecká, I., Maxová, I., Černý, R., Water and Salt Transport and Storage Properties of Mšené Sandstone. Constr. Build. Mat., 2008, Vol. 22(8), 1736-1748.

[14] Malicki, M. A., Walczak, R., Evaluating soil salinity status from bulk electrical conductivity and permittivity. Eur. J. Soil. Sci., 1990, Vol. 50, 505-514.

[15] W. Skierucha, Accuracy of soil moisture measurement by TDR technique. Int. Agrophys., 2000, Vol. 14, 417-426.

[16] Heimovaara, T. J., Design of triple wire time domain reflectometry probes in practice and theory. Soil Sci. Soc. Am. J., Vol. 57, 1410-1417.

[17] Jiřičková, M., Černý, R., Chloride Binding in Building Materials. J. Build. Phys., Vol. 29(3), 189-200.

[18] Pel, L., Kopinga, K., Kaasschieter, E. F., Saline absorption in calcium-silicate brick observed by NMR scanning. J. Phys. D: Appl. Phys., Vol. 33, 1380-1385.

[19] Pavlík, Z., Jiřičková, M., Fiala, L., Černý, R., Inverse Modelling of Salt Diffusion and Advection in Building Materials. Research in Building Physics and Building Engineering, 2006, London, Taylor and Francis, 155-160.

List of participants

Prof. RNDr. Ivan Baník Ph.D.
Slovak University of Technology
Faculty of Civil Engineering
Radlinského 11
813 68 Bratislava
SLOVAKIA

Ing. Vlastimil Boháč CSc.
Slovak Academy of Sciences
Institute of Physics, SAS
Dúbravská cesta 9
845 11 Bratislava 45
SLOVAKIA

Prof. Ing. Robert Černý, DrSc.
Czech Technical University
Faculty of Civil Engineering
Thákurova 7
16629 Prague
CZECH REPUBLIC

Ing. Danica Fidríková
Slovak Academy of Sciences
Institute of Physics
Dúbravská cesta 9
84511 Bratislava
SLOVAKIA

MSc. Marcin Gapski, PhD student
Wojskowa Akademia Techniczna
Faculty of Mechatronics
Kaliskiego 2
00-908 Warsaw
POLAND

D.Sc. Darius Gawin Ph.D., M.E.
Technical University of Lodz
Department of Building Physics &
Building Materials
Al. Politechniki 6
90-590 Lodz
POLAND

Mgr. Matúš Holúbek
Slovak University of Technology
Faculty of Civil Engineering
Radlinského 11
813 68 Bratislava
SLOVAKIA

Ing. Jan Kočí
Czech Technical University
Faculty of Civil Engineering
Thákurova 7
166 29 Prague 6
CZECH REPUBLIC

Ing. Václav Kočí
Czech Technical University
Faculty of Civil Engineering
Thákurova 7
16629 Prague 6
CZECH REPUBLIC

Prof. Piotr Koniorczyk, Ph.D., DSc., Eng.
Military University of Technology
Institute of Aviation Technology
Kaliskiego 2
00-908 Warsaw
POLAND

Ing. Daniel Kopkáně
Brno University of Technology
Faculty of Civil Engineering
Veveří 95
60200 Brno
CZECH REPUBLIC

Ing. Tomáš Korecký
Czech Technical University
Faculty of Civil Engineering
Thákurova 7
166 29 Prague 6
CZECH REPUBLIC

prom. fyz. Ol'ga Koronthályová CSc.
Slovak Academy of Sciences
Institute of Construction and Architecture
Dubravska cesta 9
845 03 Bratislava
SLOVAKIA

Mgr. Jozef Kováč
Constantine the Philosopher University
Tr. A. Hlinku 1
949 74 Nitra
SLOVAKIA

Ing. Ludovít Kubičár, DrSc.
Slovak Academy of Sciences
Institute of Physics SAS
Dubravska cesta 9
845 11 Bratislava
SLOVAKIA

Ing. Peter Matiašovský, CSc.
Slovak Academy of Sciences
Institute of Construction and Architecture
Dúbravská cesta 9
845 03 Bratislava 45
SLOVAKIA

doc. RNDr. Igor Medveď, Ph.D.
Constantine the Philosopher University
Faculty of Natural Sciences
Tr. A. Hlinku 1
94974 Nitra
SLOVAKIA

Ing. Peter Mihálka, PhD.
Slovak Academy of Sciences
Institute of Construction and Architecture
Dubravska cesta 9
845 03 Bratislava
SLOVAKIA

Mgr. Ján Ondruška, PhD.
Constantine the Philosopher University
Faculty of Natural Sciences
Tr. A. Hlinku 1
94974 Nitra
SLOVAKIA

Ing. Gabriela Pavlendová Ph.D.
Slovak University of Technology
Faculty of Civil Engineering
Radlinského 11
813 68 Bratislava
SLOVAKIA

doc. Ing. Zbyšek Pavlík, Ph.D.
Czech Technical University
Faculty of Civil Engineering
Thákurova 7
166 29 Prague 6
CZECH REPUBLIC

Prof. Mgr. Jan Toman, DrSc.
Czech Technical University
Faculty of Civil Engineering
Thákurova 7
166 29 Prague 6
CZECH REPUBLIC

RNDr. Anton Trník, Ph.D.
Constantine the Philosopher University
Faculty of Natural Sciences
Tr. A Hlinku 1
94974 Nitra
SLOVAKIA

Prof. Ing. Jiří Vala, CSc.
Brno University of Technology
Faculty of Civil Engineering
®i¾kova 17
60200 Brno
CZECH REPUBLIC

Ing. Eva Vejmelková, Ph.D.
Czech Technical University
Faculty of Civil Engineering
Thákurova 7
166 29 Prague 6
CZECH REPUBLIC

Ing. Viliam Vretenár, PhD.
Slovak Academy of Sciences
Institute of Physics
Dúbravská cesta 9
84511 Bratislava
SLOVAKIA

Assoc. Prof. Janusz Zmywaczyk, Ph.D
Military University of Technology
Faculty of Mechatronics
Kaliskiego 2
00-908 Warsaw
POLAND

Ing. Tereza Kulovaná
Czech Technical University
Faculty of Civil Engineering
Thákurova 7
166 29 Prague 6
CZECH REPUBLIC

Ing. Miloš Jerman, PhD.
Czech Technical University
Faculty of Civil Engineering
Thákurova 7
166 29 Prague 6
CZECH REPUBLIC

Ing. Miroslava Lapková
Czech Technical University
Faculty of Civil Engineering
Thákurova 7
166 29 Prague 6
CZECH REPUBLIC

RNDr. Vratislav Tydlitát, CSc.
Czech Technical University
Faculty of Engineering
Thákurova 7
166 29 Prague 6
CZECH REPUBLIC

doc. Ing. Juraj Veselský, PhD.
Slovak University of Technology
Faculty of Civil Engineering
Radlinského 11
813 68 Bratislava
SLOVAKIA

Dominika Trefon-Radziejewska, MSc.
Silesian University of Technology
Institute of Physics
Krzywoustego 2
44-100 Gliwice
POLAND

prof. RNDr. Július Krempaský, DrSc.
Slovak University of Technology
Faculty of Electrical Engineering and
Information Technology
812 19 Ilkovičova 3
Bratislava
SLOVAKIA

Prof. Bimal K. Sarkar, Ph.D.
VIT University
Department of Physics
Vellore 632014
632014 Tamil Nadu
INDIA

Dr. Ulf Hammerschmidt, Dipl. Phys.
Physikalisch-Technische Bundesanstalt 1.74
Bundesallee 100
38 116 Braunschweig
GERMANY

Prof. Ing. Oldrich Zmeskal, CSc.
Brno University of Technology
Faculty of Chemistry
Purkynova 118
612 00 Brno
CZECH REPUBLIC

Ing. Lenka Dohnalova
Brno University of Technology
Faculty of chemistry
Purkynova 118
612 00 Brno
CZECH REPUBLIC

Title	Thermophysics 2011 – Conference Proceedings
Editor	Oldřich Zmeškal
Publisher	Brno University of Technology, Faculty of Chemistry, Purkyňova 464/118, CZ-612 00 Brno
Print	Brno University of Technology, Faculty of Chemistry, Purkyňova 464/118, CZ-612 00 Brno
Edition	first
Year of first edition	2011
Number of pages	278
Number of copies	70
ISBN	978-80-214-4345-7